The use of Optical Biosensors for Kinetic Analysis: A Critical Appraisal

by

Paul Edwards.

a thesis submitted in candidature
for the degree of
Doctor of Philosophy
and the
Diploma of Imperial College
at the University of London

Department of Chemistry

Imperial College of Science, Technology and Medicine,
London

July 1998

Abstract

The evaluation and interpretation of data from the resonant mirror optical biosensor, IAsys, is discussed with emphasis on the kinetic data. Various aspects of the biosensor and sensor surface design are investigated for suitability to kinetic analysis.

The IAsys biosensor utilises a cuvette format containing a sample well and the sensing surface. In order to monitor molecular interactions one of the binding partners (the ligand) must be attached to the sensor surface , often via a carboxymethyl CMD layer (CMD), while the other partner (the ligate) binds from solution. Stirring within the cuvette is investigated to determine the conditions for which mass transport limitations can be excluded.

Kinetic analysis of biosensor data relies upon the concentration of the ligate being in excess over the ligand and therefore effectively constant so that pseudo-first order conditions prevail. Any change in the ligate concentration may adversely effect the constants determined and this is possible with the 'closed' cuvette design. Second order equations are derived and the deviations from the first order conditions investigated.

Sensor surfaces coated with a CMD layer may also effect the kinetic constants determined in which the kinetics of differing interactions were monitored on both CMD and planar (No CMD) sensor surfaces. Deviations from the expected first-order behaviour are investigated and explanations for these deviations proposed.

Finally, a comparison of kinetic constants determined from the stop-flow fluorescence and IAsys is presented and recommendations made in order for IAsys to produce kinetic results which mirror those obtained in solution.

Acknowledgements.

I would like to thank Dr. Denise Pollard-Knight for initiating this PhD prior to her departure from Affinity Sensors and to her successor Dr. Peter Lowe for helpful suggestions throughout the course of this research. I am also indebted to my industrial supervisors, Dr. Robert Davies and Dr. Colin Maule, and my academic supervisor Dr. Robin Leatherbarrow, for their help and guidance throughout the course of this research.

Finally, I would like to thank my family and friends, especially those at Affinity Sensors, for their support and understanding during the last few years.

Contents.

Figures

Tables:

Table 9.7: The association and dissociation rate constants derived for the interaction of three fluorescein conjugates with anti-FITC mab immobilised on an amino surface 240

Abbreviations:

A) Textual

^{125}I HSA	^{125}I labelled HSA
BSA	Bovine serum albumin
CI-2	Chymotrypsin inhibitor 2
CMD	Carboxymethyl dextran
cpm	counts per minute
D1.3Fv	Fv antibody fragment to hen egg lysozyme
Da	Daltons
DMF	Dimethylformamide
DNA	Deoxyribonucleic acid
EDC	1-ethyl-3-(3-dimethylaminopropyl)-carbodiimide
ELISA	Enzyme linked immunosorbant assay
FITC	Fluoresein isothiocyanate.
HEL	Hen egg lysozyme
HSA	Human serum albumin
IgG	Immunoglobulin G
IRS	Internal reflectance spectroscopy
mab	Monoclonal antibody
mbp	Maltose binding protein
NHS	N-hydroxysuccinimide
PBS	Phosphate buffered saline
PBS/T	Phosphate buffered saline containing 0.05% Tween 20.
RAMFc	Rabbit Anti-mouse Fc
RIA	Radioimmunoassay
SPR	Surface plasmon resonance
TE	Transverse electronic
TIR	Total internal reflection
TM	Transverse magnetic
UHP water	Ultra high purity water

B) Equation symbols.

A	Extent of the first phase of association or dissociation
B	Extent of the second phase of association or dissociation
G	Immobilised species (ligand)
k_{ass}	Association rate constant
k_{diss}	Dissociation rate constant
K_A	Association equilibrium constant
K_D	Dissociation equilibrium constant
L	Species in solution (ligate)
R_0	Initial IAsys response
R_{eq}	Equilibrium IAsys response
R_{max}	Maximal IAsys response equal to the capacity of the ligand
R_t	IAsys response at time t
R_∞	IAsys response at infinity
ν	Initial rate
β	factor converting IAsys response to concentration
θ_c	Critical angle

Chapter 1

Biosensors.

1.1 Introduction.

A biosensor may be defined as an analytical device that incorporates both a biological recognition component and a transducer as major elements as shown in figure 1.1.

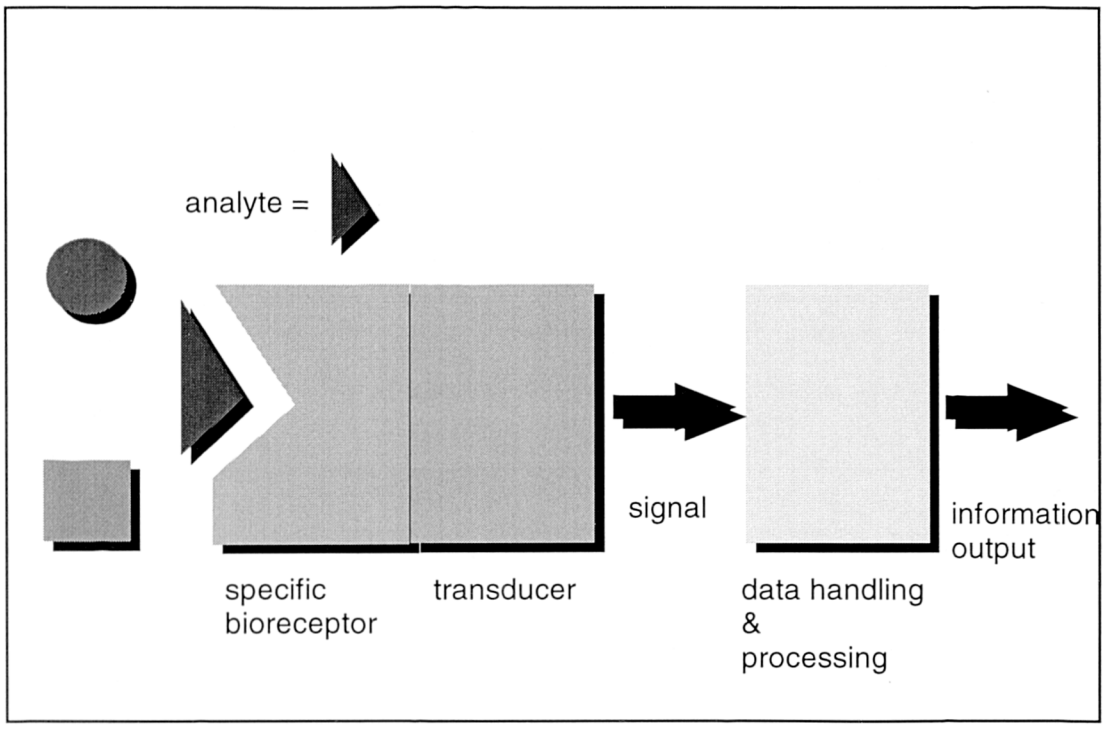

Figure 1.1: *Schematic diagram of a biosensor.*

The biological sensing element produces a physical or chemical change due to the presence of the analyte and therefore provides the specificity of the biosensor. A transducer converts this change in the sensing element into an electrical signal which can be processed into a suitable form.

Ideal requirements for a biosensor are that it should be able to:-

(1) allow rapid detection and quantification within the required concentration range ideally in 'real-time'.

(2) detect the binding event without the need for additional steps and reagents, a so-called direct assay or measurement.

(3) be regenerable to allow multiple measurements on the same surface.

(4) detect binding events in unprocessed samples such as serum.

1.2 Biosensor transducers

The development of biosensors has become increasingly important as demonstrated by the larger number of research papers published each year. There are four main transducer types currently used for biosensor construction and these are listed below:

(1) Electrochemical, which can be further divided into amperometric and potentiometric (Vadgama et al., 1989, Morgan et al., 1996).

(2) Gravimetric including quartz crystal microbalances (Thompson et al 1991), surface acoustic waves (Zellers et al., 1988).

(3) Calorimetric (Mosbach. 1991).

(4) Optical such as total internal reflection fluorescence (Noy et al., 1992), ellipsometry (Ruzgas et al., 1992), surface plasmon resonance (Karlsson et al., 1991), waveguides (Cush et al., 1993) and interferometry (Fattinger et al., 1993)

An optical biosensor forms the basis of this thesis and as such this overview is restricted to surface sensitive optical techniques

1.3 Surface sensitive optical techniques.

Surface sensitive techniques have gained increased importance in the analysis of biospecific interactions due to the ability to immobilise the recognition element to a surface thus eliminating the need for separation methods. Furthermore, evanescent wave techniques (see 1.3.2) can often allow direct measurement of surface reactions without an appreciable interference from the solution phase.

1.3.1 Reflectance techniques

1.3.1.1 Reflectometry

When polarised light is reflected at an interface close to the Brewster angle its polarisation is sensitive to the adsorption of protein. In a measuring instrument, the reflected beam is split into parallel (p) and perpendicular (s) components by a beam splitter. Both components of the reflected light are detected by photodiodes to produce a ratio of intensities, $S_t = I_p/I_s$. Following the analysis of Buijs et al., (1996), the adsorbed amount (Γ) can be calculated by

$$\Gamma_t = Q\frac{\Delta S}{S_0} \qquad (1.1)$$

where S_0 is the initial ratio of intensities on a bare surface, ΔS is S_t-S_0, and Q is the calibration factor. Q is a complicated factor, related to parameters such as the thickness and refractive index of the layers used. For example, Buijs et al (1996) used a silicon slide and calibrated the system with a thin silica wafer of known thickness and refractive index.

This technique uses inexpensive equipment to obtain data rapidly and therefore has the ability to measure kinetic parameters. However, the difficulty in determining the Q-factor and the amount of calibration required may limit its use where absolute values of adsorbed amounts are required. In addition, the measurements are performed through the sample solution and therefore the sample must be transparent.

1.3.1.2 Ellipsometry

Traditionally this technique is used for films of greater than 100 nm. In ellipsometry the change in the state of polarisation of light caused by reflection from a planar surface is measured to give information about deposited, transparent films. The polarisation of the incident beam is characterised by the ratio of amplitudes (A_i) and the difference in phases (D), between parallel and perpendicular reflected components. The change in these parameters upon reflection resulting from a change in refractive index(n_f) or thickness (d_f) can be determined. (Tronin, 1994. Stenberg and Nygren, 1982. Nygren, 1993)

For very thin films such as protein monolayers it is difficult to return both the refractive index and film thickness. Further limitations are: that the surface must be reflective, which restricts the surface choice to metals or silicon; both the incident and reflected light must pass through solution; and that the equations used for iteration assume that the surface of the film is smooth and that it has a constant refractive index throughout.

1.3.1.3 Reflection interference spectroscopy

A change in the interference spectrum caused by reflections at the interface of a thin substrate layer is measured (Duschl and Hall, 1991). The intensity of interfering light at the interfaces is given by

$$I = I_1 + I_2 + 2\sqrt{I_1 I_2 \cos\left(\frac{2\pi\Delta}{\lambda}\right)} \qquad (1.2)$$

where I_1 and I_2 are the intensity of the reflected beam, Δ the film thickness, and λ the incident light wavelength. The reflected intensity plotted against λ gives the spectral interferogram from which the optical thickness can be calculated. Measurable interference requires a thickness of 0.5-10μm. As the thickness of biological layers is

around 5-10 nm an interference layer with a thickness of around 2μm with a refractive index similar to the biological layer is used.

The use of this interference layer may be regarded as a disadvantage of this technique. The absolute thickness of the analyte layer under investigation can not be accurately calculated because of the assumption inherent in the calculation that both the interference layer and the protein layer have the same refractive index.

Changes in layer thickness can be monitored rapidly. Reflection interference spectroscopy has been used to characterise antigen-antibody (Brecht et al 1992) and DNA-intercalators (Piehler et al, 1997) interactions, gas sensing and the detection of hydrocarbons in water (Gauglitz et al, 1993), and the interaction of transport proteins with bilayers (Striebel et al, 1994)

1.3.2 Evanescent wave optical biosensors

These transduction methods are based upon an optical property best understood in its use for internal reflectance spectroscopy (IRS) (Place et al., 1985). Light passes through a high (refractive) index (n_1) medium to an interface of a lower refractive index (n_2) medium (Harrick. 1967). Above a certain angle, termed the critical angle θ_c , the light is totally internally reflected (TIR). An electromagnetic field called the evanescent wave is generated in the lower index medium perpendicular to the surface (Sutherland and Dahne. 1987). The penetration depth (d_p) of the evanescent wave is the distance at which the field strength has fallen to $1/e^{th}$ value at the interface, and depends upon various parameters as shown in equation 1.3.

$$d_p = \left(\frac{\lambda}{4\pi}\right)\left(n_1^2 Sin^2\theta - n_2^2\right)^{-\frac{1}{2}} \qquad (1.3)$$

λ is the wavelength of light, n_1 and n_2 the refractive index values of the high and lower, sample index layers respectively. θ is the angle of reflection of the light.

The evanescent wave decays exponentially from the surface (figure 1.2) and is sensitive to changes in refractive index at or near the TIR interface. Thus any molecules binding to this surface will cause a change in nature of the reflected light.

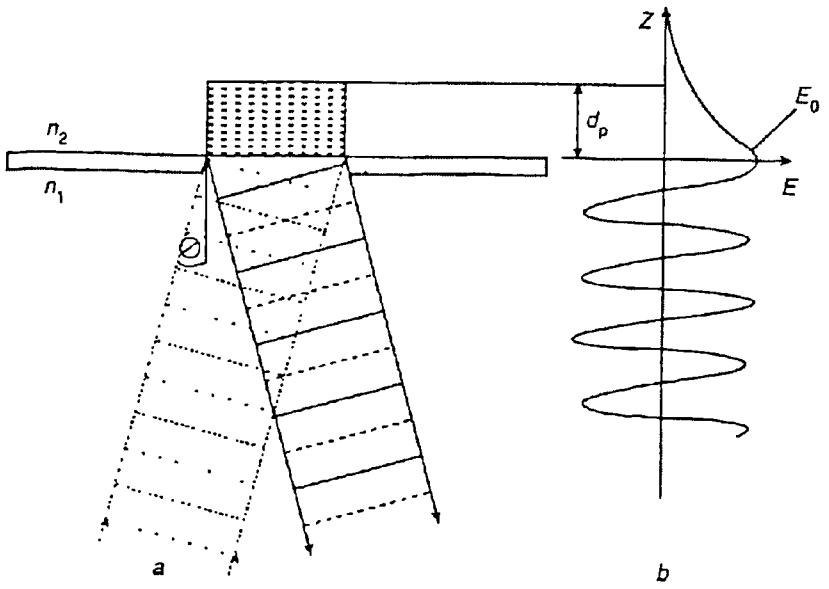

Figure 1.2: *The generation of an evanescent wave at the interface between the transducer and the sample medium. The evanescent wave is produced providing that the refractive index $n_1 > n_2$ and θ is larger than the critical angle θ_c. b shows the electric field amplitude, E, together with d_p, the penetration depth of the evanescent wave, with Z being the distance from the surface interface.*

The theory of IRS forms the basis of several differing sensing devices and these will be described briefly.

1.3.2.1 Surface plasmon resonance.

At visible wavelengths and most angles a metal acts as a mirror reflecting most of the incident light. However, at specific wavelengths or angles energy is transferred to electrons on the surface of the metal. This transfer of energy to the electrons, termed surface plasmons, occurs only when the quantum energy of the photon exactly matches that of the surface plasmons. Excitation of the plasmons causes almost all of the incident light to be absorbed resulting in a dip in the intensity of the reflected light

(Liedberg et al., 1983). The wavelength (or angle) at which this occurs, the resonance wavelength (or angle) can be determined from the intensity drop of the reflected light. The surface plasmons on the metal surface are charged clouds of electrons but they behave as single charged particles. Oscillation of a proportion of their energy is in the plane of the metal causing an evanescent wave to be generated.

SPR has been commercialised by the BIAcore instrument (BIAcore, Sweden). The reflectivity of the TM polarised light is monitored as a function of incident angle, at a constant wavelength of light. The change in resonant angle measured as a 'dip' in reflectance (Lofas et al, 1991). The configuration of the BIAcore instrument is shown in figure 1.3. The dark bounds represent the angles at which resonance was induced with the corresponding drop in reflectance. For example band 1 could represent the surface prior to protein adsorption while band 2 shows the angle after adsorption.

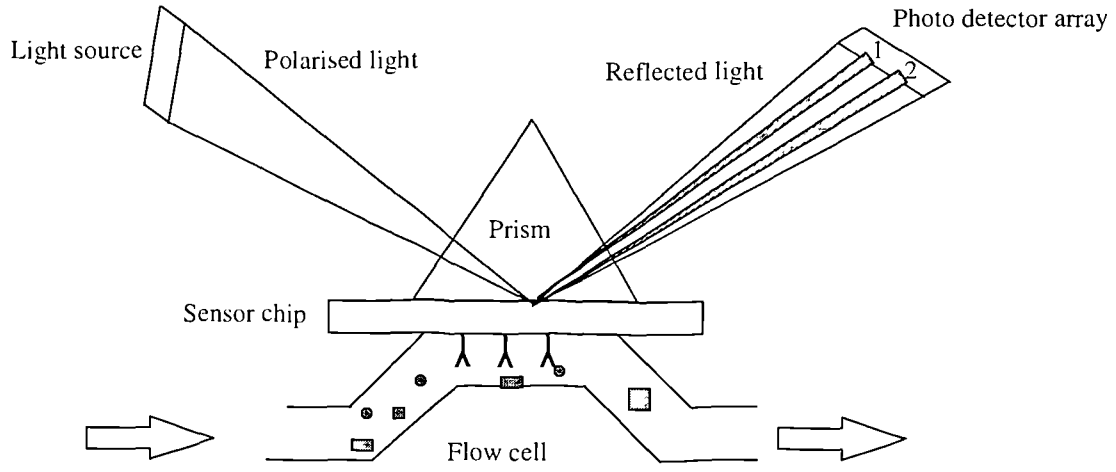

Figure 1.3: *The configuration of the BIAcore SPR biosensor. Polarised light strikes the sensor chip at a variety of angles and a dip in intensity of the reflected light is observed. The angle of incidence at which this dip occurs is dependant upon the refractive index of the material within the evanescent field.*

1.3.2.2 Waveguides

At discreet angles of incidence light is coupled into a high refractive index material sandwiched between two low RI media and propagates by total internal reflection within the high RI layer. This waveguide structure is shown in figure 1.4. If this waveguide is sufficiently thin, propagation of the light will occur at one angle only and the waveguide is termed a monomode waveguide.

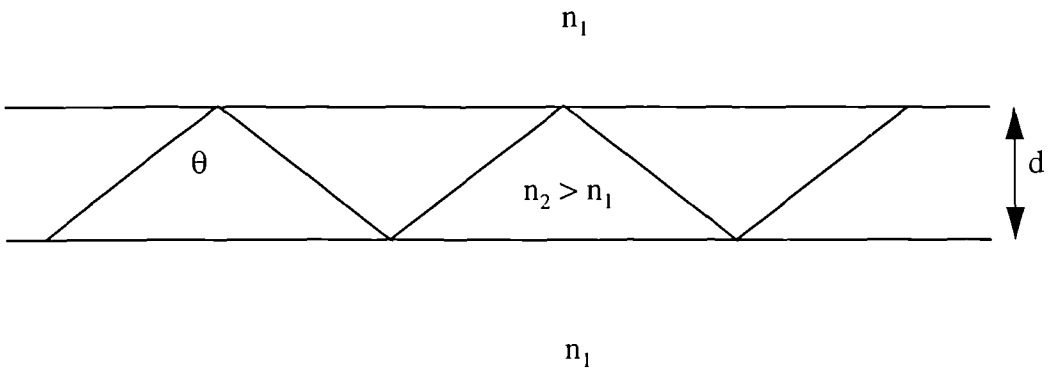

Figure 1.4: *Waveguide structure in which a high refractive index material,n_2, with a thickness of d is sandwiched between two low RI media. Light is propagated along the waveguide when coupled at a specific angle, θ.*

Light can be coupled into waveguides by a number of methods. In the end-fire technique, the waveguide is interrogated by light, over a range of angles, at one of its ends by means of a lens. At one of the angles of the incident light, light will propagate down the waveguide (figure 1.5a). Prism coupling involves a high index prism close to the waveguide surface. A beam of light is totally reflected of the bottom face of the prism and provided that the high index waveguide layer is close enough the reflection is frustrated and some of the light tunnels through and propagates down the waveguide (figure 1.5b). Gratings of the correct periodicity can also be used for coupling. An external beam of light with a specific wavelength will be coupled into the waveguide at the correct angle of incidence (figure 1.5c and section 1.3.2.2.4).

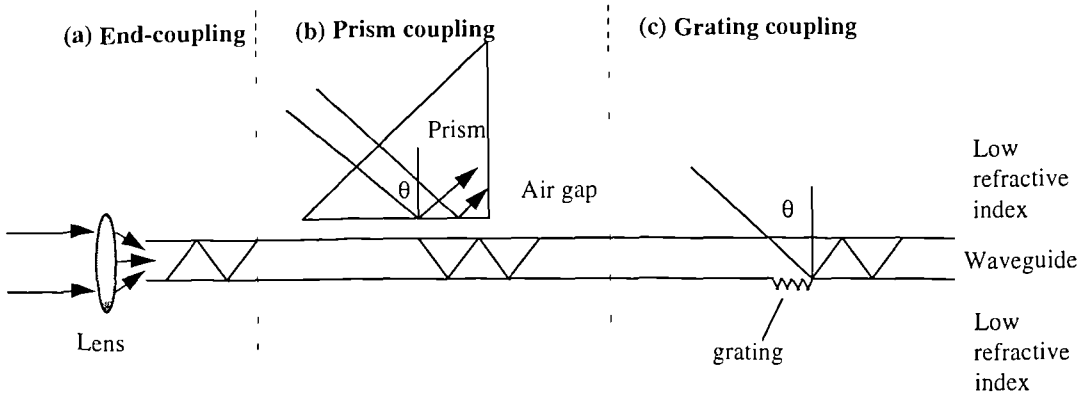

Figure 1.5: *Coupling into waveguides. (a) End-coupling: Polarised light is directed into the end of a waveguide by means of a lens. (b) Prism coupling: Light, directed on to a prism at an angle θ, undergoes TIR at the bottom edge of the prism. The air gap is sufficiently small to allow light to tunnel into the waveguide. (c) Grating coupling: Light strikes the grating at an angle θ and is propagated along the waveguide.*

1.3.2.2.1 Total internal reflection fluorescence

An evanescent wave of the appropriate wavelength will excite fluorescent molecules. The emitted light detected is a function of: the quantum yield; the extinction coefficient; the concentration of the fluorophore; and a constant incorporating instrumental factors. The nature of the evanescent wave means that fluorescent molecules in solution may also be excited in addition to those binding to the surface.

Investigating the competitive adsorption of proteins onto glass slides allowed Lassen and Malmsten, (1996) to reduce the contribution from the bulk fluorescent to approximately 10% of the total fluorescence. This was achieved by limiting the concentration of the labelled proteins and the amount of protein adsorbed to slides. The same authors also investigated protein adsorption onto polymers of different charges and hydrophobicities (Lassen and Malmsten, 1997). Other examples, using prism coupling, include the measurement of tracer diffusion through polymer films (Santore and Kaufman, 1996), and the investigation into the effects of shear rate, pH, and ionic strength upon mass transport to a surface (Cha and Beissinger, 1996).

In addition to the prism 'waveguide', both planar waveguides and optical fibres have been used. The fibre optic system is the most sensitive configuration due to a superior collection efficiency defined as the ratio between the intensities of the induced evanescent and excitation fields (Domenici et al., 1995) and consists of a high refractive index core surrounded by a lower refractive index outer layer or cladding. Light directed down an optical fibre undergoes TIR and an evanescent wave is generated. In order to monitor interactions a small piece of the cladding is removed to expose the core to which ligand is attached. Binding of analyte to the ligand occurs within the evanescent field at the uncladded region. The reaction is monitored by measuring the reflected light signal when it has returned into the cladded region. The core can be straight (Domenici et al., 1995) or tapered (Feldman et al., 1995) with the latter giving an enhanced evanescent field and thus fluorescent signal. A tapered optical fibre has shown a sensitivity for an antigen of 4 pM (Feldman et al., 1995) while using a sandwich format 60 nM of IgG was detected using a tapered optical fibre loop immunosensor (Hale et al, 1996).

Femtomolar (10^{-15} M) sensitivity has been reported using a dual channel etched silicon nitride thin-film integrated optical waveguide. A thin layer of Si_2O_3N on silica is etched to produce two parallel channels. Using a prism to couple the light, the device is placed in a flow cell. The bioselective layer is immobilised to one channel only and a red emitting label used to detect binding (Plowman et al., 1996). Given the nature of the evanescent field, fluorescent labelling is not required as the change in reflected light is also sensitive to refractive index changes. However, the use of fluorescent labels can increase the sensitivity of the techniques.

1.3.2.2.2 Attenuated Total Reflectance (ATR).

Energy absorbed from the evanescent wave attenuates the intensity of the internally reflected light beam. The surface of the low index material is coated with a film which absorbs light or simply allows it to leak away from the waveguide. Incident light is directed onto this film and the attenuated light intensity measured as a function of the incident wavelength. There have been few reports on this technique for biosensing although ATR has been used to study immunological reactions (Ockman, 1978. Arwin, 1985).

1.3.2.2.3 Interferometry

The difference interferometer uses polarised light focused onto a TiO_2-SiO_2 grating in order to propagate both the TE and TM components along a waveguide. The sensor responds to changes in the refractive index within the evanescent field. The molecular surface concentration on the surface is obtained by monitoring the relative phase difference, $\Delta\phi$, between the TE and TM components as shown in figure 1.6 (Fattinger et al., 1993).

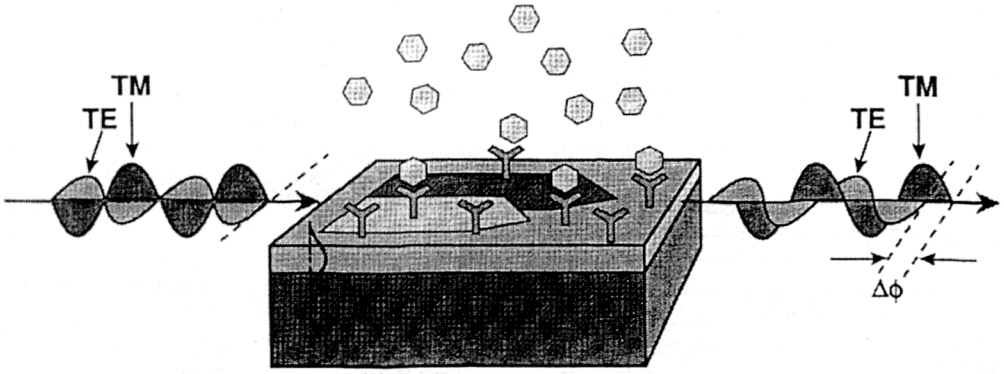

Figure 1.6: *The difference interferometer. Changes in the relative phase $\Delta\phi$ are monitored giving a measure of the molecular coverage. TE: Transverse electronic; TM: transverse magnetic*

$\Delta\phi$ is determined by dividing the emerging beam into two equal intensity beams. One of these beams undergoes an additional $\pi/2$ phase change between the TE and TM components. Interference between the TE and TM components of each beam is caused by a prism tilted to 45°. The intensities of the light from the prisms allows $\Delta\phi$ to be calculated. The surface coverage can be determined by the use of a conversion factor ,z, such that

$$\Gamma = z.\frac{\Delta\phi(t)}{2\pi} \qquad (1.4)$$

where z contains information about the concentration dependence of the RI of protein solutions and the interaction length, the distance over which the TE and TM components interact with the sample. (Stamm and Lukosz., 1996).

The difference interferometer has been used to monitor avidin adsorption to its surface and subsequent biotinylated BSA binding (Stamm and Lukosz., 1993). Interactions between adsorbed anti-human IgG with human IgG, and hepatitis β surface antigen (HBsAg) with anti-HBsAg using protein A immobilised to the waveguide have also been investigated (Schlatter et al., 1993). It has been recently reported that 0.3 nM rabbit IgG was detected by immobilising avidin onto the waveguide and binding biotinylated goat anti-rabbit IgG (Stamm and Lukosz, 1996). Interferometry has been shown to be more sensitive than either SPR or grating couplers (Huber et al., 1992).

1.3.2.2.4 Integrated optical grating couplers.

Adsorption of molecules to a waveguide surface changes its thickness. This change in thickness causes a change in the effective refractive index of the TE and TM components propagating within the waveguide, ΔN_{TE} and ΔN_{TM} respectively. The effective index can be monitored by either measuring the input-coupling angle or the output-coupling angle as illustrated in figure 1.7. The input coupler measures the incident laser angle at which light propagates along the waveguide and is detected at the end of the waveguide. The output coupler differs in that laser light is directed along the waveguide by end-coupling and it is the angle at which light is coupled out of the waveguide that is monitored (Lukosz ,1991).

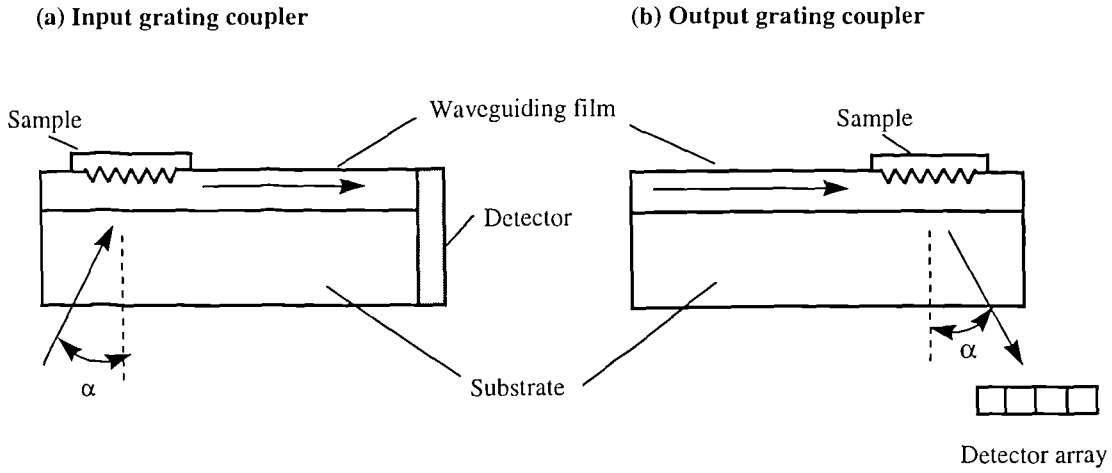

Figure 1.7: *Input/output grating couplers (a) Input coupling: Light is directed onto the grating and coupled into the waveguide before being detected at the end of the waveguide. The in-coupling angle is measured. (b) Output coupling: Light is end-coupled into the waveguide and coupled out by a grating. The out-coupling angle is measured.*

The effective refractive index of both polarisations can be determined from either the input or output coupling angle, α, of each polarisation

$$N = n_{air} \sin\alpha + l\frac{\lambda}{\Lambda} \tag{1.5}$$

where n_{air} is the refractive index of air, λ the wavelength, Λ the grating period, and l the diffraction order. The index change of both polarisations, ΔN_{TE} and ΔN_{TM} are determined by the change, $\Delta\alpha$, in angle α.

$$\Delta N = n_{air}\Delta(\sin\alpha) \tag{1.6}$$

The determination of ΔN_{TE} and ΔN_{TM} allows the calculation of the refractive index (n_F) and thickness (d_F) of the adsorbed layer by solving the mode equations for a single layer waveguide (Tiefenthaler and Lukosz, 1989), which in turn allows the surface coverage (Γ) to be determined

$$\Gamma = \frac{(n_F - n_C)d_F}{(dn/dc)} \tag{1.7}$$

where n_c is the refractive index of the bulk solution. In general the coefficient dn/dc for globular proteins is approximately 0.185 cm^3/g and this is probably sufficient to determine the surface coverage for such proteins. However, other molecules may have highly different values and in this instances the correct value should be sought.

Input grating couplers have been used to investigate the binding of rabbit anti- human IgG to immobilised human IgG down to a concentration of 1nM (Nellen and Lukosz, 1990). The input coupling method has now been used in a commercial sensor (BIOS-1 Artificial Sensing Instruments, Switzerland) developed by Tiefenthaler (Tiefenthaler, 1993). Bernard and Bosshard (1995) have used the sensor to monitor protein-protein interactions, Kurrat et al (1997) have described the adsorption of HSA and BSA onto the waveguide, and Polzius et al (1993) used the instrument to monitor monoclonal antibody production in animal cell culture on-line. In a similar manner output grating couplers have been used to investigate adsorption and binding interactions (Clerc and Lukosz, 1993,1994,1997 and Lukosz et al 1991a and 1991b).

A modified input coupler has been proposed by Brandenburg and Gombert (1993) in which, instead of a discrete angle of incidence illuminating the grating at one time, a range of angles (i.e. a wedge beam) are used. The coupling angle found from the drop in intensity of the reflected light is observed as a dark line on a CCD array.

Alternatively, both the input and output grating couplers can be used together. The bidiffraction grating coupler has two gratings of different periodicities etched onto a TiO_2 waveguide (Brecht et al., 1992 Fattinger, 1993). The advantage of this arrangement is that the outcoupled beam from the output grating propagates in a direction different from that outcoupled by the grating used for incoupling. This has the effect of spatially separating the two outcoupled beams reducing stray light and improving the signal to noise ratio.

1.3.2.2.5 The Critical Sensor

This uses the difference in the effective refractive index (N_{eff}) between areas on a waveguide which are shielded and unshielded. Upon adsorption of protein to the unshielded area this difference will change as the N_{eff} of the shielded area will remain constant (Schipper et al., 1995). The critical sensor directs the divergent light beam, striking the interface between the shielded and unshielded area, in such a way that half is reflected (R) and half is transmitted (T) as shown in figure 1.8. A change in the critical angle causes a change in the difference between R and T (Schipper et al., 1996,1995).

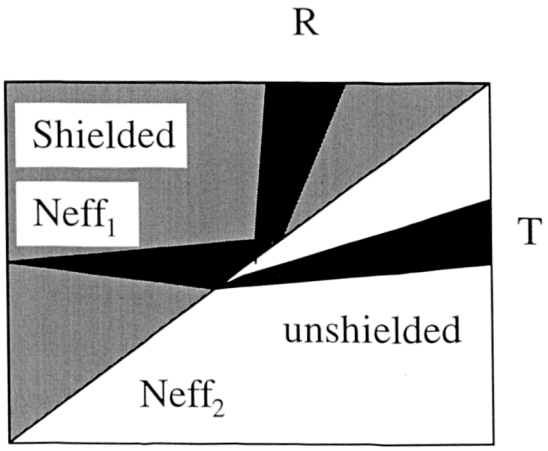

Figure 1.8: *The critical sensor: The difference in the critical angle is measured by monitoring the difference in intensities between the reflected (R) and transmitted (T) light intensities.*

The critical sensor has been shown to be capable of monitoring immunological reactions by detecting the binding of concentrations of anti-HSA monoclonal antibody down to around 5nM. (Schipper et al., 1995) to adsorbed HSA. This technique has the advantage of simplicity and ease of use but it is at present unable to detect low concentrations of small molecules without the use of a competition format.

1.3.2.2.6 IAsys Resonant Mirror instrument.

The construction of this device is shown in figure 1.9 and consists of a high refractive index dielectric resonant layer such as titania with a thickness of around 100 nm. Separating this layer from a prism is a thin (1μm) , low refractive index layer such as silica which is sufficiently thin to allow light to couple into the resonant layer. Polarised laser light at 670 nm is scanned in a 10° arc across the prism by means of a rocking laser. At a specific angle, the resonant angle ϕ, light couples into the high index layer and propagates along this layer for about 1mm before coupling out.

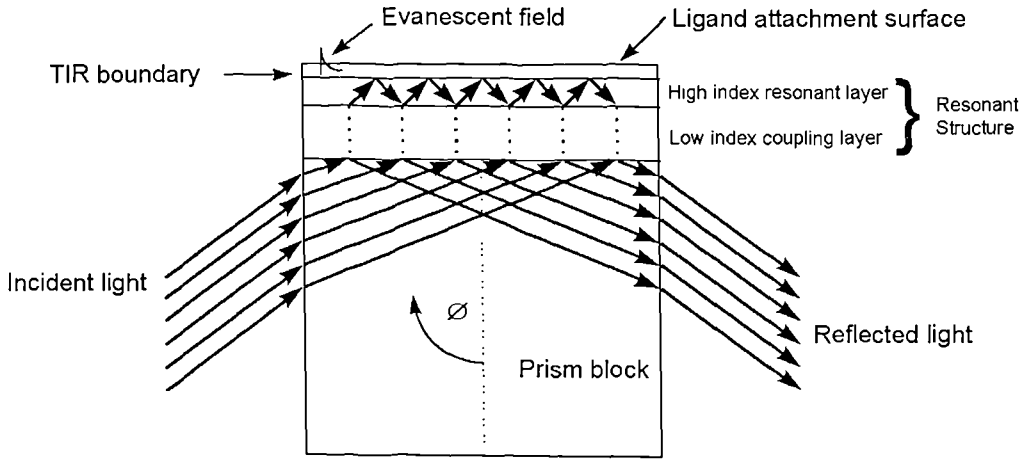

Figure 1.9: *The structure of the Resonant Mirror:*

In common with waveguides both the TE and TM polarisations are propagated. However, in contrast to SPR there is no dip in intensity of reflected light at the resonance angle. There is however, a change in phase of the reflected light upon resonance (Cush et al., 1993). The phase undergoes at 2π change on passing through resonance and is π out of phase at the resonance peak (figure 1.10).

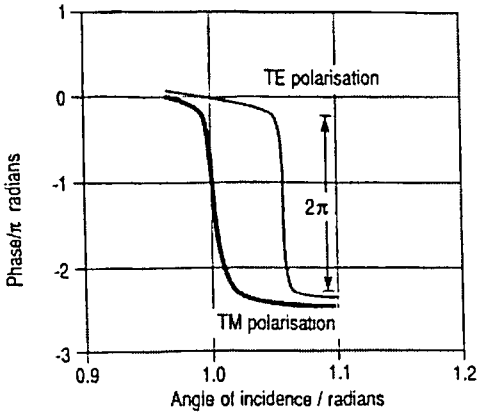

Fig. 2. Phase of light reflected from Resonant Mirror

Figure 1.10: *Phase of light reflected from the resonant mirror. At a specific angle of incidence, the resonant angle, an evanescent* field *is generated and a* π *change in phase is observed. There is a total of* 2π *change is phase.*

This change in phase in the reflected light is monitored by passing both the TE and TM components through an analyser at 45° to the polarisation axis. The resulting output gives zero signal away from resonance and sharp peaks of light at resonance. In this manner the two components can act as references to each other. In practice it is the TE component that is monitored as is more sensitive to refractive index changes and produces a sharper resonant peak. The TM component acts as the reference. Monitoring the intensity peak allows the change in resonant angle to be monitored as a function of time and therefore respond to changes in refractive index on the sensing surface (Buckle et al., 1993).

1.4 Attachment of biomolecules to the sensor surface

In order to monitor specific bio-macromolecular interactions it is necessary to attach one of the partners, the ligand, to the sensor surface. Biosensor responses are proportional to the volume of protein which itself is proportional to cube-root of the molecular weight and occur when a water (or salt) molecule is displaced by the macromolecule of higher refractive index. Direct adsorption of the ligand onto sensor surfaces is unsuitable in most cases despite being a rapid and convenient method. Adsorption of proteins onto solid surfaces often results in a low specific activity and

hence sensitivity due to the inaccessible orientation of the recognition site towards the surface (Ulbrich et al, 1991); denaturation of the ligand can also occur (Butler et al., 1992). The adsorbed ligand may 'leach' from the surface resulting in a drop in sensitivity with time (Niveleau et al., 1993. Underwood and Steele, 1991). Non-specific binding to surfaces is also appreciable although this can be reduced by incubating the surface with a non-specific protein prior to ligate binding (Bhatia et al., 1989). This may however further bury the ligand resulting in a drop in specific activity.

Covalent attachment of the ligand is therefore preferable in order to eliminate the leaching while improving the biological activity. Gold surfaces used for SPR devices utilise the fact that aliphatic thiols form closely packed and covalently attached monolayers (Williams, 1988) which can be used to attach biomolecules. Inorganic dielectric layers such as silica can be silanised in order to introduce different chemical moieties such as amino, epoxy, diol, thiol, aldehyde or carboxylate. (Borchert et al., 1982. Ernst-Cabrera and Wilchek, 1987. Bhatia et al., 1989). It has been shown that attachment via silanes provide greater stability to detergents and low pH than adsorption (Jönsson et al., 1985).

Despite this covalent coupling the ligand is still anchored close to the surface and susceptible to denaturation and masking of biological activity. Non-specific binding may also be high but can be reduced by the use of detergents, or varying the pH or ionic strength (Williams and Blanch. 1994). An alternative approach is to use a hydrogel to which the ligand can be attached (Lofas and Johnsson., 1990). A hydrogel is a three-dimensional water-binding polymeric structure containing a large amount of water (typically more than 95% by weight). The hydrogel used in the IAsys and BIAcore instruments is carboxymethylated dextran (CMD). This is coupled to the sensor surface via either silane chemistry for dielectric material or thiol/epichlorohydrin chemistry for SPR. The CMD matrix extends 190nm from the surface in buffers below physiological concentration and to 140nm above physiological (Wigren et al., 1995). This matrix has the advantages of :-

(a) The gel being negatively charged allows concentration of positively charged ligand molecules (Johnsson et al., 1991). A positively charged ligand can be achieved by using an immobilisation buffer with a pH below the pI of the ligand and a low ionic strength.

(b) The ligand is 'held' away from the surface of the sensor surface in a hydrophilic environment and as such the immobilised ligand retains a greater activity (Lofas et al., 1993). Furthermore binding to the ligand within the flexible CMD may be less influenced by steric hindrance.

(c) The CMD matrix extends away from the sensor surface by a value of 100 nm and therefore gives a larger attachment area than planar surfaces. As a consequence responses are often larger on CMD than planar surfaces although given the exponential decay of the evanescent field from the surface, reactions at the sensor surface will result in larger responses than those further from the sensor surface such as those within the dextran matrix.

(d) Allowing covalent attachment of the ligand through the carboxyl groups on the CMD (Lofas and Johnsson., 1990). The most common method is primarily through lysine groups on the ligand using EDC/NHS chemistry. There are however other immobilisation chemistries available (O'Shannessy et al., 1992).

(e) Low non-specific binding (Lofas and Johnsson., 1990)

A schematic representation of the CMD matrix after ligand immobilisation is shown in figure 1.11 showing immobilised ligand with multiple attachments to the matrix together with CMD-CMD and CMD-ligand-CMD linkages. The energy profile of the evanescent field is also shown demonstrated the drop in intensity with increasing distance from the surface.

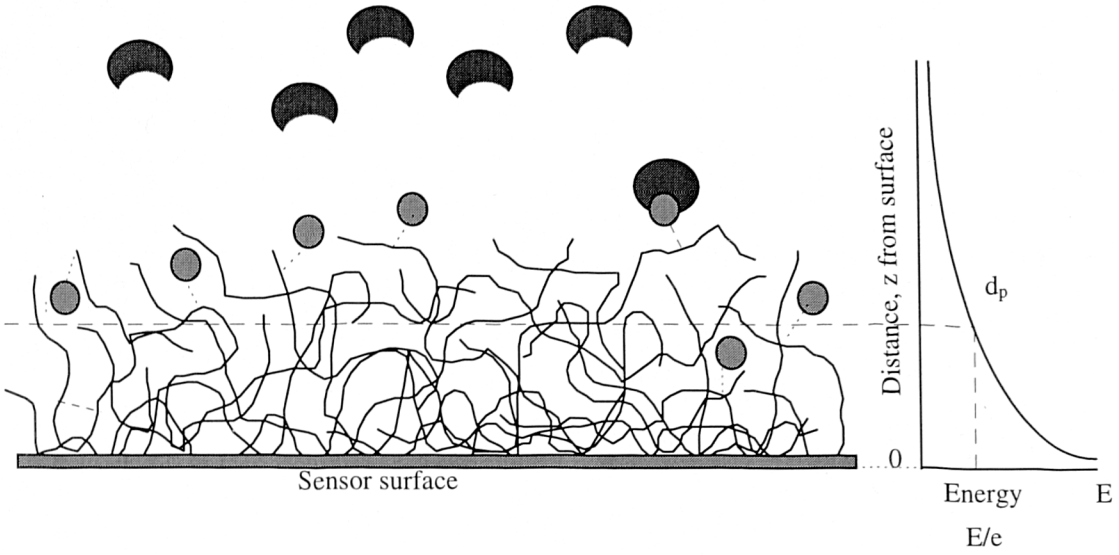

Figure 1.11: *Schematic representation of the CMD matrix after ligand immobilisation illustrating CMD-ligand, CMD-ligand-CMD and CMD-CMD linkages.* ● *represents the ligand and* ◖ *the ligate. ---- the linkages*

The use of the carboxymethyl dextran gel may however prevent large molecules from entering the evanescent field. Watts et al, (1994) recommended that planar surfaces be used for interactions involving cells and biomolecules above a molecular weight of 1x 10^6 Da. However, interactions between large molecules on CMD have been observed. Tobacco Mosaic virus (M_r 40MDa) has been immobilised to CMD and the binding of specific antibodies monitored. (Pellequer and Van Regenmortel, 1993).

Coupling through lysine groups introduces the possibility of random coupling if the ligand has more than one available lysine group and hence different sub-populations of binding sites with different accessibilities and reactivities. Site-specific immobilisation can eliminate these sub-populations by attaching through groups away from the active site. Depending upon the single chemical group present, the coupling used can be thiol-disulphide exchange (Johnsson et al., 1995), aldehyde and sulphydryl coupling (Lofas et al., 1995), hydrazide coupling (O'Shannessy et al., 1992), chelate linkages of oligohistidine tags on bacterially expressed proteins

(O'Shannessy et al., 1992. Gershon and Khilke., 1995) or via photoactivatable reagents (Gao et al., 1995). Orientated immobilisation has be achieved by the use of a sandwich format in which an antibody able to specifically bind one of the biomolecules is immobilised onto the sensor surface (Karlsson et al., 1991). Rabbit anti-mouse Fc can be used to capture murine monoclonal antibodies while protein A, G or L can also be used. Streptavidin has been used to capture biotinylated protein (Johnsson et al., 1995) and is the preferred route for DNA and RNA immobilisation (Jost et al., 1991. Buckle et al 1996).

Chapter 2.

Biospecific interactions

2.1 Introduction.

The rate of a chemical reaction is governed by both the physical transport of the reactants together and their specific binding. The specific binding of two species can be described by equation 2.1

$$G + L \underset{k_{diss}}{\overset{k_{ass}}{\rightleftharpoons}} GL \qquad (2.1)$$

where k_{ass} and k_{diss} are the association and dissociation rate constants respectively.

For a biochemical interaction the situation is more complicated. The larger size of the biochemical reactants influences both the physical transport and the specific binding. The larger size and hence smaller diffusion coefficients, means that the diffusion of the reactants together becomes important. The translational diffusional coefficient (D_A) is defined by the Stokes-Einstein relationship

$$D_A = \frac{k_B T}{6\pi \eta r_A} \qquad (2.2)$$

where η is the solvent viscosity, k_B the Boltzmann constant, r_A the radius of the reactant and T the absolute temperature.

The maximum association rate constant in solution is one in which the binding rate is not limited by the mass transport of the two reactants together. The diffusional association rate (k_a) defined as the rate at which the two spherical species come into contact is given by

$$k_a = 4\pi(D_G + D_L)(r_G + r_L) \qquad (2.3)$$

where D_G and D_L are the diffusion coefficients of G and L having interaction radii of r_G and r_L respectively. Provided that the hydrodynamic radii (r'_G and r'_L) are equal to the interaction radii and that the two interacting molecules are equal in size then a

diffusion limited collision rate of around 10^9 $M^{-1}s^{-1}$ is calculated (Berg and Von Hippel, 1985).

In addition to translational diffusion, rotational diffusion also occurs and the rotational diffusional constant ($D_{rot.}$) can be calculated from the hydrated volume of the reactant (V_h) , assuming a spherical shape.

$$D_{rot} = \frac{k_B T}{6\pi V_h r_A} \qquad (2.4)$$

The biochemical association rate is thought to occur via the diffusion controlled formation of an unstable encounter complex (Creighton, 1993), followed by its rearrangement to the final complex as shown in equation 2.5 below

$$G + L \underset{k_{-1}}{\overset{k_1}{\rightleftharpoons}} \{G\bullet\bullet\bullet\bullet\bullet\bullet L\} \underset{k_{-2}}{\overset{k_2}{\rightleftharpoons}} GL \qquad (2.5)$$

These encounter complexes are not observed and their structures remain unknown. The binding rate is still proportional to the free concentration of reactant but is slower than the diffusion controlled k_1. This is due to the encounter complex being unstable and dissociating more rapidly than it completes binding.

The encounter complex is formed when the two reactants diffuse sufficiently close to one another to be mutually influenced by one other (Northrup and Erickson, 1992). Charges within both reactants cause the molecules to attract each other and the reactants are brought together. The reactive sites within each molecule often make up only a small fraction of the surface area available. The reactants continue to approach each other and charged groups/dipole moments guide the molecules to complementary sites on each reactant. (Novotny and Sharp., 1992, Honig and Nicholls., 1995). Long range electrostatic forces, which decay as $1/r^2$ in a vacuum, are reduced some 80-fold in water.

For example, Kozack and Subramaniam (1993) have investigated electrostatic interactions and their effect upon diffusional motion. It was found that point mutations on charged residues near the binding site exerted the greatest influence on steering the protein into a favourable conformation for binding. Further evidence for the influence of electrostatic influences comes from the asymmetric charge on horse cytochrome c. The charge distribution in the cytochrome c indicates a large dipole moment of 300 Debye units with the dipole axis passing through what is thought to be the binding site. This allows it and its redox partners (Cytochrome c oxidase/reductase) to become orientated favourably and mutually by their electric fields (Koppenol and Margoliash., 1982). In addition the association rate constant has been shown to be highly dependent upon ionic strength (I) and thus electrostatic interactions are important in orientation of the dipole. (Van Leeuwen., 1983).

The binding rate can be reduced by polar water molecule being attracted to, and orientated around, the charged groups so that the dipoles interact with the solute thus reducing the steering ability of the groups (Sharp and Honig, 1990). This water must be removed upon complex formation and the electrostatic energy is increased. This desolvation process may oppose the formation of the complex and so lowering the association rate constant.

In addition to the electrosteering, the matching of topography of the two reactant surfaces is important (MacCullum et al., 1996). For example proteins tend to bind on planar binding sites, while peptides generally bind to ridge type sites, and smaller ligands to cavities. Most protein binding sites are concave with high curvatures (i.e. pockets) for small ligands but with low curvatures for antigens. The reason for the concave shape is thought to be three fold. Firstly, the curvature can cause diffusion away from the cavity to be lower than from flat surfaces or through solvents (Cram., 1983). Secondly, electrostatic fields are enhanced and focused in cavities whereas solvents quench these on flat or convex protein surfaces (Klapper et al., 1986). Finally, hydrophobicity of the surface is a function of its sites curvature relative to that of the water molecule thus reducing the quenching of the charged groups by the polar water molecule (Nicholls et al.,1991).

Other interactions between the two molecules also govern the orientation of the reactants in the encounter complex (Náray-Szabó., 1993). Short range forces also operate to bind the two molecules together. Van der Waals contacts (Ysern et al., 1994), H-bonds and salt bridges (Chacko et al., 1995), and interfacial solvent networks (McPhalen and James., 1998) also contribute to the overall configuration of reactants. Van der Waals and hydrophobic forces operate over 2 - 4 Å and are symmetrical in nature, hydrogen bonds are directional and require orientation of the relevant groups.

The final complex is formed by solvent exclusion (Hydrophobic effect) and conformational changes between the two reactants (Colman et al., 1987; Bhat et al., 1990,1994). The hydrophobic effect involves the removal of water from the active site in order for the interactants to become closer. The structure of the protein domain does not change substantially and any changes tend to be small and often within the error of crystallographic structures. Conformational changes, such as movements of rigid domains or subunits also occur, in order to ensure a better 'fit' between the two molecules. Ligands may bind between two domains which then engulf the ligand. This may maximise the interaction and reduce solvent interactions.

2.2 Methods available for kinetic and equilibrium analysis.

From equation 2.1 the rate of dissociation is related to the concentration of complex and the rate of association is related to the concentration of both G and L as shown in equation 2.6

$$[G][L]k_{ass} = k_{diss}[GL] \qquad (2.6)$$

Many conventional methods rely upon determining the bound and/or free concentration of one of the interacting species at equilibrium, and using this data to construct a Scatchard plot (Scatchard, 1949) from equation 2.7.

$$\frac{[GL]}{[L]} = K_A([G]_{max} - [GL]) \qquad (2.7)$$

Plotting the ratio of bound concentration ([GL]) to free concentration ([L]) against the bound concentration produces a straight line from which the K_A ,the association equilibrium constant (k_{ass}/k_{diss}) can be determined from the slope. $[G]_{max}$ is the capacity of G for L and is determined from the abscissa intercept.

2.2.1 Immunoassays.

These solid phase assays utilise the ease of separation of complexed and uncomplexed biomolecules when one species is attached to the solid phase and usually determines the affinity, not the separate rate constants. The detection of the complexed molecule is often performed using an enzyme label producing a colour when incubated with a suitable substrate (Beatty et al 1987a,b; Fuchs et al. 1995), or is detected by radioactivity with the binding partner in solution being radiolabelled (R.I.A.). However these are solid phase determinations of the overall affinity of the reaction involving a labelled molecule. Competition assays have been developed in order to determine the solution phase affinity of unlabelled molecules such as that of Friguet et al (1985) with later modifications by Stevens (1987) . Here, a premix of the two interacting species is allowed to reach equilibrium. The free concentration of one of the interactants is then determined. A second method involves the determination of the amount of free antigen in the solution phase which will inhibit the binding of a particular concentration of antibody by 50%. (Nieto et al. 1984; Holland and Stewart. 1991). Methods have also been developed to determine the individual rate constants such as the dissociation rate constant (Larvor et al. 1994) but diffusional effects should be taken into account (Nygren et al 1987).

All of these assays involving solid phase attachment rely upon the fact that the signal generated by the binding species, regardless of whether it is absorbance or radioactive counts, is proportional to the bound species. This is invariably not the case due to

heterogeneity of the solid phase reactant (Butler et al, 1992), and steric hindrance (Cowen and Underwood, 1988).

2.2.2 Calorimetry

This involves the measurement of heat changes occurring during a reaction (Janin, 1995; Gomez et al, 1995). There are two main types of instruments exploiting these changes, the differential scanning calorimeter (DSC) and the isothermal titration calorimeter (ITC). The DSC is used mainly for determining ΔH of protein unfolding.

The ITC (Wiseman et al., 1989) allows the determination of ΔH, the association equilibrium constant and the stoichiometry of the reaction in solution by monitoring the heat change when one reactant reacts with another. One of the reactants is placed in a sample cell and, together with a reference cell, is surrounded by an adiabatic jacket. Increasing volumes of the other reactant is added while the cell contents are stirred. A plot of heat change against reactant/reactant ratio is plotted after adjusting the data for heat changes due to dilution. This technique has a maximum K_A value of around 1×10^8 M (Wiseman et al., 1989) given the small changes in temperature at the low concentrations needed to span ten-times above and below the K_A.

2.2.3 Affinity Chromatography

These techniques involve the covalent linkage of a ligand onto a column matrix and its interaction of the reactant in solution as it passes down the column. The concentration of the reactant and its elution volume allows a Scatchard plot to be constructed and the affinity to be determined from linear regression analysis. Alternatively the affinity can be obtained from non-linear regression analysis of the data without linearisation.

There are two main methods for determining the affinity from column elution volumes, zonal (Dunn and Chaiken, 1974) and frontal (Nichol et al,1974). These differ experimentally only in the volume of reactant passed down the column and hence in the calculation stage. The zonal approach involves the addition of a small volume of reactant of a known concentration. This however has the disadvantage of

not accurately determining the concentration in the mobile phases due to continual dilution (Winzor et al 1991). Frontal analysis eliminates this by the addition of sufficient solution to ensure that the elution profile contains a plateau from which the elution volume can be measured.

Chromatography not only allows the affinity between ligand and solute in a 1:1 stoichiometry. Affinities can be calculated from multivalent species (Eilat and Chaiken 1979; Hogg and Winzor, 1985) and from solution reactions in which a competitor binds either to the ligand or the solute thus altering the elution volume compared to the volume in the absence of competitor (Hogg et al, 1991). Dissociation rate constants have also been determined using chromatography (Moore and Walters, 1987, Munro et al 1994).

2.2.4 Fluorescence.

This technique is important in determining the kinetics of molecular binding because of its high sensitivity. In addition, it is capable of making rapid measurements in solution with no requirement to separate the reactants or complex.

Fluorescent molecules absorb electromagnetic radiation at one wavelength and emit it at a longer wavelength. The difference being termed the Stokes shift. During the lifetime of the molecule (a few ns or less) it may transfer some, or all, of its energy resulting in a change in fluorescence which can be used to determine affinities and rate constants (Dandliker and Levison, 1967). The fluorescence of a molecule can either be intrinsic or extrinsic. Intrinsic fluorescence arises from tryptophan residues within the molecule but the fluorescence changes from binding are small and protein dependent resulting in a low sensitivity. Extrinsic fluorescence results from the labelling of a molecule with a fluorophore such as fluorescein isothiocyanate (FITC) or fluorescein maleimide. This labelling increases the fluorescence change and hence sensitivity but the labelling may affect the binding properties under investigation.

Binding often results in a change in fluorescence intensity or a change in its polarisation. Fluorescence quenching due to energy transfer from the fluorophore is often used to monitor interactions at equilibrium or as a function of time. Equilibrium

methods allow the affinity to be calculated from a Scatchard plot. If the reaction is followed with time then association and dissociation rates can be measured from non-linear regression analysis of the data (Voss, 1993). For rapid reactions stop-flow devices have been described in which the reactants are injected into a optical cell rapidly and the change in fluorescence is monitored with mixing occurring within a millisecond.

Fluorescence polarisation measurements are based upon the observation that fluorescent molecules emit light at different planes to that used for excitation due to the molecular rotation that has occurred between excitation and fluorescence (Checovich et al., 1995). The polarisation is proportional to the molecules rotational relaxation time which, provided that the viscosity and temperature are constant, is proportional to the molecular volume. Measurement of the intensity of light emitted in the horizontal (I_{II}) and vertical ($I_{\perp}$) planes can be used to calculate the polarisation value P as

$$P = \frac{I_{II} - I_{\perp}}{I_{II} + I_{\perp}} \qquad (2.8)$$

High polarisation values mean the molecule is large whereas low values mean it is small. Upon binding of another macromolecule to the fluorescently labelled macromolecule there will be an increase in molecular volume and hence polarisation which can be monitored at equilibrium, or as a function of time using stirred or stopped-flow apparatus. Polarisation does however have a molecular weight limit in that large molecules binding of increasingly large molecules will produce decreasing changes in polarisation. At present the limit is around 100.000 Da (Checovich et al., 1995).

Fluorescence as a technique has found many applications in kinetic and equilibrium measurements because of its ability to measure rapid reactions in solution with high sensitivity. However, the requirement to fluorescently label molecules means that the native molecule is no longer the species under investigation. Furthermore,

photobleaching and inner filter effects mean that experiments should be carefully designed.

2.2.5 Other methods

Other techniques used to characterise biomolecular interactions include analytical ultracentrifugation (Day, 1990), nuclear magnetic resonance, capillary electrophoresis, light scattering, equilibrium dialysis and electron spin resonance (Winzor and Sawyer, 1995).

2.3 Evanescent wave optical biosensors for kinetic analysis.

As outlined in chapter 1, evanescent wave biosensors monitor refractive index changes on the sensor surface when a ligate from solution binds to a ligand attached to the sensor surface. There are currently four commercially available instruments for the monitoring of biomolecular interactions all of which use the evanescent wave. Biacore (Biacore, Sweden) and IBIS (Intersens Instruments BV, Holland) instruments are based on the SPR principle, whereas IAsys (Affinity Sensors, UK) is based upon the resonant mirror technique, and BIOS-1 (Artificial Sensing Instruments. Switzerland) uses grating coupling. Despite these differences all four monitor biomolecule interactions at a sensor surface.

The strategy used for the analysis of biomolecular interactions involves four steps: (i) covalent attachment of the ligand to the sensor surface, (ii) binding of the ligate, (iii) replacement of the ligate solution with buffer to initiate dissociation, and (iv) regeneration of the ligand by removal of the ligate. The regeneration step allows multiple ligate binding on one ligand immobilised sensor surface.

The binding and dissociation of the ligate is shown for the IAsys instrument in figure 2.1 and it is these two steps which when analysed define the interaction.

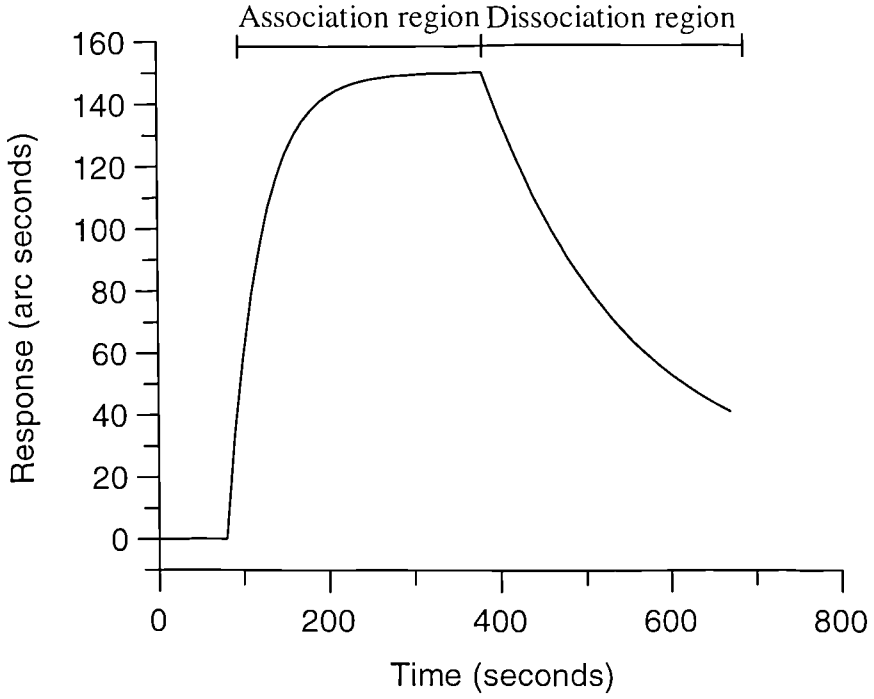

Figure 2.1: *IAsys profile showing the association and dissociation of the ligate.*

From the association data at differing concentrations kinetic and equilibrium constants can be determined, while from the dissociation data the dissociation rate constant can be calculated.

2.3.1 Determination of kinetic constants from biosensor data

Equation 2.1 for the interaction of two molecules is equally valid for the interaction with one of the species immobilised to the sensor surface. From equation 2.1 let G be the immobilised species (ligand), L the species in solution(ligate), and GL the complex with k_{ass}, and k_{diss} the association and dissociation rate constants respectively.

$$\frac{d[GL]}{dt} = k_{ass}[G][L] - k_{diss}[GL] \qquad (2.9)$$

For biosensor experiments the concentration of L in solution is usually in excess over the concentration of immobilised ligand G and is therefore considered constant. Under these pseudo-first order conditions the concentration of free ligand sites decreases with ligate binding, and so the concentration of free ligand sites at time, t is equal to the maximum number of sites ($[G_0]$) minus the sites bound to ligate ($[GL]_t$).

$$\frac{d[GL]}{dt} = k_{ass}([G_0]-[GL]_t)[G]-k_{diss}[GL]_t \qquad (2.10)$$

Complex formation results in a change in response (R_t) which is directly proportional to [GL]. The term [G_0] presenting the starting concentration of ligand sites is likewise proportional to the binding capacity for the ligate as defined by the biosensor R_{max}. Equation 2.10 can therefore be written as

$$\frac{dR_t}{dt} = k_{ass}(R_{max} - R_t)[L]-k_{diss}R_t \qquad (2.11)$$

Multiplying out the brackets and rearranging gives

$$\frac{dR_t}{dt} = k_{ass}R_{max}[L]-R_t(k_{ass}[L]-k_{diss}) \qquad (2.12)$$

Initially extraction of the kinetic constants from such biosensor instruments relied upon linearisation of the data (Karlsson et al ,1991). For each ligate concentration, [L], plotting dR_t/dt against R_t should give a straight line of slope $k_{ass}[L]+k_{diss}$. The slopes corresponding to differing concentrations of L were then plotted against ligate concentration to give a straight line whose slope was equal to the association rate constant and whose intercept was equal to the dissociation rate constant. However, given the short comings of linearisation of data such as the compounding of errors (Leatherbarrow, 1990) and the fact that association data from biosensors often fails to produce a single straight line when linearised, non-linear regression was introduced (O.Shannessy et al., 1993. O.Shannessy 1994) using the equation derived below

Rearranging of equation 2.12 in terms of an integral gives

$$\int \frac{dR_t}{k_{ass}R_{max}[L]-R_t(k_{ass}[L]-k_{diss})} = \int dt \qquad (2.13)$$

Integration produces

$$\frac{\ln(k_{ass}[L]R_{\max} - R_t(k_{ass}[L] - k_{diss}))}{-k_{ass}[L] + k_{diss}} = t + c \qquad (2.14)$$

When t= 0 $R_t = 0$ and therefore

$$c = \frac{\ln(k_{ass}[L]R_{\max})}{-(k_{ass}[L] + k_{diss})} \qquad (2.15)$$

Inserting into equation 2.14

$$\frac{\ln(k_{ass}[L]R_{\max} - R_t(k_{ass}[L] - k_{diss}))}{-k_{ass}[L] + k_{diss}} = t - \frac{\ln(k_{ass}[L]R_{\max})}{k_{ass}[L] + k_{diss}}$$

Rearranging and multiplying by $-k_{ass}[L]+ k_{diss}$

$$\ln\left(\frac{k_{ass}[L]R_{\max} - R_t(k_{ass}[L] + k_{diss})}{k_{ass}[L]R_{\max}}\right) = -(k_{ass}[L] + k_{diss})t$$

Taking exponentials

$$\left(\frac{k_{ass}[L]R_{\max} - R_t(k_{ass}[L] + k_{diss})}{k_{ass}[L]R_{\max}}\right) = e^{-(k_{ass}[L] + k_{diss})t}$$

Multiply by $k_{ass}[L]R_{max}$

$$k_{ass}[L]R_{\max} - R_t(k_{ass}[L] + k_{diss}) = k_{ass}[L]R_{\max}e^{-(k_{ass}[L]+k_{diss})t}$$

$$R_t(k_{ass}[L] + k_{diss}) = k_{ass}[L]R_{\max} - k_{ass}[L]R_{\max}e^{-(k_{ass}[L]+k_{diss})t}$$

$$R_t(k_{ass}[L] + k_{diss}) = k_{ass}[L]R_{\max}(1 - e^{-(k_{ass}[L]+k_{diss})t})$$

$$R_t = \frac{k_{ass}[L]R_{\max}}{k_{ass}[L] + k_{diss}}(1 - e^{-(k_{ass}[L] + k_{diss})t}) \qquad (2.15)$$

The term $\frac{k_{ass}[L]R_{\max}}{k_{ass}[L]+k_{diss}}$ is usually replaced by R_{eq}, the equilibrium response for a given ligate concentration such that equation 2.15 becomes

$$R_t = R_{eq}(1-e^{-(k_{ass}[L]+k_{diss})t}) \tag{2.16}$$

Application of the above equation to binding data at different concentrations allows k_{on} to be determined for each concentration, where $k_{on} = (k_{ass}[L]+k_{diss})$. Thus a plot of k_{on} against ligate concentration, [L], gives a straight line with a slope k_{ass} and an intercept of k_{diss} in the same manner as derived using linearisation of the data. The value of k_{diss} from the intercept is often close to zero with substantial error and so can only be imprecisely measured.

The dissociation rate constant can, however, be determined from the dissociation phase of the ligate interaction when the ligate solution is replaced with buffer. Here the concentration of [L] is taken to be zero and the first order decay in signal is given by:.

$$\frac{dR}{dt} = -k_{diss}R_t \tag{2.17}$$

Integration gives

$$R_t = R_o\, e^{-k_{diss}t} \tag{2.18}$$

Thus fitting the dissociation phase to the above equation permits the dissociation rate constant to be determined provided that the concentration of L is zero i.e. there is no rebinding of the dissociated ligate to the immobilised ligand (chapter 7).

2.3.2 Equilibrium constant determination from biosensor data.

2.3.2.1 Scatchard analysis

The association equilibrium constant, K_A (unit: M^{-1}), according to Langmuir (1918) is the ratio of the association rate constant to the dissociation rate constant. The dissociation equilibrium constant, K_D (unit: M) is a composite of the rate constants:

$$K_A = \frac{k_{ass}}{k_{diss}} = \frac{1}{K_D} \tag{2.19}$$

An alternative method of determining K_D uses the equilibrium responses at differing concentrations of ligate.

At equilibrium there is no net flux of ligate between sensor surface and bulk solution and $\frac{dR}{dt} = 0$ with R_t becoming R_{eq} thus equation 2.12 becomes

$$k_{ass}(R_{max} - R_{eq})[L] - k_{diss}R_{eq} = 0$$

$$k_{ass}(R_{max} - R_{eq})[L] = k_{diss}R_{eq} \tag{2.20}$$

Dividing by k_{diss} [L]

$$K_A R_{max} - K_A R_{eq} = \frac{R_{eq}}{[L]} \tag{2.21}$$

This is equivalent to the Scatchard equation (equation 2.7) and in this case a plot of $\frac{R_{eq}}{[L]}$ against R_{eq} gives a straight line with a slope of $-K_A$.

2.3.2.2 Binding isotherm

It is also possible to plot equilibrium responses against ligate concentration to determine the K_D of the interaction.

Dividing both sides of equation 2.20 by k_{diss} and rearranging gives

$$K_A R_{max}[L] = R_{eq}(1 + K_A[L])$$

Dividing by R_{eq}

$$\frac{K_A R_{max}[L]}{R_{eq}} = 1 + K_A[L]$$

Dividing by $K_A R_{max}[L]$ and taking the reciprocal

$$R_{eq} = \frac{K_A R_{max}[L]}{1 + K_A[L]}$$

Division of the right hand side of the equation by K_A

$$R_{eq} = \frac{R_{max}[L]}{K_D + [L]} \qquad (2.22)$$

Thus from a plot of R_{eq} against [L] the K_D can be found by non-linear regression analysis. A consequence of this equation is that the K_D of the reaction is equal to the concentration of L which gives a R_{eq} of one half of the R_{max} value

2.4 Potential problems of biosensor kinetic techniques

Evanescent wave techniques monitor refractive index changes on sensor surfaces and therefore in order to detect that change any interaction must result in a measurable change in refractive index. This may present problems with low molecular weight molecules. If the M_r is too low for direct visualisation then competition experiments may be required although there have been reports of the detection of biotin (244 Da) and theophylline (180 Da) binding directly (Karlsson and Stählberg., 1995).

Other complications influencing biosensor data are generally thought to be due to the use of a surface to investigate solution kinetics.

The binding of ligate to the ligand attached to the sensor surface requires the efficient delivery of ligate. If delivery of ligate is slower than the specific binding the measured kinetics will be limited by this mass transport effect. Glaser (1993) has modelled the transport of ligate to the Biacore CMD sensor surface in two dimensions. When the reaction is rapid, or with high ligand immobilisation, or at low flow rates the binding

may be mass transport limited. Hall et al. (1996) investigated the assumption of constant ligate concentration in the flowing buffer and found that a maximum association rate constant of around 1 x 10^6 $M^{-1}s^{-1}$ could be measured at flow rates up to 30µl/minute using the Biacore instrument (the highest possible at that time).

A further complication is the movement of the ligate through the CMD hydrogel which has been found to slow the measured interactions as modelled by Schuck (1996). Schuck and Minton (1996) have proposed a new approach based on a two compartment description of transport which allows the determination of rate constants up to 100 fold faster than previously possible.

In addition to the mass transport issue, the association data from biosensors often fails to be accurately described by the single exponential equation derived from integration of the pseudo-first order equation. In fact the data are better fitted with an equation with two exponential terms at higher ligate concentrations (equation 2.23.).

$$R_t = A\left(1-\exp^{-k_{on(1)}t}\right)+B(1-\exp^{-k_{on(2)}t}) \qquad (2.23)$$

A and B are the extents of the two phases with rate constants $k_{on(1)}$ and $k_{on(2)}$ respectively. The use of this equation will be described in more detail in chapter 6.

Dissociation data often fails to be described by the single exponential decay equation (equation 2.18). Instead, dissociation data are better fitted using equations that make no assumption as to the completeness of dissociation. This is usually achieved by the incorporation of an offset term such as equation 2.24

$$R_t = R_o\, e^{-k_{diss}t} + R_\infty \qquad (2.24)$$

where R_∞ is the offset term equivalent to the response after infinite time.

Dissociation data have also been fitted by assuming there are two dissociation processes occurring described by two separate rate constants (equation 2.25)

$$R_t = Ae^{k_{diss(1)}t} + Be^{-k_{diss(2)}t} \quad (2.25)$$

A and B are the extents of the two dissociation phases having rate constants of $k_{diss(1)}$ and $k_{diss(2)}$ respectively.

Several reasons for this non-Langmuirian behaviour have been suggested, including mass transport effects. The Langmuirian equation assumes a 1:1 interaction which is not the case with antibody/antigen reactions. However, while bi- and multi-valencey have been found to produce non-ideal behaviour (Kalinin et al., 1995) there are several reports of biphasic kinetics on surfaces for reactions which should only possess a 1:1 stoichiometry (Fisher et al., 1994. Corr et al., 1994 Oddie et al., 1997). Ligand heterogeneity caused by random amine linkages is also likely to be an important factor (Oddie et al., 1997. O'Shannessy and Winzor., 1996) as is steric hindrance caused by ligate binding (Edwards et al., 1995. Bowles et al. 1997). These complicating factors make the careful design of the experiment extremely important (Edwards et al., 1995., 1997. Karlsson and Fält. 1997).

The use of numerical integration together with global fitting of all the data has allowed a wider range of models to be fitted to the biosensor data including mass transport, conformational changes upon binding, ligand heterogeneity (Fisher and Fivash., 1994., Morton et al., 1995. Myszka et al., 1997.).

The affinity in solution has been determined using the instruments as purely concentration determinants using initial rates (Karlsson.1994) or on-rates (Nieba et al., 1996)

While most literature has focused on the Biacore and IAsys instruments interaction kinetics have been investigated using difference interferometry (Schlatter et al, 1993), elipsometry (Martensson et al, 1993) and input grating coupling (Bernard and Bosshard, 1995).

2.5 Objective of the research.

Given the difficulty in interpretation of biosensor data as outlined above a detailed investigation into biosensor kinetic data was instigated. The purpose was to attempt to investigate the causes of the non-ideality of the association and dissociation data often observed with evanescent wave biosensors. The IAsys resonant mirror biosensor was used to investigate these deviations and attempts made to eliminate, or substantially reduce, these deviations. Several biological systems were used for this investigation. Most of the early work focused on the interaction of chymotrypsin inhibitor 2 (CI-2) with chymotrypsin, an interaction with a 1:1 stoichiometry. Assumptions made in the kinetic analysis of biosensor data will be investigated, such as the influence of mass transport and the general applicability of the pseudo first-order analysis to biosensor data.

Kinetic constants obtained with IAsys were compared to solution fluorescence measurements to determine whether the biosensor results can, at least in some cases, be related to those in solution, and if not at what stage the measurement techniques diverge. For these comparative measurements proteins containing a single thiol group were labelled with fluorescein maleimide and the interaction of an anti-fluorescein antibody with these conjugates investigated.

Chapter 3

Materials and Methods.

3.1.Materials

3.1.1 Chemicals

All reagents were of Analytical grade or better. General reagents were obtained from Sigma Chemical Company (Poole, Dorset, UK) or Fisher Scientific (Loughborough, Leicestershire, UK). Fluorescein-5-maleimide, and Coomassie Plus Protein reagent were from Pierce and Warriner (Chester, UK). 1,3,4,6,tetrachloro-3α,6α diphenylglycouril, Fluorescein (sodium salt) and succinyl-Ala-Ala-Pro-Phe p-nitrophenolanilide were from Sigma Chemical Company (Poole, Dorset, UK). Colloidal gold particles (30nm) were from British Biocell International (Cardiff, UK). Radiolabelled $Na^{125}I$ was purchased from ICN Biomedicals Ltd. (Thame, Oxfordshire, UK).

Polymerised glutaraldehyde (4.2%) was prepared by the addition of 500 µl of 0.1 M NaOH to 5 mL of 5% glutaraldehyde (EM grade), obtained from Sigma Chemical Company. After a thirty minute incubation at room temperature the reaction mixture was neutralised by the addition of 500 µl of 0.1 M HCl.

3.1.2 Biochemicals

Human Serum Albumin (HSA) and anti-HSA monoclonal antibody (anti-HSA mab) were from Biogenesis (Bournemouth, Dorset, UK). Lysozyme, Bovine Serum Albumin (BSA), β-casein, bovine α-chymotrypsin, cytochrome c from *Saccharomyces cerevisiae*, papain, and mouse ascites fluid containing FITC monoclonal antibody (anti-FITC mab) were obtained from Sigma Chemical Company. Rabbit Anti-mouse Fc (RAMFc) was from ICN. Recombinant Chymotrypsin Inhibitor 2 (CI-2) was from Imperial College, London and maltose binding protein (mbp) was a kind gift of Dr. A. Cass, also at Imperial College. Cambridge. D1.3Fv was a kind donation from Dr. A. Gill (University College London,)

3.2 Methods.

The immobilisation of ligands to either CMD, planar amino or planar carboxyl surfaces followed standard protocols. As such, a typical immobilisation will be described in detail for each of the surfaces. Deviations from these standard protocols, such as immobilisation buffer, ligand concentration, and immobilisation time, will be indicated in the relevant text. All experiments were performed at 22 °C using a solution volume of 200 µl in the cuvette unless otherwise stated.

3.2.1 Immobilisation.

3.2.1.1 CMD

The use of EDC/NHS chemistry to covalently link the ligand, via its amino groups, to the carboxyl groups on the CMD is described below with the reaction scheme shown in figure 3.1.

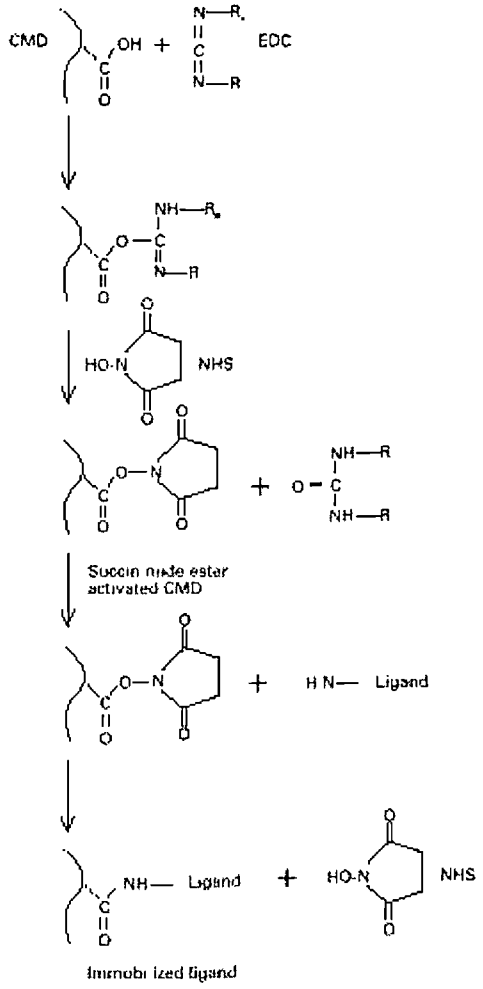

Figure 3.1: *The reaction scheme for the immobilisation of ligands to CMD via EDC/NHS chemistry.*

In detail, four additions of 200 µl of PBS/T are made to the cuvette, aspirating after each addition. A fifth addition is made and a baseline established. Thus the cuvette has had five washes of PBS/T. A premix of EDC/NHS is prepared with concentrations of 0.2M and 50 mM respectively. The PBS/T is aspirated from the cuvette and three washes of the EDC/NHS mixture added. After a seven minute activation period, the cuvette is washed 5 times with PBS/T and a baseline established. The cuvette is then washed with immobilisation buffer five times. The ligand is then usually diluted 1/10 into the immobilisation buffer in the cuvette, although complete replacement of the cuvette contents is possible, and incubated for 10 minutes. To deactivate the NHS esters, five washes of 1M ethanolamine pH 8.5 (5 x 200 µl) are performed which reacts with the free esters and, given the high ionic strength, removes any electrostatically bound ligand from within the CMD matrix. After a two minute incubation in ethanolamine, the cuvette is washed with PBS/T (5 x 200 µl). If the ligand is known to be stable to regeneration solution then the cuvette is washed with 5 x 200 µl of regenerant for 2 minutes followed by a re-equilibration in PBS/T. This conditioning is usually repeated at least once more to completely remove non-covalently bound material. The amount immobilised is then determined as the response difference in PBS/T baseline after EDC/NHS and the final preconditioning steps. A typical immobilisation profile is shown in figure 3.2.

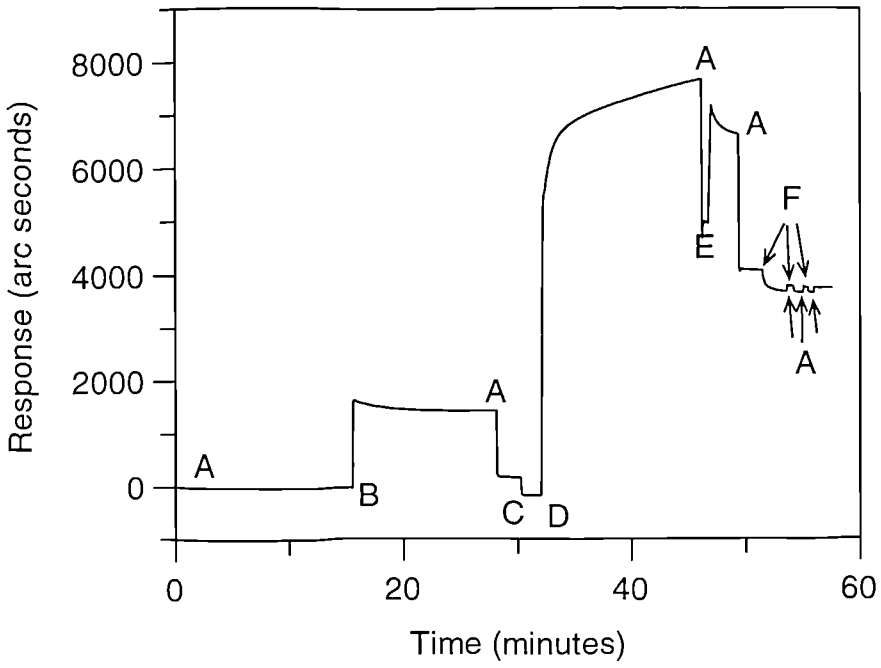

Figure 3.2: *A typical immobilisation profile on CMD. A, represents the addition of PBS/T; B, the addition of EDC/NHS; C, 10 mM acetate pH5.0 (immobilisation buffer); D, the ligand; E, 1 M ethanolamine pH8.5; F, 100 mM HCl (Regenerant).*

3.2.1.2 Planar carboxylate surfaces

The chemical groups used to link the ligand to the sensor surface are the same as the CMD surface and thus the same EDC/NHS chemistry is used. However there are certain differences in the methodology arising from the planar surface. The concentration of ligand used for immobilisation is often higher (~0.1-1 mg/ml) as the surface is unable to electrostatically concentrate the ligand as efficiently as the CMD. Furthermore the presence of Tween in any of the buffers prior to immobilisation severely reduces, and often prevents, attachment due to the coverage of Tween on the surface. The removal of reactive NHS esters is facilitated by the use of a concentrated solution of a non-specific protein which, in addition to reacting with the esters, also adsorbs to the surface. This 'blocking' of the surface helps to prevent non-specific binding of the ligate. With these points in mind a typical immobilisation is described.

A baseline is established in 10 mM phosphate pH 7.4 by washing the cuvette with 5 x 200 µl. The EDC/NHS premix, at the same concentrations as those for the CMD

immobilisation, is added and reacted for 7 minutes. A baseline is then established in the phosphate buffer by adding 5 x 200 µl of buffer followed by five washes with immobilisation buffer. The immobilisation is achieved by the dilution of ligand into the cuvette (1/10), although direct replacement is possible and incubated. After immobilisation, a buffer wash (5 x 200 µl) is performed with the ligand being conditioned with regenerant for 2 minutes. The baseline buffer is then changed to PBS and the blocking reagent added and left for 10 minutes. The blocking reagent is often BSA or β-casein at concentrations around 5 mg/ml. After the blocking step a PBS baseline is re-established and conditioned with regenerant as before. A typical planar carboxylate immobilisation trace is shown in figure 3.3.

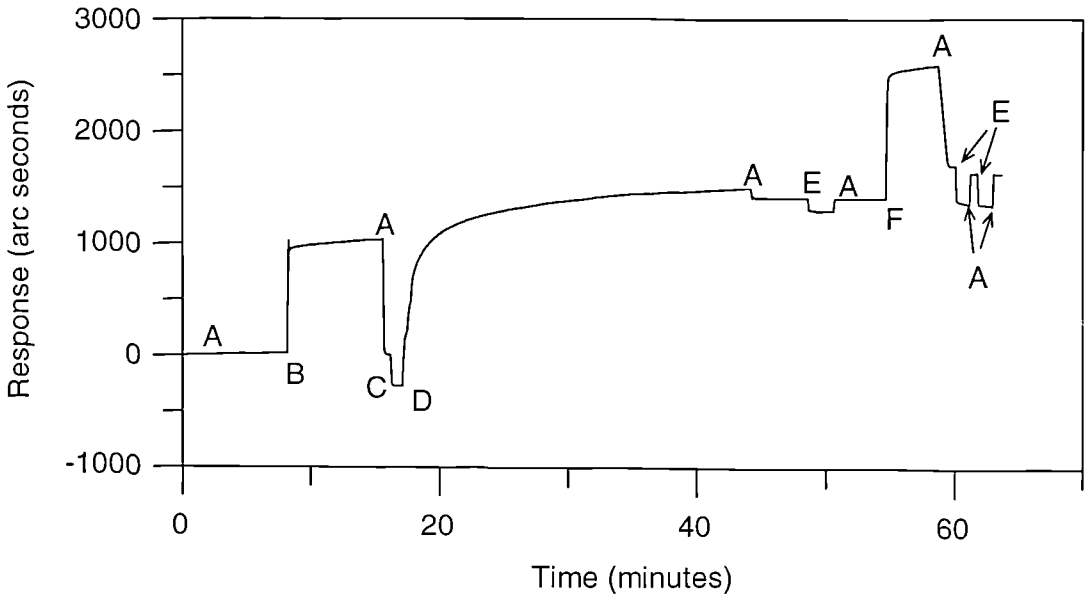

Figure 3.3: *A typical immobilisation profile on a carboxylate surface. A, represents the addition of 10 mM phosphate pH 7.74; B, the addition of EDC/NHS; C, 10 mM acetate pH5.0; D, ligand; E, 100 mM HCl; F, blocking reagent such as BSA or β-casein.*

3.2.1.3 Planar amino surfaces

In common with the planar carboxylate surface, the amino surface should be 'blocked' with a non-specific protein but the immobilisation chemistry is different due to the presence of amino groups on the sensor surface. The chemistry used is to link the

amino groups on the ligand to the amino groups on the sensor surface via polymerised glutaraldehyde (see figure 3.4).

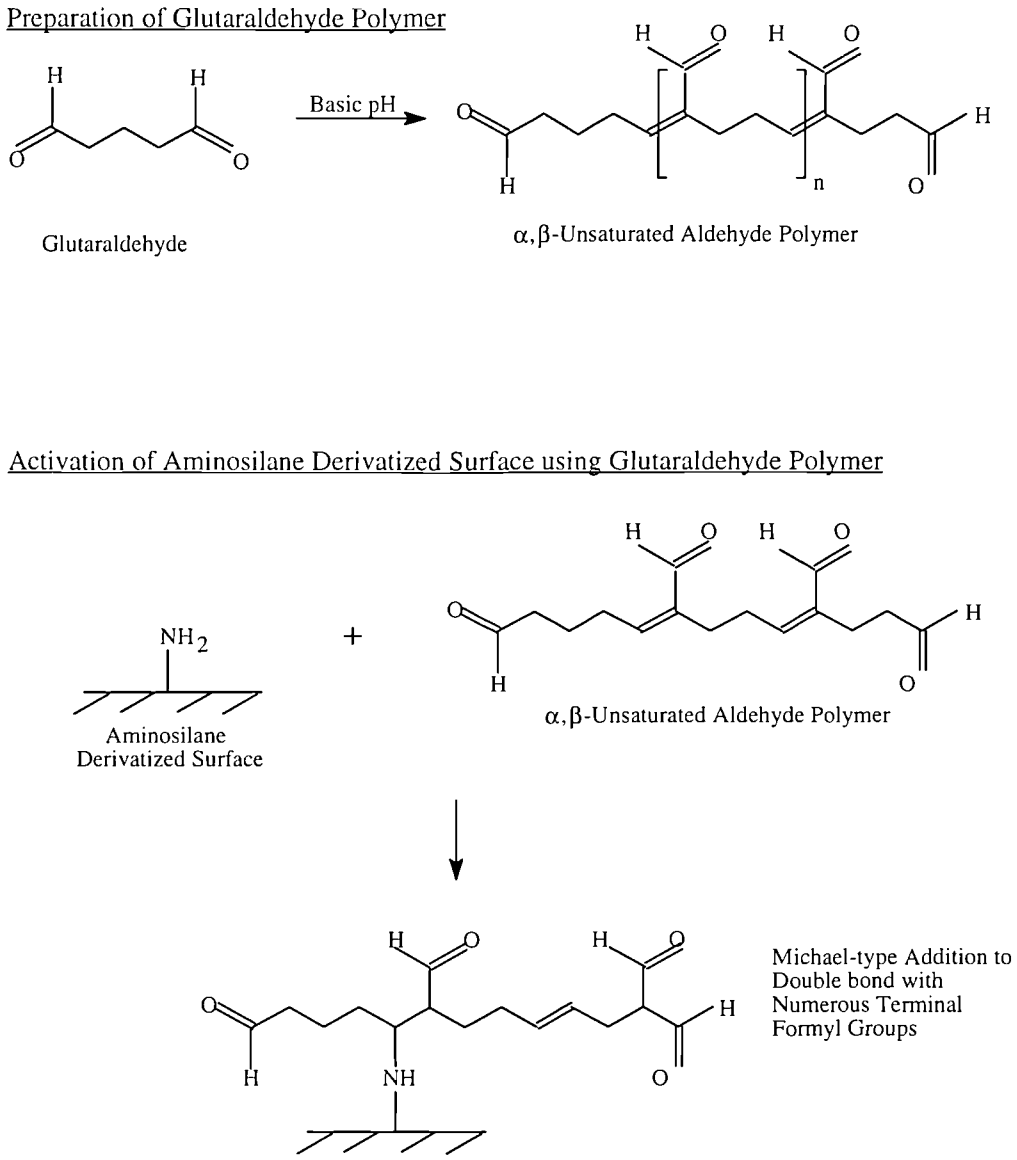

Figure 3.4: *A reaction scheme for the preparation of polyglutaraldehyde and its subsequent use in the immobilisation of ligands to an amino surface.*

A baseline is established with 5 x 200 µl of 10 mM phosphate buffer pH 7.4. The polymerised glutaraldehyde is added to the cuvette (3 x 200 µl) and incubated for 30 minutes. The cuvette is then washed in the phosphate buffer (4 x 200 µl) with a final

volume in the cuvette of 180 µl. Ligand is then diluted into the cuvette at the required concentration and allowed to react. The remainder of this method is identical to the planar carboxylate method. A typical trace is shown in figure 3.5

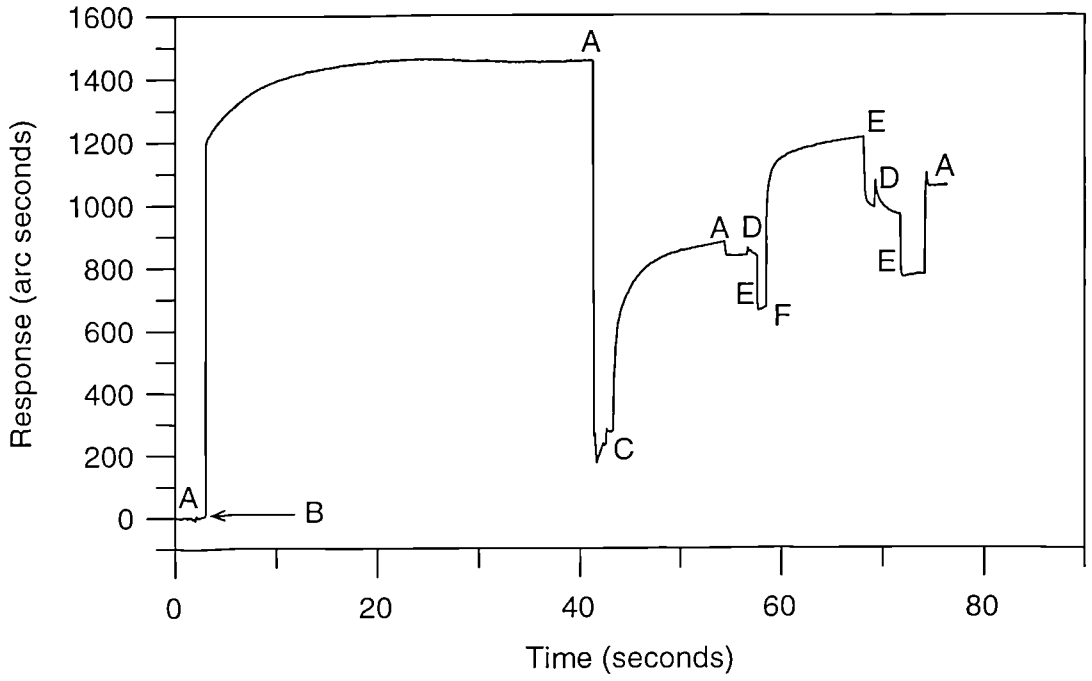

Figure 3.5: *A typical immobilisation profile on an amino surface. A, represents the addition of 10 mM phosphate pH 7.4; B, the addition of polymerised glutaraldehyde; C, the addition of Ligand; D, 100 mM HCl; E, PBS; F, blocking reagent such as BSA or β-casein.*

3.2.2 Effect of stirrer height on the binding rate

To a planar, underivatised sensor surface, lysozyme was adsorbed at a concentration of 5 mg/ml for 15 minutes from 10 mM phosphate buffer pH 7.4. Colloidal gold particles (30 nm) were added to 9.625 x 10^9 particles/ml in the cuvette by the injection of 5 µl of a stock solution of colloidal gold (3.85 x 10^{11} particles/ml) to 195 µl of phosphate buffer. These particles were allowed to interact for 5 minutes at varying stirrer speeds at stirrer heights of 2 mm and 0.6 mm.

3.2.3 Effect of stirrer rate on the rate of binding

In addition to the above stirrer experiment involving gold particles, the chymotrypsin/CI-2 system was investigated. Chymotrypsin was immobilised on a CMD sensor surface by the addition of 50 µl of 1 mg/ml stock solution to 150 µl of 10 mM acetate pH 5.0 in the cuvette. This immobilisation was performed for 10 minutes, followed by an ethanolamine wash and preconditioning with 10 mM HCl. An immobilisation response of 1500 arc seconds was achieved. A solution of CI-2 was prepared in PBS/T at a concentration of 5.7 µg/ml (640 nM). To 180 µl of PBS/T in the cuvette, 20 µl of the CI-2 solution added and allowed to bind for three minutes. The binding was repeated at differing stir rates in triplicate. After each binding the stir rate was altered to 100% and the bound CI-2 removed by a two minute 10 mM HCl wash.

3.2.4 Effect of glycerol on the binding rate.

3.2.4.1 Planar surface

Glycerol solutions at 24% and 48% w/w were prepared in UHP water. BSA solutions in different viscosity media were prepared by dissolving 5 mg of BSA into 10 ml of 24% and 48% glycerol solutions together with 10 ml of UHP water giving a final concentration of 500 µg/ml. A further dilution in to the appropriate solution was made to give a concentration of 150 µg/ml. To planar, underivatised sensor surfaces 180 µl of either the 24%, 48% or the UHP water added to the cuvette and a baseline established for 5 minutes. After this equilibration, 20 µl of BSA in the relevant viscosity medium was added and adsorbed for 10 minutes. Each viscosity solution was tested in triplicate using a different sensor surface.

3.2.4.2 CMD surface

Chymotrypsin was immobilised to a CMD sensor surface using EDC/NHS chemistry at a concentration of 250 µg/ml in 10 mM acetate pH 5.0 for 10 minutes. After an ethanolamine wash and conditioning with 10 mM HCl an immobilisation response of 1500 arc seconds was achieved. Solutions of CI-2 in 48, 20, 10, 5, 2.5, 1.25, and 0.625% glycerol were prepared at a concentration of 1240 nM. A 1240 nM solution of CI-2 was also prepared in PBS/T. To 180 µl of the relevant viscosity

solution, 20 µl of the appropriate CI-2 solution was added and allowed to bind for 5 minutes. After this time, the chymotrypsin was regenerated with 10 mM HCl.

3.2.5 Adsorption isotherm for HSA on a planar surface

HSA solutions at differing concentrations were prepared in 10 mM phosphate pH7.4 in order to give the following concentrations when diluted 1/10 into the cuvette. These final concentrations were 100, 10, 5, 2.5, 1.25, 0.625, and 0.31 µg/ml. The adsorption of each of these solutions was monitored for five minutes followed by treatment with a two minute wash with 0.1M NaOH / 1% SDS solution. This solution removed adsorbed HSA in preparation for the next concentration. Each concentration was performed in triplicate.

3.2.6 Radiolabelling of HSA with ^{125}I

HSA was dissolved in PBS to a concentration of 10 mg/ml. 1 mg/ml of 1,3,4,6,tetrachloro-3α,6α— diphenylglycouril (Iodogen) was prepared in dichloromethane and 200 µl added to a glass vial. The solvent was evaporated using a nitrogen stream leaving the Iodogen on the glass walls. To this vial, 1.5 mL of the HSA solution and 5 µl of Na^{125}I were added and mixed for 1 hour. A PD10 column was equilibrated with 3 column volumes (3 x 3 mL) of PBS followed by 1.5 mL of 10 mg/ml HSA to block the column. Three column volumes of PBS, 10 mM acetate pH 5.0, and then PBS were passed down the column. The reaction solution was then passed down the column and eluted with PBS collecting 12 drop fractions (~0.5 mL). The counts in each vial were monitored using a gamma counter at a distance of approximately 0.6m. The fractions containing ^{125}I HSA were pooled. The activity was determined by measuring the cpm of two 5 µl aliquots. The HSA concentration of the pooled material was determined using Coomassie Plus Protein reagent. HSA standards at 100,200,300, and 400 µg/ml were prepared in PBS. The pooled ^{125} I HSA was diluted 1/25 in PBS. To 1 mL of coomassie reagent, 50 µl of the standards, PBS only (blank) or the diluted sample were added in duplicate. The absorbance at 595 nm was measured and the concentration determined from the standard curve which allowed the specific activity of the ^{125}I HSA to be calculated.

3.2.7 Investigation into depletion using ^{125}I HSA.

Anti-HSA mab was immobilised to CMD surfaces at two loadings. The high loading of 2800 arc seconds was achieved by immobilising at 339 µg/ml in 10 mM acetate pH 5.0 for 10 minutes. The immobilisation response was determined after three 2 minute washes with 100 mM HCl. The immobilisation of anti-HSA mab at a concentration of 8 µg/ml for 10 minutes gave a response after acid conditioning of 600 arc seconds. A further CMD surface was immobilised with chymotrypsin at 10 µg/ml in acetate pH 6.0 for 10 minutes which, after conditioning with 10 mM HCl, gave an immobilisation response of 650 arc seconds.

^{125}I HSA was diluted in PBS and PBS/T to concentrations of 500, 24, and 9 nM. The binding of these solutions were monitored for 10 minutes. Two 5 µl aliquots of the starting material were counted together with two 5 µl aliquots of the cuvette contents after binding. The instrument response after PBS or PBS/T wash was measured and the ligand regenerated with the acid regenerant. The 9 nM solution was only used for the high loaded surface due to small shifts with the low and control surfaces.

3.2.8 Affinity determination of ^{125}I HSA binding to CMD immobilised anti-HSA mab

A CMD sensor surface with anti-HSA mab immobilised to a response of 600 arc seconds was prepared by the use of a 10µg/ml solution in 10 mM acetate pH 5.0. Solutions of each of the ^{125} I HSA and native HSA were prepared in PBS/T. Each solution was diluted 1/10 into the cuvette, to give final concentrations of between 2 and 250 nM, and bound for 5 minutes. The ligand was regenerated with 100 mM HCl for 2 minutes.

3.2.9 Enzymatic determination of the kinetic parameters for the interaction of chymotrypsin with CI-2.

A 1 mg/ml solution of chymotrypsin was prepared in PBS/T which was further diluted to give a 100 nM solution. The substrate (succinyl-Ala-Ala-Pro-Phe-p-nitrophenylanilide) was prepared in PBS/T to a concentration of 1.0 mM. CI-2 was prepared at differing concentrations in PBS/T ranging from 2 µM to 100 nM. To 10 µl of the chymotrypsin solution was added to 880 µl of PBS/T in a 1 mL spectrometer cuvette. To this solution, 10 µl of one of the CI-2 solutions was added, mixed, and

incubated for 15 minutes. After this time, 100 µl of the substrate was added, the cuvette inverted to mix the contents, and the absorbance at 412nm monitored for 10 minutes. The absorbance measurements were repeated at the different CI-2 concentrations including 0 nM and the initial rates of substrate hydrolysis converted to M/s by multiplying by the extinction coefficient of the product (8480 $M^{-1}cm^{-1}$). The dissociation rate constant was determined by preforming the chymotrypsin/CI-2 complex and then diluting this into a solution of substrate. To 100 µl of a 1 mM solution of chymotrypsin 100 µl of 10 mM CI-2 was added and equilibrated for 1 hour. After this time, 5 µl of this premix was added to 1 mL of 0.1 mM substrate and the increase in absorbance at 412nm monitored.

3.2.10 Binding of ^{125}I HSA to immobilised anti-HSA mab

Anti-HSA mab was immobilised by adding 200 µl of 10 µg/ml solution in 10 mM acetate pH 5.0 to a CMD sensor surface and incubating for 10 minutes. The binding of 220 µg/ml HSA in PBS/T was followed for different contact times up to 30 minutes. The binding response after PBS/T wash was recorded and the amount of ^{125}I HSA bound determined by counting a 100 µl aliquot of the 10 mM HCl regeneration solution. The regeneration time was two minutes. The cpm obtained from different binding responses also allowed the calibration factor to be calculated.

3.2.11 Stoichiometry of HSA/anti-HSA mab system

Anti-HSA mab was immobilised at differing concentrations to separate CMD blocks in order to obtain differing immobilisation responses. The concentration range used was 1 to 500 µg/ml in 10 mM acetate buffer pH5.0. HSA at 3 µM was then added to each of the sensor surfaces and the saturating response measured.

3.2.12 Effect of ligand loading upon the kinetics of chymotrypsin/CI-2 interaction.

To produce differing immobilisation responses on CMD surfaces, chymotrypsin was immobilised from 10 mM acetate pH 6.0 at concentrations of 2,10,50,200,500 and 2500 µg/ml for 10 minutes. The ligand was conditioned with 10 mM HCl for 2 minutes. Seven CI-2 concentrations from 1.8 to 124 nM in the cuvette were bound for 10 minutes by diluting 1/10 into the cuvette. For example, 20 µl of 1240 nM added to 180 µl of PBS/T in the cuvette produces at concentration in the cuvette of 124 nM.

Dissociation was monitored by the replacement of the CI-2 solutions with PBS/T buffer. The CI-2 solutions were removed completely by a two minute wash for 10 mM HCl.

3.2.13 Dissociation in the presence of ligand for chymotrypsin/CI-2.

Using chymotrypsin immobilised to CMD the effect of ligand in the dissociation buffer was investigated. CI-2 at a final concentration of 124 nM was bound for 5 minutes. Dissociation was then induced by the addition of PBS/T and the dissociation monitored for 10 minutes. The chymotrypsin was regenerated with 10 mM HCl for 2 minutes. CI-2 was rebound for 5 minutes and dissociation in PBS/T containing 1μM chymotrypsin followed for 20 minutes and then regenerated as before. Finally CI-2 binding was repeated as above and the dissociation monitored by washing with PBS/T every 3 minutes.

3.2.14 Purification of anti-FITC mab

The monoclonal anti-FITC antibody (isotope IgG_1) was purified from mouse ascites fluid using a 1 mL Protein G column (A.C.L., Cambridge, UK). The column was washed with 20 column volumes of 20 mM acetate pH5.0. The ascites fluid was then diluted 1/8 in the acetate buffer. Using a 500 μl injection loop, the diluted ascites fluid was loaded onto the column at a flow rate of 0.3ml/min. The column eluate was monitored at 280nm. When the baseline had returned to its pre-injection value, a further 500 μl of the diluted ascites fluid was added, after which when the baseline had been re-established a further 500 μl of ascites fluid was added. When a baseline in the running acetate buffer had been achieved for a final time the IgG fraction was eluted with 0.1M glycine pH3.0 collecting 0.5 mL fractions. The fractions were neutralised with an equal volume of 50 mM carbonate buffer pH11.0. The column was cleaned with 8M urea and stored in 20% ethanol at 4°C. The fractions giving an absorbance at 280nm were pooled and their concentration determined using Coomassie plus reagent with anti-HSA mab as standard.

3.2.15 Dissociation of anti-FITC mab from immobilised FITC on CMD surface in the presence of fluorescein (sodium salt).

The FITC was immobilised to a CMD sensor surface by activating the CMD matrix six times with EDC/NHS solutions. Each activation had a duration of 7 minutes. A 1M solution of ethylenediamine pH8.5 was then added and incubated for 10 minutes. A 5 mg/ml solution of FITC in acetate buffer pH5.0 was added and allowed to immobilise for 10 minutes. After washing with PBS/T, an immobilisation response of 220 arc seconds was achieved. The binding of 400 nM anti-FITC mab in PBS/T was monitored for 5 minutes. Dissociation was measured for 5 minutes by the addition of PBS/T containing varying concentrations of fluorescein-Na. The fluorescein-Na concentrations were 0, 1.4 nM, 14 nM, 140 nM. 280 nM, 1.4 μM and 140 μM.

3.2.16 Calibration of planar surfaces with ^{125}I HSA.

^{125}I labelled HSA was prepared following the previous methodology to a specific activity of 2.42Mbq/mg. Varying dilutions of this ^{125}I HSA was prepared in PBS. Underizatised planar surfaces were used for the adsorption of various concentrations of ^{125}I HSA. The responses produced after 5 minutes following a PBS wash were noted and the sensor surface removed from the cuvette mounting. The sensor surface was then counted for 1 minute.

3.2.17 Kinetic comparison of planar and CMD surfaces using the lysozyme/D1.3Fv interaction.

3.2.17.1 Carboxylate

Lysozyme at 1 mg/ml was prepared in UHP water. After EDC/NHS activation of the carboxylate surfaces, lysozyme was immobilised by adding 50 μl of the lysozyme solution to 150 μl of acetate buffer in the cuvette. After conditioning with 100 mM HCl, 413 arc seconds were immobilised. The remaining activated sites were blocked with 1 mg/ml cytochrome c. D1.3Fv was bound 0.25 to 32 nM for 10 minutes regenerating with 100 mM HCl after each binding.

3.2.17.2 CMD

Lysozyme was immobilised at 10 µg/ml in 10 mM acetate buffer pH 5.0 for 5 minutes and after acid conditioning 484 arc seconds were immobilised. D1.3Fv was bound for 10 minutes at differing concentrations as used for the carboxylate surface. Regeneration was achieved with 100 mM HCl.

3.2.17.3 Amino

After reacting the amino groups on the surface with 4.2% polymerised glutaraldehyde, 20 µl of 1 mg/ml lysozyme added to 180 µl of phosphate buffer in the cuvette and immobilised for 10 minutes. After conditioning with 100 mM HCl, 367 arc seconds were immobilised. The remaining sites were blocked with 1 mg/ml cytochrome c. D1.3Fv at the concentrations used for the carboxylate were bound for 5 minutes.

3.2.18 Kinetic comparison of planar and CMD surfaces using the HSA/anti-HSA mab interaction.

Both of these species were used as the ligand to determine whether the kinetic are sensitive to which of the partners is the ligand.

3.2.18.1 Carboxylate

530 µg/ml of anti-HSA mab in 10 mM acetate pH5.0 was immobilised for 5 minutes which after conditioning with 100 mM HCl gave an immobilisation response of 105 arc seconds. The remaining sites were blocked with 50 mg/ml β-casein for 10 minutes. HSA at concentrations ranging from 6 to 1510 nM were bound in PBS/T for 5 minutes. Regeneration was achieved by the use of 100 mM HCl.

HSA was immobilised at 1 mg/ml in acetate buffer pH5.0 for 5 minutes. After preconditioning a response of 220 arc seconds was observed. the free sites were blocked as above. Anti-HSA mab at concentrations of 1 to 1130 nM in PBS/T were bound for 5 minutes followed by regeneration in 100 mM HCl.

3.2.18.2 CMD

Both anti-HSA mab and HSA were immobilised to the CMD at concentrations of 10 µg/ml in 10 mM acetate pH5.0 for 2 minutes in order to control the immobilisation responses. After conditioning with 100 mM HCl the response from anti-HSA mab

immobilised was 2023 arc seconds and the response from HSA immobilised was 999 arc seconds. HSA or anti-HSA mab were then bound at the same concentration range used for the carboxylate surface for 10 minutes and then regenerated with 100 mM HCl.

3.2.18.3 Amino

HSA was immobilised at 122 µg/ml and anti-HSA mab at 339 µg/ml. After conditioning responses for anti-HSA mab and HSA immobilisation were 591 and 244 arc seconds respectively. The sites were blocked with 50 mg/ml β-casein. The ligate, either HSA or anti-HSA mab, were bound for 5 minutes at the same concentration ranges as used for the carboxylate.

3.2.19 Determination of the association rate constant by initial rate analysis

Chymotrypsin was immobilised to CMD at a concentration of 50 µg/ml in 10 mM acetate pH 6.0 for 10 minutes. The capacity of this surface (R_{max}) was obtained by the addition of a saturating concentration of CI-2 (6.7µM). Binding of this CI-2 solution for twenty minutes produced a saturating equilibrium response. Regeneration of the immobilised chymotrypsin was afforded by a 2 minute wash with 2 mM HCl. To determine the initial rates of binding a range of CI-2 concentrations (1-200 nM) in the cuvette were bound for 1 minute. After each binding the chymotrypsin was regenerated with 2 mM HCl for 2 minutes.

3.2.20 Equilibrium titration for chymotrypsin/CI-2 interaction.

To a chymotrypsin immobilised CMD cuvette (3.2.19) containing 90 µl of PBS/T, 10 µl of 160 nM CI-2 added and the response recorded until equilibrium was approached. A further 10 µl of 160 nM was added and another equilibrium response obtained. Further additions of CI-2 produced further equilibrium responses. These additions were 5 µl of 320 nM, 10 µl of 320 nM, 10 µl of 640 nM, 20 µl of 640 nM, and finally a further 20 µl of 640 nM CI-2.

3.2.21 Determination of the solution affinity of Chymotrypsin/CI-2 using IAsys

CI-2 at a concentration of 64 nM was prepared in PBS/T. Chymotrypsin at concentrations ranging from 2 to 1000 nM were prepared in PBS/T. To 100 µl of the CI-2 solution, 100 µl of each of the chymotrypsin concentrations were added and incubated for 2 hours at room temperature. After this time 100 µl of each premix was added to a CMD cuvette with chymotrypsin immobilised having a response of 970 arc seconds and bound for 5 minutes. Each binding was followed by a 10 mM HCl regeneration.

3.2.22 Conjugation of cytochrome c to fluorescein

Fluorescein maleimide was prepared by dissolving 2mg in 4ml of DMF followed by the addition of 0.7ml of PBS. Cytochrome c was dissolved in PBS to a concentration of 100 µg/ml. To 0.25ml of this diluted fluorescein, 1.25ml of cytochrome was added and incubated for 4 hours at room temperature with mixing. To reduce the positive charge on the conjugate, 50 µl of 5 mg/ml succinic anhydride in DMF was added and incubated for 1 hour at room temperature. A PD10 column was washed with 3 column volumes of PBS followed by 1.5ml of 1 mg/ml cytochrome c in PBS. The column was then washed with 3 column volumes of PBS, followed by 3 column volumes of acetate buffer pH5. 0, and then 3 column volumes of PBS/T. The reaction mixture was passed down the column and eluted with PBS/T collecting 0.5ml fractions. The fractions were monitored at 280nm, 490nm, and in the presence of Coomassie Protein reagent at 595nm. The fraction containing labelled protein were pooled and the concentration determined using Coomassie Protein reagent with cytochrome c as standard.

3.2.23 Conjugation of Papain to fluorescein.

To 1.25ml of 200 µg/ml of papain in PBS, 0.25ml of stock fluorescein maleimide was added and incubated for 4 hours at room temperature with mixing. To the reaction mixture, 50 µl of 5 mg/ml succinic anhydride in DMF was added and incubated for 1

hour. A PD10 column was equilibrated as 3.2.20 but blocked with 1 mg/ml of papain in PBS. The absorbance of the eluted fractions were monitored as previous.

3.2.24 Conjugation of maltose binding protein (mbp) to fluorescein.

To 1.25 ml of 350 µg/ml mbp in PBS, 250 µl of stock fluorescein maleimide added. A PD10 column was equilibrated and blocked with 1 mg/ml of mbp and the eluted fractions monitored as before.

3.2.25 The interaction of anti-FITC mab with CMD immobilised fluorescein conjugates

The conjugates were immobilised to CMD surfaces in 10 mM acetate buffer pH5.0 using the standard EDC/NHS chemistry.

3.2.25.1 Cytochrome c conjugate

Cytochrome c conjugate was immobilised at 0.2 µg/ml for 10 minutes which after ethanolamine wash and 100 mM HCl conditioning gave a response of 120 arc seconds. Purified anti-FITC mab was bound at concentrations between 0.6 and 12 nM for 5 minutes regenerating with 100 mM HCl for 2 minutes after each binding cycle. On the higher anti-FITC mab concentrations of 12,8,4, and 2 nM dissociation of the complex was monitored in PBS/T. A higher loaded surface was prepared for the equilibrium titration experiment. This was achieved by immobilising the conjugate at 15 µg/ml to give an immobilisation response of 2500 arc seconds.

3.2.25.2 Papain conjugate.

Papain conjugate was immobilised at 0.5 µg/ml to CMD for 10 minutes giving a response after 100 mM HCl of 167 arc seconds. Purified FITC antibody was then bound at concentrations up to 12 nM in PBS/T for 5 minutes. The dissociation was followed for the higher concentrations of mab for 5 minutes by replacement of ligate solution with PBS/T. To illustrate the influence of rebinding in this system 1 mM fluorescein-Na was added to the PBS/T for dissociation. A higher loaded surface was prepared for the equilibrium titration experiment. This was achieved by immobilising the conjugate at 20 µg/ml to give an immobilisation response of 1988 arc seconds

3.2.25.3 maltose binding protein conjugate

The maltose binding protein conjugate was immobilised at 2 μg/ml in acetate buffer for 10 minutes to give an immobilisation response after ethanolamine and 100 mM HCl conditioning of 240 arc seconds. The binding of anti-FITC mab at a concentration range of 0.1-80 nM in PBS/T for 5 minutes was monitored.

3.2.26 Control for immobilised fluorescein conjugates.

As a control for the labelled conjugates, the unlabelled protein was immobilised to the CMD surface from 10 mM acetate pH5.0 at concentrations of 20 μg/ml (cytochrome c), 10 μg/ml (papain), and 10 μg/ml (mbp). Anti-FITC mab at a final concentration of 4 nM was bound for 5 minutes to each of the control surfaces.

3.2.27 Equilibrium titration of the immobilised fluorescent conjugates.

Using conjugate immobilised CMD surfaces from the kinetic analysis of anti-FITC mab binding, equilibrium titration experiment were performed by titrating with anti-FITC mab. The starting volume in the cuvette was 90 μl of PBS/T to which aliquots of anti-FITC mab solutions were added and the response noted upon the attainment of equilibrium. Thus for cytochrome c conjugate the concentration range in the cuvette was 0.06 to 16 nM, for the papain conjugate it was 0.1-218 nM.

3.2.28 Binding of fluorescein conjugates to anti-FITC mab immobilised on a carboxylate surface.

Immobilisation of the anti-FITC mab was achieved by incubating with 100 μg/ml anti-FITC mab for 10 minutes. A response of 360 arc seconds was obtained. After blocking with 5 mg/ml β-casein the conjugates were bound at differing concentrations in PBS/T regenerating with 4M $MgCl_2$. As a control, unlabelled protein was also bound.

3.2.29 Binding of fluorescein conjugates to anti-FITC mab immobilised on an amino surface

The anti-FITC mab was immobilised at 600 μg/ml in 10 mM phosphate buffer pH7.4 for 10 minutes. After conditioning with 4M $MgCl_2$ an immobilisation response of 400 arc seconds was achieved. The surface was then blocked with 5 mg/ml β-casein for 10

minutes followed by a further 4M $MgCl_2$ preconditioning step. The conjugates were then bound at differing concentrations in PBS/T regenerating with 4M $MgCl_2$. As in the case of the planar carboxyl surface the controls were the unlabelled material.

3.2.30 Binding of fluorescein conjugates to anti-FITC mab immobilised on a CMD surface

Anti-FITC mab was immobilised on CMD surfaces at 20 µg/ml which gave an immobilisation response after conditioning with 4M $MgCl_2$ of 550 arc seconds. Binding of the conjugates at differing concentrations in PBS/T was then monitored, regenerating with 100 mM HCl. As a control, unlabelled protein was bound in PBS/T.

3.2.31 The binding of fluorescein conjugates to anti-FITC mab bound to CMD immobilised RAMFc

RAMFc was immobilised to CMD at a concentration of 100 µg/ml for 10 minutes. After an ethanolamine wash and preconditioning with 100 mM HCl, 2200 arc seconds of RAMFc were immobilised. Anti-FITC mab was then bound at 15 µg/ml for 5 minutes. After a PBS/T wash then conjugate was then bound for 5 minutes. After this time, dissociation was followed for 5 minutes in PBS/T and then the conjugate-anti-FITC mab complex removed by 100 mM HCl for 2 minutes.

3.2.32 The binding of fluorescein conjugates to anti-FITC mab bound to carboxylate immobilised RAMFc

RAMFc was immobilised to carboxylate at a concentration of 500 µg/ml for 10 minutes. After preconditioning with 100 mM HCl, 1100 arc seconds of RAMFc were immobilised. The surface was then blocked with β-casein. Anti-FITC mab was then bound at 15 µg/ml for 5 minutes. After a PBS/T wash then conjugate was then bound for 5 minutes. After this time, dissociation was followed for 5 minutes in PBS/T and then the conjugate-anti-FITC mab complex removed by 100 mM HCl for 2 minutes.

3.2.33 Controls for HSA/anti-HSA mab system.

β-casein was immobilised on aminosilane and carboxylate surfaces at 5 mg/ml from phosphate buffer for 10 minutes and conditioned with 100 mM HCl for 2 minutes. A further 5 mg/ml was immobilised and bound for 10 minutes. Following further

conditioning, anti-HSA mab was incubated at 339 μg/ml for 5 minutes. Any binding was removed by 100 mM HCl and 1 mg/ml HSA incubated for 5 minutes. The control for the binding of HSA on the CMD surface was to immobilised RAMFc at 100 μg/ml in acetate for 10 minutes. After preconditioning with 1M formic acid, HSA at 1 mg/ml in PBS/T was bound for 3 minutes. The control for anti-HSA mab binding on CMD was to immobilise BSA at 10 μg/ml to give an immobilisation response of 800 arc seconds. Anti-HSA mab was then bound at 2.2 μM in PBS/T for 3 minutes.

3.2.34 Controls for the Chymotrypsin/CI-2 system

To a RAMFc CMD sensor surface, CI-2 at 1240 nM was diluted 1/10 into the cuvette containing PBS/T and bound for four minutes. Any binding was removed by a two minute wash with 1 M formic acid.

3.2.35 Controls for the lysozyme/D1.3Fv system

The same controls used for the HSA/anti-HSA mab system were used for the binding of D1.3Fv to immobilised lysozyme. Binding of 15 nM solutions of D1.3Fv to casein immobilised amino or carboxylate surfaces were monitored for five minutes. The binding of 15 nM D1.3Fv to RAMFc served as the control for the CMD surface.

3.2.36 Controls for the FITC/anti-FITC mab interaction.

HSA was immobilised to a CMD sensor surface at a concentration of 200 μg/ml in 10 mM acetate to give a response after conditioning with 100 mM HCl of 1600 arc seconds. FITC antibody at 1 μM was allowed to bind for 2 minutes. The control for the amino surface was to immobilise β–casein as described for the anti-HSA mab/HSA controls. Anti-FITC mab was then bound for 5 minutes at a concentration of 1.1 μM in PBS/T

Chapter 4

Interaction kinetics on CMD.

4.1 Introduction.

There are several factors that need to be investigated in order to verify the applicability of the biosensor and the CMD hydrogel to the study of molecular interactions. Firstly, the relationship between instrument response and binding needs to be established. It is then important to investigate the stoichiometry and kinetics of ligate binding. A final point, which is specific to the CMD matrix, is the effect ligand loading has on the observed behaviour. This chapter presents a detailed analysis of each of these factors.

4.2 The relationship between binding and instrument response.

All the studies within this thesis depend upon ligate binding generating a proportional instrument response. In order to confirm this relationship, the amount of ligate bound to the immobilised ligand was measured directly using ^{125}I HSA binding to CMD immobilised anti-HSA mab and compared to the IAsys response. In order to vary the amount bound, differing incubation times were used. The amount bound (cpm) and the instrument response are plotted as a function of binding time in figure 4.1.

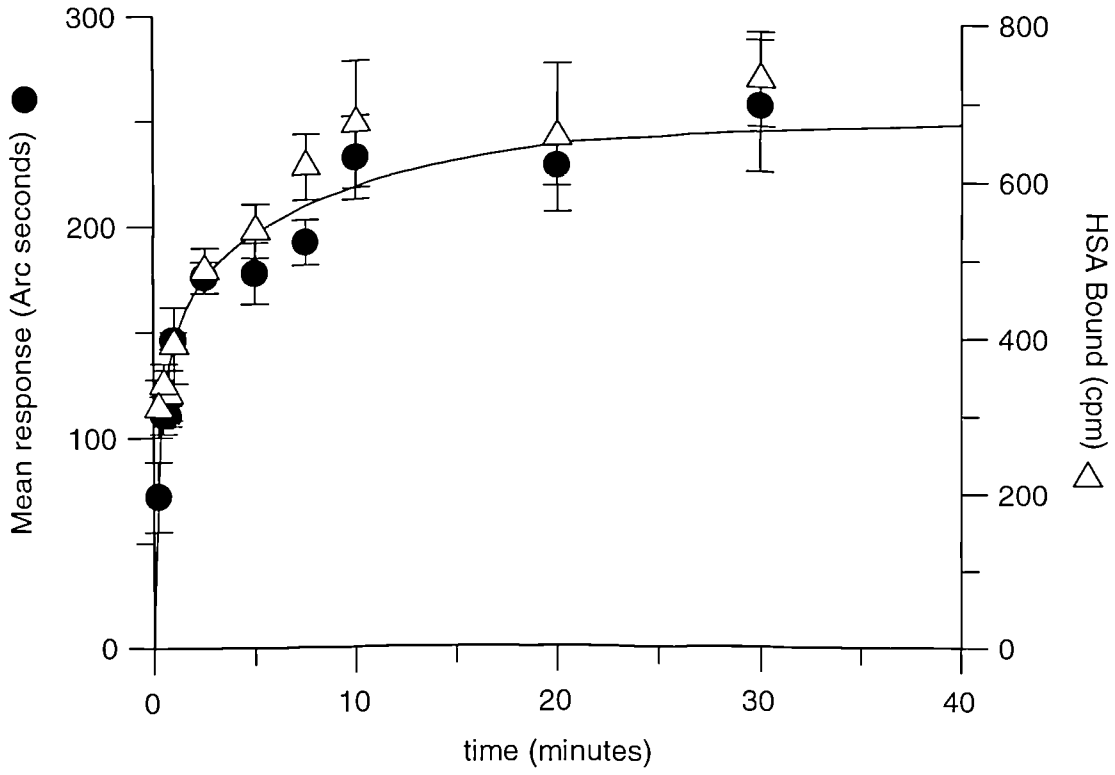

Figure 4.1: *Effect of incubation time upon the IAsys instrument response (solid circles) and amount of bound ^{125}I HSA measured in cpm (open triangles) when binding to anti-HSA mab immobilised on CMD. All data points are means of triplicate values, and errors represent the standard error of the mean (SE) The solid line shows a double exponential fit.*

From figure 4.1, the relationship between the amount of ^{125}I HSA bound and the IAsys response can be determined. This relationship is plotted in figure 4.2

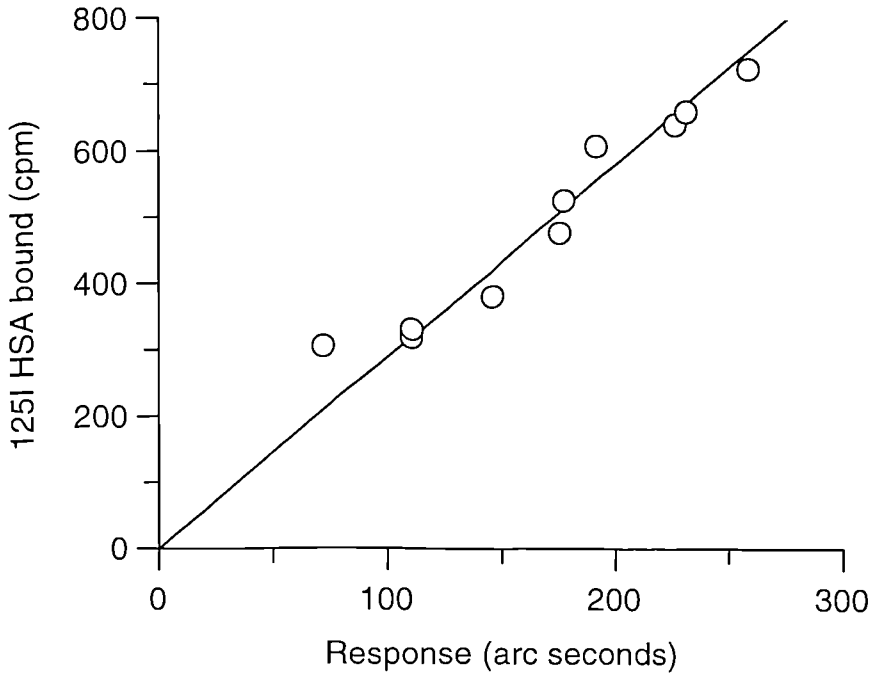

Figure 4.2: *Relationship between cpm and instrument response for the binding of ^{125}I HSA to CMD immobilised anti-HSA mab. The best line through the data using linear regression is shown.*

From the data in figure 4.2 it is evident that there is a linear relationship between instrument response and amount bound (cpm) and as such the instrument response is proportional to the amount of ligate bound.

It is possible to obtain further information regarding the cpm/instrument response relationship using figure 4.2. A calibration factor relating the instrument response to the total amount of ligate on the surface can be obtained with knowledge of the sensor surface area and the specific activity of the ^{125}I HSA.

The slope of figure 4.2 was 2.906 cpm = 1 arc second.
The specific activity of the ^{125} I HSA solution was 0.5MBq/mg and the sensor surface area was 20mm^2. Together, these result in the relationship:

$$\underline{1 ng/mm^2 = 206 \text{ arc seconds}}$$

Knowledge of this calibration factor allows the conversion of IAsys response to a concentration term which is essential for second order data analysis (Chapter 7)

4.3 Stoichiometry of binding.

In the previous section it was established that the instrument response was proportional to the binding of ligate. However, the stoichiometry was not measured. The effect of the amount of ligand attached to the CMD matrix upon the measured binding activity was investigated by immobilising anti-HSA mab and binding HSA at a saturating concentration. The stoichiometry (f) is calculated as the molar ratio of the immobilised anti-HSA mab response to that of the HSA binding response such that

$$f = \frac{\left(\frac{Binding\ \mathrm{Re}sponse\ for\ HSA}{68{,}000}\right)}{\left(\frac{Binding\ \mathrm{Re}sponse\ for\ Anti-HSA}{150{,}000}\right)} \qquad (4.1)$$

where 68,000 and 150,000 are the molecular weights of HSA and anti-HSA mab respectively. As illustrated in figure 4.3 at high immobilisation responses the stoichiometry is low but with decreasing immobilisation response the stoichiometry increases. Extrapolation to infinite dilution gives a maximum stoichiometry of approximately 2 molecules of HSA per molecule of anti-HSA mab.

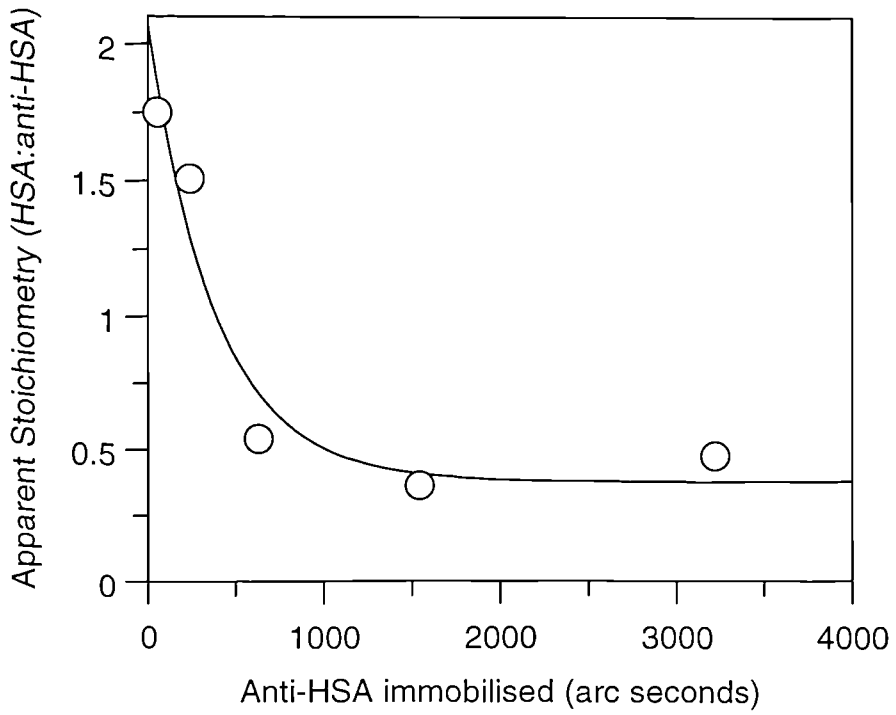

Figure 4.3: *Dependence of the binding stoichiometry between HSA and anti-HSA mab upon the amount of anti-HSA mab immobilised to the CMD surface.*

From figure 4.3 the advantage of using low loadings in order to approach the maximal stoichiometry is seen. However, lowering the immobilisation response also lowers the binding response and thus a compromise often must be made.

4.4 Association kinetics.

The binding of ligate to immobilised ligand is expected to be described by the integrated rate equation possessing a single exponential term (equation 2.16). This is indeed the case at lower ligate concentrations. However, at higher ligate concentrations the association data are not well described by the single exponential equation but are well described by an equation containing two exponential terms shown in equation 4.2 below

$$R_t = A(1-\exp(-k_{on(1)}t) + B(1-\exp(-k_{on(2)}t) \qquad (4.2)$$

where the instrument response, R_t, varies with two apparent on-rates ($k_{on(1)}$ and $k_{on(2)}$) having extents of A and B respectively. This is illustrated in figure 4.4

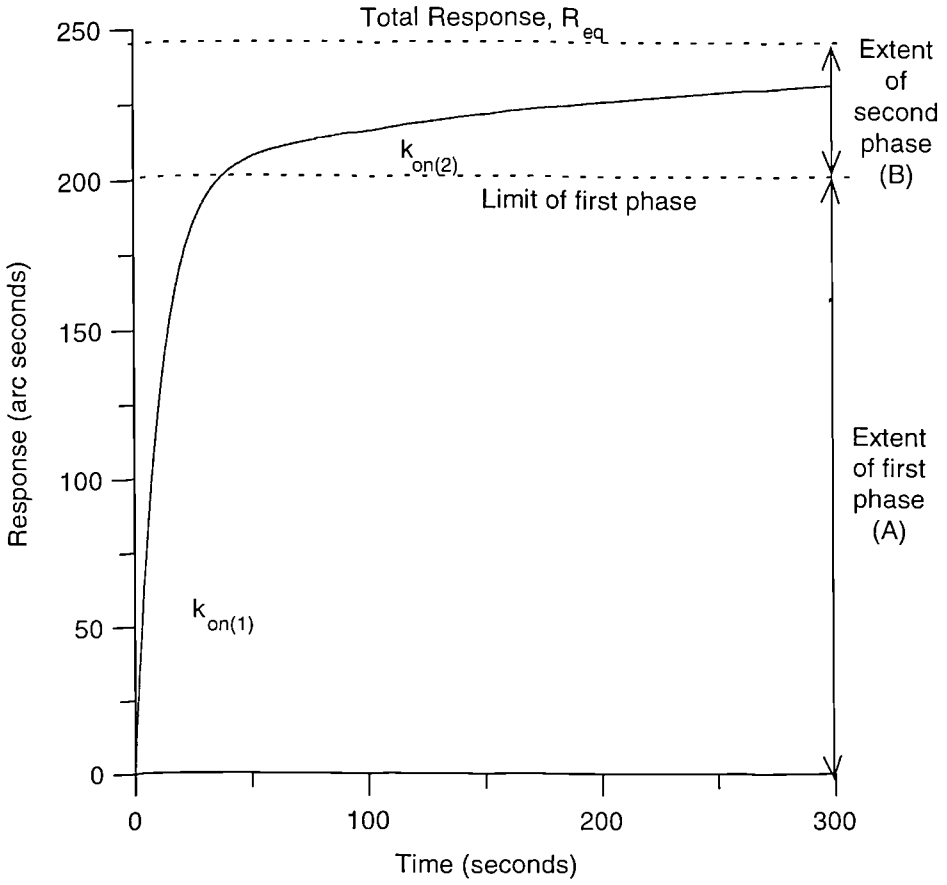

Figure 4.4: *A binding curve simulated by the use of a double exponential equation with an order of magnitude difference in on-rates ($k_{on(1)}>k_{on(2)}$). The extents of the two phases are shown on the figure.*

To illustrate this concentration dependence figures 4.5-4.7 show binding data at a high concentration of ligate fitted to both the single and double exponential equation together with the residual error plots. In addition, lower ligate concentration data are shown fitted to a single exponential equation. These biological systems used in these figures differ in their binding ratios such that HSA binding to immobilised anti-HSA mab has a 2:1 ratio (figure 4.5), anti-HSA mab binding to immobilised HSA has a ratio of 1:2 (figure 4.6), and CI-2 binding to immobilised chymotrypsin has a ratio of 1:1 (figure 4.7).

.

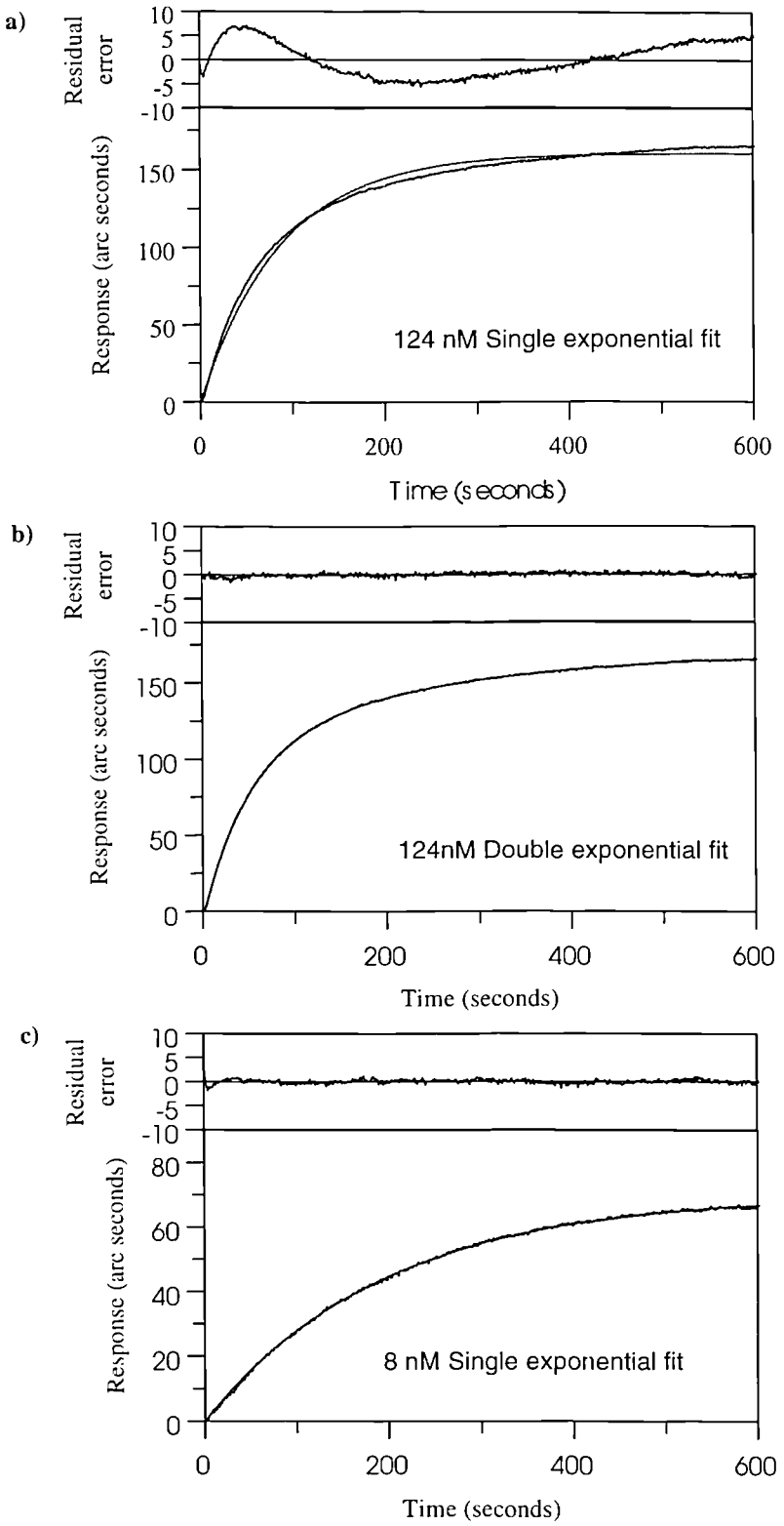

Figure 4.5: *The concentration dependence of the fit for anti-HSA mab binding to HSA immobilised on a CMD surface. a) shows the single exponential fit to 124 nM anti-HSA mab binding. b) the double exponential fit to 124 nM anti-HSA mab. c) single exponential fit to 8 nM anti-HSA mab. The residual error plots are shown above the fitted data for each fit.*

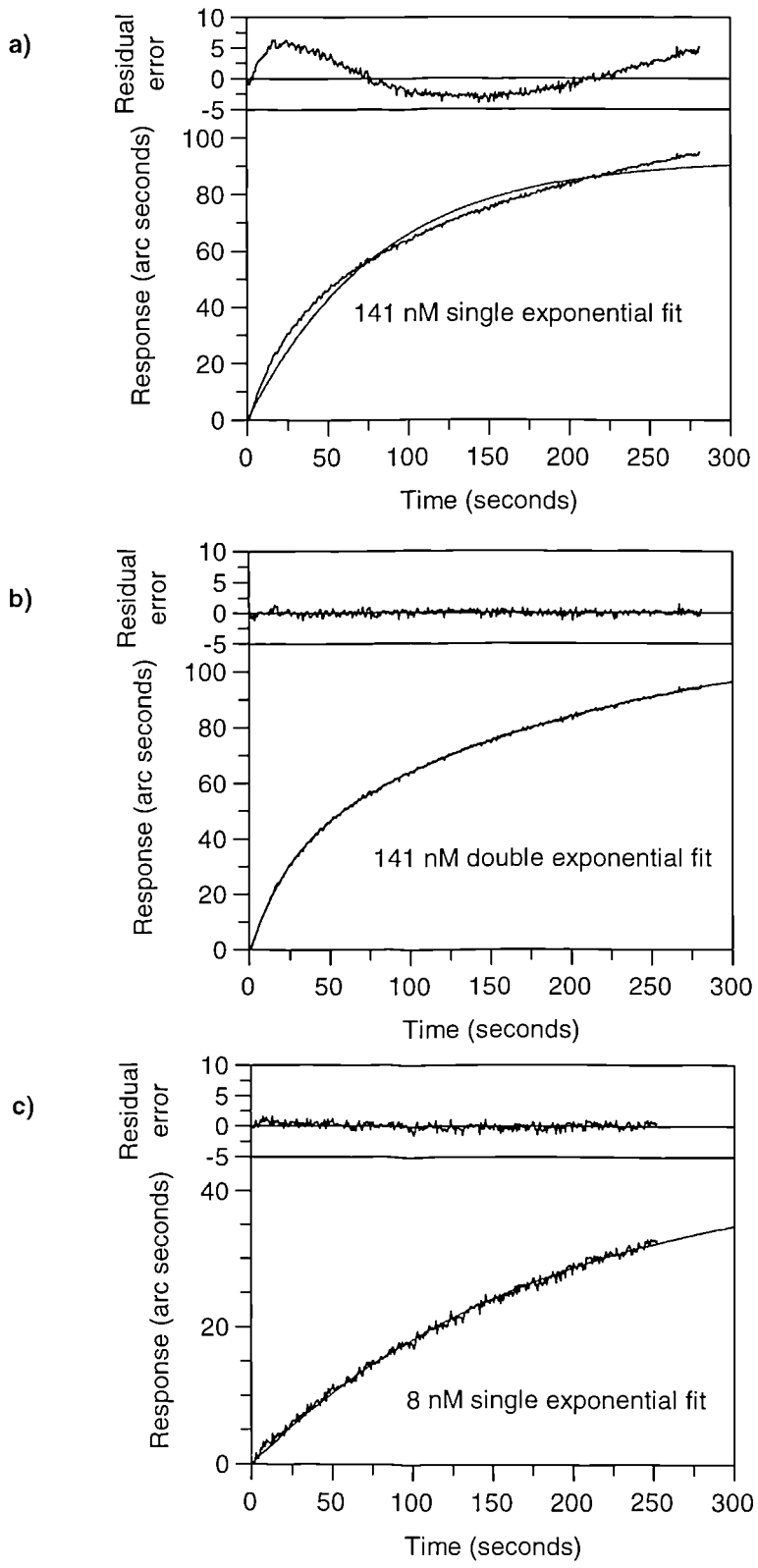

Figure 4.6: *The concentration dependence of the fit for HSA binding to anti-HSA mab immobilised on a CMD surface. a) shows the single exponential fit to 141 nM HSA binding. b) the double exponential fit to 141 nM HSA. c) single exponential fit to 8 nM HSA. The residual error plots are shown above the fitted data for each fit*

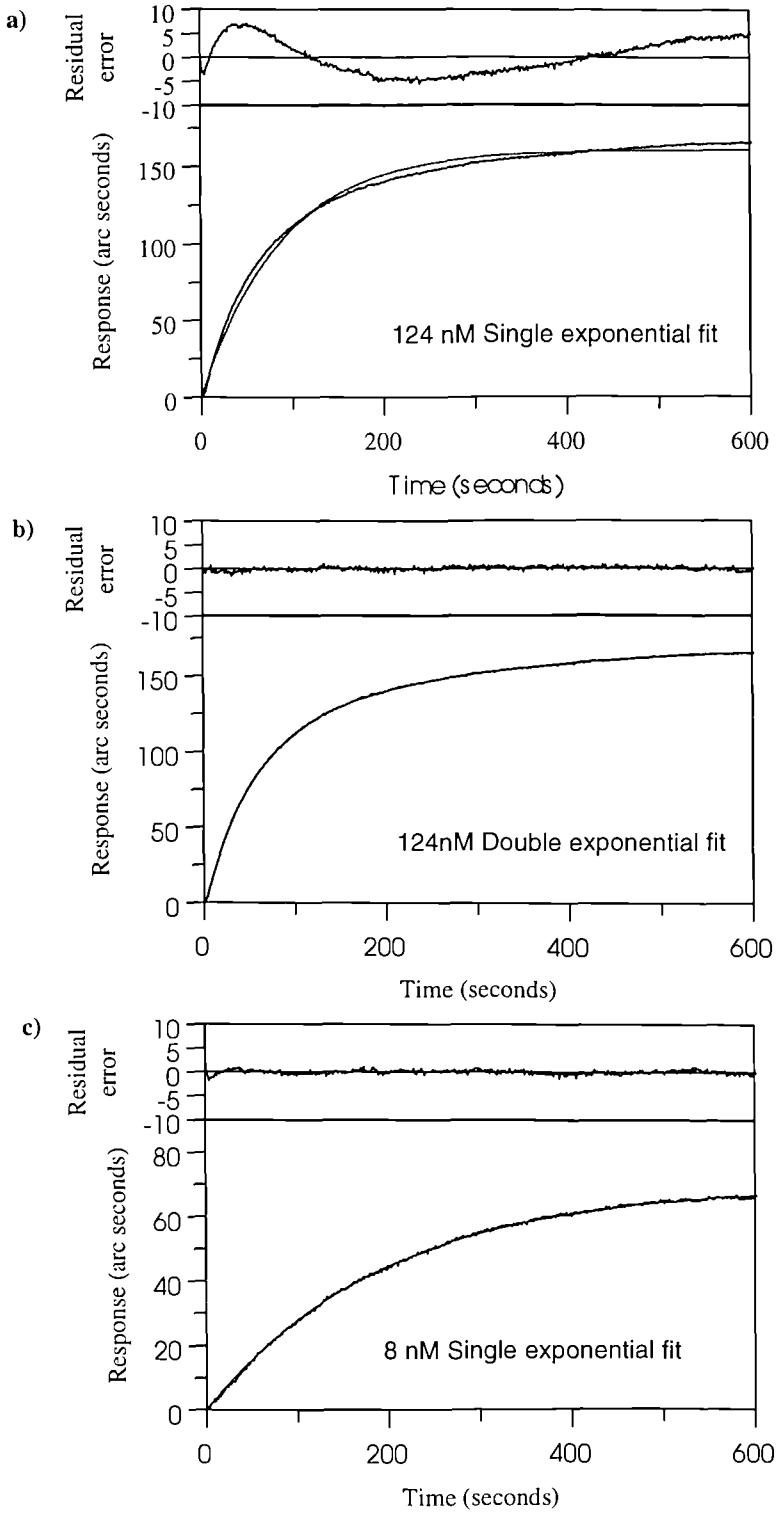

Figure 4.7: *The concentration dependence of the fit for CI-2 binding to chymotrypsin immobilised on a CMD surface. a) shows the double exponential fit to 124 nM CI-2 binding. b) the single exponential fit to 124 nM CI-2. c) single exponential fit to 8 nM CI-2. The residual error plots are shown above the fitted data for each fit*

For all these systems the overall trend was the same. At higher ligate concentrations the data were not well described by the single exponential equation (equation 2.16) but well described by an equation containing two exponential terms (equation 4.2). The k_{on} values derived from curve fitting were used to construct a secondary plot of k_{on} against ligate concentration. At low concentrations the k_{on} from the single exponential equation can be used. At the higher ligate concentrations, as the data are described by two apparent k_{on} values, it is necessary to determine which of these two values should be used. Figure 4.8 shows the kinetic plot for the interaction of CI-2 binding to immobilised chymotrypsin.

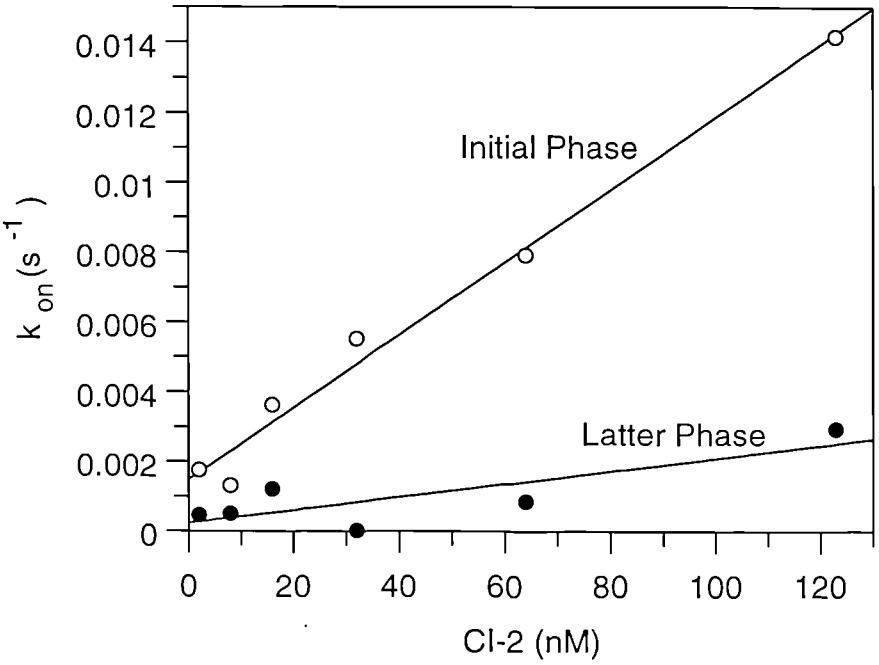

Figure 4.8: *The concentration dependence of the two on-rates determined by fitting the data for CI-2 binding to immobilised chymotrypsin from application of the double exponential equation.*

The slope of the line from the use of $k_{on(1)}$ values (initial phase) is steeper than that from the $k_{on(2)}$ (latter phase) and as a result the initial phase is more rapid than the latter phase.

It is possible to determine which of the two on-rate values should be used for the determination of kinetic constants by comparison was other techniques. The CI-2/chymotrypsin interaction has been studied in solution from the inhibition kinetics

(Longstaff et al, 1990) which revealed an association rate constant of 3.8 x 10^6 $M^{-1}s^{-1}$ and a dissociation rate constant of 6 x 10^{-3} s^{-1} and thus an affinity of 1.6 nM. To ensure that the CI-2/chymotrypsin interaction used in this study has similar reaction kinetics, the system was re-investigated monitoring hydrolysis of the substrate, succinyl-Ala-Ala-Pro-Phe p-nitrophenylanilidc. Binding of CI-2 results in inhibition, and so reduces the hydrolysis rate.

The initial rate (v) of substrate hydrolysis in M/s was plotted against CI-2 concentration (figure 4.9). Using equation 4.3 below the K_D (K_i) of the system was determined

$$v = v_0\left(1 - \frac{I}{(K_D + I)}\right) \tag{4.3}$$

where v_0 is the initial rate in the absence of CI-2, I is the concentration of CI-2, and K_D the dissociation equilibrium constant (affinity).

The resulting K_D must be adjusted to account for the substrate acting as a competitive inhibitor of the enzyme. When the CI-2 dissociates from the chymotrypsin, the substrate may bind preventing the CI-2 from rebinding. The correction factor is

$$1 + \frac{[S]}{K_M} \tag{4.4}$$

The concentration of the substrate was 0.1 mM and the K_M is 0.04 mM (DelMar et al., 1979) giving a corrected K_D of 1.84 nM.

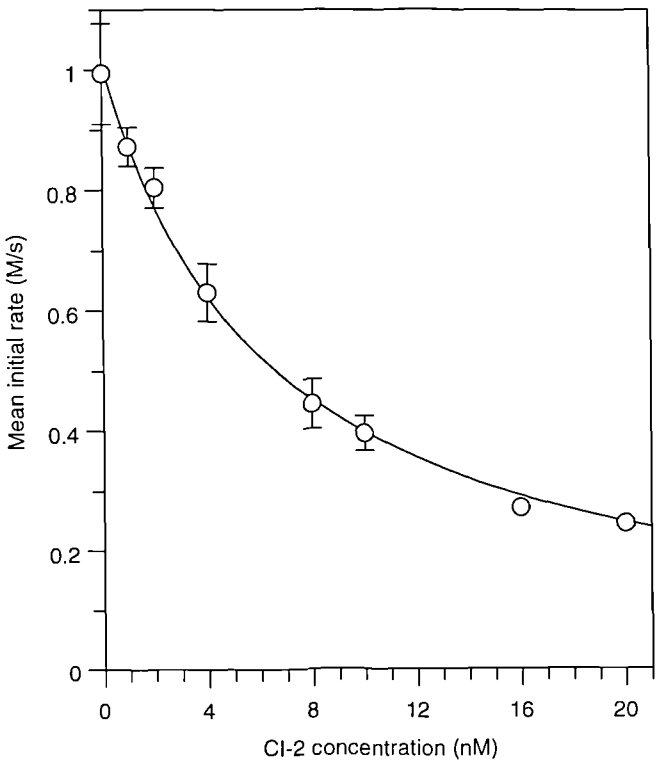

Figure 4.9: *The initial rate of succinyl-Ala-Ala-Pro-Phe-p-nitrophenylanilide hydrolysis by chymotrypsin in the presence of CI-2 with an enzyme concentration of 1 nM and a substrate concentration of 0.1 mM. The data represent a mean of three readings with the standard error of the mean shown. The solid curve is the best fit to the data using equation 4.3*

The dissociation rate constant was obtained by the addition of a concentrated premix of CI-2 and chymotrypsin. Dissociation of the CI-2 from the chymotrypsin was monitored as an increase in absorption at 412nm with time (figure 4.10). Non-linear regression analysis of the data to equation 4.5 (Longstaff et al., 1990) allows the k_{diss} to be calculated.

$$A = A_0 + \frac{k_{cat}[E]_0(k_{diss}t + \exp^{-k_{diss}t} - 1)}{k_{diss}} \qquad (4.5)$$

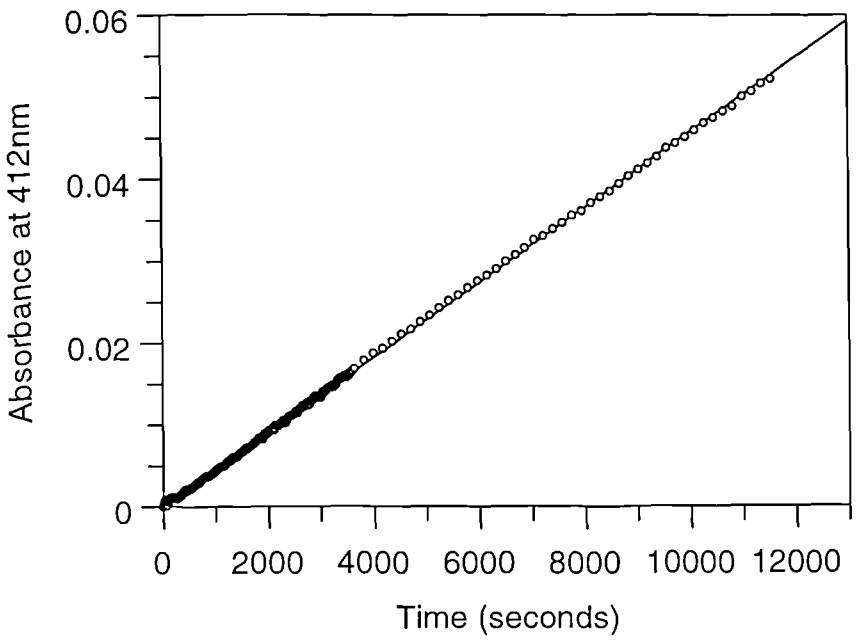

Figure 4.10 : *The recovery in absorbance with time from a preformed CI-2/chymotrypsin complex. The line represents the best fit of the data to equation 4.5*

Figure 4.10 shows the fit to the data using equation 4.5 with k_{cat} = 45 s^{-1} (DelMar et al., 1979) and the initial concentration of enzyme ($[E]_0$) = 100 nM giving a k_{diss} value of 8 x 10^{-3} s^{-1}. Combining this k_{diss} with the K_D determined from figure 4.9 gives a k_{ass} of 4.3 x 10^6 $M^{-1}s^{-1}$.

The association rate constant from IAsys is obtained from the slope of the secondary kinetic plot and as such can be used to determine which k_{on} value should be used to determine association kinetics. From the two slopes in figure 4.8 association rate constants of 3 x 10^5 $M^{-1}s^{-1}$ and 2 x 10^4 $M^{-1}s^{-1}$ were determined for the initial and latter phase respectively and clearly the $k_{on(1)}$ value is closer to that obtained from the spectroscopic experiment. It is therefore this on-rate that should be used in combination with the k_{on} value from single exponential fitting when determining rate constants from plots of on-rate against ligate concentration.

The binding curves for the interaction of ligate with immobilised ligand often fail to be adequately described by the expected integrated rate equation (equation 2.16) especially at higher ligate concentrations. At these higher concentrations the data are

fitted well be the inclusion of a second exponential term (equation 4.2). This trend is not a result of the binding ratio. The same concentration dependence is seen in figures 4.5-4.7 with differing binding ratios. When the data require fitting to equation 4.2 two rate constants are calculated. From comparison to a solution based technique, it is the first, rapid on-rate ($k_{on(1)}$) that should be used to construct the kinetic plot of on-rate against concentration. At the lower concentrations which are well fitted to the single exponential equation this on-rate should be used. It is therefore possible to construct the kinetic plot using on-rate values from both single (low ligate concentrations) and double (higher ligate concentrations) exponential equations.

4.5 Dissociation kinetics.

The dissociation of ligate from immobilised ligand initiated by the replacement of the ligate solution with buffer is expected to be described by a first order decay process (equation 2.18). This is, however, often not the case. There have been numerous reports of biphasic dissociation and incomplete dissociation (O'Shannessy et al., 1993. Bondeson et al., 1993. Rova et al., 1995). The dissociation data often show incomplete dissociation and are therefore better described by inclusion of an offset term into the dissociation equation (equation 2.24). The effect of including the offset is shown in figure 4.11 with data generated using equation 2.18 with an R_0 of 300 arc seconds and a k_{diss} of 5×10^{-3} s^{-1} (dotted line). The solid line shows the dissociation curve for the same R_o and k_{diss} but with an offset of 100 arc seconds generated by application of equation 2.24.

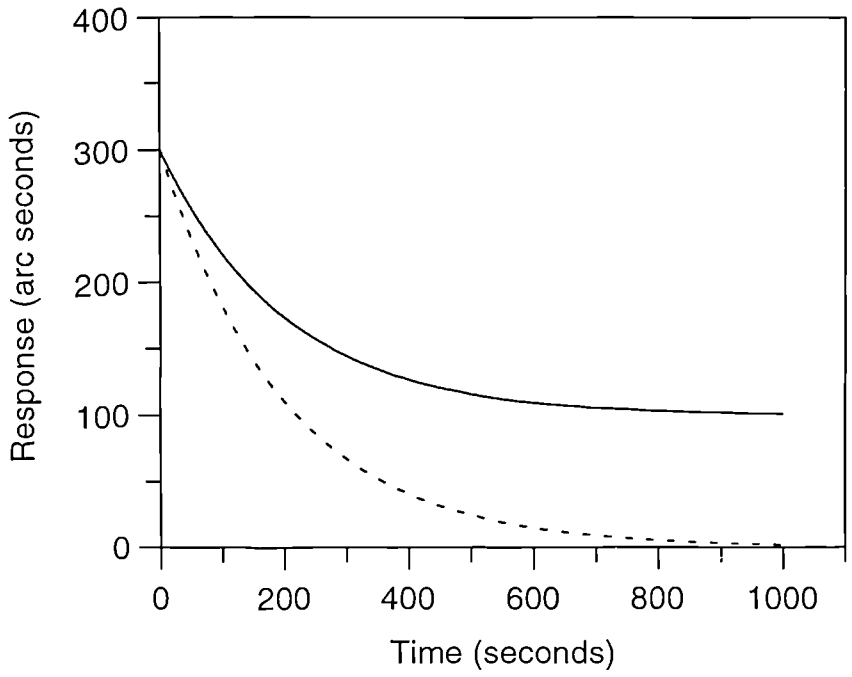

Figure 4.11: *Simulated dissociation data showing the effect of an offset value. The dotted line data was generated using equation 2.18 with a R_0 value of 300 arc seconds and a k_{diss} value of 5 x 10^{-3} s^{-1}. The solid line was generated using equation 2.24 using the same R_0 and k_{diss} values but with the inclusion of an offset term of 100 arc seconds.*

Another approach to fitting incomplete dissociation profiles is to assume that the incomplete dissociation is due to rebinding of the dissociated ligate. A situation further supported by data in 4.5.1. Under these circumstances it is possible to fit data using a second order dissociation equation which can allow for rebinding. This is described in greater detail in chapter 7.

4.5.1 The effect of free ligand in the dissociation buffer.

Hindered diffusion of the ligate from the immobilised ligand is thought to be an important factor in the deviation of dissociation profiles from the expected first order decay process. In order to reduce the possibility of rebinding, it is possible to include competing ligand within the dissociation buffer. This approach was investigated with two systems; chymotrypsin/CI-2 and FITC/anti-FITC mab.

4.5.1.1 Chymotrypsin/CI-2

In order to investigate rebinding, dissociation was performed in the presence of 1 mM chymotrypsin, and the dissociation profile compared with dissociation initiated with four washes of PBS/T and with a dissociation profile arising from washing every three minutes. Figure 4.12 shows a comparison of the dissociation profiles.

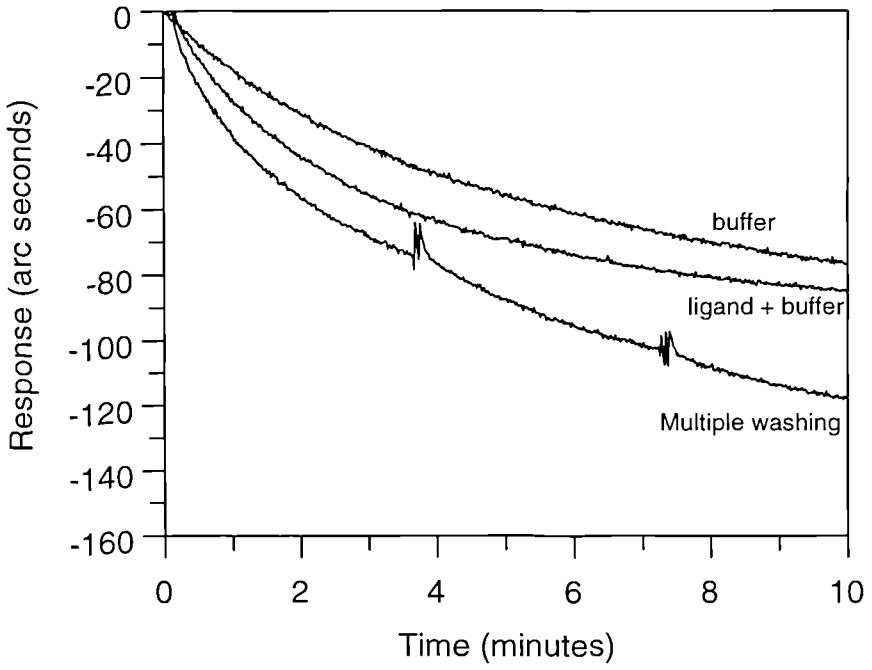

Figure 4.12: *The influence of multiple washing and the presence of free ligand in the dissociation buffer upon the dissociation of CI-2 from immobilised chymotrypsin. The time is taken from the start of dissociation such that the response at this time is 0. The binding response was 150 arc seconds.*

Both the data from multiple washing and that in the presence of chymotrypsin show a fast initial decrease in response with time compared to that in buffer. The buffer and the buffer containing ligand reach a constant response above the baseline. Multiple washing, however, allows the response to continue to decrease.

4.5.1.2 FITC/anti-FITC mab

Fluorescein isothiocyanate (FITC) was immobilised to CMD surfaces and the effect of differing concentrations of fluorescein (sodium salt) upon the dissociation rate of FITC mab from the immobilised FITC was monitored. Figure 4.13 shows the dissociation profiles obtained in the presence of differing fluorescein concentrations. The dissociation rate constants derived from curve fitting to a single exponential with and without an offset and to a second order equation (second order analysis is explained in detail in chapter 7) are plotted in figure 4.14.

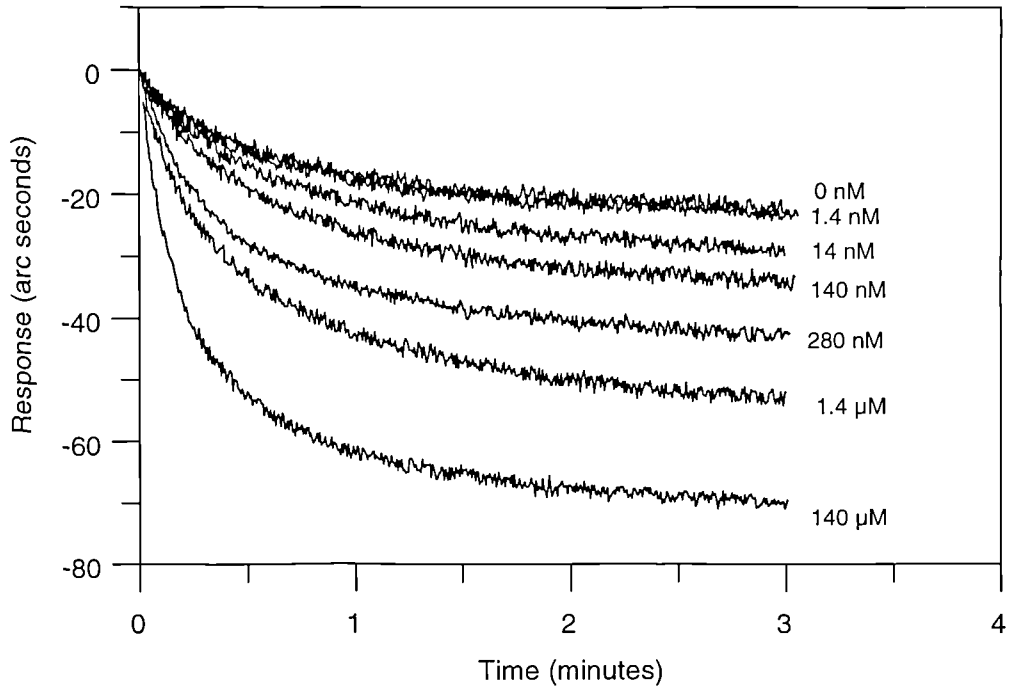

Figure 4.13: *The dissociation of anti-FITC mab from CMD immobilised FITC in the presence of differing concentrations of fluorescein (Na salt).*

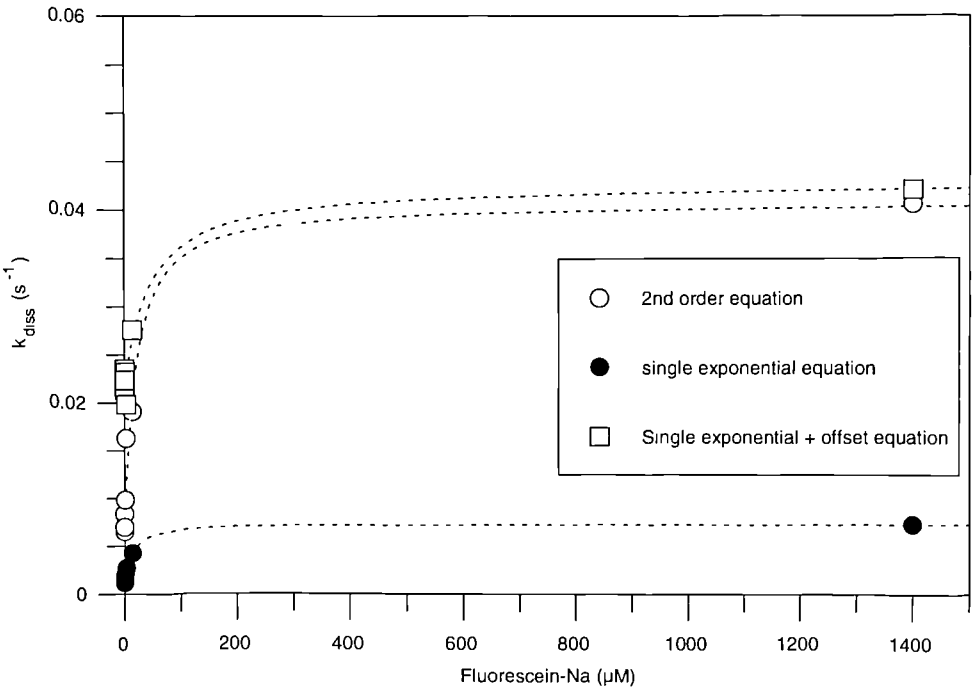

Figure 4.14: *The dissociation rate constant derived from data in figure 4.13 by using a single exponential dissociation equation with and without an offset, together with second order analysis.*

It has been proposed that in certain instances the valencey of the interaction influences the manner of dissociation (MacKenzie et al., 1996. O'Shannessy et al., 1993. Malmborg et al., 1992). While the valency is important, this does not account for the biphasic nature of the CI-2 dissociation.

The maximum dissociation rates determined from both the second order equation and the single exponential equation with an offset value are similar with values of 3.95 x 10^{-2} s^{-1} and 4.1 x 10^{-2} s^{-1} respectively. However, the later equation returned a high dissociation rate in the absence of fluorescein-Na thus affecting the total increase in dissociation rate constant observed. For the single exponential equation with an offset a two-fold increase was seen whereas for the second order equation an change from 6 x 10^{-3} s^{-1} to 3.95 x 10^{-2} equates to almost a ten-fold increase.

The dissociation curves are often poorly fitted using the first order decay equation (equation 2.18) but can be well described by the inclusion of an offset term within the

equation (equation 2.23). Data obtained by including a competing ligand within the dissociation buffer, or repeated buffer replacements, causes the dissociation to become closer to completion. Therefore when determining dissociation kinetics it is advisable to include competing ligand in the dissociating buffer or to use only the initial portion of data for conventional first order analysis with equation 2.18.

4.6 Saturation (binding) isotherms.

The equilibrium IAsys response can be used to construct a plot of equilibrium response (R_{eq}) against ligate concentration ([L]) from which the K_D can be calculated by application of equation 2.22. Linearisation of this isotherm can be achieved by plotting the $R_{eq}/[L]$ against [L], the slope of which is equal to $-K_A$ according to equation 2.21. An example of both these approaches is shown in figure 4.15

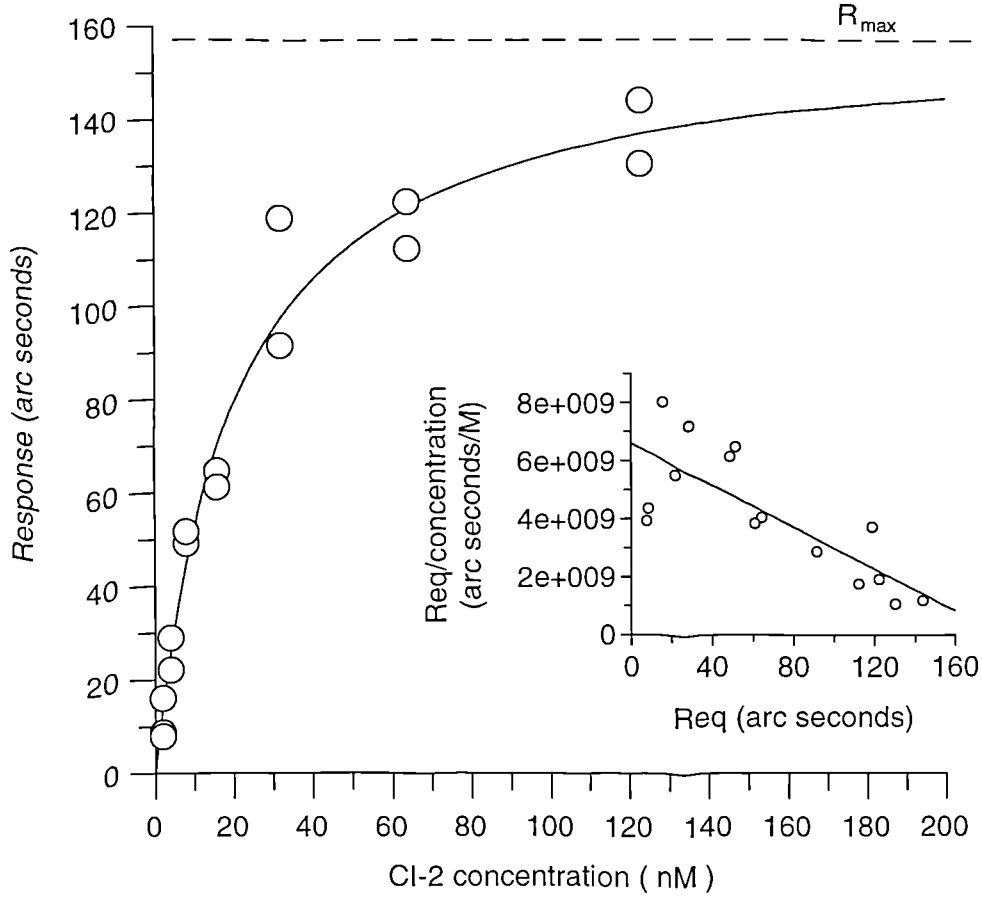

Figure 4.15: *Typical plot of equilibrium response of CI-2 binding to immobilised chymotrypsin. The solid line shows the best fit curve to the data (equation 2.22), and a Scatchard plot of the same data is inset.*

4.7 Effect of ligand loading.

The effect of ligand loading upon the kinetic and equilibrium constants for the interaction of CI-2 with CMD immobilised chymotrypsin was investigated. Chymotrypsin was immobilised at differing concentrations in order to achieve differing immobilisation responses. The loadings obtained at each of the concentrations are shown figure 4.16 with a concentration range of 2 to 2500 μg/ml giving a loading range of 333 to 1110 arc seconds. The graph resembles a saturation curve with a plateau region above 500 μg/ml or about 1000 arc seconds.

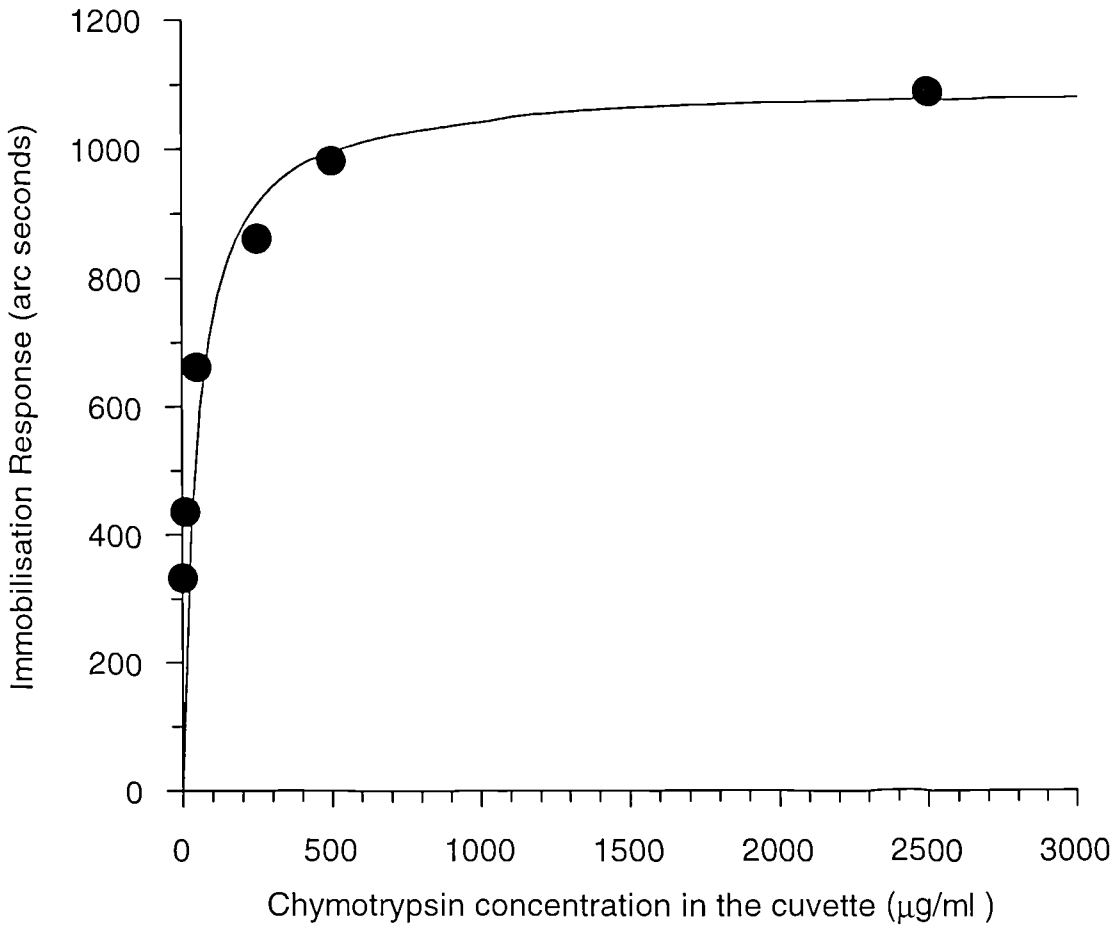

Figure 4.16: *Amount of chymotrypsin immobilised to the CMD surface measured as biosensor response in arc seconds as a function of the initial chymotrypsin concentration.*

The highest loading represents a binding capacity of 300 arc seconds whereas the lowest has a capacity of 60 arc seconds.

4.7.1 Effect of ligand loading upon the association rate constant.

The association rate constant was determined by plotting a kinetic plot for six CI-2 concentrations at each loading level. Data were fitted to both the single and double exponential equations with the best fit determining which of the on-rates used in the kinetic plot. At the higher concentrations the data were fitted well with the double exponential equation and therefore $k_{on(1)}$ was used.

From plots of on-rate against CI-2 concentration at the different loadings the effect of loading upon the association rate constant was determined. Figure 4.17 shows that a plateau is observed at lower loadings while at higher loadings there is a decrease in the rate constant.

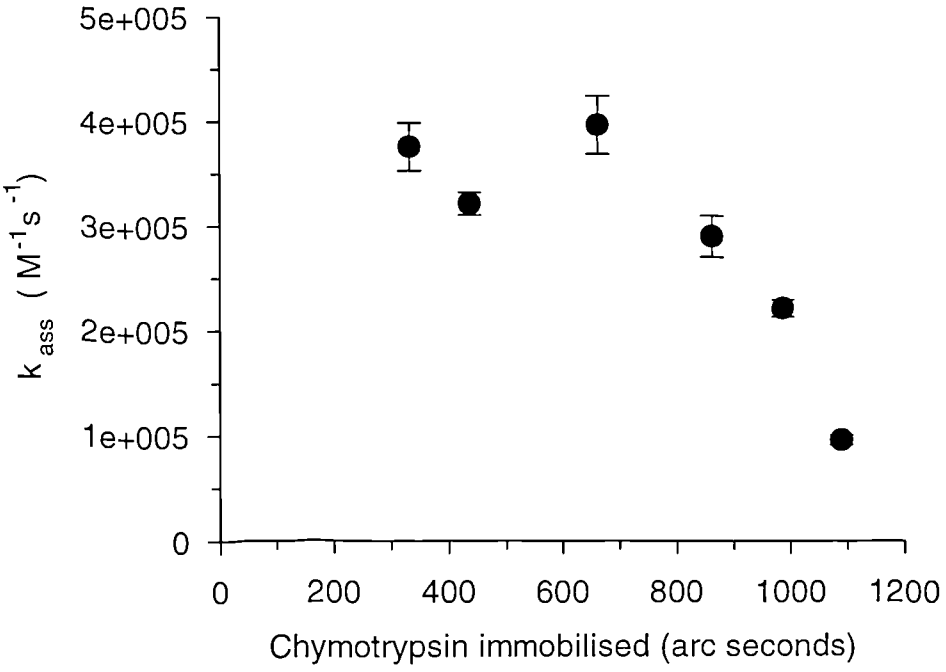

Figure 4.17: Effect of ligand loading upon the association rate constant for the interaction of CI-2 with immobilised chymotrypsin. The rate constants were estimated in duplicate at each CI-2 concentration for each chymotrypsin loading.

4.7.2 Effect of ligand loading upon the dissociation rate constant.

It should be possible to determine the influence of loading upon the dissociation rate constant by plotting the intercept of the kinetic plot against loading. However, given the high errors associated with the determination of the dissociation rate constant in this manner the direct fitting of the dissociation data was preferred (equation 2.18).

Dissociation from the higher CI-2 concentrations of 124,64, and 32 nM was used in duplicate so that there are six replicates for each loading level. The effect is shown is shown in figure 4.18 with the dissociation rate constant decreasing above a loading of 800 arc seconds from 7 x 10^{-3} s^{-1} to 4 x $10^{-3}s^{-1}$.

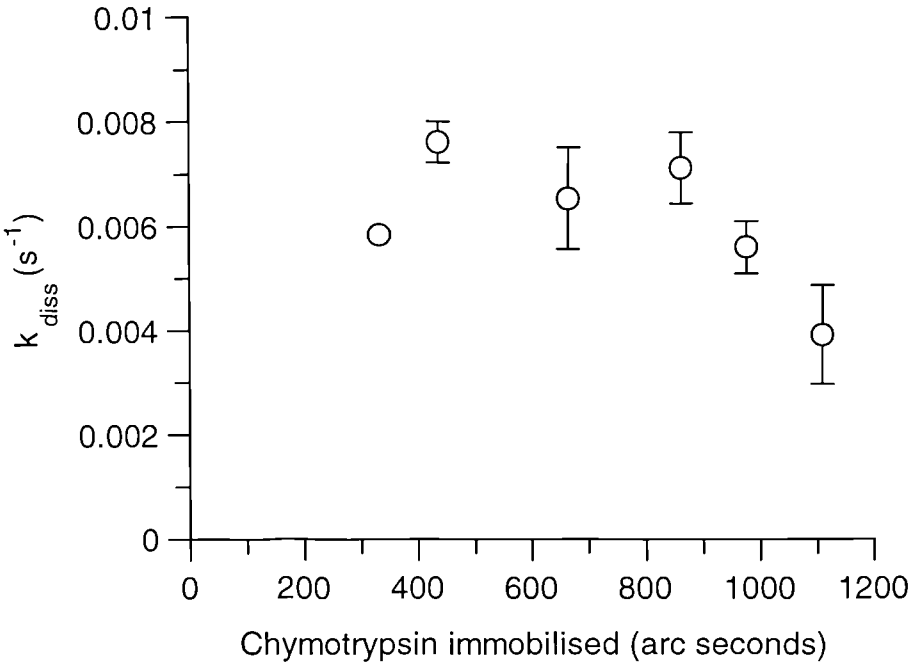

Figure 4.18: *The effect of ligand loading upon the dissociation rate constant for the interaction of CI-2 from immobilised chymotrypsin. The values are the means of the dissociation rate constants determined from three different CI-2 concentrations (124, 64,32 nM) in duplicate by application of equation 2.18.*

4.7.3 Effect of ligand loading upon the dissociation equilibrium constant.

The dissociation equilibrium constant can be determined in two ways. Firstly as a simple ratio between the dissociation rate constant to the association rate constant. Secondly from a binding isotherm showing the equilibrium response against concentration such as figure 4.15. The K_D determined from the isotherm plotted against loading level is shown in figure 4.19.

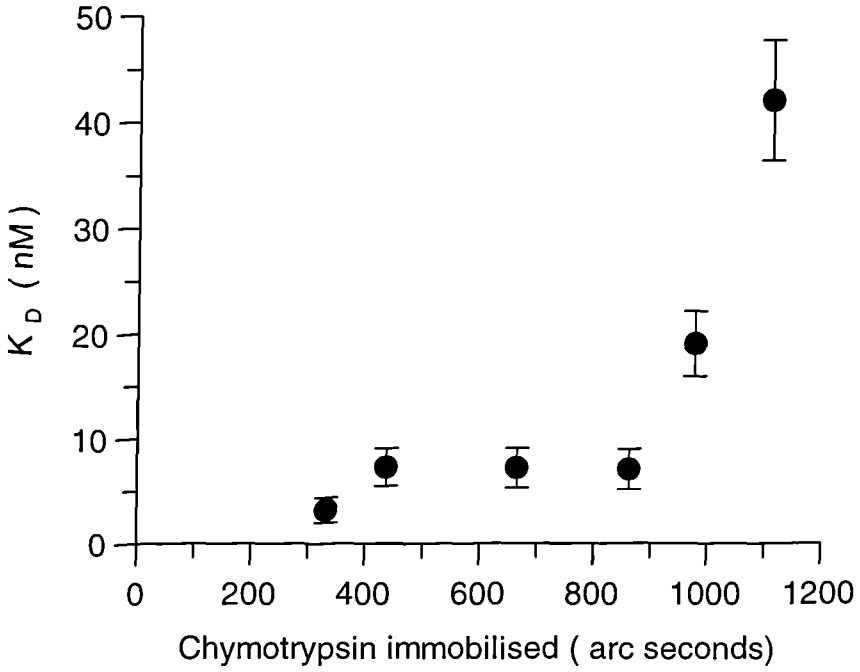

Figure 4.19: *Effect of chymotrypsin loading within the CMD matrix upon K_D determined from isotherm plots such as figure 4.18 for CI-2 binding.*

4.7.4 Effect of ligand loading upon the extents obtained from curve fitting

The extent of the second phase (B) from curve fitting of the 124 nM and 15 nM CI-2 with the double exponential equation is shown in figure 4.20 as a function of ligand loading. The extent is expressed as a percentage of the total extent (A+B). For the lower concentration of 15 nM the percentage extent of the second phase is around 40 % and largely unaffected by the loading. In contrast, the contribution of the second phase for the 124 nM CI-2 concentration increases with increasing loading from 40% to 90%.

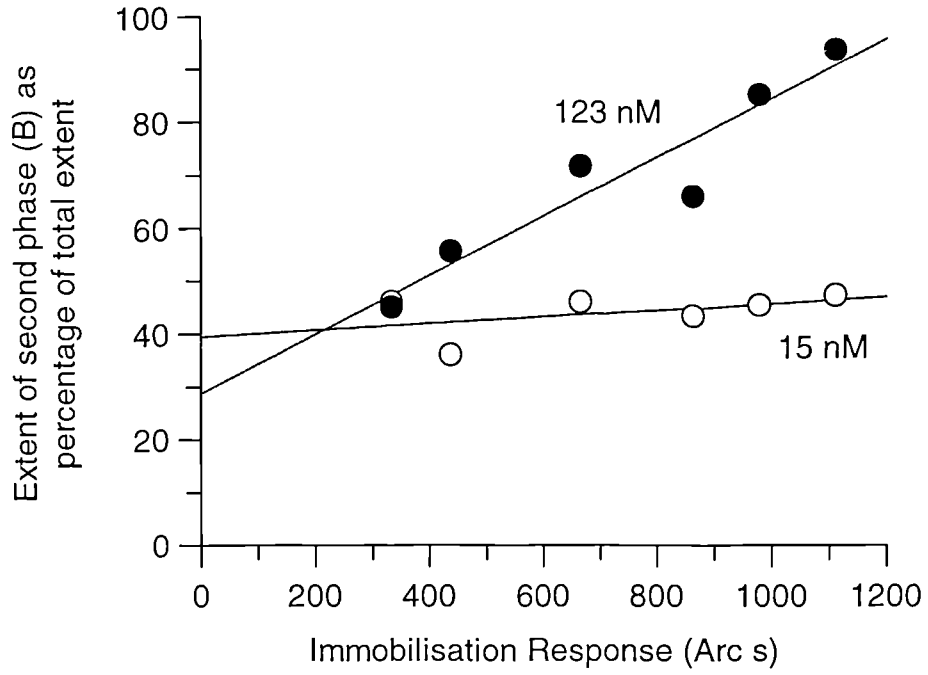

Figure 4.20: *Variation in the contribution of the extent of the slow association phase as a percentage of the total response for the interaction of CI-2 with differing loadings of chymotrypsin. The open circles represent data from the interaction of 15 nM CI-2 while the solid circles represent 124 nM CI-2.*

Ligand loading has a profound influence upon both the kinetic and equilibrium constants determined using a CMD matrix on the IAsys instrument. The effect on the association rate constant is shown in figure 4.17 with a plateau value of around 4 x 10^5 $M^{-1}s^{-1}$ while at higher loadings lower values are measured. At the higher loading of 1110 arc seconds the apparent rate has dropped by a factor of four. The dissociation rate constant determined from curve fitting of the CI-2 data reveals that at the higher loadings the dissociation rate constant decreases (figure 4.18). This is probably due to the rebinding of the CI-2 within the CMD matrix. The K_D determined from the isotherm plot also shows a dependence (figure 4.19) with the highest K_D observed at higher loadings.

4.8 Discussion.

In the case of all the biological systems studied the binding of low ligate concentrations are well described by an equation containing a single exponential term. At higher ligate concentrations the association data are better fitted by the inclusion of a second exponential term. There have been several recent publications highlighting this deviation (Edwards et al., 1995, 1997. Morton et al., 1995., Khilko et al., 1993). O'Shannessy and Winzor, (1996) highlighted the possible causes of the apparent biphasic nature of biosensor data. They cited that the factors expected to cause this biphasic nature included (a) Mass transport (b) Valency considerations (c) Immobilised ligand density (d) Inhomogeneity of either the ligand or ligate (e) Immobilisation chemistry (f) Rebinding, Parking problems and Volumetric effects. While it is recognised that valency considerations are important in the application of the pseudo first order equation, this is unlikely to be the major cause of the deviation observed. It is also unlikely that either the ligand or the ligate were heterogeneous in nature prior to use as all reagents were greater than 90% pure. The experiments designed to illustrate the concentration dependence in the fitting were performed at low immobilisation levels at the maximum stir rate in order to eliminate or substantially reduce mass transport effects.

4.8.1 Proposed models for biphasic association curves.

4.8.1.1 Binding involves more than a single step.

Some authors have proposed that the binding of ligate to immobilised ligand involves more than a single step such as isomerisation (Fisher et al., 1994. Morton et al., 1994). It is possible that the biphasic instrument response could reflect an event after the initial binding. For example the ligand, ligate or surface may undergo a conformational change resulting in a change in refractive index as described by equation 4.6

$$G + L \underset{k_{-1}}{\overset{k_1[L]}{\rightleftharpoons}} GL \underset{k_{-2}}{\overset{k_2}{\rightleftharpoons}} (GL)' \qquad (4.6)$$

Alternatively the ligand or the surface may undergo a change prior to binding in order to expose hidden binding sites described by equation 4.7

$$G + L \underset{k_{-1}}{\overset{k_1}{\rightleftharpoons}} GL \underset{k_{-2}}{\overset{k_2[L]}{\rightleftharpoons}} (GL)' \qquad (4.7)$$

The two mechanisms can be distinguished by the concentration dependence of the second phase. For the chymotrypsin/CI-2 interaction there is a slight concentration dependence in the rate of the second phase with an increase in ligate concentration causing an increase in the rate. Clearly this is inconsistent with equation 4.7 in which the rate of the second phase should decrease with increasing ligate concentration. It is however consistent with equation 4.6. Equation 4.6 predicts that the events after the initial binding are responsible for the second phase and not due to slow binding of later ligate. The linear relationship between the cpm and instrument response demonstrated in figure 4.2 suggests that the kinetic scheme in equation 4.6 is not correct as the amount bound from cpm reflects both the first and second phases and not just the first initial phase.

4.8.1.2 Heterogeneity of the immobilised ligand.

The presence of more than one type of binding site caused by a heterogeneous ligand (Khilko et al., 1995. O'Shannessy et al., 1993) could occur given the nature of the immobilisation procedure. The random nature of the EDC/NHS coupling through lysine groups within the ligand would be expected to produce immobilised ligand with differing affinities. For example if two different binding sites were present then two distinct phases would be observed with the magnitude of the two phases reflecting the relative proportions of the two populations. In the reaction scheme in equation 4.8 the two classes of ligand are denoted G and G' with the rate of ligate binding to each of the classes given by k and k' respectively.

$$G + L \underset{k_{-1}}{\overset{k_1[L]}{\rightleftharpoons}} GL \qquad G' + L \underset{k_{-1}'}{\overset{k_1'[L]}{\rightleftharpoons}} G'L \qquad (4.8)$$

At low ligate concentrations only the high affinity sites would be occupied and so a single exponential curve could fit the data provided that the difference in the affinity of the two sites were substantially different. At high ligate concentrations all sites would be occupied and therefore show biphasic kinetics. Recently, the influence of the random coupling of the EDC/NHS reaction has been proposed to account for data failing to conform to a model assuming binding homogeneity. Oddie et al (1997) showed that the data from anti-ferritin Fab' fragments binding to immobilised ferritin followed the expected homogeneity model. However, when the ferritin molecule was dissociated to its subunit dimer possessing one Fab binding site prior to immobilisation the binding data showed significantly deviation from the homogeneous model. This difference was ascribed to the ferritin molecule having 12 anti-ferritin Fab' binding sites per molecule and thus the immobilisation procedure had little effect on the majority of free binding sites. In a further paper, Kortt et al (1997) compared the affinity for an anti-viral neuraminidase antibody for the anti-idiotype 11-1G10 antibody. In order to eliminate antibody bivalency monovalent Fab fragments and recombinant scFvs were used. It was found that immobilisation of the 11-1G10 fragments reduced the affinity for NC41 compared to site directed immobilisation via C-terminal thiol residue and from solution equilibrium measurements using the biosensor to determine the concentration of free ligate. When the NC41 fragments were immobilised through amine groups the affinity for 11-1G10 was retained. The authors suggest that the non-specific immobilisation through amine groups close to the active site of the 11-1G10 reduced the affinity.

4.8.1.3 Steric hindrance/Parking problem

Steric hindrance caused by the binding of ligate to immobilised ligand at the limits of the CMD would be expected to prevent ligate from entering the CMD or reduce the rate at which the ligate diffuses through the CMD matrix. This may therefore give a

more constrained environment than in free solution. The steric hindrance can be directly observed from the change in stoichiometry of HSA binding to anti-HSA mab as illustrated in figure 4.3. At the high immobilisation levels a stoichiometry of 0.5 is observed. Only by reducing the immobilisation response can a stoichiometry close to that expected in solution be determined. Furthermore, figure 4.20 shows the contribution of the second phase is dependant upon the loading of the ligand with a contribution to the overall extent being an extrapolated value of 30% at 0 loading to 90% at the highest loading. This is also in agreement with the proposal of steric hindrance which would be expected to be exaggerated at higher loadings.

This hindered access would be expected to affect the rate and equilibrium constants derived from the sensor with the effect exacerbated at higher loadings. Figures 4.17-4.19 support this hindered access proposal.

A schematic diagram can therefore be constructed illustrating the steric hindrance within the CMD matrix. The ligand could be immobilised such that its ligate binding site is inaccessible or the CMD matrix or an adjacent occupied ligand site may restrict access, or the ligand binding may be unhindered (Figure 4.21) (Edwards et al., 1995,1997)

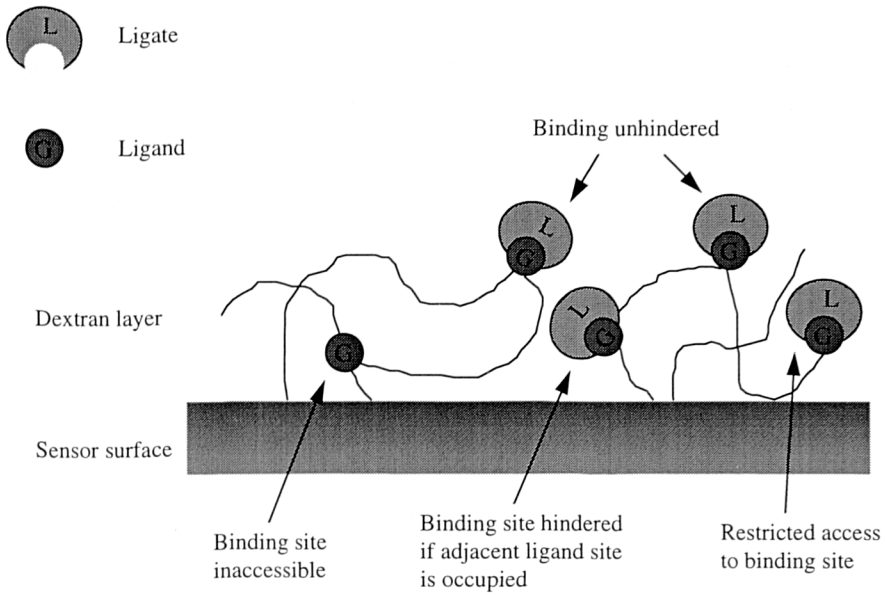

Figure 4.21: *Schematic diagram showing some of the processes that may contribute to the observed kinetic behaviour when ligate binds to ligand immobilised on CMD. Binding may be unhindered by the CMD; alternatively, the binding site may be inaccessible or present restricted access. In addition, the binding of ligate at one site may occlude binding at other sites*

Chapter 5

Mass transport

5.1 Introduction

The interaction of two reactants is governed by the rate at which they come into contact and the rate at which specific binding occurs. When two or more processes occur, the measured rates will be limited by the slowest. Therefore, if the diffusion of the two reactants together is the slowest step then only the diffusion rate will be measured. In such circumstances the reaction is described as diffusion limited. However, if the specific binding events are rate limiting, then the measured rate will reflect that of the specific binding reaction. In this reaction limited situation the transport of reactants is faster than the consumption. Between these two extremes lie reactions that are termed diffusion influenced.

For most antibody/antigen interactions the rate of association is significantly less than the diffusional association rate ($\approx 1 \times 10^9$ $M^{-1}s^{-1}$) with values between 0.5-5 x 10^6 $M^{-1}s^{-1}$ (Náray-Szabó., 1993) and hence measured rates tend to be reaction limited. This situation is, however, not always true. For example, electrostatic interactions can significantly alter the measured rates (Novotny and Sharp., 1992). Just as the measured association rate constant can be affected by diffusion so can the measured dissociation rate constant. If the transport of the dissociating reactant away from its binding partner is slower than the rate of dissociation then there is the possibility of rebinding. This would have the effect of slowing the measured dissociation rate constant.

When one reactant is attached to a solid surface its diffusion coefficient is reduced to zero and thus only the solution reactant is free to diffuse. This results in a higher probability that diffusional control will operate. There have been numerous investigations into diffusion at the macromolecular level on cell surfaces (Model and Omann., 1995. Berg and Von Hippel, 1985. Shoup and Szabo, 1982) and on solid surfaces such as ELISA plates (Nygren and Stenberg., 1985. Stenberg et al., 1986). For example, Nygren et al., (1987) have shown that the initial binding of antibody to immobilised antigen was diffusion limited and that the dissociation rate constant could be increased with stirring. Stenberg and Nygren (1985) demonstrated that stirring maintains a constant concentration above the surface resulting in an increase in the amount of adsorbed protein to the surface. On solid surfaces there is a 'stagnant'

layer through which the binding partner must cross in order to bind. The partner must diffuse through this layer prior to binding and thus its thickness has a great influence upon the measured binding rates. On ELISA plates this layer has a thickness of around 50μm (Stenberg and Nygren., 1985) but can be reduced with stirring. The thickness of the unstirred layer can be determined using Ficks second law of diffusion by monitoring the initial rate or flux of binding, J, and combining equations 5.1 and 5.2 below (Eddowes., 1987)

$$J = K_{diff}(c_{sol.} - c_{surf.}) \tag{5.1}$$

where

$$K_{diff} = \frac{D}{x} \tag{5.2}$$

in which c_{sol} and c_{surf} are the concentrations (g/m^3) of ligate in solution and on the surface respectively, D is the diffusion coefficient (m^2/s) , and x is the unstirred layer thickness (m). From these units, the initial rate of binding/adsorption should be in $g/m^2/s$. For this calculation it is assumed that the concentration of the ligate in solution is in excess over that on the surface. In addition, the surface is assumed to behave as an infinite sink such that every surface contact causes an attachment and that no steric constraints are operating.

Other insights into the influence of mass transport can be obtained by examining another parameter. The Damkoehler number is the ratio of the maximum reaction rate to that of the diffusional transport rate through a water film of thickness R (Stenberg et al., 1986)

$$Da = \frac{Rk_{ass}\Gamma_0}{D} \tag{5.3}$$

Where Γ_0 is the total surface concentration of binding sites. The lower the Damkoehler number the less the reaction is influenced by mass transport.
Stirring or flow lowers the 'stagnant' layer thickness by increasing the efficiency of transport to the surface-attached reactant and hence lowers the Damkoehler number.

Both the IAsys and Biacore instruments use a hydrogel matrix and attachment to the CMD layer no longer reduces the diffusional coefficient of the immobilised reactant (ligand) to zero (Karlsson et al., 1994). The hydrogel matrix acts as a flexible anchorage for the ligand. This flexibility causes the diffusional coefficient to be greater than that expected from attachment to a solid surface but lower than achieved in free solution. However, an unstirred layer still exists and can therefore play an important role in the determination of kinetic parameters. The situation is further complicated by the additional diffusion through the hydrogel prior to binding. If the kinetic rates determined by IAsys are to be directly comparable to solution the mass transport of the ligate to the immobilised ligand must be appreciably faster than the binding. This chapter investigates how mass transport can be detected in IAsys data and ways in which it can be substantially reduced. Comparison with flow based sensors such as the BIAcore instrument together with ELISA technology will be made.

5.2 Effects of mass transport upon association data.

The influence of mass transport on experimental data can be observed in several ways and are illustrated below.

5.2.1 Non-linear derivative plots.

In chapter 2 a derivative equation describing the rate of complex formation with time (dR/dt) was derived (Equation 10). Karlsson et al. (1991) used this to calculate k_{on} by plotting dR/dt against R. A constant binding rate is indicative of a mass transport limited reaction and this is shown by a plateau region prior to the expected decrease in slope (Glaser, 1993). The transformation from a mass transport to a reaction limited situation is not abrupt and between these extremes a positive curvature may be observed reflecting partial mass transport conditions. This is illustrated in figure 5.1

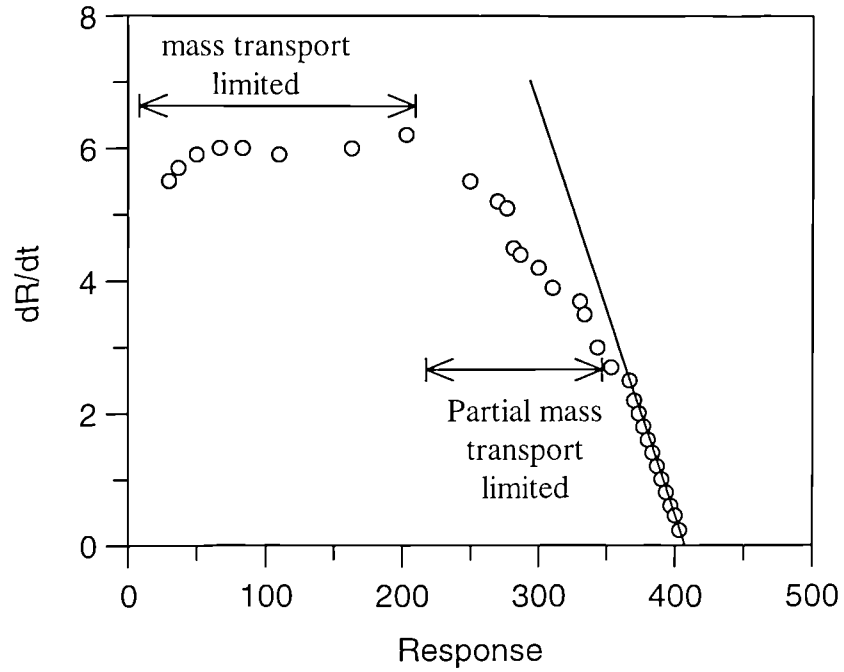

Figure 5.1: *A plot of the rate of change of response (R) with time (t), (dR/dt), against Response. Mass transport limited conditions are seen between response values of 0 to 200 arc seconds with a constant binding rate. There is then a gradual approach to reaction limited conditions shown by the straight line through the latter data points.*

5.2.2 Sigmoidal binding curves

The influence of mass transport can, depending upon its magnitude, be seen in experimental data as a linear portion of the binding curve. This linear portion prior to binding causes the binding curve to appear sigmoidal. This is, however, often difficult to observe in typical experiments.

5.2.3 Lower k_{on} values

As mass transport limiting conditions cause a lowering of the association rate constant, performing the experiment under different conditions, such as varying ligand immobilisation levels, will change the association rate constant. When plotting the pseudo first-order rate constant, k_{on}, against ligate concentration, this will be seen as an change in slope (figure 5.2).

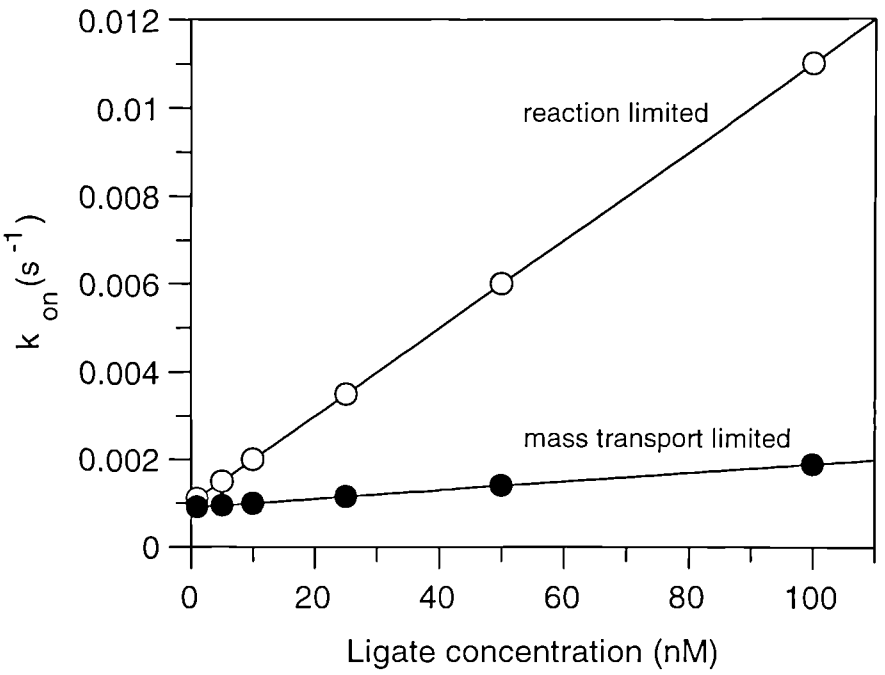

Figure 5.2: *The influence of mass transport upon the pseudo-first order rate constant.*

5.3 Experimental investigation into mass transport .

The assumption that the rate of binding measured by IAsys is that of the intrinsic binding and not the mass transport limited rate is paramount in the determination of kinetic constants. With this in mind, a detailed investigation was instigated using the previously discussed methods to detect mass transport in experimental data.

5.3.1 The influence of stirring

IAsys ensures efficient mixing within the cuvette well by the use of a stainless steel stirrer. This vibro-stirrer vibrates vertically at 126 Hz and is illustrated in figure 5.3. The amplitude can be selected by the user, with a setting of 100 being the maximum.

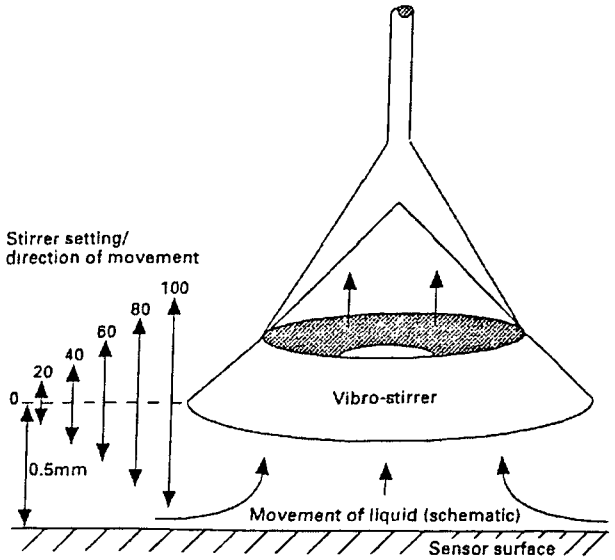

Figure 5.3: *The vibro-stirrer: The stirrer vibrates at a fixed frequency with the user able to determine the amplitude.*

The efficiency of this vibro-stirrer is therefore paramount in measuring interaction kinetics and thus its suitability was investigated.

If the binding rate is diffusion limited then a faster, more efficient delivery of ligate to immobilised ligand will increase the binding rate. Binding rates will therefore be unaffected by varying the stir rates (amplitudes) provided the reaction is not diffusion limited. Figure 5.4 shows the effect varying the stir rate has upon the k_{on} values determined for the binding of CI-2 to immobilised chymotrypsin on a CMD surface. At low stir rates the k_{on} is low but reaches a constant k_{on} value at stir rates above 60 The initial rates of binding also follow the same trend with a plateau after a setting of 60 (data not shown)

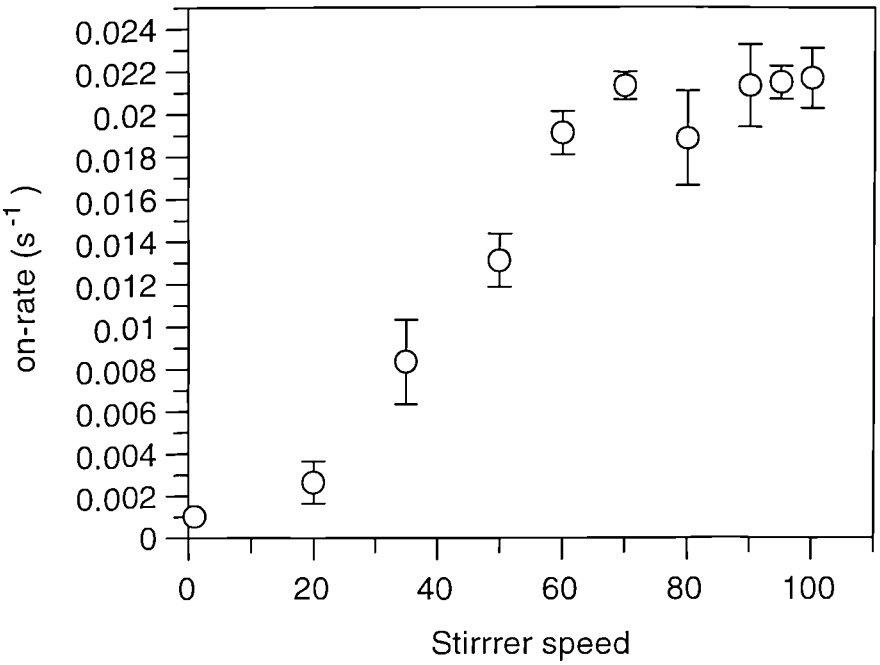

Figure 5.4: *The on-rate, determined from a single exponential fit of 32 nM CI-2 binding to immobilised chymotrypsin as a function of stirrer amplitude (setting). Above a setting of around 60 a constant on-rate is determined.*

The dR/dt plot (Figure 5.5) shows the change from kinetic through to mass transport limited conditions for the CI-2 data at stirrer speeds of 100 (kinetic limited), 35 (partial mass transport limited) and 1 (mass transport limited). While it is difficult to observe any plateau regions indicating mass transport, the differences in rate are obvious.

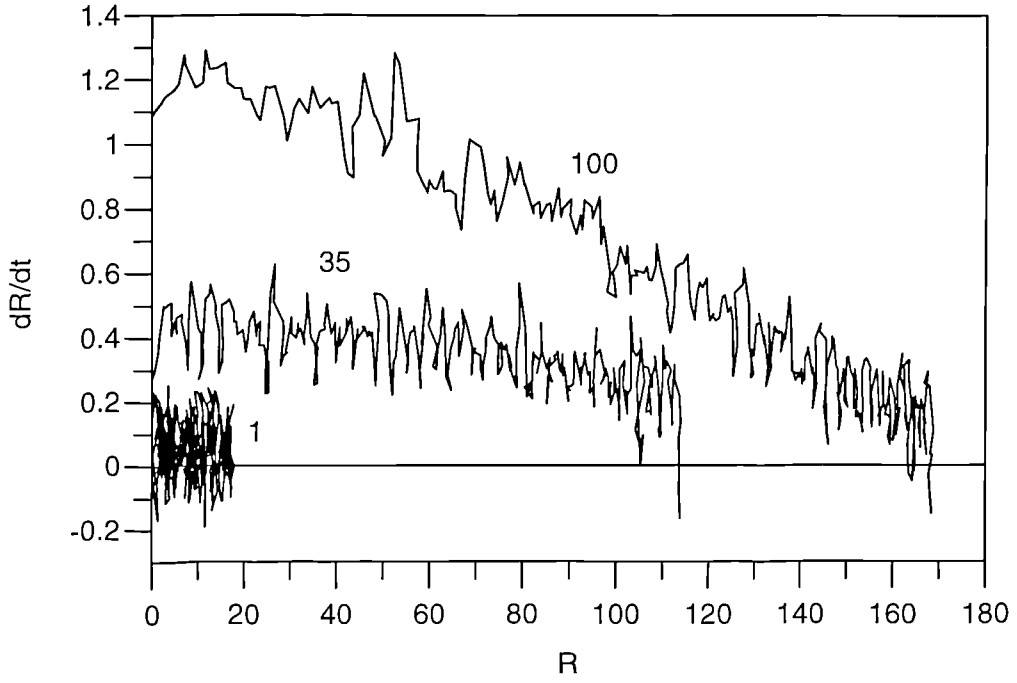

Figure 5.5: *The influence of stirrer amplitude upon the dR/dt against R plot for the interaction of 32 nM CI-2 with CMD immobilised chymotrypsin. The change in dR/dt at the three amplitude settings is evident.*

Furthermore, figure 5.6 shows an overlay of the binding profiles at different stir speeds for the interaction of 64 nM CI-2 with immobilised chymotrypsin. The curves are essentially superimposable above a setting of around 60. Below this value the binding curves have lower responses with linear binding curves at the lower stir rates suggesting mass transport limitations.

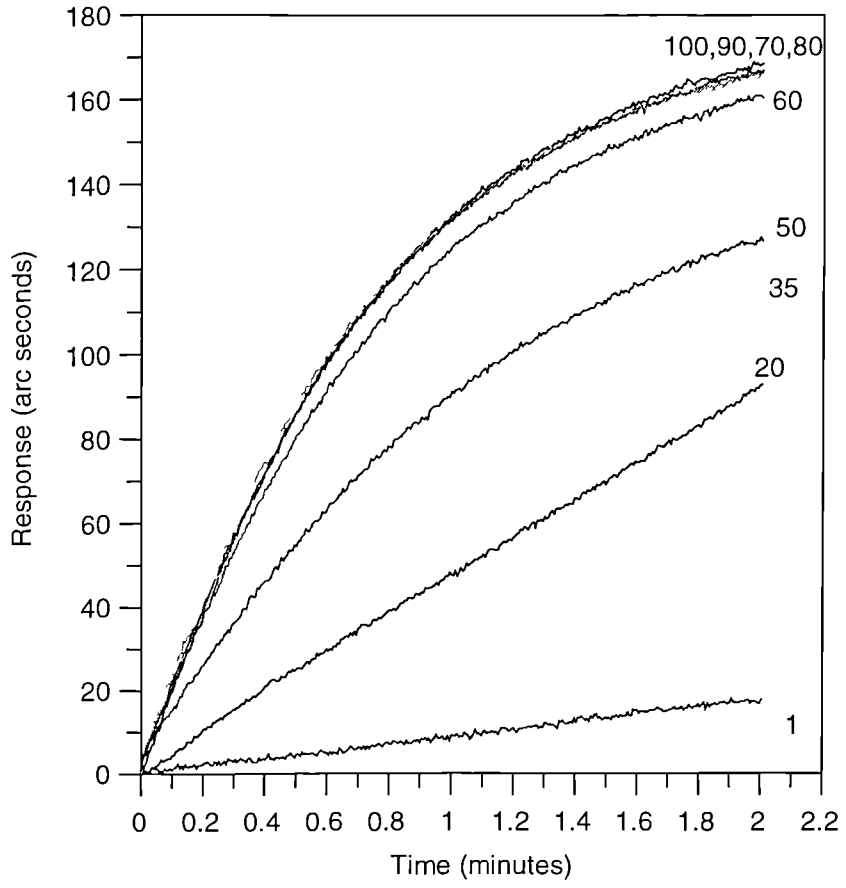

Figure 5.6: *Overlay of the first two minutes of association data for the interaction of 64 nM CI-2 with immobilised chymotrypsin at differing stirrer amplitudes. The stirrer amplitudes are shown on the figure.*

The influence of stirrer amplitude upon the measured on-rates has been shown in the previous figures. Mass transport also influences the calculated rate constants from the plot of on-rate against ligate concentration as shown in figure 5.7. The binding of differing concentrations of CI-2 to chymotrypsin immobilised on CMD was performed at stirrer amplitudes of 10 and 100. The association rate constants for each stirrer setting determined from the slope of the plot reveal a four-fold difference with k_{ass} values of $7.69 \pm 0.3 \times 10^4$ $M^{-1}s^{-1}$ and $1.95 \pm 0.05 \times 10^4$ $M^{-1}s^{-1}$ for the high and low stirrer setting. The dissociation rate constant determined from the intercept is also affected by the change in stirrer setting. At a setting of 10, a k_{diss} of $8.19 \pm 3.43 \times 10^{-5}$ s^{-1} is obtained while at 100 a value of $3.20 \pm 0.17 \times 10^{-3}$ s^{-1} is determined.

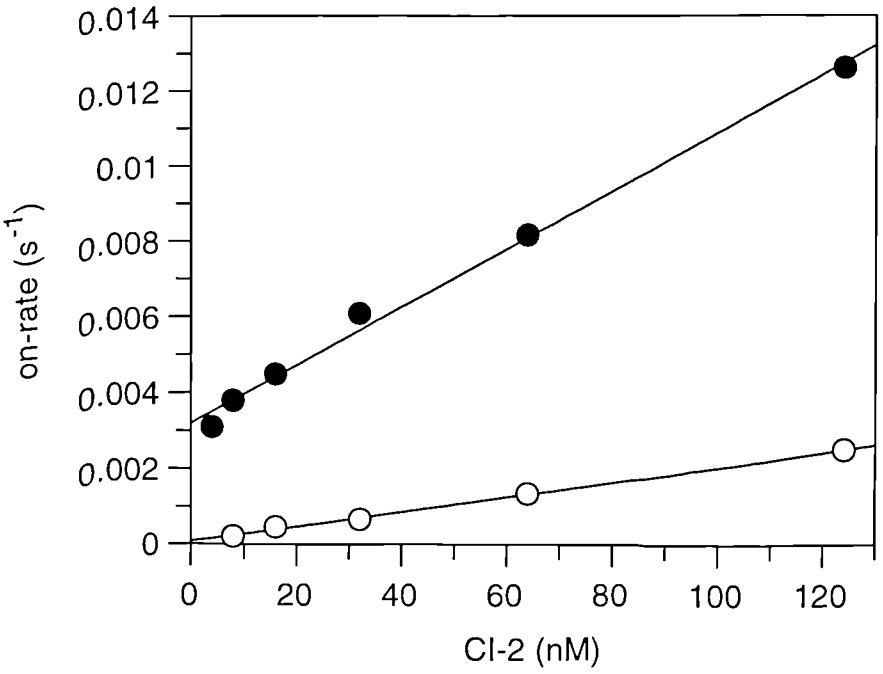

Figure 5.7: *The influence of stirrer amplitude upon the association and dissociation rate constants. The open circles represent data from a stirrer setting of 10 while the closed circles represent a setting of 100.*

5.3.2 Viscosity.

While the intrinsic binding rate will not be influenced by an alteration in solution viscosity, the rate of diffusion will (Berg and Von Hippel, 1985) and therefore viscosity changes provide a simple and convenient method for the determination of mass transport effects. From the Stokes-Einstein relationship (equation 2.2), altering the viscosity will alter the diffusion coefficient such that the coefficient is inversely proportional to the viscosity. For a kinetic controlled binding, changing the viscosity of the interaction buffer will not effect the rate.

Performing this experiment does however, entail the correction of the primary data due to the influence of the solvent refractive index η on the data. The $\eta_{water} = 1.33$ and that of protein is 1.5 giving a $\Delta\eta$ of 0.17. In 48% glycerol, however, the solution η value is higher resulting in a lower $\Delta\eta$ and hence a lower instrument response. The primary data must therefore be scaled to allow for this decrease in sensitivity before being subjected to either initial rate or k_{on} analysis. Figure 5.8 shows the effect of

viscosity upon the binding rate of 124 nM CI-2 to immobilised chymotrypsin with the rate being unaffected up to glycerol concentrations of 10% (η/η_0 = 1.7). Above this relative viscosity the rate of binding decreases indicating mass transport limitations. However, the assumption must be made that glycerol does not interfere with the binding of the ligate to the ligand.

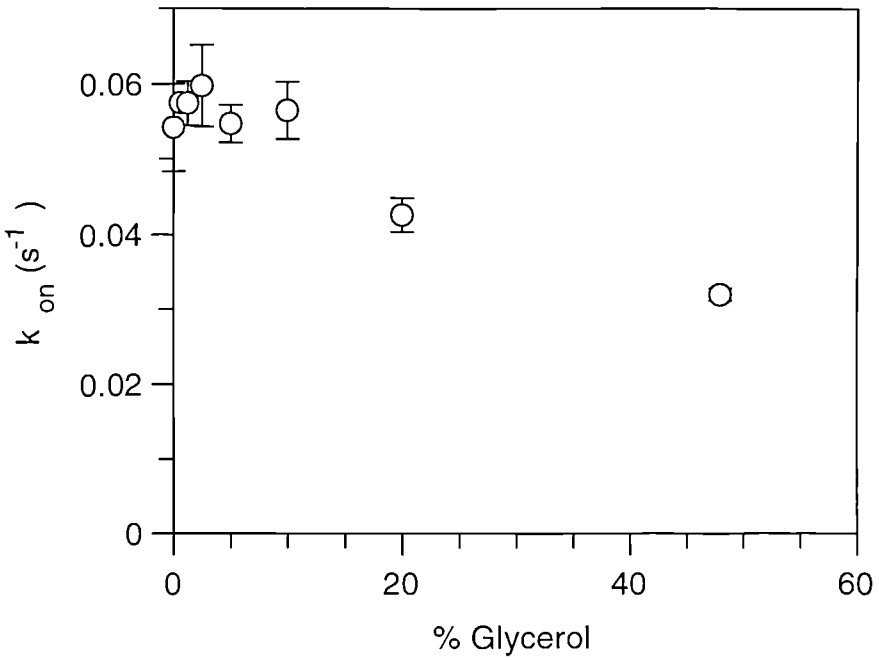

Figure 5.8: *The influence of solution viscosity (% glycerol) upon the on-rate of 124 nM CI-2 to CMD immobilised chymotrypsin.*

5.3.3 Stirrer height

The thickness of the unstirred layer is not only influenced by the speed of the stirrer but also its height above the sensor surface. This was investigated by measuring the binding rates at height settings of 0.6 mm and 2 mm. The binding rates were reduced upon raising the stirrer to 2 mm and the plateau values were decreased by approximately 13%. However, the plateau region was observed at the same stirrer setting of 60 (figure 5.9)

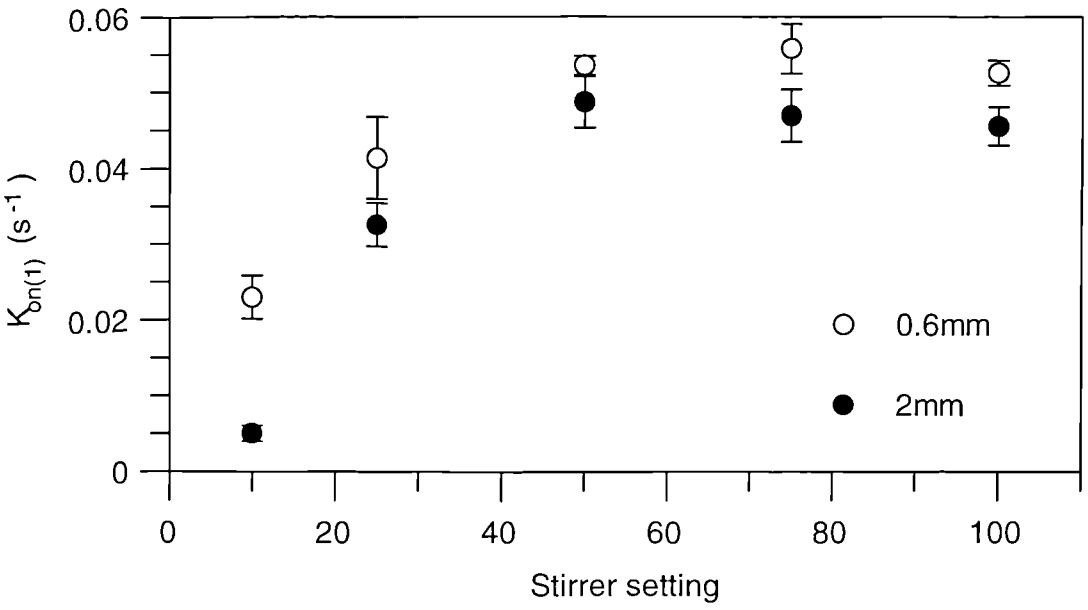

Figure 5.9: *The effect of stirrer height on the on-rate determined at differing stirrer amplitudes for the interaction of 30 nm colloidal gold to lysozyme adsorbed to an bare sensor surface.*

5.3.4 Unstirred layer thickness

The unstirred layer thickness is ultimately the defining parameter in the rate of transport to the CMD or sensor surface provided that the bulk solution is efficiently mixed. Combining equations 5.1 and 5.2 allows the thickness of the unstirred layer to be calculated. The parameters that can be altered are the concentration and, indirectly by changing the viscosity, the diffusion coefficient allowing an estimate of the unstirred layer thickness.

Using a planar underivatised surface, BSA at 15 µg/ml was adsorbed from three solutions of differing viscosities. Following corrections for refractive index differences, the unstirred layer thickness was calculated below from the initial binding rate.

J = Binding flux from the initial rate of binding.

At 0% viscosity the initial rate was 90 arc seconds/second

To convert response to a concentration term, the calibration factor of 600 arc seconds = 1ng/mm^2 for a planar surface is used (the determination of this value is described in chapter 7)

$$90/600 = 0.15 ng/mm^2/s$$

$$= 1.5 \times 10^{-4} g/m^2/s$$

D = Diffusion coefficient = 6.1 x 10^{-11} m^2/s (Cantor and Schimmel, 1980)

Concentration = 15 µg/ml

=15 g/m^3

Inserting into

$$x = \frac{D}{J}(c_{sol.}) \qquad (5.4)$$

$$= 6.1 \text{ µm.}$$

A similar calculation can be performed for different viscosity solutions, altering the value of D in each solution by using the Stokes-Einstein equation (equation 2.2). Layer thicknesses of 6.2 µm and 7.4 µm were determined in 24% and 48% glycerol respectively.

The unstirred layer can also be found by varying the solution concentration thus altering the binding flux. The adsorption of HSA at differing concentrations to a planar sensor surface was monitored and an increase in layer thickness with decreasing concentration from a value of 4 µm to 9 µm was found as shown in figure 5.10. These values are, however, within the value from the viscosity experiments and as such seems plausible that the thickness lies between these values. The 10 µg/ml solution gave a thickness of around 5 µm which agrees reasonably well with that obtained previously in different viscosity solutions.

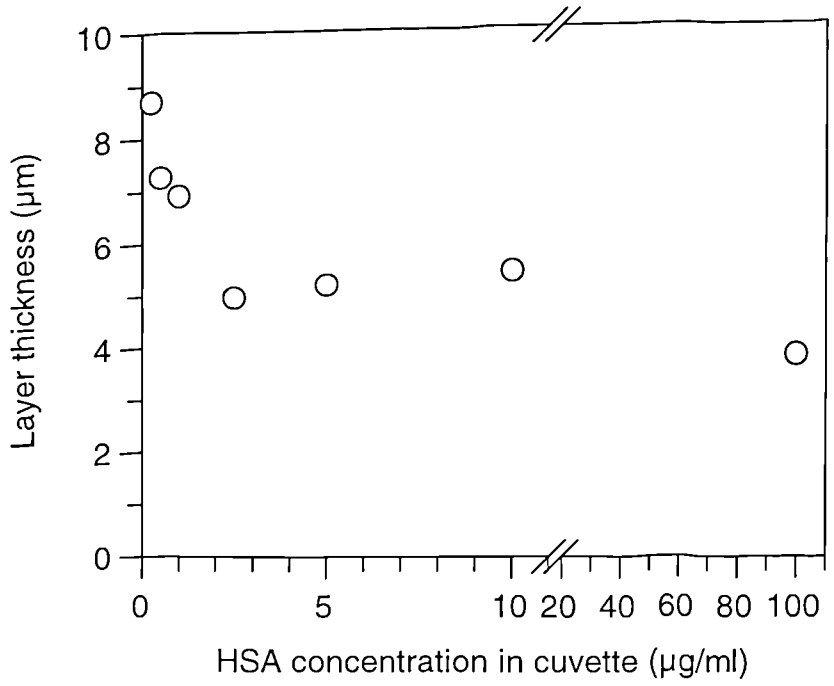

Figure 5.10: *The calculated unstirred layer thickness, determined from initial rate analysis of adsorption data, as a function of HSA concentration.*

5.4 Discussion.

Biosensor experiments require the attachment of the ligand to the sensor surface and as such can be considered a heterogeneous technique with many similarities to ELISA technology. Due to the attachment to the surface there will be a 'stagnant' layer through which the ligate must diffuse from the bulk solution to the immobilised ligand. Minimisation of this layer is therefore essential in reducing the mass transport influence. In ELISA technology this unstirred layer is usually reduced by stirring within the wells or by means of gentle shaking. Without stirring the thickness of this layer is around 30µm and the time taken to diffuse through this layer is equal to (x^2/D) for which a value of around 15 seconds is obtained for a typical value for D of 6 x 10^{-11} m^2/s. Biosensors reduce this layer thickness by either stirring (IAsys) or flow (Biacore). In the case of IAsys the thickness of the unstirred layer is approximately 5 µm, which would give a diffusional time of 0.5 seconds.

The stirrer amplitude dependence of the k_{on} has been investigated for the CI-2/chymotrypsin system demonstrating a plateau region around a setting of 60. As there is a linear relationship between the setting and amplitude of the stirrer spanning the

whole range up to 100 it may be concluded that reactions performed at stir rates above a setting of 60 are not greatly influenced by mass transport. Indeed, the layer thickness of around 6 μm calculated on planar surfaces at different viscosities would give a diffusional time of 600 ms, equivalent to two data points using IAsys at its fastest collection rate. The values determined at different HSA concentrations seem to show that at the lower concentrations the layer thickness becomes 9 μm. The increase in calculated unstirred layer thickness with decreasing concentration is likely to be due to the assumption that the solution concentration is in excess over the surface concentration being invalid.

It is useful to compare the thickness of the 'stagnant' layer as a result of laminar flow through the Biacore flow cell. The flow cell dimensions have been used to determine the diffusional layer thickness (Karlsson., 1991. Karlsson et al., 1994. Glasser, 1993) by equation 5.5

$$x = \sqrt[3]{\frac{D.h^2.b.l}{flw}} \tag{5.5}$$

where h, b, and l are the height, width and length of the flow cell and flw the linear flow rate through the cell. The effect of the flow rate on the diffusional layer is shown in figure 5.11 with values of h,b, and l of 50 μm, 0.3 mm, and 0.8 mm respectively and a value of 6 x 10^{-11} m^2/s for D .

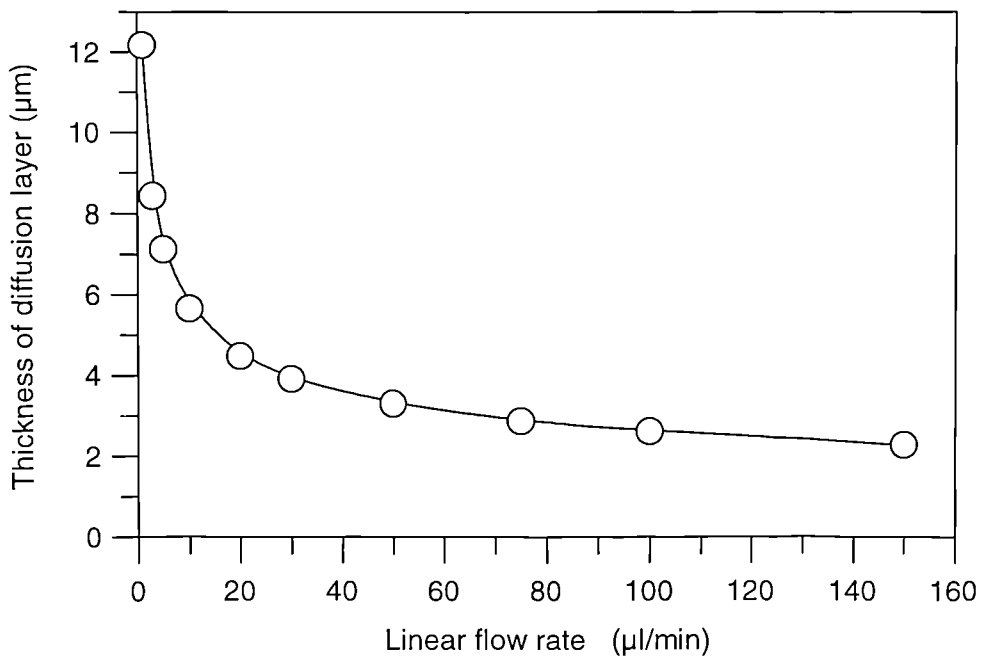

Figure 5.11: *The calculated unstirred layer thickness as a function of linear flow rate through a flow cell of height 50 µm, width 0.3 mm, and length 0.5 mm.*

The manufacturer now recommend the use of flow rates above 30µl/min for kinetic analysis, a rate which yields a diffusional layer thickness of 4µm. Comparison of this value with those from the IAsys suggest that both methods reduce the unstirred layer thickness to similar levels. Data in figure 5.12 shows the layer thickness derived by initial rate analysis for the binding of CI-2 to immobilised chymotrypsin. The value for the diffusion coefficient of CI-2 was unknown and therefore an estimate of 2 x 10^{-10} m^2/s was used. While the exact value for the diffusional coefficient is unknown this value represents a 'ball-park' figure which is comparable with that of pancreatic ribonuclease (mw = 13683) and lysozyme (mw = 14100) of 1.19 x 10^{-10} m^2/s and 1.04 x 10^{-10} m^2/s respectively (Cantor and Schimmel, 1980).

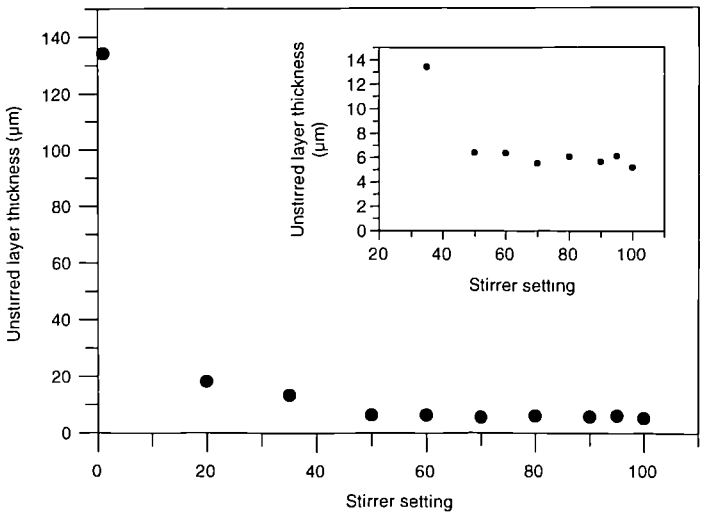

Figure 5.12: *The unstirred layer thickness for the interaction of 124 nM CI-2 with CMD immobilised chymotrypsin assuming a diffusion coefficient of 2 x 10^{-10} m^2/s for CI-2.*

The influence of glycerol upon the binding rate is the best indication of mass transport limitations. From figure 5.8 the rate is dependent on the viscosity above 10% glycerol levels (rel. visc. 1.7) while below this there seems to be a plateau. The viscosity dependence at these higher % values suggests a diffusional limitation. However, the increase in glycerol concentration may interfere with the normal binding.

The use of the Da number (equation 5.3) to access whether the reaction rate measured is influenced by mass transport has been described by Stenberg et al. (1986) for ELISA technology, Sadana and Sii (1991) for fibre optic biosensors and by Yarmush (1997) for the Biacore instrument. Here it will be used for IAsys data assuming that the ligate (mw 9200) has to traverse an unstirred layer of thickness 5 µm (5 x 10^{-4} cm) before binding to the ligand which has a capacity of 200 arc seconds for the ligate (1.08 x 10^{-11} moles/cm^2) . The diffusional coefficient, D, is 2 x 10^{-6} cm^2/s and the association rate constant is 5 x 10^5 $M^{-1}s^{-1}$ (5 x 10^8 cm^3/mole s). This gives a Da number of 2.7 indicating that the reaction CI-2/Chymotrypsin reaction is not mass transport limited under these conditions.

The experimental data suggest that under the conditions employed in the course of a normal experiment the data generated will not be limited by mass transport. The degree of mass transport influence also depends on the capacity of the immobilised ligand for the ligate. Myszka et al (1997) have used global fitting of an equation incorporating a mass transport term. This term must be determined first by performing the experiment at a high immobilisation level, and then the affinity can be determined by the using this value in conjunction with the simple bimolecular equation. While this may be a valid approach it does significantly lengthen the kinetic determination. A further complication is the influence of diffusion through the CMD matrix (Schuck 1996) which would be expected to slow the measured rates. This diffusion through the CMD matrix would be unaffected by a variation in flow rate or stirrer speed. The influence of this CMD matrix is discussed further in chapter 6.

Chapter 6

A Comparison of Interaction kinetics on CMD and Planar Surfaces.

6.1 Introduction.

The influence of polymer solutions upon the diffusion of macromolecules has been investigated in studies unconnected with biosensor technology. Johnson et al, (1996) showed that the diffusional constants decrease in the presence of polymer gels compared to those in solution and that this decrease is more severe for large macromolecules. In a previous publication by the same authors (1995) the effect of ionic strength on the diffusivity and partitioning of negatively charged macromolecules into negatively charged sulphated agarose was investigated. It was found that altering the ionic strength of the solutions did not change the relative diffusivity but the partitioning coefficient was dramatically changed.

The use of the surface attached CMD matrix on biosensors may be expected to have an influence upon the kinetics of biomolecular interactions. This influence will be greater under conditions of high ligand immobilisation or slow stirring (or low flow rate on the BIAcore instrument). However, several authors have questioned the applicability of the CMD matrix for the determination of kinetic constants comparable to solution phase measurements. Schuck (1996) has modelled the effect of various parameters on the interaction kinetics determined with the CMD matrix. The matrix was split into discrete segments in the z-axis through which ligate must permeate in order to bind to ligand sites deeper within the matrix. In the model no account was made of lateral movement. Using this compartmental model the influence of various parameters was investigated, including the concentrations of both ligand and ligate, the exponential decay of the evanescent field, and the thickness of the CMD matrix. It was concluded that the CMD has an effect upon the kinetics at lower association rate constants than expected and that it is the thickness of the CMD layer which has the most profound effect. Schuck (1996) therefore recommended the reduction in the CMD thickness which could be achieved by the use of lower molecular weight CMD or by the use of a derivatised planar surface such as an aminosilane surface (Watts et al., 1994).

Given the change in the diffusivity in the presence of polymer solutions, in the studies by Johnson et al (1996) the diffusion coefficients were halved in comparison to the solution values, the influence of the CMD matrix on surface attached reactions was

investigated. The conclusions by Schuck were investigated by comparing kinetics obtained on planar carboxylate and amino surfaces with those obtained on CMD. In order to compare the planar and CMD surfaces, the sensitivity of the planar surface was determined.

6.2 Sensitivity of planar surfaces

The sensitivity of the planar surface, in terms of arc s/ng/mm^2, was determined by adsorbing differing concentrations of radiolabelled HSA onto planar surfaces. The entire surface was then placed, after washing with buffer, in a gamma counter. The IAsys response and the cpm values were noted and are plotted in figure 6.1.

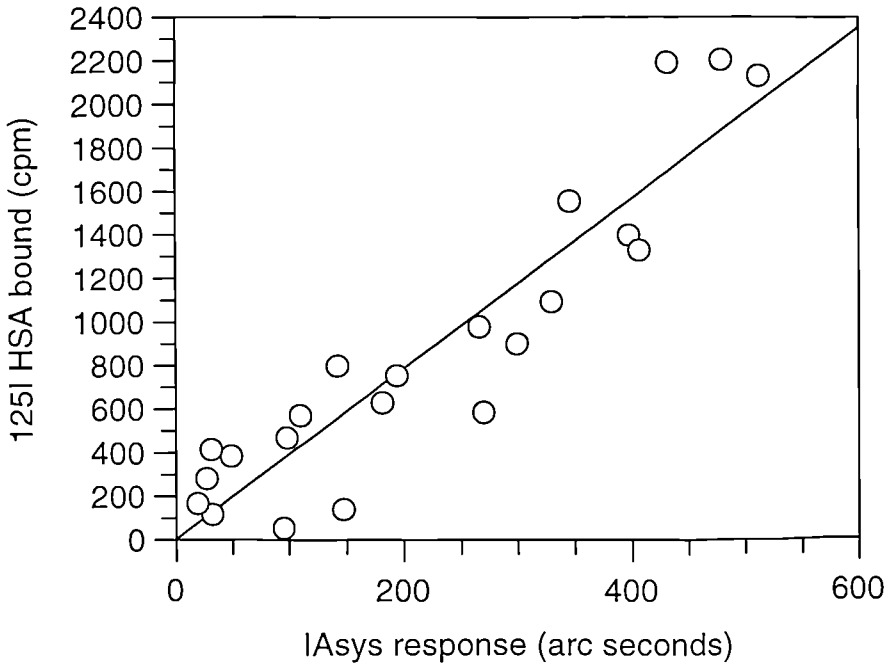

Figure 6.1: *Calibration plot for the planar surface. The ^{125}I HSA cpm were determined from measurement of the sensor surface, with the IAsys response noted prior to radioactive measurement.*

The calibration factor for planar surfaces was determined in a similar manner to that of the CMD surface (section 4.2). Using values for the specific activity and surface

area of 2.5 MBq/mg and 16 mm^2, a calibration factor of $1ng/mm^2$ = 615 arc seconds was calculated.

6.3 Kinetic comparison of planar and CMD surfaces.

In order to compare the kinetics of association and dissociation, three different biological systems were used with three types of sensor surfaces. The sensor surfaces were CMD, planar aminosilane and planar carboxylate, the carboxylate being obtained directly from the aminosilane surface. The biological systems were anti-HSA mab/HSA, Lysozyme/D1.3Fv, and chymotrypsin/CI-2.

6.3.1Anti-HSA mab/HSA

Both the HSA and the anti-HSA mab were immobilised separately to the surfaces and anti-HSA mab or HSA bound respectively. This allowed, in addition to the surface comparison, an investigation into any ligand dependence of the interaction kinetics

6.3.1.1 The binding of HSA to immobilised anti-HSA mab.

The binding of HSA to immobilised anti-HSA mab was investigated by non-linear regression analysis using either single or double exponential equations for each of the three surfaces. The resulting k_{on} values were plotted against their respective concentrations and are shown in figure 6.2

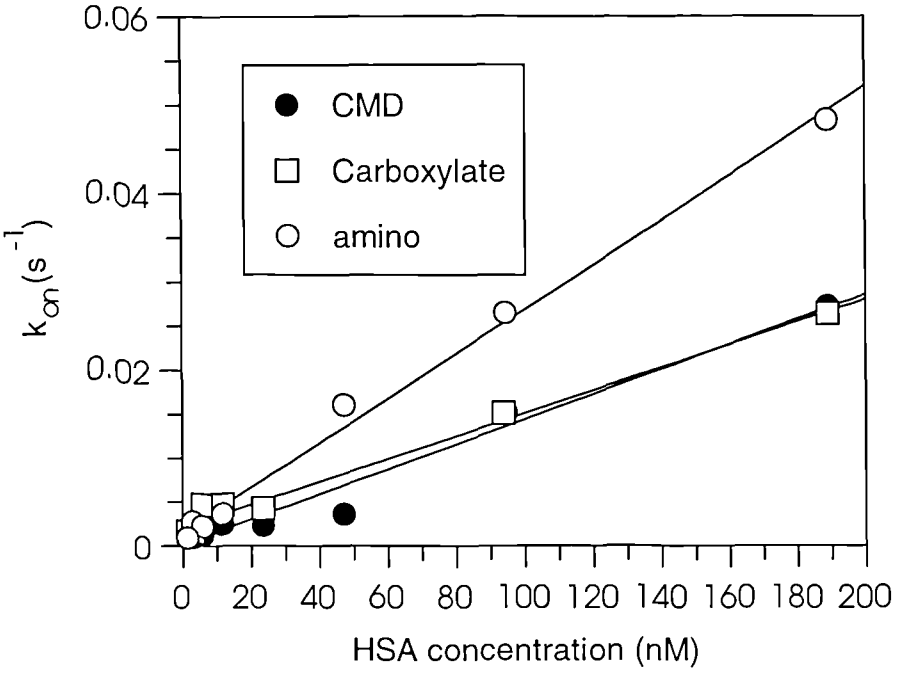

Figure 6.2: *A plot of on-rate against HSA concentration for the binding of HSA to anti-HSA mab immobilised to CMD, or planar amino or carboxylate surfaces. The on-rates were determined by application of single or double exponential association equations (equations 2.16 and 2.23 respectively). In the case of the double exponential equation producing the best fit, the first on-rate ($k_{on(1)}$) was used.*

The association and dissociation rate constants given by the slope and intercept for each of the three surfaces are shown in table 6.1

Surface	k_{ass} ($M^{-1}s^{-1}$)	k_{diss} (s^{-1})	K_D (nM)
Amino	$2.53 \pm 0.09 \times 10^{5}$	$1.56 \pm 0.72 \times 10^{-3}$	6.2 ± 2.9
Carboxylate	$1.31 \pm 0.07 \times 10^{5}$	$2.09 \pm 0.51 \times 10^{-3}$	15.9 ± 3.9
CMD	$1.43 \pm 0.10 \times 10^{5}$	$1.75 \pm 7.8 \times 10^{-4}$	1.2 ± 5.3

Table 6.1: *Comparison of the association and dissociation rate constants obtained from the data in figure 6.2. Also shown is the K_D determined from the ratio of the two rate constants.*

The association rate constant for the carboxylate and CMD surfaces are essentially the same, while that from the amino surface is almost two-fold higher. The dissociation rate constant from the planar surfaces are, within error, the same. It is difficult to assign a value for the CMD surface given the high error but it may be that this value is similar to that determined for the planar surfaces. The nature of the k_{on} vs. concentration plot means that k_{diss} values are frequently poorly defined, as the intercept is close to zero.

Inspection of the shape of the binding curve from the amino surface illustrates the higher rate, a rapid increase in response with a rapidly achieved plateau. Figure 6.3 shows such a plot for all three surfaces at a HSA concentration of 1.5 μM. When the binding responses are normalised in relation to each of their final values, such as in figure 6.4, both the CMD and the carboxylate curves are identical. This is despite the higher CMD binding response in comparison to the carboxylate. The amino reaches its plateau rapidly which is indicative of a faster on-rate.

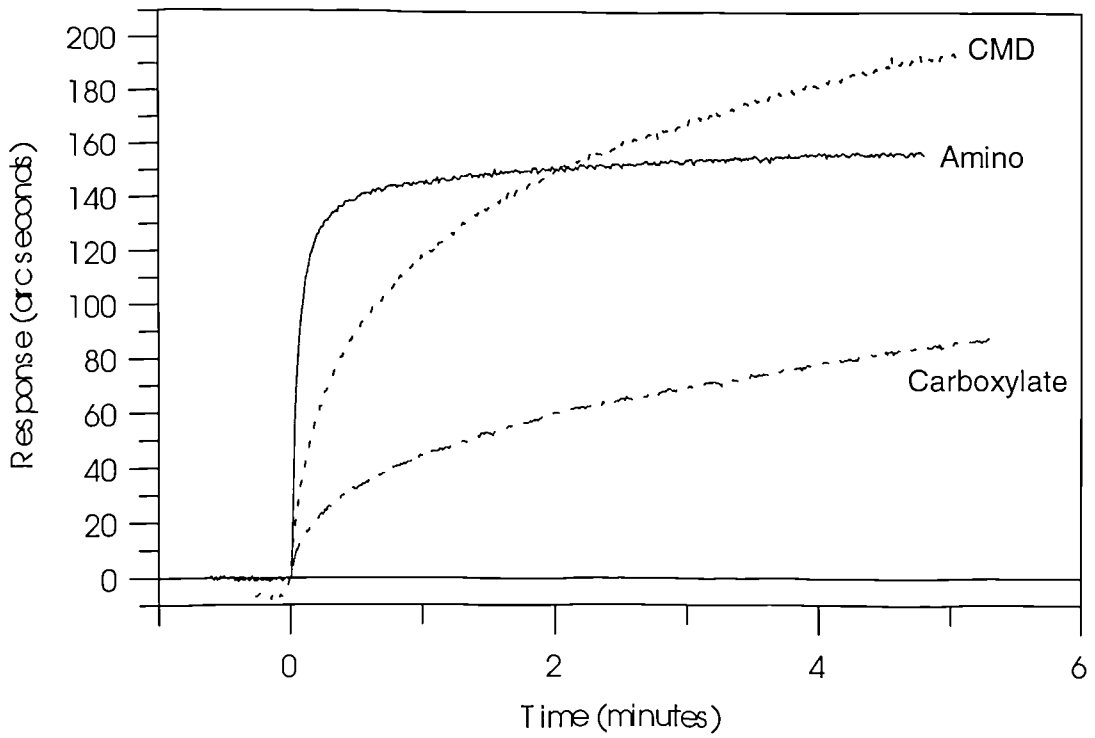

Figure 6.3: *The time course of HSA binding at 1.5 μM to anti-HSA mab immobilised to CMD, or planar amino or carboxylate surfaces.*

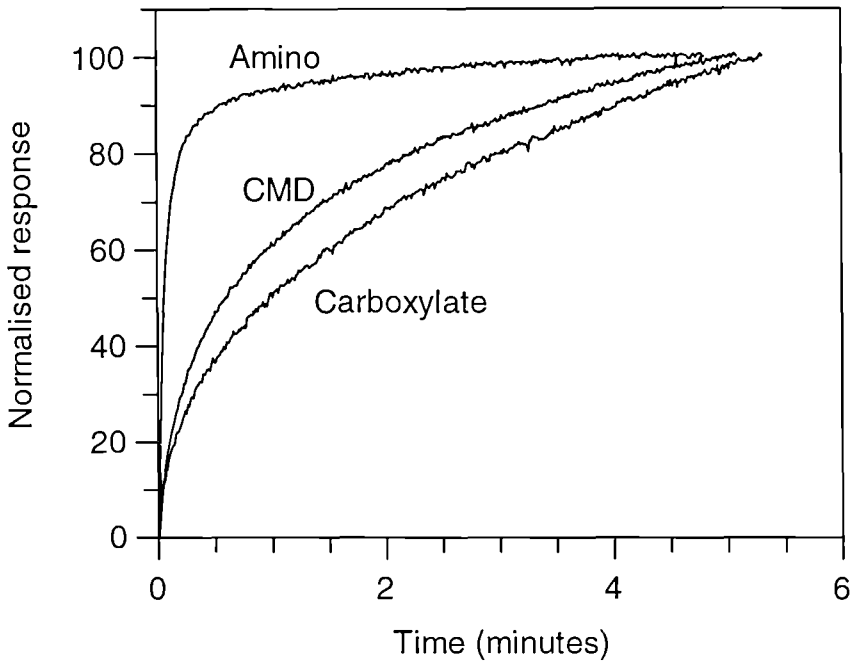

Figure 6.4: *Normalised data in relation to the final IAsys response for data in figure 6.3*

The high errors associated with calculating dissociation rate constants from the intercept of k_{on} vs. [L] plots makes any definite conclusion difficult, although all the values are similar within error. The dissociation rate constant on the CMD surface gives a lower rate but this is coupled with a higher error.

In view of these poorly defined intercepts describing the k_{diss}, direct fitting of the dissociation phase was therefore performed. The data were fitted to a single exponential dissociation equation with (equation 2.24) and without an offset (equation 2.18). It was found that the data were fitted better by the equation containing the offset. Figure 6.5 shows the dissociation phase data with the fitted curve. The values determined on the different surfaces using the equation containing the offset were 2.15 $\pm$ 0.03 x 10^{-4} s^{-1}, 2.28 $\pm$ 0.12 x 10^{-4} s^{-1}, and 2.29 $\pm$ 0.04 x 10^{-4} s^{-1} on the amino, carboxylate, and CMD surfaces respectively.

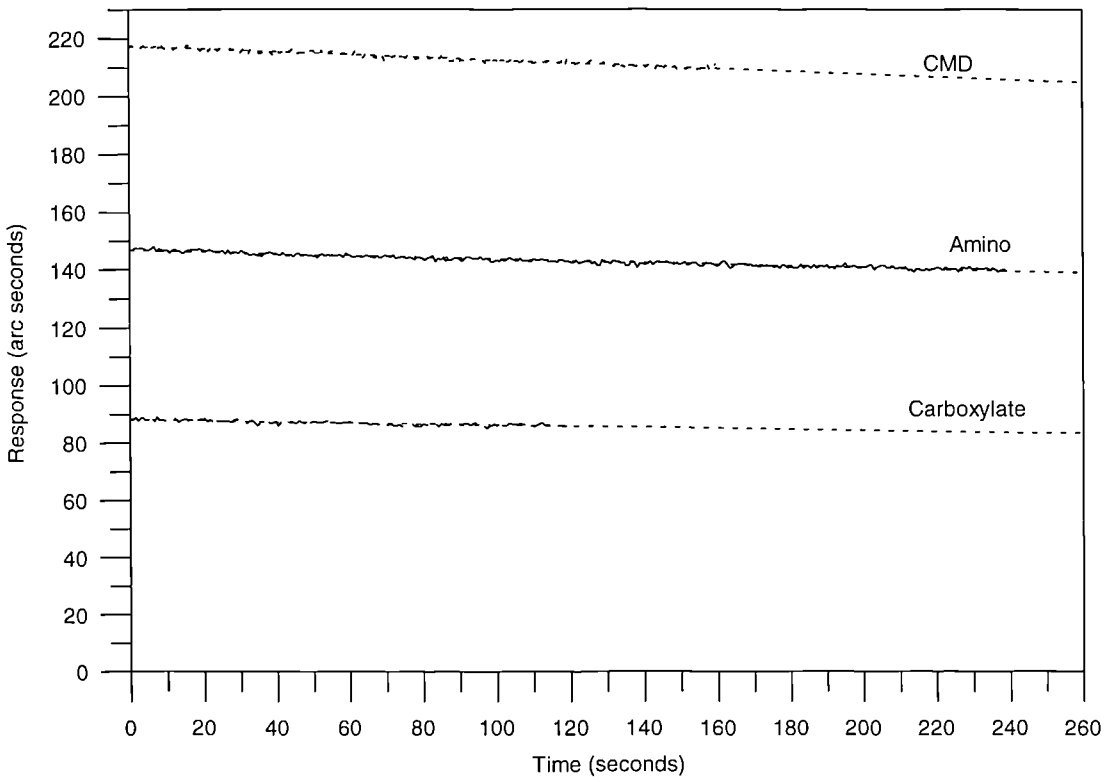

Figure 6.5: *The dissociation profile for HSA, bound at a concentration of 1.5 μM, from anti-HSA mab immobilised to CMD, or planar amino or carboxylate surfaces. The dotted lines show the best fit to an single exponential dissociation equation containing an offset (equation 2.24).*

6.3.1.2 The binding of anti-HSA mab to immobilised HSA

The binding of anti-HSA mab was investigated in a similar manner. In contrast to the HSA binding, there appears to be no surface dependence in the kinetics of the interaction as demonstrated in figure 6.6.

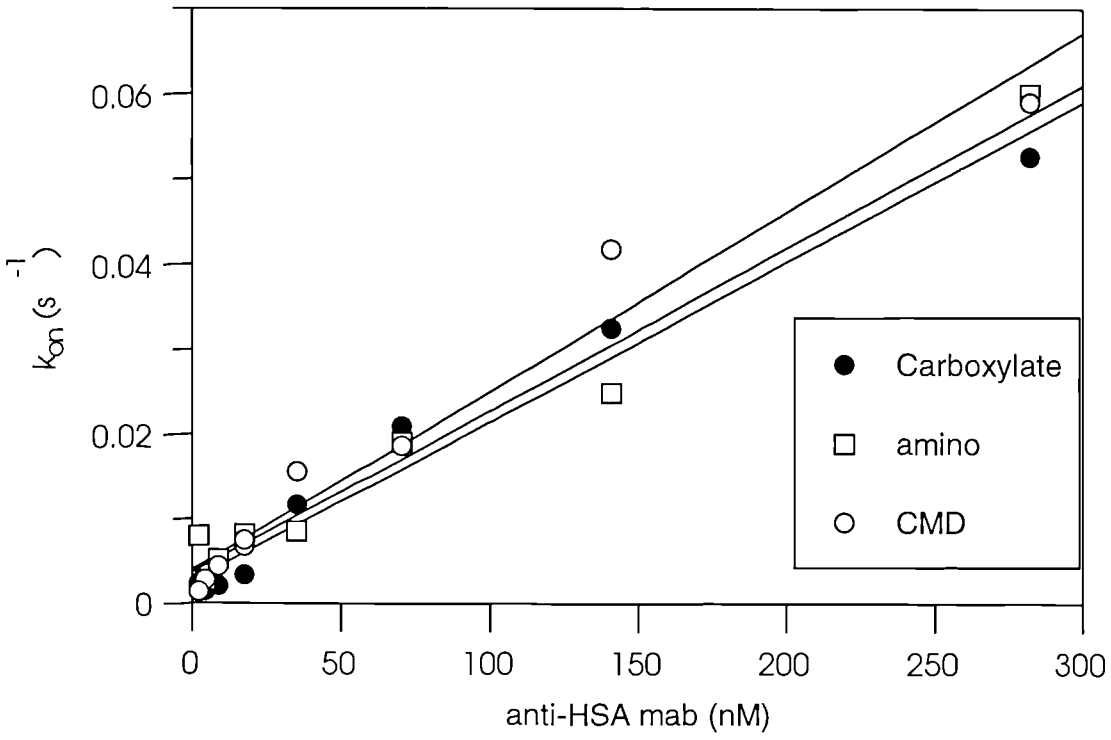

Figure 6.6: *A plot of on-rate against anti-HSA mab concentration for the binding of anti-HSA mab to HSA immobilised to CMD, or planar amino or carboxylate surfaces. The on-rates were determined by application of single or double exponential association equations (equations 2.16 and 2.23 respectively). In the case of the double exponential equation producing the best fit, the first on-rate ($k_{on(1)}$) was used.*

Table 6.2 shows the derived association and dissociation rate constants.

Surface	k_{ass} ($M^{-1}s^{-1}$)	k_{diss} (s^{-1})	K_D (nM)
Amino	$1.91 \pm 0.13 \times 10^{5}$	$3.67 \pm 1.47 \times 10^{-3}$	19.2 ± 7.8
Carboxylate	$1.87 \pm 0.13 \times 10^{5}$	$2.71 \pm 1.51 \times 10^{-3}$	14.5 ± 8.1
CMD	$2.11 \pm 0.16 \times 10^{5}$	$3.97 \pm 1.71 \times 10^{-4}$	18.8 ± 8.2

Table 6.2: *Comparison of the association and dissociation rate constants obtained from the data in figure 6.6. Also shown is the K_D determined from the ratio of the two rate constants.*

The association rate constant on all the surfaces was around 2 x 10^5 $M^{-1}s^{-1}$ while the dissociation rate constant revealed that the rate from the CMD surface was lower that that from the planar surfaces. Once again the error on the CMD value makes any definite conclusion regarding the k_{diss} difficult.

Data at 1.13 μM anti-HSA mab reveals that the binding responses on the CMD surface are about five times higher than on the two planar surfaces (figure 6.7).

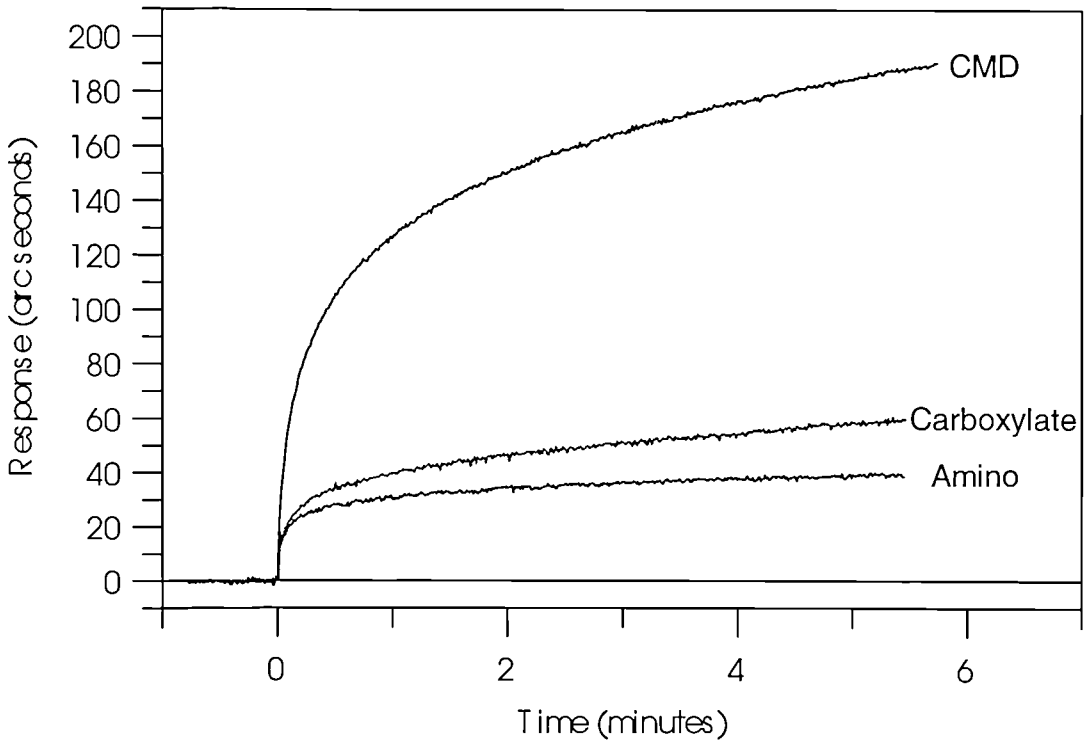

Figure 6.7: *The time course for anti-HSA mab at 1.13 μM binding to HSA immobilised on CMD, or planar amino or carboxylate sensor surfaces.*

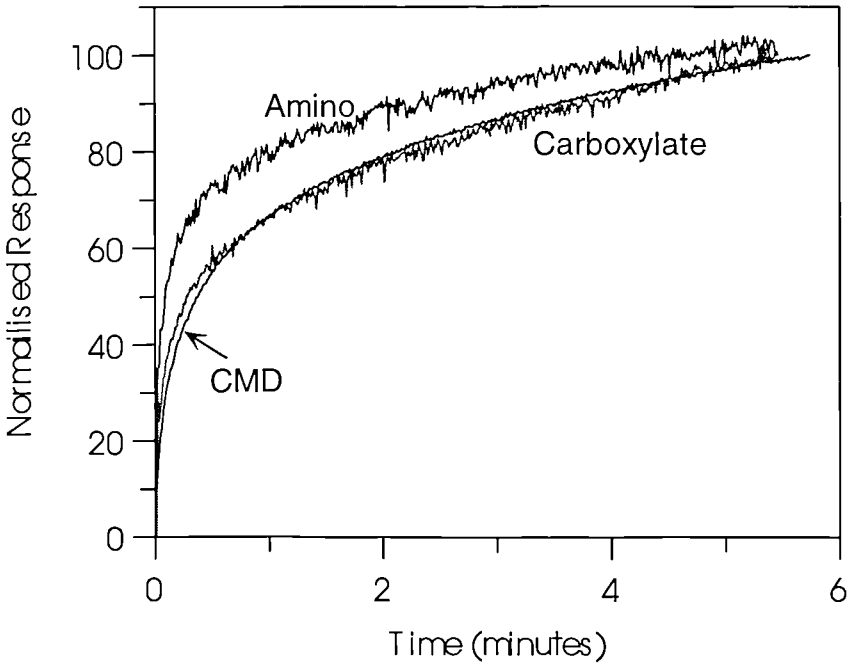

Figure 6.8: *Normalised data from figure 6.7.*

Figure 6.8 shows that the normalised data are essentially the same and therefore the rate of binding at this concentration is independent of the surface type. The data in figure 6.6 show that this independence is maintained over the concentration range investigated.

The poorly defined k_{diss} from the intercept necessitated direct analysis of the dissociation phase. The dissociation phases for all three surfaces were fitted to a single exponential dissociation equation with and without an offset. In common with the HSA dissociation, the data for the anti-HSA mab dissociation were fitted better with the equation containing an offset. Figure 6.9 shows the dissociation data at 1.13 μM anti-HSA mab with the fitted curve.

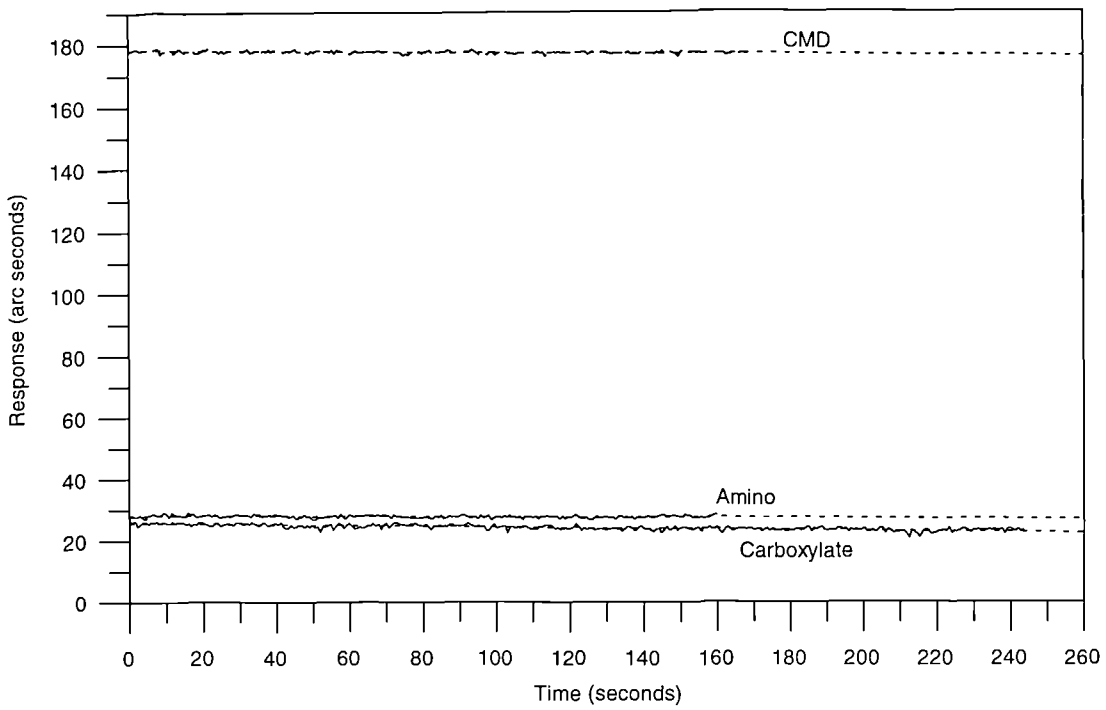

Figure 6.9: *The dissociation profile for anti-HSA mab, bound at a concentration of 1.13 μM, from HSA immobilised on amino, CMD, and carboxylate surfaces. The dotted lines show the best fit to an single exponential dissociation equation containing an offset.*

The dissociation rate constant values determined were 1.95 ± 0.22 x 10^{-4} s^{-1}, 5.39 ± 0.18 x 10^{-4} s^{-1}, and 5.55 ± 0.33 x 10^{4} s^{-1} on the amino, carboxylate, and CMD surfaces respectively.

6.3.2 Lysozyme/D1.3Fv

In order to compare kinetics using a further system, the interaction of lysozyme with D1.3Fv was chosen. In addition to the comparison of kinetic data on the three surfaces and this interaction has a faster dissociation rate and as such any differences arising from a surface change may be easier to observe than for the slower HSA/anti-HSA mab dissociation.

The binding of D1.3Fv to lysozyme immobilised on the three surfaces showed little surface dependence as can be seen from figure 6.10.

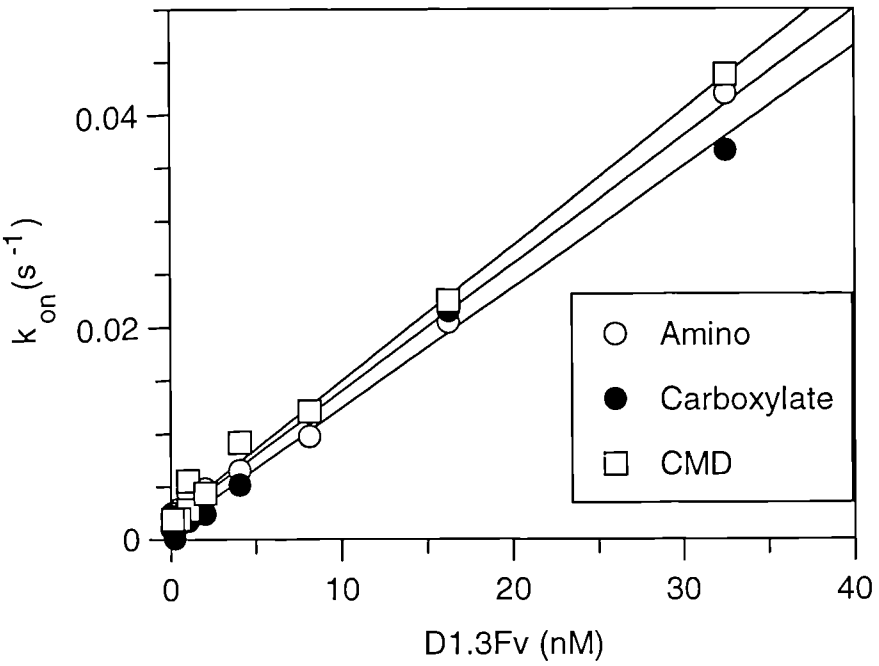

Figure 6.10: *A plot of on-rate against D1.3Fv concentration for the binding of D1.3Fv to lysozyme immobilised to CMD, or planar amino or carboxylate surfaces. The on-rates were determined by application of single or double exponential association equations (equations 2.16 and 2.23 respectively). In the case of the double exponential equation producing the best fit, the first on-rate ($k_{on(1)}$) was used.*

The association and dissociation rate constants determined from this plot are tabulated below (table 6.3)

Surface	k_{ass} ($M^{-1}s^{-1}$)	k_{diss} (s^{-1})	K_D (nM)
Amino	$1.21 \pm 0.04 \times 10^{6}$	$1.96 \pm 0.39 \times 10^{-3}$	2.6 ± 0.5
Carboxylate	$1.14 \pm 0.04 \times 10^{6}$	$1.01 \pm 0.46 \times 10^{-3}$	0.9 ± 0.4
CMD	$1.28 \pm 0.03 \times 10^{6}$	$2.16 \pm 0.43 \times 10^{-3}$	1.7 ± 0.3

Table 6.3: *Comparison of the association and dissociation rate constants obtained from the data in figure 6.10. Also shown is the K_D determined from the ratio of the two rate constants.*

The association rate constants derived from all three surfaces are essentially the same, within error, although the rate from the CMD surface may be slightly higher. This increase is observed on the normalised plot for 16 nM D1.3Fv (figure 6.11) with the curve from the CMD surface slightly above those from the other two surfaces (figure 6.12).

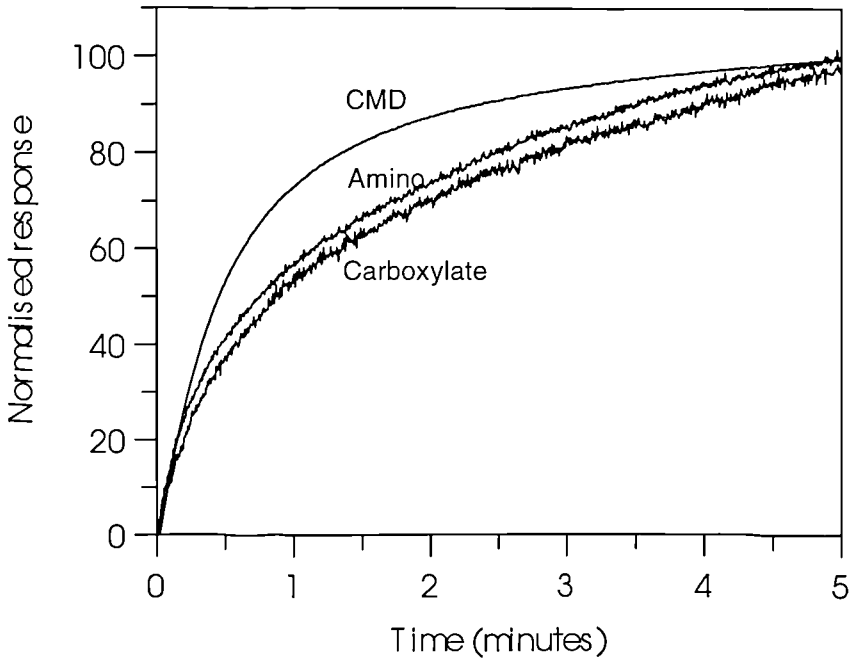

Figure 6.11: *Normalised binding responses for the interaction of 16 nM D1.3Fv with lysozyme immobilised on CMD, amino, and carboxylate sensor surfaces.*

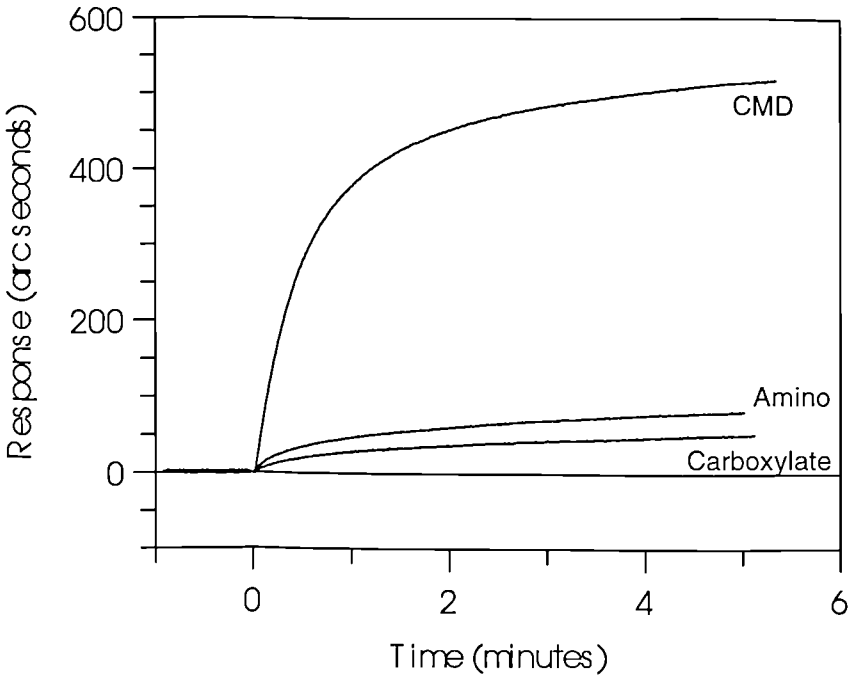

Figure 6.12: *The time course for the binding of 16 nM D1.3Fv to lysozyme immobilised on CMD, amino, and carboxylate surfaces.*

As with the HSA/anti-HSA mab system a comparison of the dissociation rate constants is difficult given the errors associated with this value. A more accurate comparison can be obtained from direct fitting of the dissociation phase. In order to highlight any differences the dissociation rate constant was determined by curve fitting. using the same equations used for the HSA/anti-HSA mab study. The equation containing the offset fitted the data better and this fit is shown in figure 6.13 together with the experimental data for 32 nM D1.3Fv.

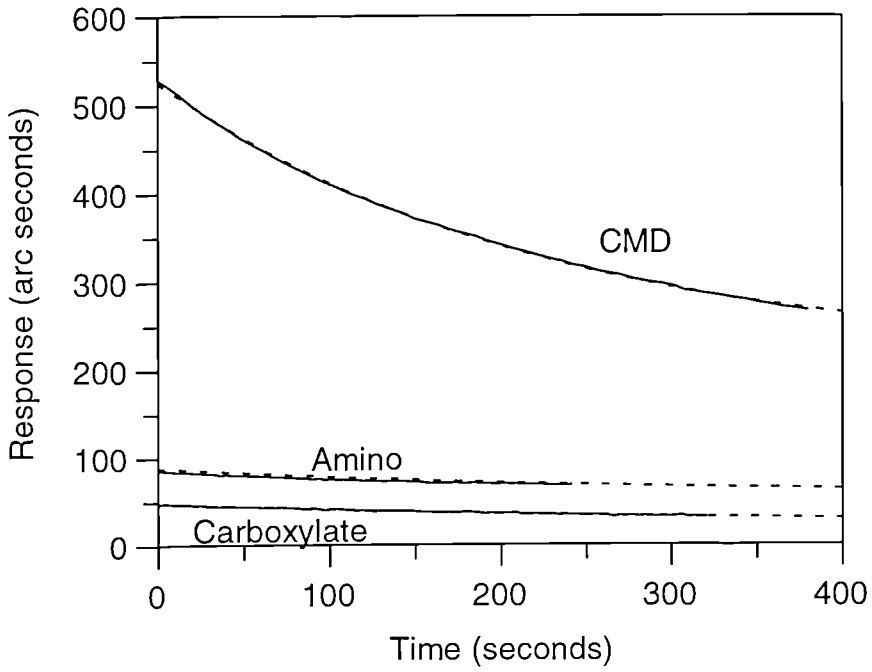

Figure 6.13: *The dissociation profile for D1.3Fv, bound at a concentration of 32 nM, from lysozyme immobilised on CMD, amino, and carboxylate surfaces. The dotted lines show the best fit to an single exponential dissociation equation containing an offset.*

The dissociation rate constant values from this curve fitting were 4.03 ± 0.27 x 10^{-3} s^{-1} for the amino surface, 3.59 ± 0.26 x 10^{-3} s^{-1} for the carboxylate, and 4.44 ± 0.06 x 10^{-3} s^{-1} for the CMD surface.

6.3.3 Chymotrypsin/CI-2

It was found that the chymotrypsin was only active when immobilised to the CMD matrix. Immobilisation to either of the planar surfaces resulted in no binding of the CI-2 (figure 6.14) .

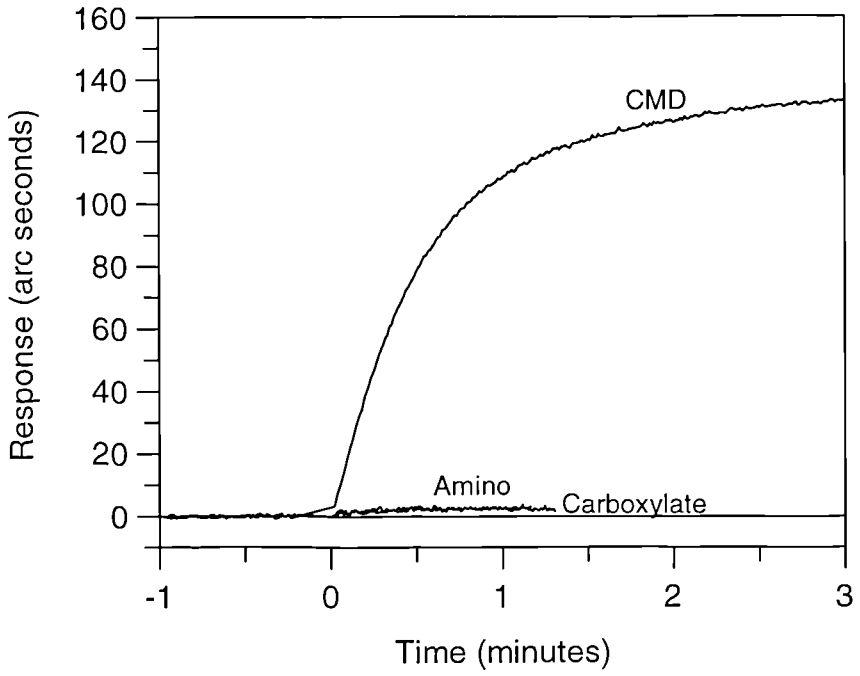

Figure 6.14: *The interaction of 124 nM CI-2 with chymotrypsin immobilised on CMD, amino, and carboxylate surfaces. Chymotrypsin was only able to bind CI-2 when immobilised on CMD.*

Immobilisation of the CI-2 also failed to bind chymotrypsin on either of the three surfaces. Instead of the binding response a rapid drop in response was observed when the chymotrypsin was added to the cuvette

6.4 Discussion.

The planar surface is three times as sensitive as the CMD surface (section 4.2) with responses of 615 and 206 arc seconds equivalent to 1ng/mm^2 respectively. The CMD surface is less sensitive due to the presence of the hydrogel preventing molecules from binding close to the sensor surface where the evanescent field is more intense. However, the CMD layer does allow multi-layers of immobilised ligand to be formed and thus usually possesses a greater capacity which in turn means a larger response for a given ligate concentration compared to planar surfaces. The CMD layer also provides a hydrophilic environment away from denaturing surface forces. The influence of these denaturing forces is evident from the interaction of CI-2 with

immobilised chymotrypsin. Immobilisation of the chymotrypsin onto a planar surface results in denaturation of the enzyme and subsequently no CI-2 binding.

The interaction between HSA and anti HSA mab has an affinity of around 2 nM with an association rate constant of approximately 2 x 10^5 $M^{-1}s^{-1}$ giving a dissociation rate constant of 4x 10^{-4} s^{-1} and may therefore be considered to be a typical example of the K_D measured by biosensor technology. The immobilisation of anti-HSA mab onto each of the surfaces followed by HSA binding from solution resulted in association rate constants which were similar for the carboxylate and CMD surfaces but higher for the interaction on the amino surface. Values for the association rate constant on the carboxylate were 1.31 and 1.43 x 10^5 $M^{-1}s^{-1}$ respectively with the amino value being almost double at 2.53 x 10^5 $M^{-1}s^{-1}$. This difference is further signified by the rapid increase in response followed by a plateau value in the time course on the amino surface. In addition, the normalised plot also shows the carboxylate and CMD surfaces having similar shape curves whereas the amino plot shows the rapid attainment of a plateau value. This difference is prevalent throughout the concentrations but is more pronounced at the higher concentrations. The chemistry of attachment is similar with coupling through the amino groups of the anti-HSA mab to either the amino surface via glutaraldehyde or to the carboxyl groups on the carboxylate or CMD via EDC/NHS. It is possible that the EDC/NHS coupling procedure is more severe than the glutaraldehyde method resulting in the lower association rate constant.

The error in the dissociation rate constant derived from the intercept of k_{on} vs. [L] plots makes any conclusion on the effect on dissociation difficult. It would seem that the dissociation rate constant is around 2 x 10^{-3} s^{-1} for the planar surfaces. Given this difficulty in defining the intercept, direct fitting of the dissociation phase provides a better comparison.. The data from all three surfaces were well fitted using a single exponential equation with an offset value giving dissociation rate constants of 2 x 10^{-4} s^{-1} . There was no discernible difference in values between any of the surfaces.

The binding of anti-HSA mab to immobilised HSA revealed that the kinetics of association were surface independent at around 2 x 10^5 $M^{-1}s^{-1}$. The assumption of a

1:1 complex is not strictly true for the interaction using either molecule as the ligand due to the bivalent nature of the antibody. While the immobilisation of the antibody followed by binding is valid to be investigated with the integrated rate equation the same is not the case when the antibody is the ligate given its ability to bridge two immobilised ligand molecules. Despite this it is possible to compare surface kinetics on different surfaces. Direct fitting of the dissociation phase was once again performed due to the poorly defined intercept vale from the plot of k_{on} vs. [L].

The dissociation of anti-HSA mab was fitted well to a single exponential decay equation containing an offset and values of 1.95 x 10^{-4} s^{-1} for the amino surface and 5.5 x $10^{-4}s^{-1}$ for both the carboxylate and CMD surfaces. The cause of the higher dissociation rate constant on the latter surfaces is unknown but may represent the error associated within three experiments.

Although a kinetic comparison in terms of ligand can not be made in the strictest sense due to the difference in ligate stoichiometry, it can be seen that there seems to be little difference between rate constants with either anti-HSA mab or HSA immobilised.

The D1.3Fv/lysozyme system has a K_D of 3 nM (Ito and Kurasawa, 1993) and a maximum stoichiometry of 1:1. Immobilisation of the lysozyme and binding of the D1.3Fv reveals no significant difference in the association rate constant between surfaces. Curve fitting of the dissociation phases gave rate constants of 4.03 x 10^{-3} s^{-1} for amino, 3.59 x 10^{-3} s^{-1} for carboxylate, and 4.44 x 10^{-3} s^{-1} for CMD with low residual errors and therefore no significant differences were observed. The activity of the immobilised lysozyme was surface dependant with 0.95 on CMD, 0.11 on carboxylate and 0.37 on amino. The low activity on the planar surfaces probably represents denaturation by surface forces with the difference between the two surfaces representing steric constraints arising from specific interactions.

Several authors have suggested that the CMD matrix will affect the kinetic constants derived from biosensors. Karlsson (1994) suggested that the kinetics would be slower by at least a factor of two compared with solution measurements because of the increase in viscosity within the gel together with the lowering of the diffusional

coefficient of the immobilised ligand. Therefore in the absence of the matrix the constants from the planar surface should be greater.

Schuck (1996) modelled the influence of several parameters on the interaction kinetic within the CMD matrix including the loading level, the thickness of the gel and the partition coefficients and found that the gel thickness was the most important factor. However, it has been reported by Karlsson and Fält (1997) and Parsons and Stockley (1997) that the curves from planar and CMD surfaces are essentially superimposable after normalisation of the responses and they therefore concluded that the matrix had little effect on the parameters determined. Subsequently, Schuck (1997) stated that the absence of any matrix influence in the study by Karlsson and Fält was due to the slow interaction kinetics and high molecular weight of the system studied.

It has been shown that the interaction kinetics on IAsys were less surface sensitive than expected from modelling (Schuck 1996). The association rate constants were similar regardless of the surface for both the two biological systems used. The dissociation rate constant was also independent of the surface used. The k_{diss} from the intercept of k_{on} vs. [L] plot showed the surface independency although with high errors. Further evidence for this surface independence was provided by direct fitting of the dissociation phase. Here, the data were well described by a single exponential decay equation incorporating an offset (equation 2.24) and returned k_{diss} values which were essentially the same for each biological system, regardless of surface. It was also found that the kinetics were not, in the case of the HSA/anti-HSA mab system, influenced by which of the binding partners was immobilised with similar rate constants determined with either the HSA or anti-HSA mab as the ligand.

These results suggest that with these biological systems tested and at these rate constants, the interaction kinetics are independent of surface. However, in certain instances immobilisation of the ligand onto a planar surface can inactivate the ligand, as demonstrated by the chymotrypsin/CI-2 system.

Chapter 7

Depletion.

7.1 Introduction.

The assumption currently inherent within the IAsys cuvette system when used for quantitative analysis is that the concentration of the ligate in solution does not alter with time. This is usually accomplished by performing the experiment under pseudo first order conditions where the concentration of ligate is in excess over the ligand and therefore effectively constant (Edwards et al., 1995). However, given that the cuvette is a closed system and that binding of the ligate to the ligand will lower the concentration in solution, the constant concentration assumption may in certain instances be in error. This is particularly likely with high affinity systems or high immobilisation levels.

In a similar manner data from the dissociation phase may, under conditions of high R_{max} values and high affinity systems, be influenced by rebinding of the dissociated ligate. When this occurs the assumption that the ligate concentration in the dissociating buffer is zero is clearly invalid and therefore the use of the integrated dissociation equation may yield inaccurate k_{diss} results.

In order to determine the extent of depletion in the IAsys cuvette, the amount of ligate removed from solution due to binding was investigated experimentally using radiolabelled HSA. Furthermore, to determine the conditions under which depletion and rebinding become severe, both second order kinetic and equilibrium equations were derived. The influence of various parameters on the rate and equilibrium constants was investigated by comparing the constants determined under first order conditions.

7.2 Measurement of ^{125}I HSA binding.

The removal of ligate from solution was measured by the binding of ^{125}I HSA to anti-HSA immobilised to CMD at two different loadings. The cpm before and after binding were counted and the % difference calculated. Figure 7.1 shows the data from binding to the higher loading of 3000 arc seconds (R_{max} = 600 arc seconds) in the presence and absence of 0.05% Tween 20. The most striking aspect of this figure is the effect of Tween upon the percentage depletion. A depletion of around 30% was found in the absence of Tween for both the 9 and 24 nM concentrations, at the 500

nM a depletion of 17% was observed. With Tween present the depletion dropped dramatically with depletion values of at worst 5% for the lowest ligate concentration of 9 nM.

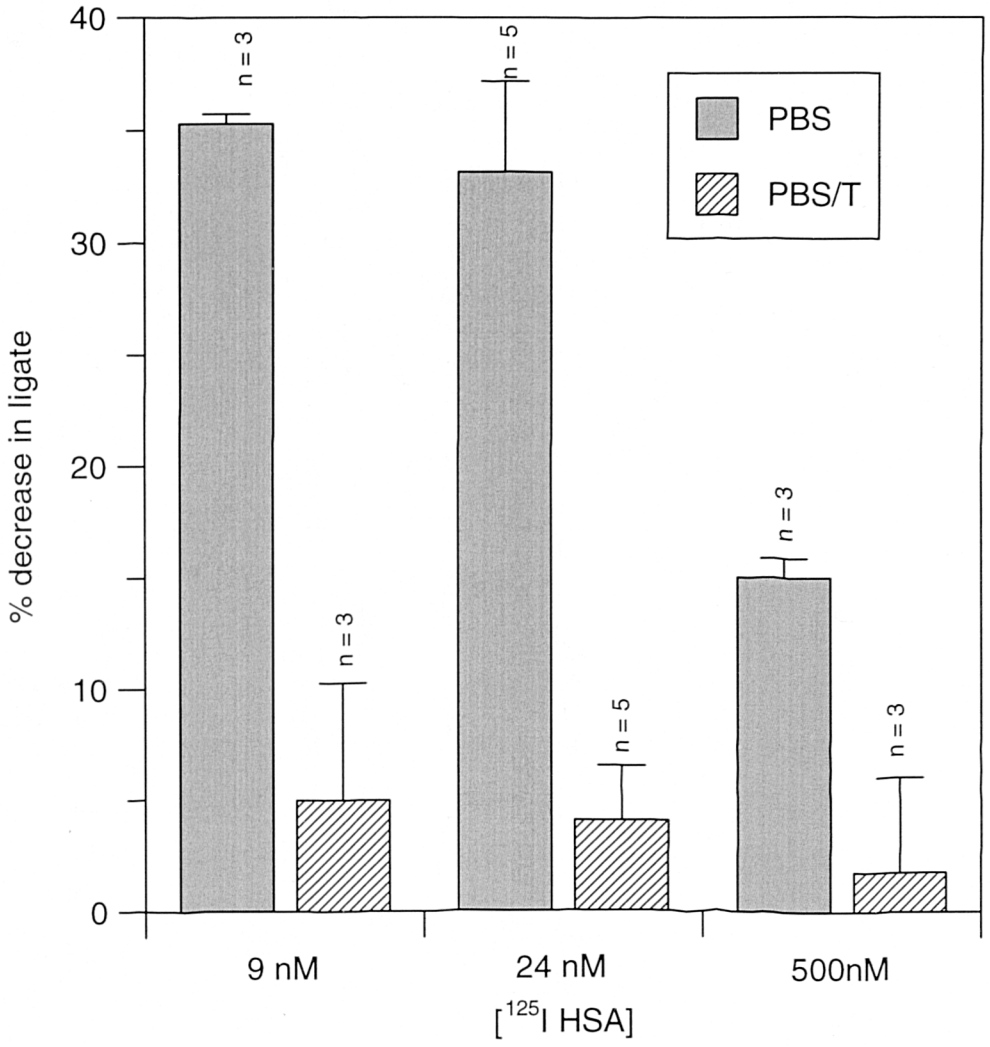

Figure 7.1: *The change in measured cpm compared to the initial value for the binding of three different* ^{125} *I HSA concentrations in the presence and absence of Tween 20 to anti-HSA mab immobilised to a response value of 3000 arc seconds.*

The high depletion observed without Tween present is due to the measurement of essentially two depletion sources. The first is the specific binding to the surface, which should be the same regardless whether Tween is present. This was found to be true with a response after 10 minutes of 250 arc seconds observed with and without Tween for the 500 nM solution. The second source arises from adsorption to the

cuvette walls, stirrer and aspirator. Lowering the capacity of the ligand for the ligate by lowering the immobilisation response would be expected to decrease the degree of depletion arising from specific interactions. Figure 7.2 shows that by immobilising anti-HSA to 625 arc seconds (R_{max} of 150 arc seconds) the depletion is reduced. In agreement with the higher immobilisation response, the depletion is higher in the absence of Tween. The depletion in the presence of Tween is negligible with, in fact, negative mean values being returned for the 24 nM solution.

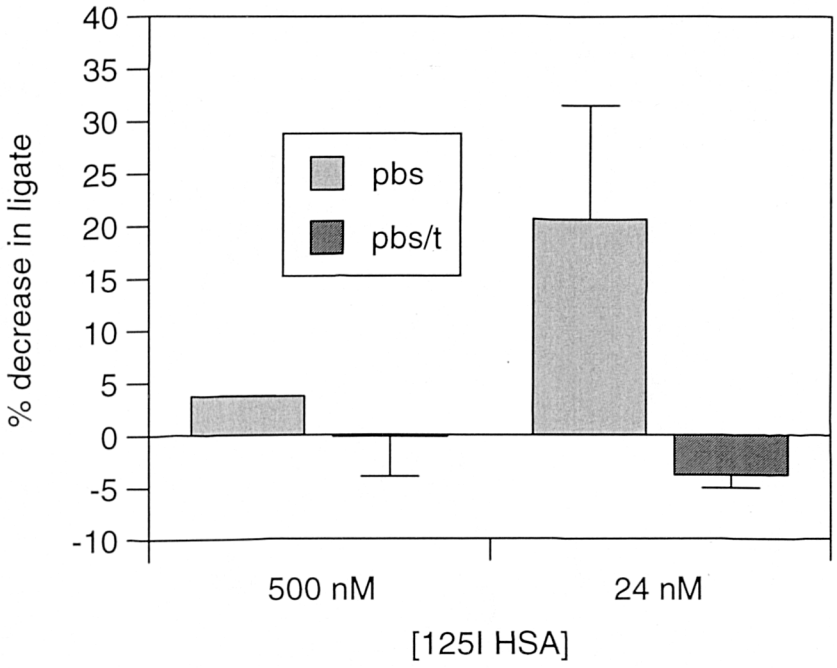

Figure 7.2: *The change in measured cpm compared to the initial value for the binding of two different ^{125} I HSA concentrations (n = 3) in the presence and absence of Tween 20 to anti-HSA mab immobilised to a response value of 625 arc seconds.*

A control surface with chymotrypsin immobilised was used for ^{125}I HSA bindings at both 500 and 24 nM. The control data in figure 7.3 show a similar pattern to that observed for the lower anti-HSA immobilised cuvette with values in PBS of 5 and 20% for the 500 and 24 nM solution respectively. Once again the values in the presence of Tween were negative and given the fact that any negative depletion value equates to generation of HSA, these negative values were assumed to represent errors in the methodology and hence the depletion was negligible.

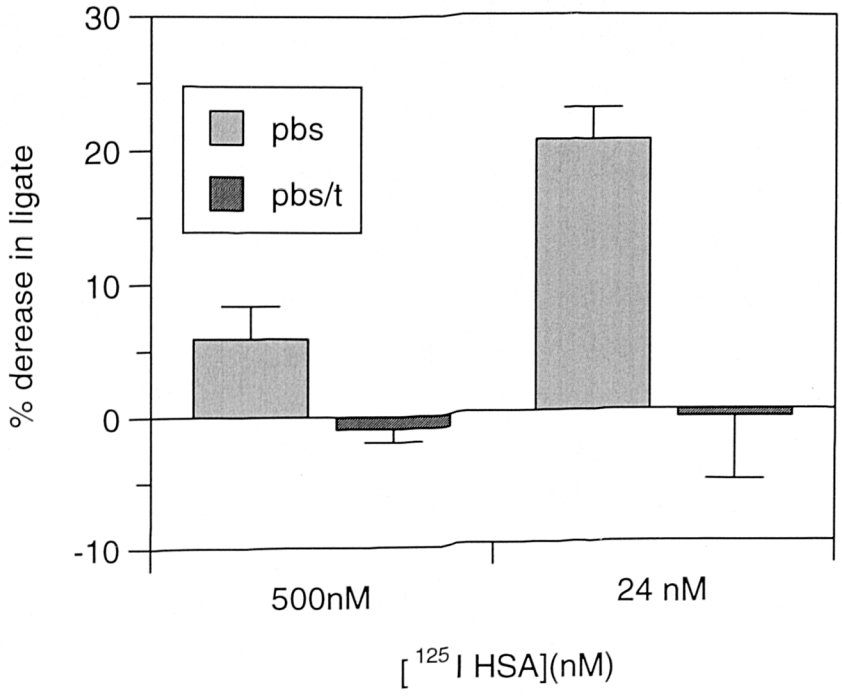

Figure 7.3: *The change in measured cpm compared to the initial value for the binding of two different* ^{125} *I HSA concentrations (n = 3) in the presence and absence of Tween 20 to chymotrypsin immobilised to a response value of 400 arc seconds.*

In order to discount that the low depletion values observed were due to a lower affinity resulting from radiolabeling, a kinetic comparison of labelled and unlabelled HSA was performed. This was achieved by binding each of the HSA solutions at differing concentrations to the high anti-HSA immobilised cuvette. From this both the association and dissociation rate constants were calculated (figure 7.4). The association rate constant for the labelled material was 1.64 x 10^5 $M^{-1}s^{-1}$, while that of the unlabelled material was 1.68 x 10^5 $M^{-1}s^{-1}$. The dissociation rate constant determined from the intercept was 1.2 x 10^{-4} s^{-1} for the labelled and 2.7 x 10^{-4} s^{-1} for the unlabelled material.

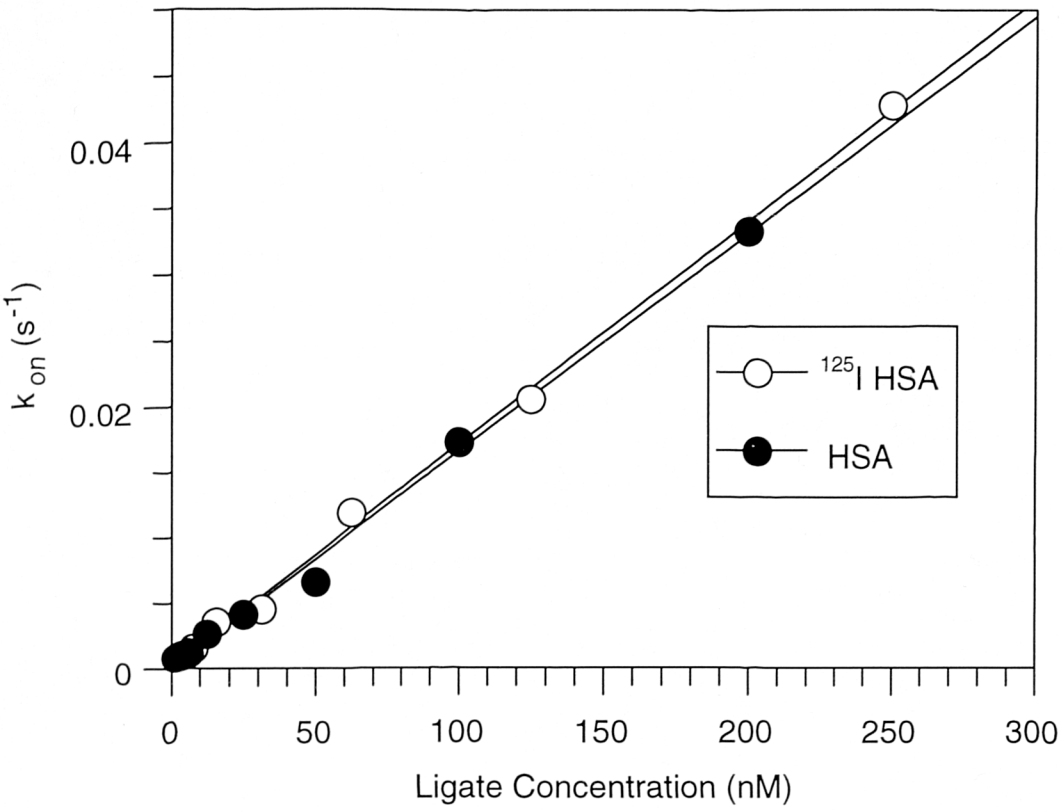

Figure 7.4: *A plot of on-rate against ligate concentration for the binding of ^{125}I HSA and unlabelled HSA to immobilised anti-HSA mab. The two solid lines represent a linear fit through the data points for both the labelled HSA and unlabelled HSA. The two sets of data points and therefore the linear fits are almost identical showing that the ^{125}I HSA labelling process has not affected the activity of the HSA.*

An alternative approach for the determination of depletion is to measure the amount of ligate bound instead of the amount of ligate free in solution after binding. It is possible to convert instrument response to a concentration term and thus determine depletion in this manner. The conversion to concentration requires a knowledge of the surface area of the sensor (16mm^2, the volume of ligate used (200µl), and the calibration factor (200 arc seconds = 1ng/mm^2) so that the conversion factor for the HSA system is 6.06 x 10^{-12} M/arc second. The depletion resulting from specific binding of ^{125}I HSA is shown in figure 7.5.

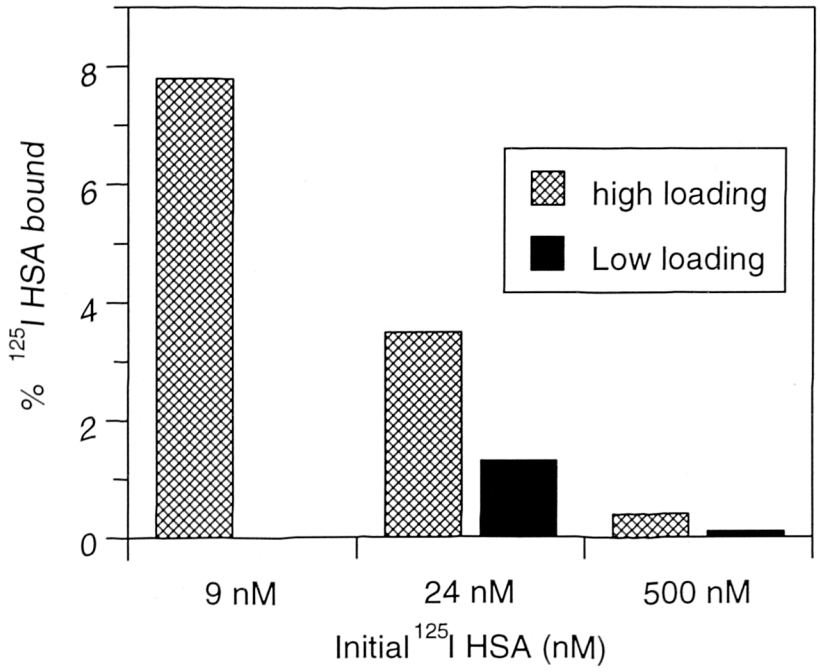

Figure 7.5: *The amount of ^{125}I HSA bound specifically to the immobilised anti-HSA as a function of initial ^{125}I HSA concentration and anti-HSA immobilisation response. The high loaded surface had an immobilisation response of 3000 arc seconds, while the low loaded surface had 625 arc seconds.*

Specific binding accounts for less than 0.5% of the total ligate concentration for the 500 nM ^{125}I HSA solution for both surface loadings. At the 24 nM concentration values of 3 and 1.2% for the high and low loadings respectively were calculated. These values, together with the 8% arising from the 9 nM solution at the high loading, are within the errors associated with the radioactive results in the presence of Tween.

7.3 Second order analysis.

In contrast to the pseudo first order analysis used routinely for the investigation of biosensor data, depletion modelling requires the use of second order equations.

7.3.1 Derivation of second order equations

The reaction between immobilised ligand, G, and ligate, L, from solution can be described by equation 7.1.

$$G + L \underset{k_{diss}}{\overset{k_{ass}}{\rightleftharpoons}} GL \qquad (7.1)$$

where k_{diss} is the dissociation rate constant and k_{ass} is the association rate constant. The rate of complex formation, GL, is given by equation 7.2.

$$\frac{d[GL]}{dt} = k_{ass}[L][G] - k_{diss}[GL] \qquad (7.2)$$

The instrument response, R, is assumed to be proportional to the concentration of complex, with the initial concentration of G and L being $[G]_0$ and $[L]_0$ respectively.

For a change in instrument response there must be R/α (g/m^2) added where α is the calibration factor in arc seconds/g/m^2.

As G is immobilised any increase in mass is from the binding of L. The number of molecules of L per m^2 is

$$\frac{R}{\alpha . M_r} . N_A \qquad (7.3)$$

where M_r is the molecular weight of L and N_A Avagadros number.

7.3.1.1 Second order association rate equation

If there is a volume V (m^3) of ligate and a total surface area S (m^2) on the device then the concentration reduction giving a response R is

$$\frac{S.R}{\alpha . M_r V} \qquad (7.4)$$

and therefore the concentration of L in the cuvette allowing for a binding response R is

$$L(R) = [L]_0 - \frac{S.R}{\alpha.M_r.V} \tag{7.5}$$

Similarly the concentrations of G and GL when a response of R is achieved are given by

$$G(R) = [G]_0\left(1 - \frac{R}{R_{\max}}\right) \tag{7.6}$$

and

$$GL(R) = \frac{[G]_0 R}{R_{\max}} \tag{7.7}$$

Where R_{max} is the maximal response when all immobilised G sites are filled.

Inserting equation 7.5, 7.6 and 7.7 into equation 7.2 gives

$$\frac{dR}{dt} = k_{ass}.\beta\left(\frac{[L]_0}{\beta} - R\right)(R_{\max} - R) - k_{diss}R \tag{7.8}$$

where $\beta = \frac{S}{\alpha.M_A V}$

Multiplying out equation 7.8 gives

$$\frac{dR}{dt} = k_{ass}\beta\left\{R^2 - \left(\frac{[L]_0}{\beta} + R_{\max} + \frac{k_{diss}}{\beta k_{ass}}\right)R + \frac{[L]_0}{\beta}R_{\max}\right\} \tag{7.9}$$

$$\frac{dR}{dt} = k_{ass}.\beta(p - R)(q - R) \tag{7.10}$$

p and q are the roots of the quadratic equation such that

$$R^2 - \left(\frac{[L]}{\beta} + R_{\max} + \frac{k_{diss}}{\beta k_{ass}}\right)R + \frac{[L]}{\beta}R_{\max} = 0 \tag{7.11}$$

This has the general solution of

$$t = \frac{1}{k_{ass}.\beta.(p-q)} \ln \frac{q(p-R)}{p(q-R)} + T \qquad (7.12)$$

Where T is the particular solution given by the boundary conditions. At t = 0, R= 0 and thus equation 7.12 has the solution

$$t = \frac{1}{k_{ass}.\beta.(p-q)} \ln \frac{q(p-R)}{p(q-R)} \qquad (7.13)$$

Rearrange to give R in terms of t

$$\ln \frac{q(p-R)}{p(q-R)} = k_{ass}\beta(p-q)t$$

$$\frac{q(p-R)}{p(q-R)} = \exp(k_{ass}\beta(p-q)t)$$

or

$$q(p-R) = p(q-R)E(t)$$

where $E(t) = \exp(k_{ass}\beta(p-q)t)$ (7.14)

thus

$$(pE(t)-q)R = pq(E(t)-1)$$

gives

$$R = \frac{pq(E(t)-1)}{pE(t)-q}$$

$$= q\left(1 - \frac{p-q}{pE(t)-q}\right) \tag{7.15}$$

in full

$$R = q\left(1 - \frac{p-q}{p\exp(k_{ass}\beta(p-q)t)-q}\right) \tag{7.16}$$

By inspection q is the equilibrium response at a given ligate concentration.

7.3.1.2 Second order dissociation rate equation

The concentration of L in the cuvette during dissociation is given by

$$L(R) = \frac{-S(R-R_0)}{\alpha.M_A V} = -\beta(R-R_0) \tag{7.17}$$

where R_0 is the initial response. The concentrations of G and GL are given by equations 7.6 and 7.7 such that the differential equation defining the rate of complex dissociation with time is

$$\frac{dR}{dt} = k_{ass}\beta\left\{R^2 - \left(R_0 + R_{\max} + \frac{k_{diss}}{\beta k_{ass}}\right)R + R_0 R_{\max}\right\} \tag{7.18}$$

This has the general solution as shown in equation 7.12

$$t = \frac{1}{k_{ass}.\beta.(p-q)}\ln\frac{q(p-R)}{p(q-R)} + T \tag{7.19}$$

Here T is $R = R_0$ at t=0

$$T = -\frac{1}{k_{ass}.\beta(p'-q')}\ln\left(\frac{q'(p'-R_0)}{p'(q'-R_0)}\right) \qquad (7.20)$$

Inserting 7.19 into 7.18 gives

$$t = \frac{1}{k_{ass}\beta(p'-q')}\left\{\ln\left(\frac{(p'-R)(q'-R_0)}{(q'-R)(p'-R_0)}\right)\right\}$$

Rearranging gives

$$\frac{p'-R}{q'-R}.\frac{q'-R_0}{p'-R_0} = \exp\left(k_{ass}\beta(p'-q')t\right)$$

$$R(t) = \frac{(p'q'-q'R_0)E(t) - p'q'+p'R_0}{(p'-R_0)E(t) - q'+R_0} \qquad (7.21)$$

where $E(t)=\exp(k_{ass}\beta(p'-q')t)$

7.3.2 Modelling of typical interactions using second order equations.

The effect of depletion on an IAsys sensor plot can be demonstrated by considering an interaction with an association rate constant of 1 x 10^6 $M^{-1}s^{-1}$ and a dissociation rate constant of 1 x 10^{-2} s^{-1} on a surface with a binding capacity (R_{max}) of 625 arc seconds. The calibration factor of 200 arc seconds is equivalent to 1ng/mm^2 and a sensor surface area of 16mm^2 together with a ligate volume of 200µl were used. Ligate concentrations were 100,50,25,10,5, and 1 nM. For comparison, first order data were also generated using equation 2.16. Both sets of binding data are shown in figure 7.6.

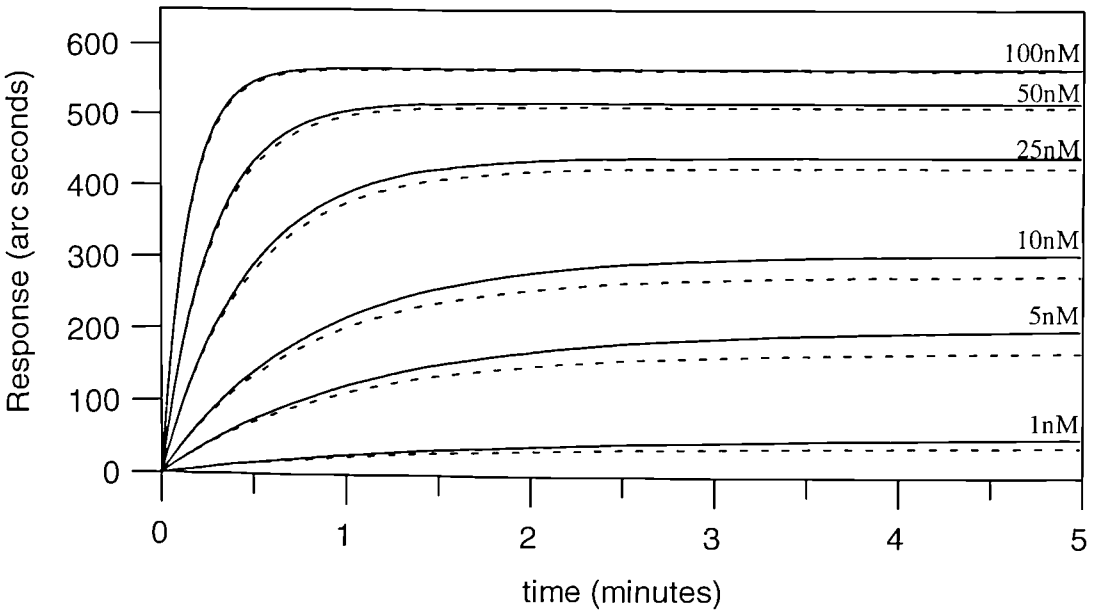

Figure 7.6: *The influence of depletion upon the binding of a 66000 Da ligate. The solid lines are generated using the pseudo-first order equation (equation 2.16) while the dotted lines are generated with the second order equation (equation 7.16).*

The deviation from the first order conditions is greater at the lower ligate concentrations, with the effect of depletion more marked for longer incubations. It may therefore be expected that depletion will effect the equilibrium values determined by a plot of equilibrium response (R_{eq}) against ligate concentration. This binding isotherm is used to determine the K_D for a reaction using the Langmuirian isotherm (equation 7.22).

$$R_{eq} = \frac{R_{\max}[A]}{K_D + [A]} \tag{7.22}$$

7.3.2.1 Equilibrium data

Despite the fact that the primary biosensor data does not require direct fitting, in contrast to the determination of the individual rate constants, the free concentration of ligate is needed. The construction of an isotherm involves the plotting of R_{eq} against the free ligate concentration. Hence, in the presence of depletion, the assumption that the free concentration is equal to that of the initial concentration is no longer valid.

The extent to which depletion affects the isotherm is related to both the capacity of the ligand for the ligate (R_{max}) and the affinity. This can be illustrated by simulating data using an R_{max} of 1250 arc seconds with a K_D of 1 nM for 300 seconds at 1 second intervals. Depletion under these circumstances is expected to be severe and this is shown by the poor fitting of the data to the Langmuirian isotherm giving a K_D value of 5 nM.

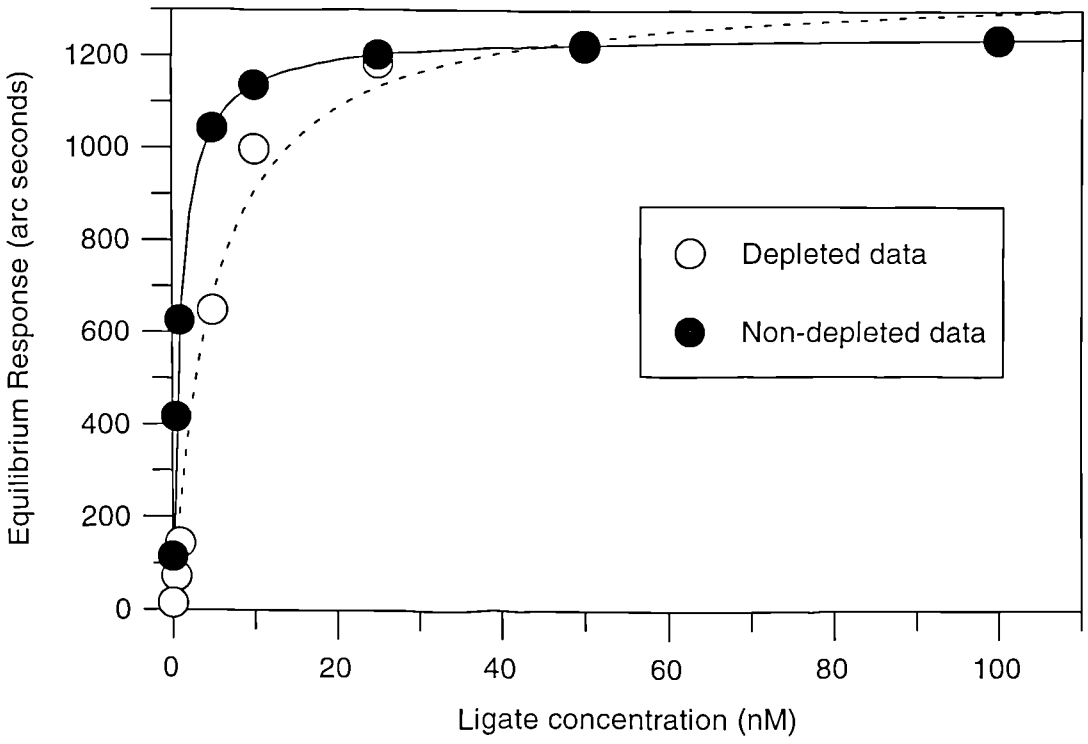

Figure 7.7: *Isotherm showing theoretical data generated assuming no depletion (closed circles) and depletion (open circles) for an interaction with an R_{max} of 1250 arc seconds and an affinity of 1 nM. Equations 2.12 and 7.16 were used to generate the non-depleted and depleted data respectively. The solid line shows the Langmuirian isotherm to the non-depleted data, while the dotted line shows the fit to the depleted data.*

The influence of R_{max} upon the depletion can be illustrated by using the same affinity as used for figure 7.7 but with an R_{max} of 200 arc seconds. This should have the effect of reducing the depletion. Data were once again simulated by both the depleted and no-depleted equation.

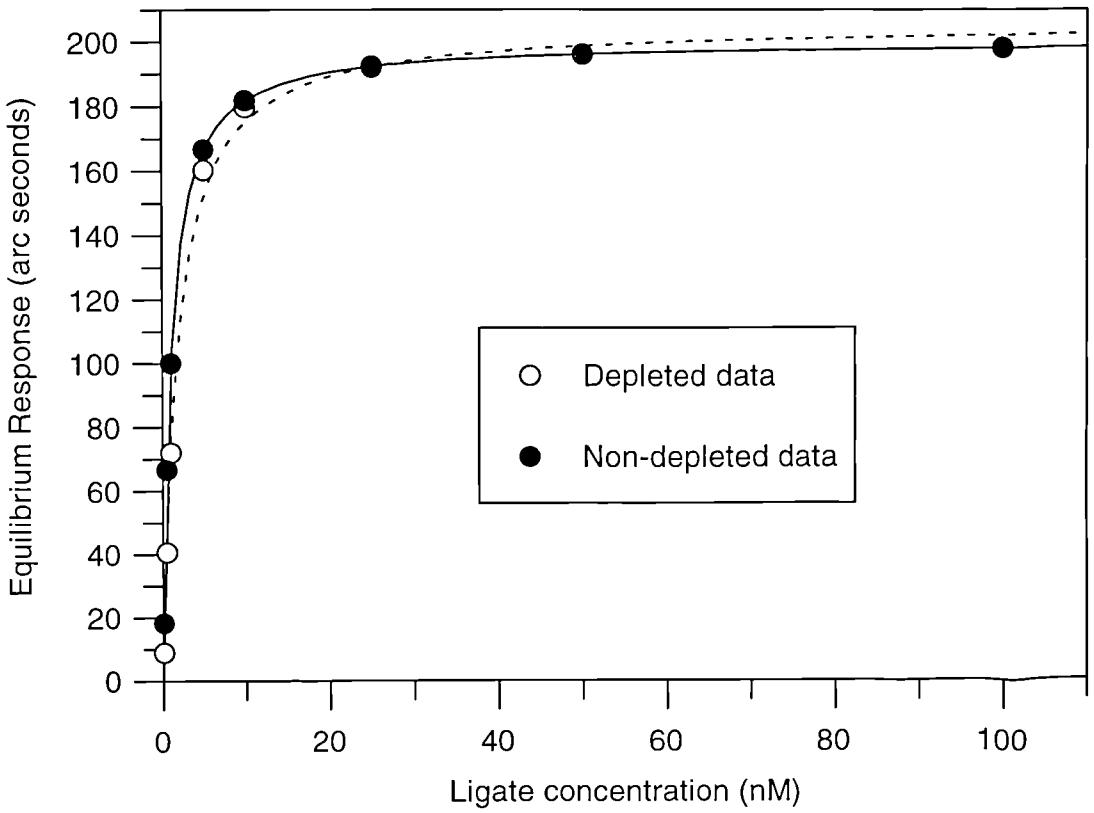

Figure 7.8: *Isotherm showing theoretical data generated assuming no depletion (closed circles) and depletion (open circles) for an interaction with an R_{max} of 200 arc seconds and an affinity of 1 nM. Equations 2.12 and 7.16 were used to generate the non-depleted and depleted data respectively. The solid line shows the Langmuirian isotherm to the non-depleted data, while the dotted line shows the fit to the depleted data.*

The deviation from the non-depleted data is less extreme than with the higher capacity simulation and the Langmuirian fit to the depleted data (dotted line) gives a K_D of 1.7 nM (error of 70%). Depletion is still evident at the lower ligate concentrations. Finally the influence of the affinity on the isotherm is shown in figure 7.9 with an R_{max} of 200 arc seconds and an affinity of 10 nM.

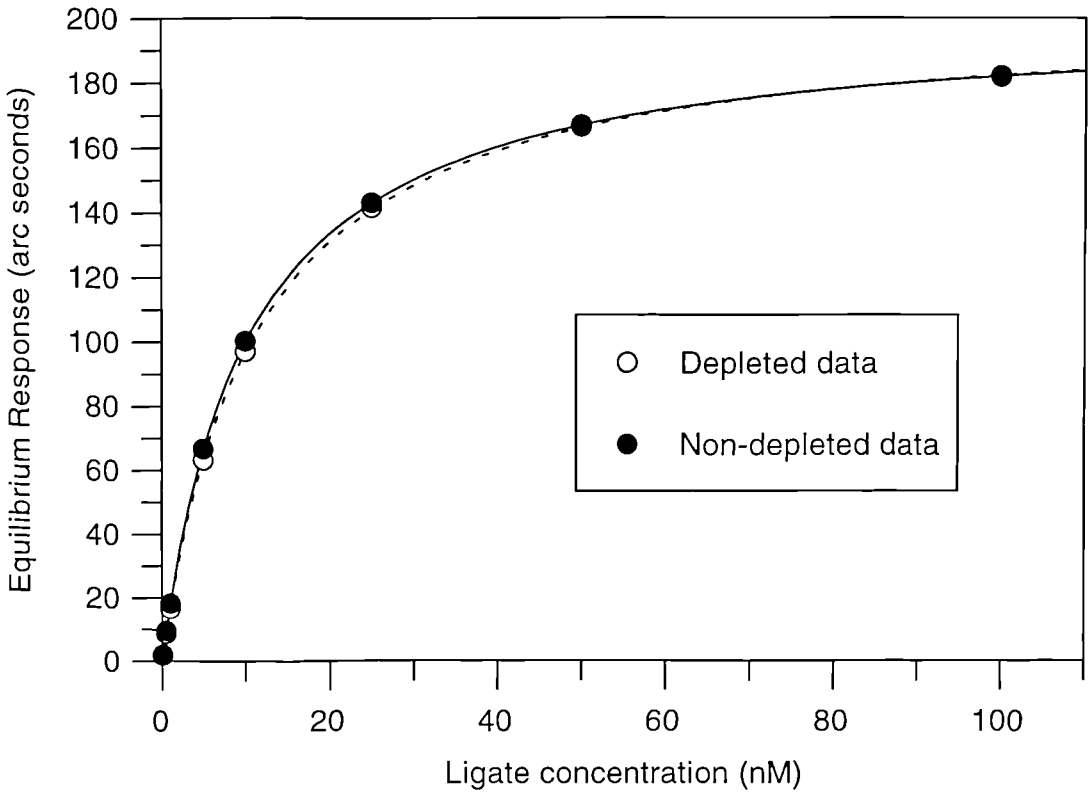

Figure 7.9: *Isotherm showing theoretical data generated assuming no depletion (closed circles) and depletion (open circles) for an interaction with an R_{max} of 200 arc seconds and an affinity of 10 nM. Equations 2.12 and 7.16 were used to generate the non-depleted and depleted data respectively. The solid line shows the Langmuirian isotherm to the non-depleted data, while the dotted line shows the fit to the depleted data.*

With a R_{max} value of 200 arc seconds and an affinity of 10 nM the two data sets are essentially superimposable. The Langmuirian isotherm fit to the depleted data gives a K_D of 10.8 nM (error of 8%).

Inspection of the data in figure 7.7 shows the importance in selection of the ligate concentration range. For equilibrium analysis it is usual to use a ligate concentration range 10 times above and below that of the K_D. At 10 times above the K_D 90% of the complex has formed which would been seen on the IAsys as approaching the R_{max} value. For the data generated by the Langmuirian isotherm this is obviously true, but for the depleted data set the values at this concentration are still some way from the

R_{max} value. Thus selection of the data at 10 times K_D would result in a poor determination of the R_{max} value with a corresponding error in the K_D value.

7.3.2.2 Calculation of the affinity in the presence of depletion

Despite the presence of depletion, the affinity of interactions can be accurately determined by the IAsys. It is possible to determine the affinity by three routes.

7.3.2.2.1 Correcting the K_D obtained from the Langmuirian isotherm.

The first involves the fitting of the data to the standard Langmuirian isotherm giving a value for K_D. This K_D value can then be corrected using the equation below

$$K_D^{corr} = K_D^{meas} - \frac{R_{max}\beta}{2} \tag{7.23}$$

The correction term is independent of the affinity and therefore an estimate of depletion can be determined with a knowledge of the R_{max}. Thus the correction for an R_{max} of 200 arc seconds would be 0.6 nM and would make the corrected affinities for the simulated data in figures 7.6 and 7.7 to be 1.08 nM and 10.1 nM. As the correction scales with the R_{max} value the correction of 1250 arc seconds is 3.75 nM giving a corrected affinity of 1.25 nM. Clearly while these corrected affinities are closer to those used to generate the data they are still higher. The reason for this discrepancy is due to the poor fit of the Langmuirian isotherm to the data resulting in a higher R_{max}, and thus K_D, than expected.

7.3.2.2.2 Correction of concentrations prior to data fitting.

An alternative method is to correct each of the data points individually for depletion. This involves the conversion of the equilibrium response to concentration using the β term and subtracting this bound ligate concentration from the initial concentration to order to give the free ligate concentration. The corrected data can then be analysed using the Langmuirian isotherm. This approach is shown in figure 7.10 for the high depleting situation shown in figure 7.7 (R_{max} = 1250 arc seconds, K_D = 1 nM).

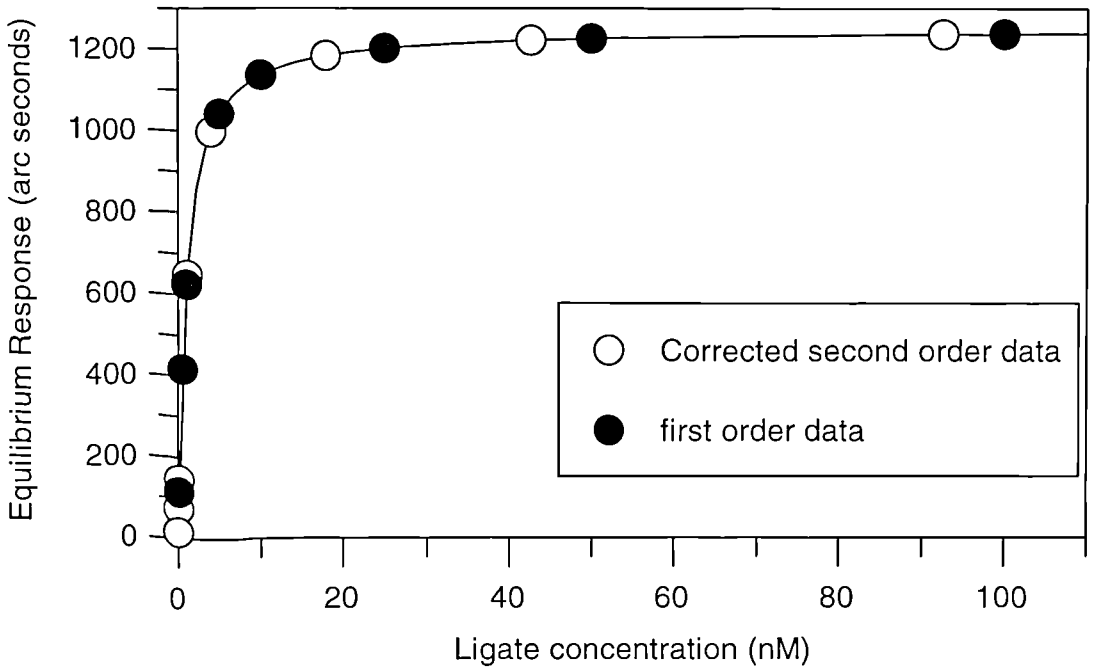

Figure 7.10: *Isotherm showing a Langmuirian fit (solid line) to the corrected depleted data (open circles) together with non-depleting data (closed circles) from the data shown in figure 7.7. The corrected second order data now lie on the Langmuirian isotherm of the first order data.*

The corrected data lies on the Langmuirian isotherm with a K_D of 1 nM and a R_{max} value of 1250 arc seconds.

7.3.2.2.3 Fitting equilibrium data using a depletion isotherm equation.

The third method is to fit the depleted data to an isotherm which allows for depletion. In the derivation of the kinetic equation (equation 7.16) the term q was found to be equal to the equilibrium response for a given ligate concentration. Therefore by solving the quadratic equation (equation 7.11) should allow the K_D of an interaction to be determined from an isotherm even in the presence of depletion.

The general solution for quadratic equations is

$$\frac{-b \pm \sqrt{b^2 - 4ac}}{2a}$$

Solving for equation 7.11 gives equation 7.24 below (positive root impossible)

$$R_{eq} = \frac{([L] + R_{max} + K) - \sqrt{([L]^2 - 2[L]R_{max}\beta + 2[L]K + (R_{max}\beta)^2 + 2R_{max}\beta K + K^2)}}{2\beta}$$

Equation 7.24

Figure 7.11 shows the fit to the data from Figure 7.7 with the depleted isotherm equation 7.24. The fit is good and the values of 1 nM for the k_D and 1250 arc seconds for the R_{max} are those used to generate the data.

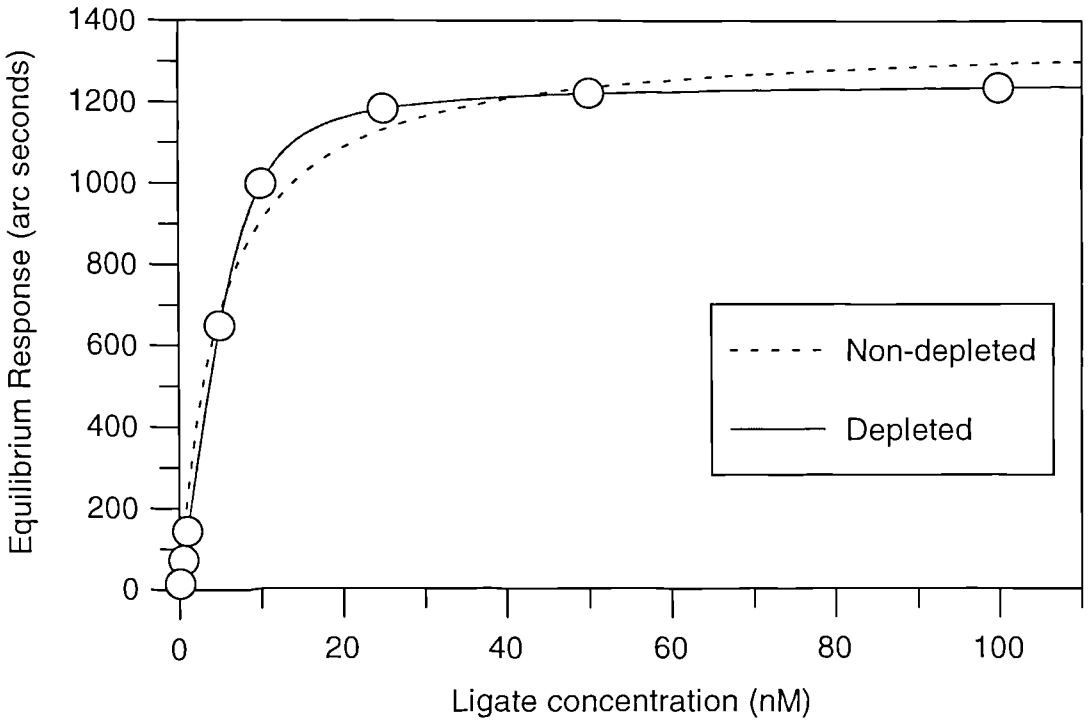

Figure 7.11: *Isotherm showing a Langmuirian fit (dotted line) together with a depleted isotherm fit (solid line) using Equation 7.24 for depleted equilibrium data in figure 7.7.*

7.3.2.3 Association data

The effect of depletion on the kinetics of an interaction can best be shown by the construction of a kinetic plot (k_{on} against ligate concentration). Therefore data simulated using the second order equation are fitted using the first order kinetic equation. This shows the effect of fitting depleted biosensor data with the first order equation and the errors in the determination of the association rate constant and dissociation rate constant.

To illustrate the effect of depletion on the determined rate values second order data were generated at a range of R_{max} values (100,200,625, and 1250 arc seconds) with an association rate constant of 1 x 10^7 $M^{-1}s^{-1}$, a dissociation rate constant of 1 x 10^{-2} s^{-1}, and using the value of β determined for a 66000 Da ligate. Data were then fitted using the first order rate equation and the determined on-rates plotted against ligate concentration for each of the R_{max} values (figure 7.12).

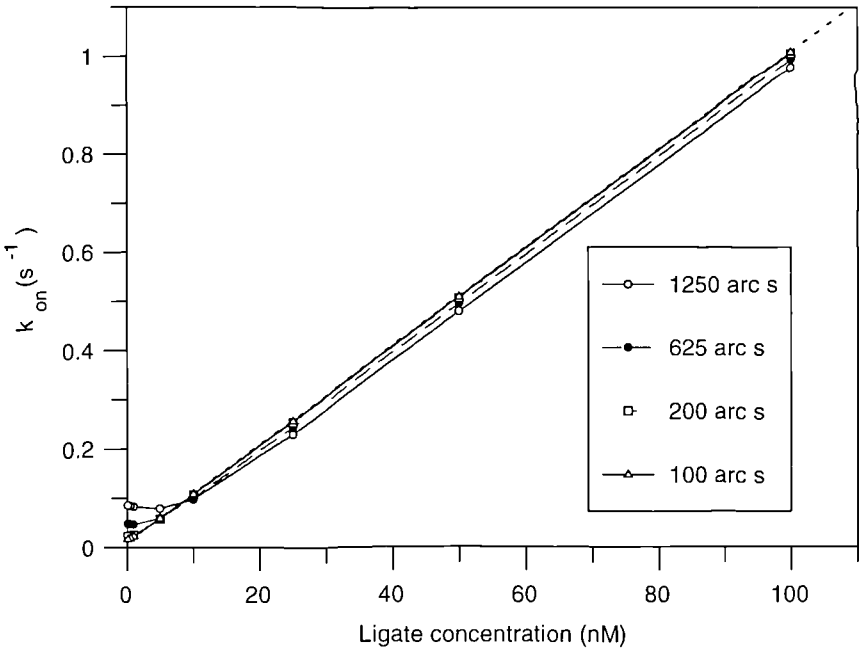

Figure 7.12: *On-rate against ligate concentration for data generated assuming depletion with a K_D of 10 nM and fitted using first order analysis. Theoretical second order data were generated using equation 7.16 for differing R_{max} values assuming a k_{ass} of 1 x 10^7 $M^{-1}s^{-1}$, a k_{diss} of 1 x 10^{-2} s^{-1} and a 66000 Da ligate.*

Depletion results in a lowering of the k_{on} value at high ligate concentrations while at lower ligate concentrations the k_{on} value is higher than expected. Thus instead of a linear plot, a curved plot is observed. This effect is more pronounced at the higher R_{max} values. Figure 7.13 shows the data in figure 7.12 but over a restricted ligate concentration range.

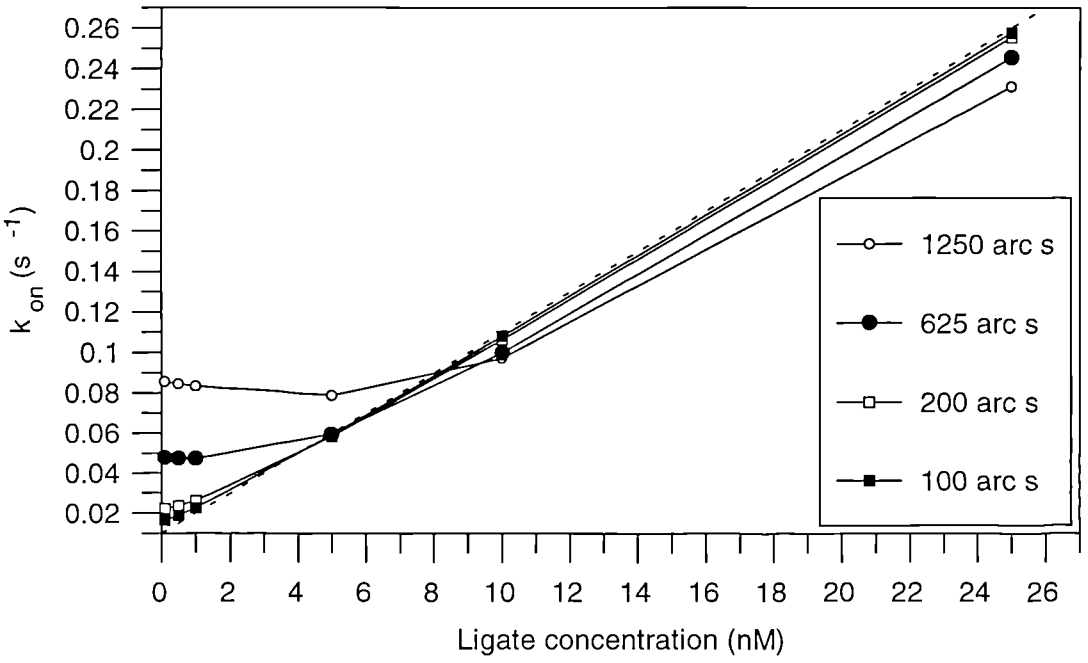

Figure 7.13: *Data from figure 7.12 but highlighting the curvature at the lower ligate concentrations.*

This highlights the curvature seen at the lower ligate concentrations with the higher R_{max} values. The dotted line is that expected from the rates used to generate the data. At the lower R_{max} values the fitted k_{on} values are close to the expected line and are less affected by depletion.

For comparison the same plots were generated using the same parameters with the exception of the association rate constant decreased to 1 x 10^5 $M^{-1}s^{-1}$. Figure 7.14 shows the data while figure 7.15 shows a restricted ligate concentration range.

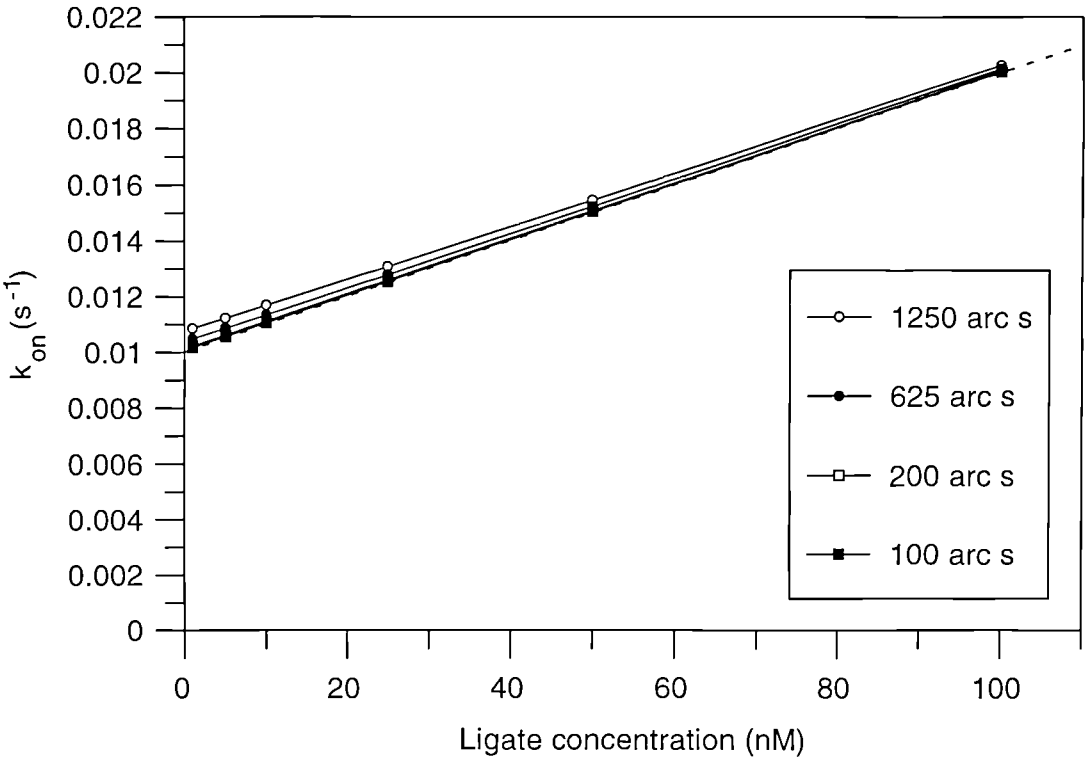

Figure 7.14: *On-rate against ligate concentration for data generated assuming depletion with a K_D of 100 nM and fitted using first order analysis. Theoretical second order data were generated using equation 7.16 for differing R_{max} values assuming a k_{ass} of* 1×10^5 $M^{-1}s^{-1}$ *a k_{diss} of 1 x 10^{-2} s^{-1} and a 66000 Da ligate. Depletion becomes appreciable at lower ligate concentrations with high R_{max} values causing a positive curvature.*

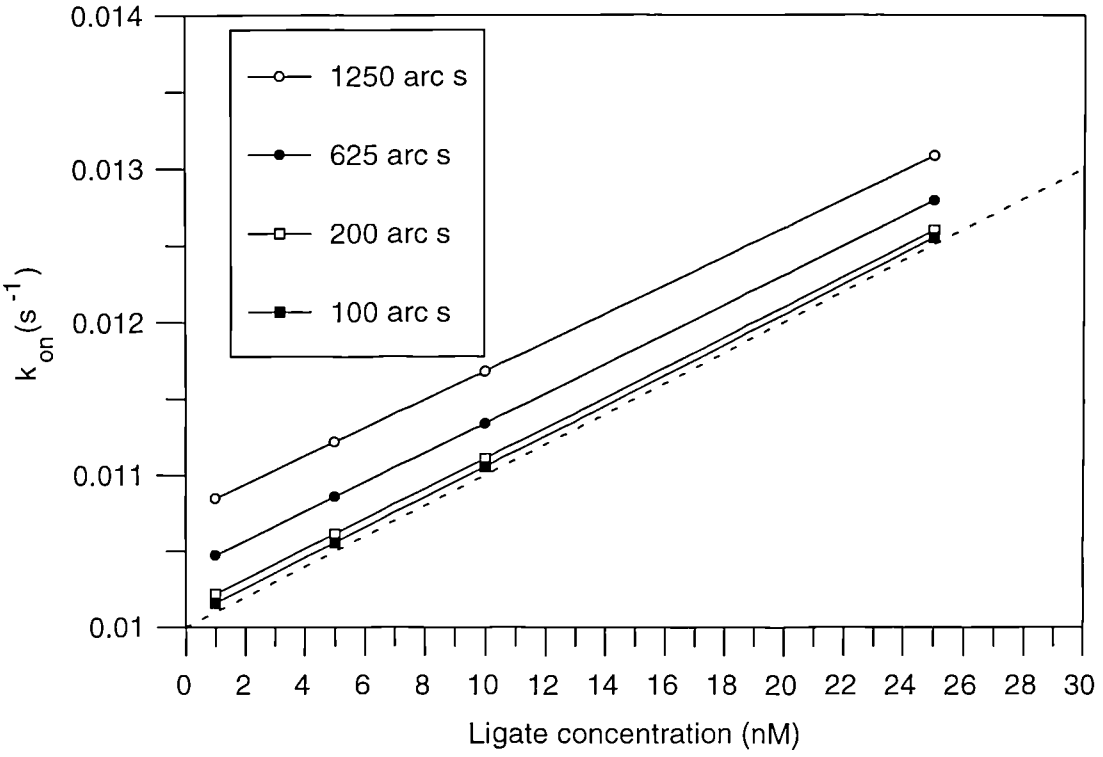

Figure 7.15: *Data from the low ligate concentrations in figure 7.14.*

7.3.2.4 Dissociation data

Due to the closed nature of the IAsys cuvette the assumption that upon dissociation the concentration of ligate in the solution is zero may not be valid. When this assumption is violated there is the possibility of rebinding of the dissociated ligate to the immobilised ligand. To investigate this, data were generated using the second order dissociation equation (equation 7.21) and this data fitted to the normal approach using equations 2.18 and 2.24 (without and without an offset value). The influence of rebinding on the dissociation phase for a 50000 mw ligate can be seen in figure 7.16 with data generated using a response at which dissociation is initiated (R_0) of 300 arc seconds for surfaces with varying R_{max} values. The association rate constant was 1 x 10^6 M^{-1} s^{-1} and the dissociation rate constant was 1 x 10^{-2} s^{-1}.

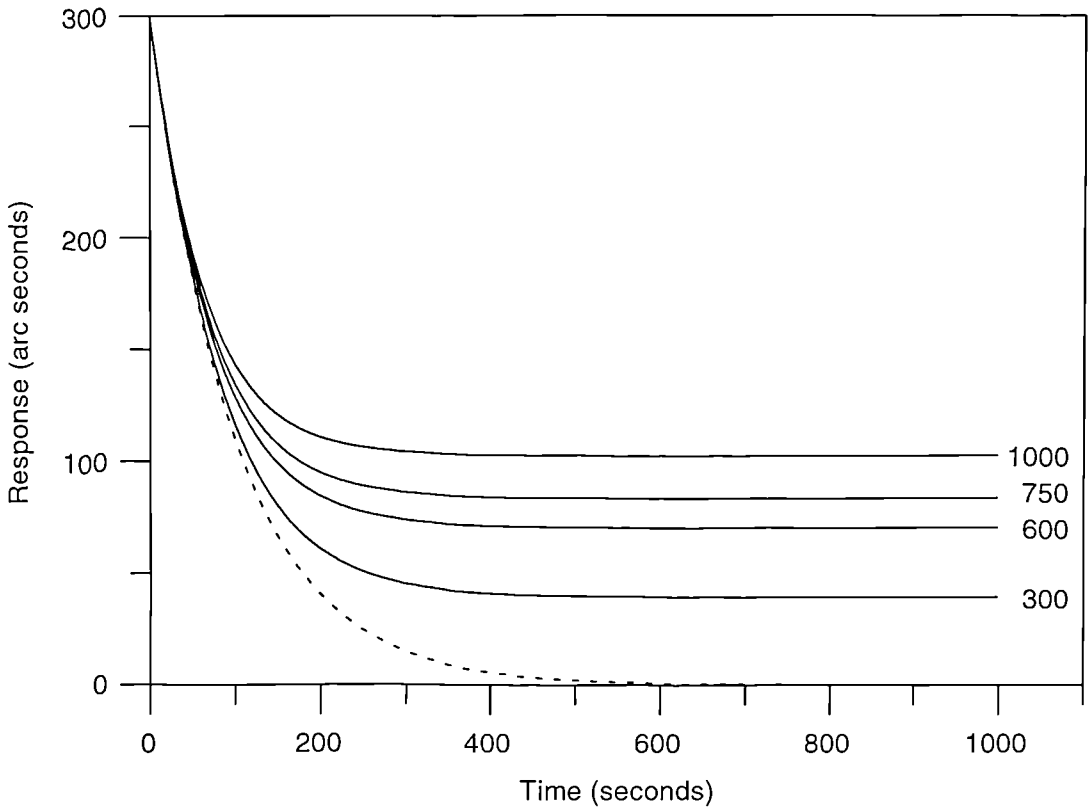

Figure 7.16: *The influence of rebinding upon the dissociation time course. The data were generated using* equation 7.21 *with a* k_{ass} *of 1 x* 10^6 $M^{-1}s^{-1}$, *a* k_{diss} *of* 1 x 10^{-2} s^{-1} *and a* R_0 *(response at which dissociation is initiated) of 300 arc seconds for surfaces with differing* R_{max} *values. The* R_{max} *values are shown to the right of the generated data. The dotted line shows the dissociation in the absence of rebinding (equation 2.18)*

As expected, the degree to which dissociation is complete is influenced by the binding capacity of the ligand. Increasing the R_{max} of the interaction causes the dissociation to become less complete with the final response being well above that expected for complete dissociation. In this example with a K_D of 10 nM, even the surface with a low R_{max} capacity of 300 arc seconds deviates from that expected in the absence of rebinding (dotted line).

In order to determine the effect of this rebinding upon the derived dissociation rate constants, data generated at the differing R_{max} values were fitted in the normal manner by either a single exponential equation (2.18), or this single exponential equation incorporating an offset (2.24), or an equation with two exponential functions (2.25).

Figure 7.17 shows the fitted curves from these equations the data generated with an R_{max} of 300 arc seconds.

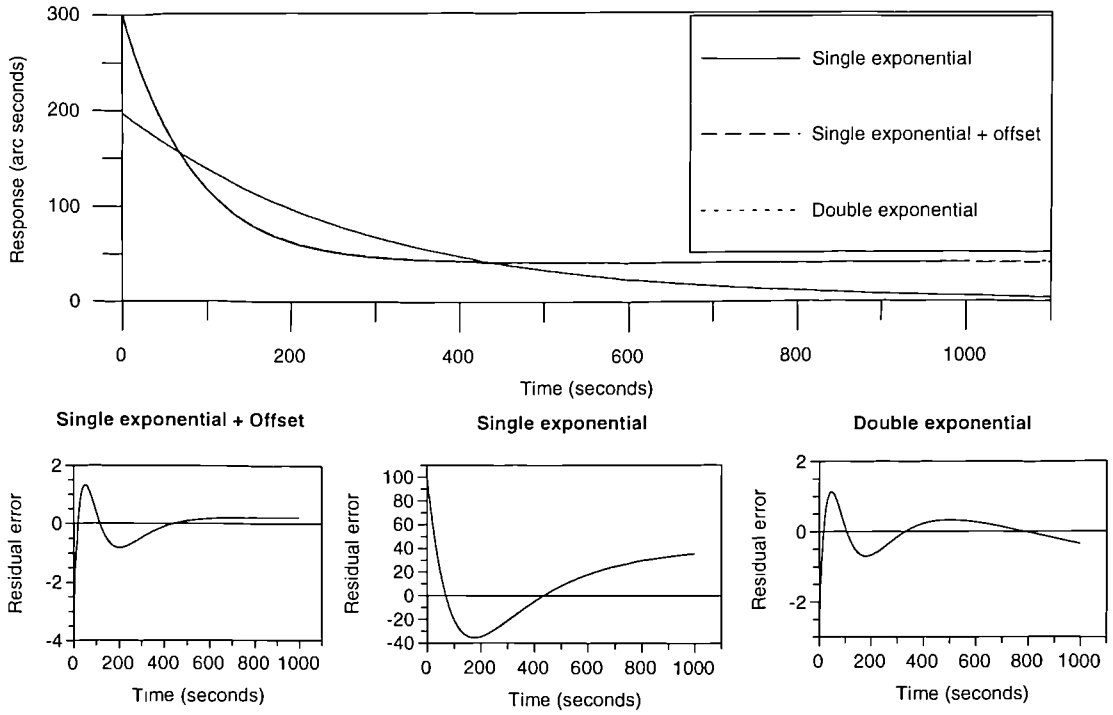

***Figure 7.17**: Curve fitting of second order dissociation data generated with R_0 and R_{max} values of 300 arc seconds and an affinity of 100 nM. Top: Dissociation time course showing the data (solid line) and the fit to the data from three different fitting equations. The data were generated using equation 7.21 with parameters of k_{ass} of 1 x 10^6 $M^{-1}s^{-1}$, a k_{diss} of 1 x 10^{-1} s^{-1} assuming a ligate molecular weight of 50000 Da. Bottom: Residual error plots showing the difference between the fitted curve and the actual data for each of the three fitting equations.*

The fit together with the residual errors shows that the single exponential equation fails to adequately describe the data. A value of 3.57 x 10^{-3} was derived from this fit and therefore a difference from the 1 x 10^{-2} s^{-1} value of 64%. In contrast, fitting to either the double exponential or the offset equations describe the data better with values of 1.22 x 10^{-2} s^{-1} ($k_{diss(1)}$) and 1.24 x 10^{-2} s^{-1} (22 and 24% difference) respectively.

By increasing the k_{diss} to 1 x 10^{-1} s^{-1} the affinity is lowered to 100 nM. Figure 7.18 shows the data from the R_{max} of 300 arc seconds over a time scale of 200 arc seconds, although all the 1000 second of data were used for fitting.

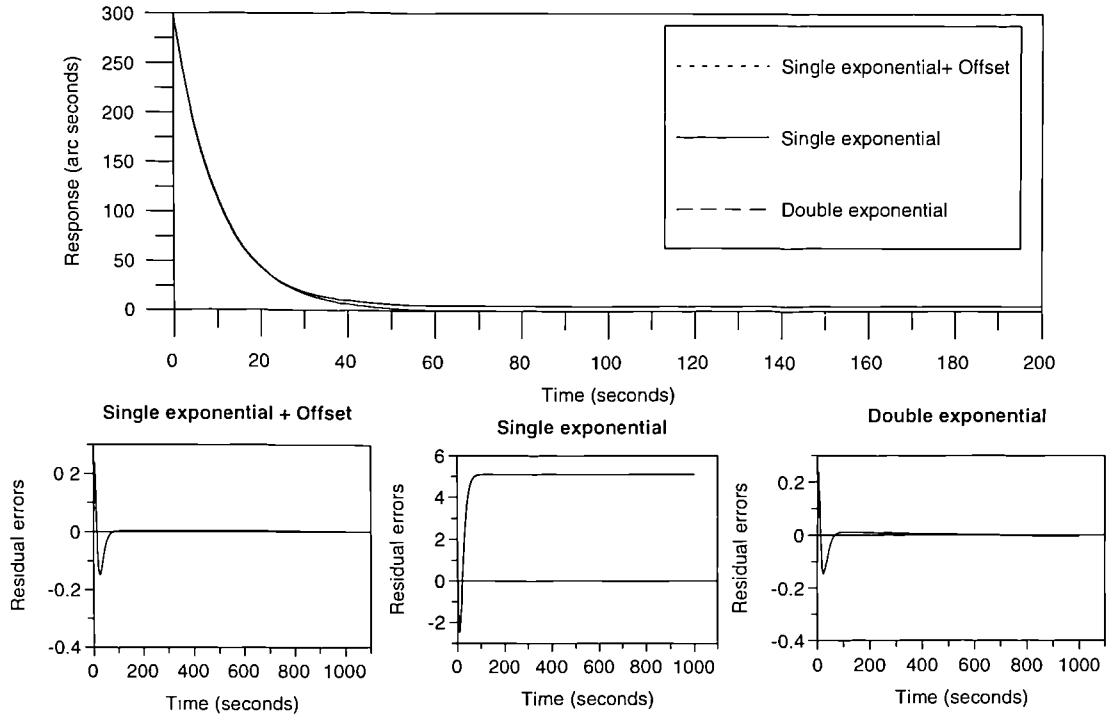

Figure 7.18: *Curve fitting of second order dissociation data generated with R_0 and R_{max} values of 300 arc seconds and an affinity of 10 nM. Top: Dissociation time course showing the data (solid line) and the fit to the data from three different fitting equations. The data were generated using equation 7.21 with parameters of k_{ass} of 1 x 10^6 $M^{-1}s^{-1}$, a k_{diss} of 1 x 10^{-1} s^{-1} assuming a ligate molecular weight of 50000 Da. Bottom: Residual error plots showing the difference between the fitted curve and the actual data for each of the three fitting equations.*

Once again the data were described well with the inclusion of an offset or by the addition of a second exponential function and returned the same k_{diss} value of 1.03 x 10^{-1} s^{-1} (3% difference). The value from the single exponential equation determined was 9.6 x 10^{-2} s^{-1} (4% difference).

Figure 7.19 shows the fitted curves from the three equations to data generated by altering the k_{diss} to 1 x 10^{-3} s^{-1} to give an affinity of 1 nM with a R_{max} of 300 arc seconds. As before, the data are well fitted to both the single + offset and the double exponential equation as shown by the magnitude of the residual errors although the errors do appear systematic. The k_{diss} values determined from these equations were 6.89 x 10^{-4} s^{-1} for the single exponential, 2.31 x 10^{-2} s^{-1} for the offset equation, and 2.02 x 10^{-3} s^{-1} for the double exponential equation giving differences of 31%, 131%, and 102% respectively.

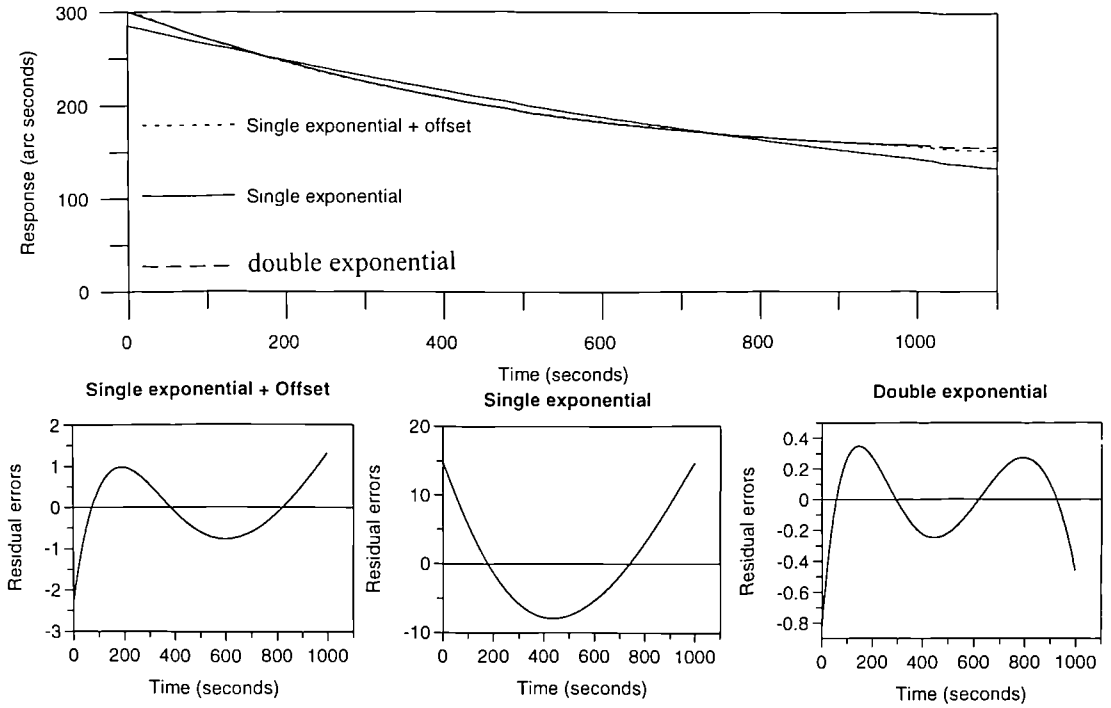

Figure 7.19: *Curve fitting of second order dissociation data generated with R_0 and R_{max} values of 300 arc seconds and an affinity of 1 nM. Top: Dissociation time course showing the data (solid line) and the fit to the data from three different fitting equations. The data were generated using equation 7.21 with parameters of k_{ass} of 1 x 10^6 $M^{-1}s^{-1}$, a k_{diss} of 1 x 10^{-1} s^{-1} assuming a ligate molecular weight of 50000 Da. Bottom: Residual error plots showing the difference between the fitted curve and the actual data for each of the three fitting equations.*

Rebinding would be expected to be worse for longer dissociation times and as such restricting the amount of data should improve the accuracy of the k_{diss}. Limiting the data window to 100 seconds improved the accuracy of the k_{diss} values from all equations but the single exponential equation once again had the lowest difference between the fitted value and that used to generate the data. However, the residual errors for the single exponential equation were higher than the other equations.

The amount of dissociation data used for fitting was scaled to the dissociation rate constant such that 1000 seconds of data were fitted for 1 x 10^{-3} s^{-1}, 100 seconds for 1 x 10^{-2} s^{-1} and 10 seconds for 1 x 10^{-1} s^{-1}. Using these time scales, data were generated at differing association and dissociation rate constants and fitted to the either the single exponential equation with or without an offset or the double exponential equation. The data are summarised in Table 7.1 below

k_{diss}	Single Exponential		Single exponential + offset		Double exponential	
	k_{diss} (s^{-1})	% difference	k_{diss} (s^{-1})	% difference	k_{diss} (s^{-1})	% difference
1 x 10^{-1}	9.59 x 10^{-2}	4.1	1.116 x 10^{-1}	11.6	1.12 x 10^{-1}	12.0
1 x 10^{-2}	9.59 x 10^{-3}	4.1	1.115 x 10^{-2}	11.5	1.119 x 10^{-2}	11.9
1 x 10^{-3}	9.58 x 10^{-4}	4.1	1.115 x 10^{-3}	11.5	1.121 x 10^{-3}	12.1

Table 7.1: *The dissociation rate constants derived from exponential curve fitting of second order data with a fixed R_0 and R_{max} of 300 arc seconds and k_{ass} of 1 x 10^6 $M^{-1}s^{-1}$. Scaling the amount of dissociation data fitted to the starting k_{diss} value used to generate the data shows the fitted k_{diss} value to be independent of the k_{diss}.*

The differences are the same regardless of the dissociation rate constant used with the affinity remaining constant by virtue of varying the association rate constant. The differences scale with the affinity of the system and not the individual rate constants

with the affinity defining the amount of rebinding and hence the extent by which the dissociation is incomplete.

The extent of rebinding is also determined by the response at the start of dissociation (R_0) in relation to the R_{max} value. Figure 7.20 shows the dissociation profiles for an interaction with k_{ass} of 1 x 10^6 $M^{-1}s^{-1}$ and a k_{diss} of 1 x 10^{-2} s^{-1} with a R_{max} value of 300 arc seconds and varying the R_0 value.

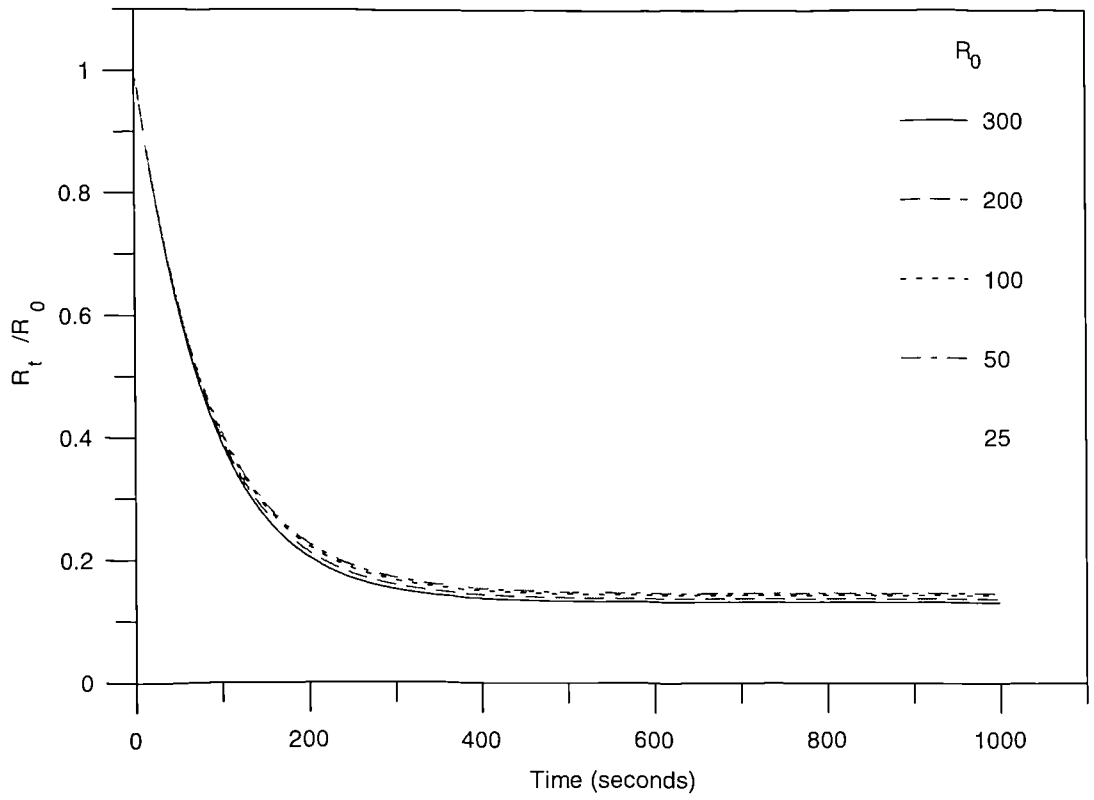

Figure 7.20: *Dissociation data generated using at different R_0 values with a constant R_{max} of 300 arc seconds. Equation 7.21 with k_{ass} of 1 x 10^6 $M^{-1}s^{-1}$, a k_{diss} of 1 x 10^{-2} s^{-1}, a R_{max} value of 300 arc seconds and a ligate molecular weight of 50000 Da with differing R_0 values. The dissociation data produced is scaled to the R_0* of each curve (R_t/R_0).

Once again the data were poorly fitted to the single exponential equation but well described by the addition of an offset value into the equation. The fit could also be improved by the reduction of the time scale in common with varying the R_{max} values.

7.4 The effect of depletion upon experimental data

Data obtained from the interaction of CI-2 with chymotrypsin immobilised at different loading levels on the CMD were analysed using the equations derived in the previous section (7.3).

7.4.1 The effect of depletion upon the association data for the CI-2/chymotrypsin interaction.

The effect of depletion upon association data can be shown by plotting the on-rate determined by second order analysis (equation 7.16) against ligate concentration. Such a plot is shown in figure 7.21 together with the corresponding on-rate from pseudo first-order analysis for the binding of CI-2 to chymotrypsin immobilised at a response of 1110 arc seconds. The second order equation assumes that the data is a simple 1:1 interaction and therefore described by a single exponential equation. In order to compare first and second order analysis, CI-2 binding data were restricted to that described by a single exponential term using the pseudo first order equation. The same data were then fitted to the second order equation. The second order equation has no on-rate term and only returns values for the association and dissociation rate constant. The on-rate in figure 7.21 for the second order analysis is calculated using the two rate constants and the CI-2 concentration.

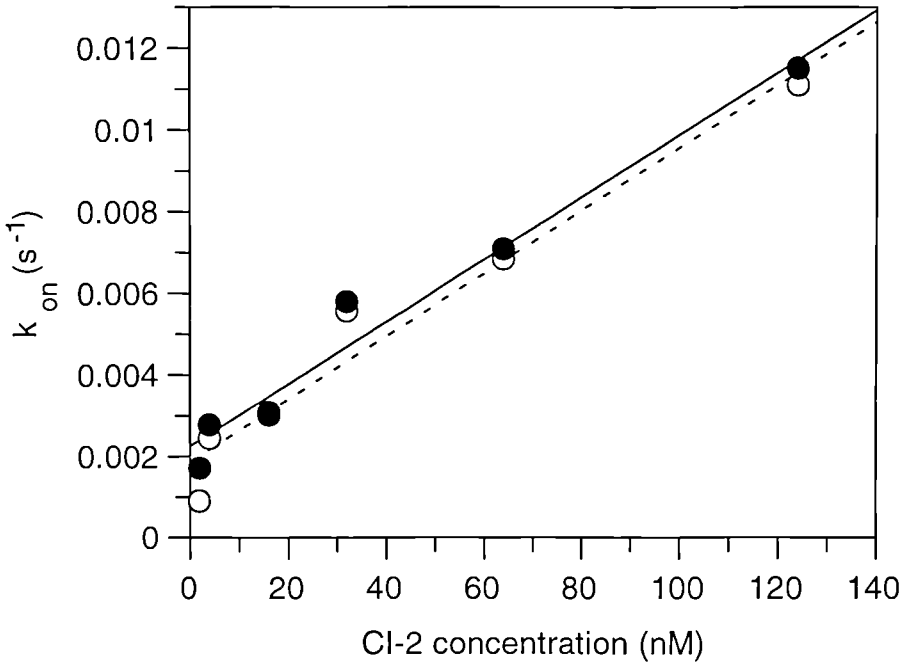

Figure 7.21: *Plot of on-rate, from both first (solid circles) and second (open circles) order analysis, against CI-2 concentration. The linear fit to the pseudo first order data is shown as a solid line, while the dashed line shows the linear fit to the second order data.*

The association and dissociation rate constants derived from the slope and intercept respectively of plots such as figure 7.21 are shown in figures 7.22 and 7.23 as a function of the chymotrypsin loading. In addition, the rate constants determined from pseudo first-order analysis are also shown.

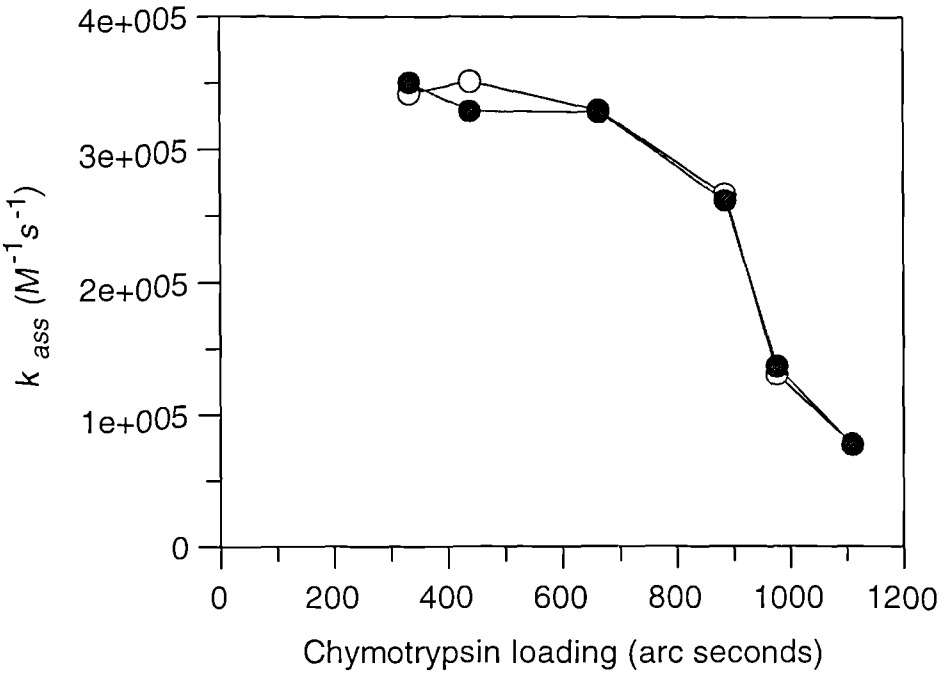

Figure 7.22: *The influence of depletion upon the association rate constant for the interaction of CI-2 with immobilised chymotrypsin. The association rate constant for both pseudo first order (solid circles) and second order (open circles) analysis of data at differing chymotrypsin loadings is shown.*

The association rate constants appear unaffected by the different analysis with no significant difference between the values obtained by either first order or second order analysis. Furthermore, the general trend in rate constants with ligand loading is maintained.

The dissociation rate constant determined from the intercept seems to be more sensitive to the analysis type. The dissociation rate constants determined from the second order analysis are lower than those obtained from first order analysis (figure 7.23) across the range of loadings investigated. However, the extent of this lowering seems independent of loading.

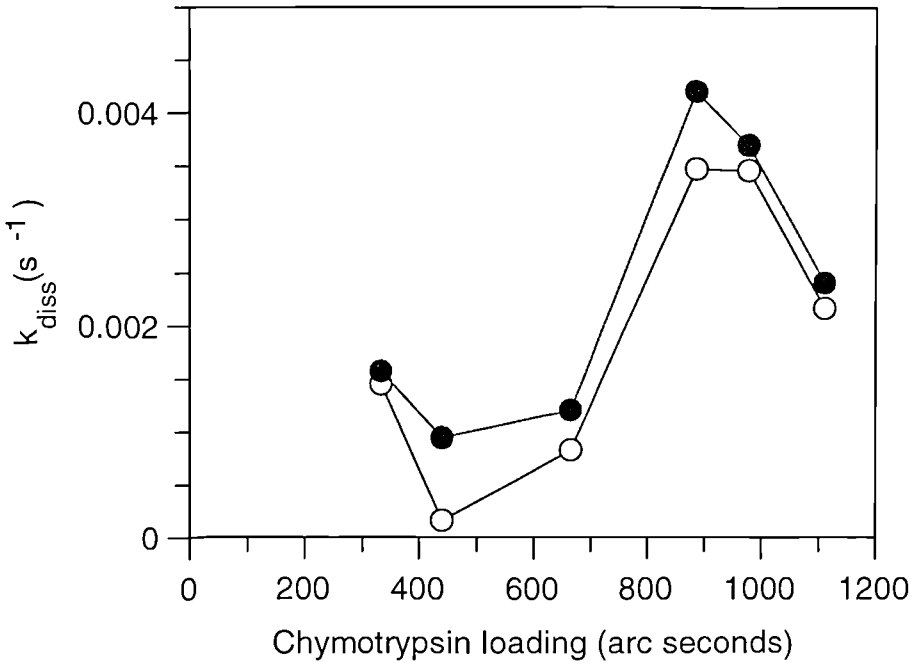

Figure 7.23: *The influence of depletion upon the dissociation rate constant, determined from the intercept of plots such as figure 7.22, against chymotrypsin loading. The open circles represent second order analysis of the experimental data while the solid circles represent pseudo first order.*

7.4.2 The effect of depletion upon the K_D for the CI-2/chymotrypsin interaction.

The ratio of the two rate constants was used to calculate K_D. Figure 7.24 shows the K_D value calculated in such a manner by both first order and second order analysis of the rate constants.

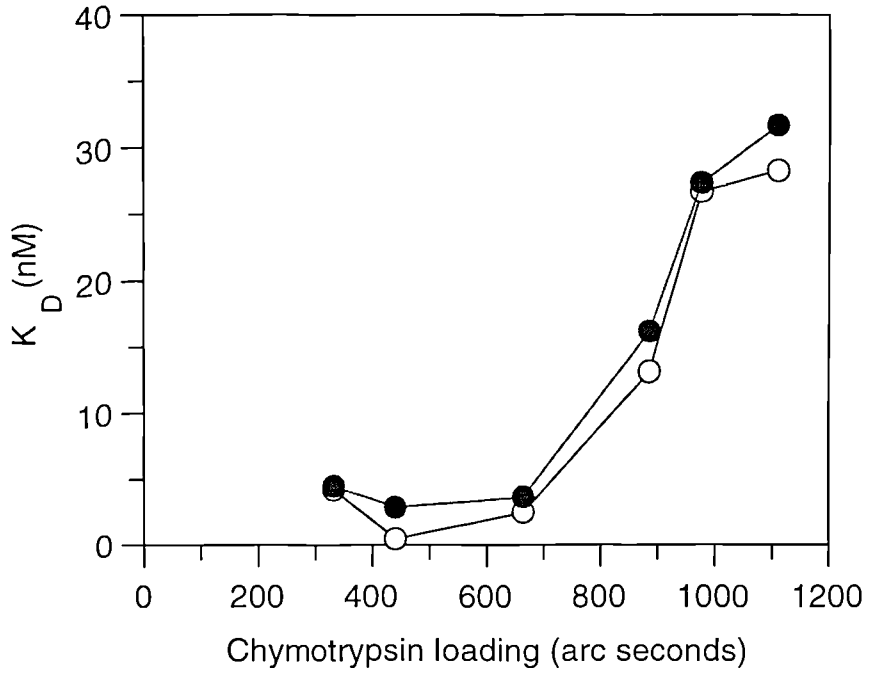

Figure 7.24: *The influence of depletion upon the K_D determined from the ratio of the two rate constants as a function of chymotrypsin loading. The open circles represent second order analysis and the closed circles, pseudo first order analysis.*

The second order analysis results in a lower K_D value, with the difference largely reflecting differences in the k_{diss} value.

The K_D was also determined from the binding isotherm of equilibrium responses. The binding isotherm for CI-2 binding to chymotrypsin immobilised to CMD at 1110 arc seconds is shown in figure 7.25 fitted to a Langmuirian isotherm (equation 7.22). Also shown on the figure are experimental data points corrected using equation 7.23 also fitted to equation 7.22. The fit to the depleted isotherm (equation 7.24) to the uncorrected data is also shown.

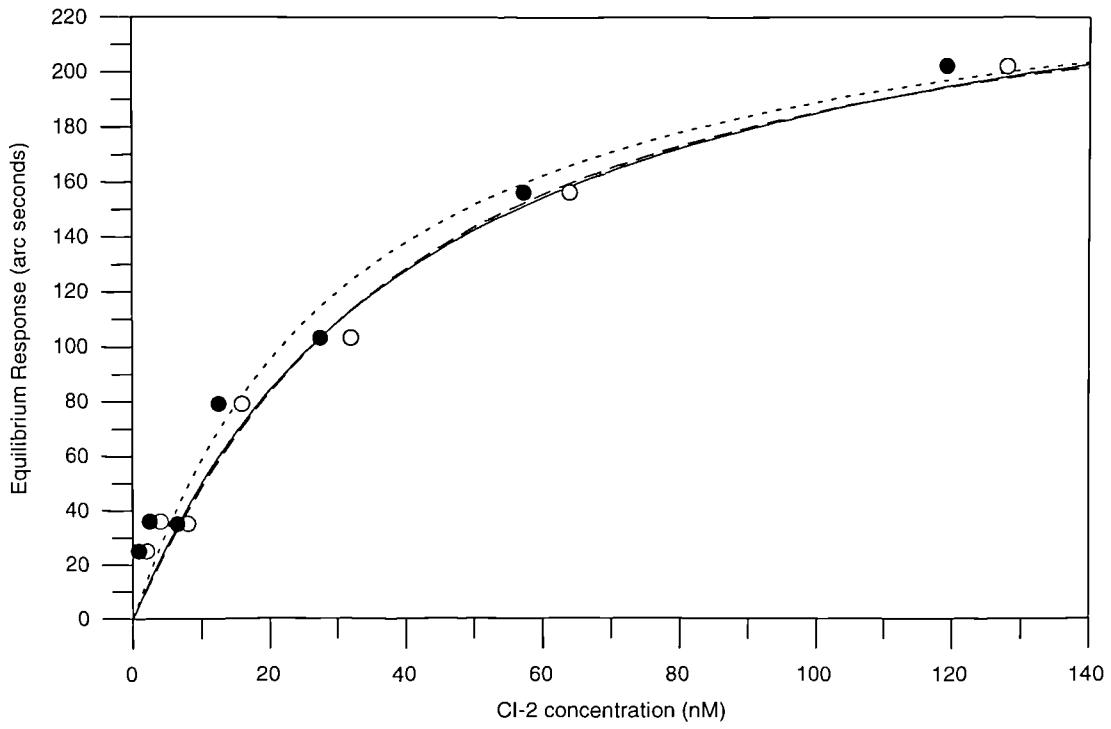

Figure 7.25: *The influence of depletion upon the binding isotherm for the interaction of CI-2 with chymotrypsin immobilised at 1110 arc seconds. Experimental data are shown as open circles and the Langmuirian isotherm as a solid line. The best fit line to the data using the depleted isotherm equation is also shown (dashed line). Experimental data were also corrected for depletion using equation 7.23 are shown as solid circles together with a Langmuirian isotherm (dotted line)*

The experimental equilibrium responses (open circles) are plotted against the CI-2 concentration and fitted to a simple Langmuirian isotherm equation as shown by the solid line. A K_D of 41 ± 10 nM was determined. Data corrected for depletion by equation 7.23 are also shown (solid circles) together with a Langmuirian isotherm (dotted line). This approach causes the data points to be shifted to the left resulting in a lower K_D value of 33 ± 9 nM. Fitting the experimental data to the depleted isotherm equation (equation 7.24) gives the fit shown as a dashed line and returns a K_D value of 33 ± 8.5 nM.

This approach was repeated for other chymotrypsin loadings and the K_D values from fitting the experimental data to first or second order conditions are shown in figure

7.26. This figure shows that the K_D from the second order analysis are lower than from first order analysis over the entire loading range investigated.

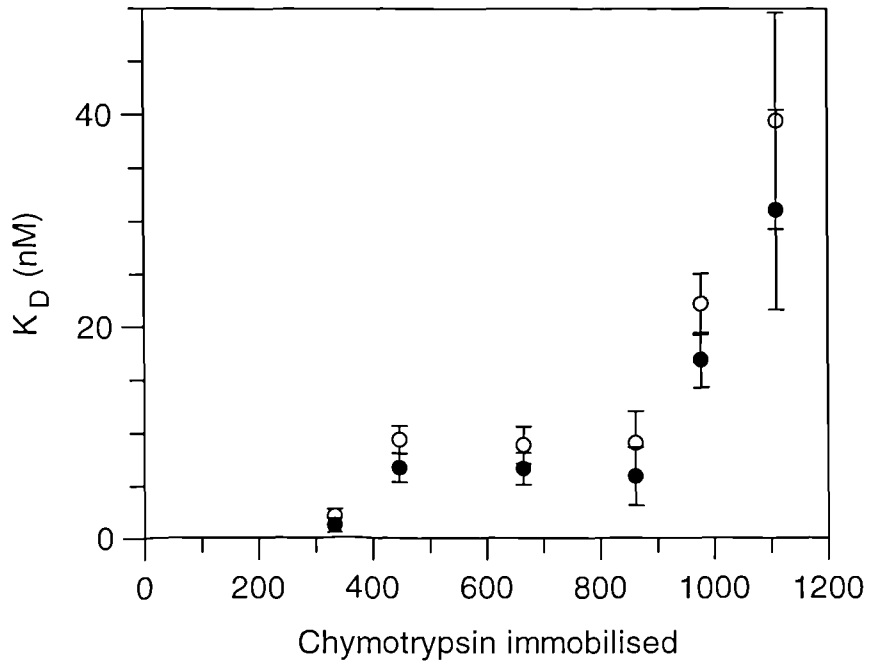

Figure 7.26: *The influence of depletion upon the K_D determined from binding isotherms of CI-2 binding to immobilised chymotrypsin. The open circles represent second order analysis using equation 7.24 while the closed circles represent first order analysis using equation 7.22 The error bars represent the standard errors from the appropriate fitting equation.*

7.4.3 The effect of depletion upon the fitted dissociation for the CI-2/chymotrypsin interaction.

The influence of rebinding would be expected to be more severe at the higher loadings and therefore CI-2 dissociation data from the highest chymotrypsin loading was investigated. The data were fitted to the single exponential equation with and without an offset together with the second order dissociation equation. The data together with the fits are shown in figure 7.27.

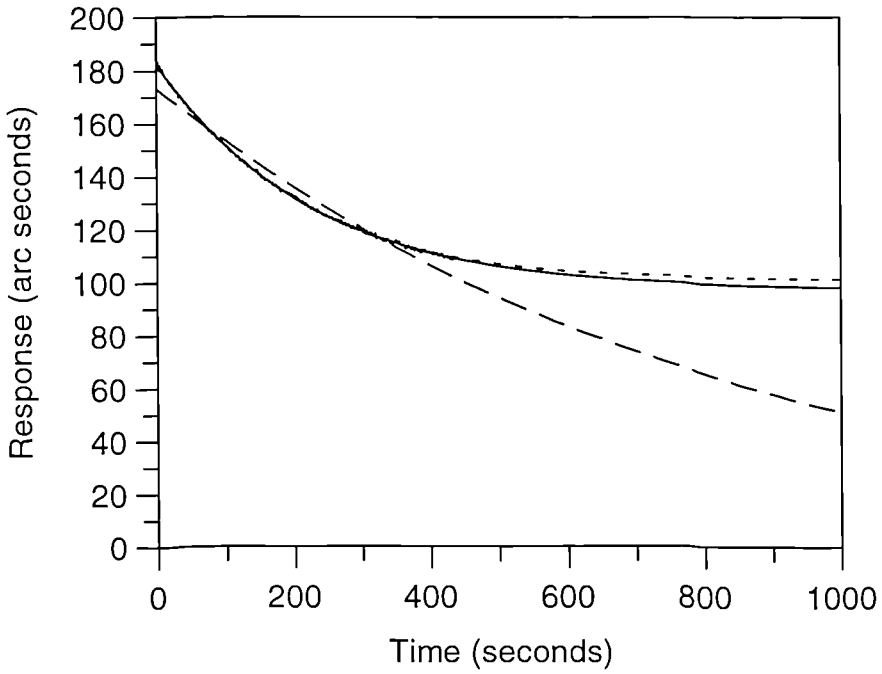

Figure 7.27: *The dissociation phase for the interaction of 124 nM CI-2 with chymotrypsin immobilised at 1110 arc seconds. The fit to the first order (single exponential) equation is shown as a dashed line while the effect of incorporating an offset is shown as a dotted line. The best fit to the second order equation is shown as a solid line.*

The fitted dissociation rate constant values from all three equations at the differing loading levels are shown in figure 7.28.

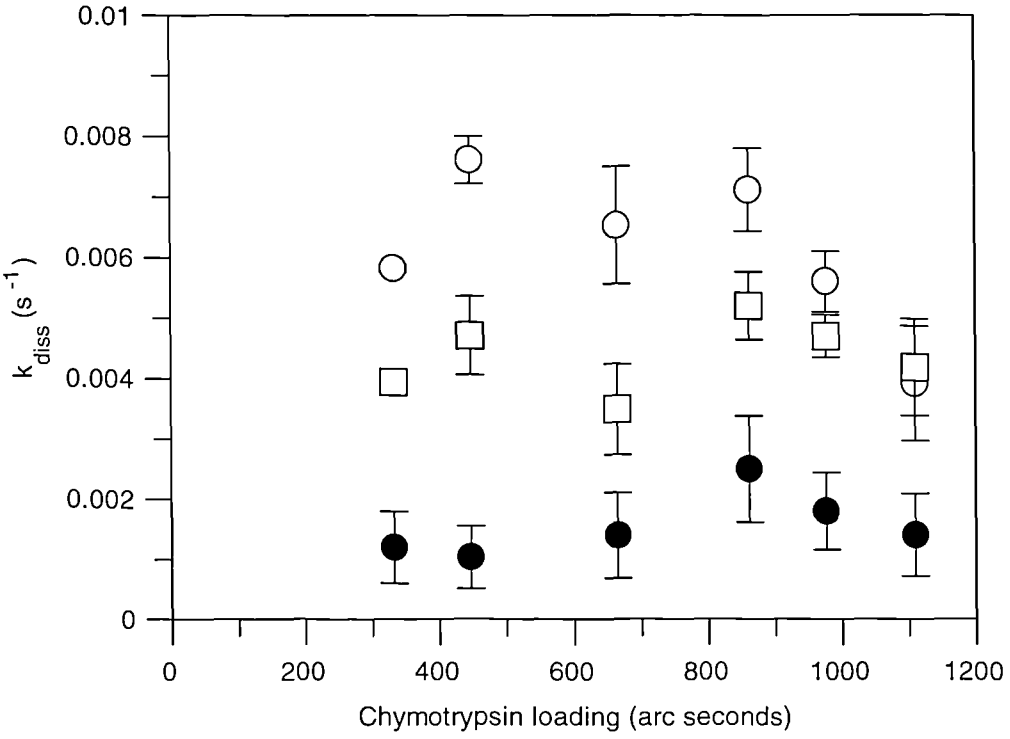

Figure 7.28: *The influence of depletion upon the dissociation rate constant determined from direct fitting of the CI-2 dissociation phase as a function of chymotrypsin loading. The open circles represent k_{diss} values determined by single exponential analysis with an offset, the closed circles single exponential analysis without an offset, and the open squares second order analysis.*

The dissociation rate constant determined from application of the dissociation equation incorporating an offset term returns k_{diss} values higher than the other equations. In addition, at the highest loading the rate is lower. Elimination of this offset causes the data to be poorly fitted with a low returned k_{diss}. Second order analysis gives k_{diss} values between the those of the other two equations and, in common with the equation without an offset, no loading dependence.

7.5 Discussion

Given that the IAsys cuvette is a closed system, depletion of the ligate concentration upon binding to ligand would be expected to occur. By its nature, depletion would be greater for longer incubations, high binding capacities (R_{max}), low ligate concentrations and high affinity interactions.

7.5.1 Theoretical

7.5.1.1 Binding isotherms

The influence of depletion on the equilibrium isotherm has been illustrated in figures 7.7 to 7.9. At high R_{max} values (1250 arc seconds) and high affinities (1 nM) depletion is severe with equilibrium values lower than expected. This lowering of the equilibrium values causes the curve to be shifted to the right such that a Langmuirian isotherm fit would give a lower affinity (higher K_D) that expected. For figure 7.7 this equates to a value of 5 nM instead of the 1 nM used to generate the data. The effect of depletion can be reduced by lowering the R_{max} value (figure 7.8) with depletion being further reduced with a lower affinity system (figure 7.9). Despite the depletion being greater for equilibrium measurements, the correct affinity can be determined providing the drop in concentration is allowed for. There are three methods available for this. The first involves correction of the K_D determined by the Langmuirian isotherm using equation 7.23. However, this does rely upon the Langmuirian isotherm describing the data, a situation which is unlikely to happen in severe cases of depletion. The second is to correct each initial ligate concentration for depletion by converting the R_{eq} value into a concentration term using β and then subtracting in order to obtain the free ligate concentration. Plotting the equilibrium values against free ligate concentration and fitting these data to the Langmuirian isotherm should give the correct K_D (figure 7.10). The final option is to fit the data to an isotherm which allows for the change in ligate concentration (equation 7.24). Using this equation allows the affinity to be determined without further manipulation of the data (figure 7.11).

7.5.1.2 Kinetic constants

7.5.1.2.1 On-rate against [Ligate] plots

The determination of kinetic constants should be influenced less by depletion as the rate tends to be governed more by the initial phase of the binding profile. In a similar manner to the isotherms, depletion is dependent upon the affinity, ligand capacity (R_{max}), and ligate concentration. At low affinities (1 nM) the deviation from the slope and intercept expected for the kinetic plot was marked. Figure 7.13 shows that depletion can be observed as an increase in the k_{on} value with decreasing ligate concentration such that instead of the expected linear relationship, the plots appear curved. This curvature results in an under estimate of k_{ass} and an over estimate of k_{diss}. This curvature is less pronounced at lower R_{max} values with only a small deviation from the expected rate constants at an R_{max} of 100 arc seconds. The deviation at the higher R_{max} values can be reduced by the use of higher ligate concentrations for which depletion will be less severe, a situation highlighted in figure 7.12.

For the 10 nM interaction, the deviation in rate constants is less marked with no obvious curvature in the data. It is noted that the higher R_{max} values cause the line to be further above that expected resulting in a small over estimate of k_{diss} (4% for 625 arc seconds) while the k_{ass} value is little changed.

Other factors are also involved in influencing the extent of depletion. The smaller the molecular weight the greater the possible depletion for a given R_{max}. However, the R_{max} is related to the ligate molecular weight and as such conversion of R_{max} values into molecular weight corrected values (R_{corr}) allows depletion to be assessed for any molecular weight ligate. Thus for example the R_{max} of 200 arc seconds in figure 7.12 equates to a R_{corr} of 0.003 for a 66000 Da ligate. For a 10,000 Da ligate the same R_{corr} corresponds to 30 arc seconds. Depletion for a 10,000 Da ligate with an R_{max} of 30 arc seconds would be the same as that for a 66000 Da ligate with an R_{max} of 200 arc seconds. The influence of molecular weight on depletion can therefore be allowed for in experimental design.

7.5.1.2.2 Directly fitted k_{diss}

The dissociation rate constant determined from direct fitting of the dissociation phases may be influenced by rebinding of the dissociated ligate to the immobilised ligand. This rebinding process can be observed as incomplete dissociation with the final dissociation response above that expected for complete dissociation. Fitting the rebinding dissociation with the single exponential equation returns a k_{diss} value which is an under-estimate as demonstrated in figures 7.17-7.19. These figures show that the data are better described by either the inclusion of an offset value within the single exponential equation or by an equation containing two exponential functions. However, both these equations over-estimate the k_{diss}. With a lowering of the k_{diss}, the difference between the initial and returned values increases. Restricting the data to 120 seconds improves the accuracy of the returned values with the single exponential equation determining the k_{diss} for all the initial values by a maximum error of 6%. The double exponential equation also fitted the data well but did so by often giving a negative value for the second k_{diss} value, illustrating that the data did not need to be described by the addition of an extra exponential term. The single exponential equation containing an offset value over-estimates the k_{diss} and this over-estimation is scaled by the initial k_{diss} value. The data generated with a 1 x 10^{-1} s^{-1} value gives a 2.6% difference in the returned k_{diss} value while a 21% difference is obtained with an initial k_{diss} of 1 x 10^{-3} s^{-1}. This increase in error is probably due to the uncertainty in the calculation of the offset value. For the slowest dissociation, over the 120 seconds the offset will not be well defined while at the faster rate the offset will be better defined. If the data are scaled in accordance with the dissociation rate constant such that the faster rate (1 x10^{-1} s^{-1}) is followed for 10 seconds and the slower (1 x10^{-3} s^{-1}) for 1000 seconds the differences between the fitted k_{diss} and that used to generate the data are the same suggesting that it is the ratio of the rate constants which determines the extent of rebinding. This is further supported by the fact that the equilibrium responses (i.e. response above the baseline) after the dissociation has been followed is dependant upon the affinity.

The response at which the dissociation is initiated (R_0) is also important. Dissociating from a response value close to the R_{max} should reduce the number of free ligand sites available for rebinding and therefore reduce the probability of this occurring. Figure

7.20 shows the dissociation profiles from a ligand with an R_{max} of 300 arc seconds with the R_0 varied. Dissociation is more complete from the curve with the R_0 of 300 arc seconds. The dissociation rate constants determined by curve fitting also follow the same trend as those determined from the variation in the R_{max} values in that the data are fitted better by the inclusion of an offset term or a second exponential but that the single exponential returns essentially the initial value by the reduction of the amount of data used.

7.5.2 Analysis of experimental data.

In order for trends in association data to be established, the importance of depletion upon the association and dissociation rate constants needs to be ascertained. The plot of on-rate against CI-2 concentration (figure 7.21) shows the influence of depletion upon the rate constants determined in such a manner. The chymotrypsin loading for this plot of 1110 arc seconds was the highest obtained, and therefore depletion is expected to be the most severe in this case. Despite this, only a small change in the association rate constant was determined although the intercept was noticeably changed. This is in agreement with the modelling in 7.3 which also showed that the dissociation rate constant determined from the intercept would be sensitive to depletion. The two rate constants determined from plots such as figure 7.21 for other loadings show that the general trend seen for pseudo first order analysis is also seen for the second order analysis. The association rate constant is unaffected by depletion as demonstrated from the agreement between the pseudo first order and second order values (Figure 7.22). The trend in the dissociation rate constant observed by both equations is also seen although the second order analysis results in k_{diss} values which are below those of the pseudo first order approach. Using the ratio of these rate constants to define K_D (figure 7.24) supports the finding that the affinity is decreased with increasing loading as does the determination of the K_D from the isotherm (figure 7.26). The values determined from these two different approaches for both the second order and pseudo first order analysis are similar.

The dissociation phase of the interaction of 124 nM CI-2 with chymotrypsin immobilised at 1110 arc seconds was fitted to first order dissociation equations with and without an offset. In addition, second order analysis was also performed (figure

7.27) . The fitting of the data with the first order equation without an offset resulted in a poor fit. The fit was improved by the introduction of an offset term allowing for the incomplete dissociation of the CI-2. A similar fit was achieved by the second order analysis. In terms of k_{diss} values, the first order equation without the offset gave 1.44 ± 0.4 x 10^{-3} s^{-1}, while the incorporation of an offset gave a higher value of 4.2 ± 0.1 x 10^{-3} s^{-1}. The second order equation gave a value between the two of 4.1 ± 0.03 x 10^{-3} s^{-1}. The loading dependence of the fitting of the dissociation can be seen in figure 7.28. Both the second order and the first order equation containing the offset gave k_{diss} values which showed no real dependence. However, the k_{diss} from the offset equation suggest that at the higher loading a slower dissociation is observed due to rebinding of the CI-2.

Depletion in the IAsys instrument does occur (Hall et al., 1997) but its influence can be reduced to acceptable levels by experimental design such as avoiding high R_{max} values and low ligate concentrations. In the dissociation phase, rebinding may become a problem with high affinity systems. When determining k_{diss} values high R_{max} values should be avoided and the dissociation initiated from a starting value close to the R_{max} value. When depletion or rebinding are observed both kinetic and equilibrium equations incorporating second order conditions can be applied.

Finally non-specific adsorption to the walls of the cuvette, stirrer or aspirator would also lead to depletion. While these were not modelled, the data for ^{125}I HSA binding to a control block of chymotrypsin suggest that these sources of depletion are negligible.

Chapter 8

Alternative analysis of biosensor kinetic data

8.1 Introduction.

The analysis of biosensor data is not restricted to the determination of either the association and dissociation rate constants or the equilibrium constants by the application of the integrated rate equations or binding isotherms respectively. Alternative methods of determining the rate and equilibrium constants have been derived by several authors (Karlsson 1994, Nieba et al. 1996, Hall and Winzor. 1997). For example, the determination of the affinity constant in solution using a biosensor was first proposed by Karlsson (1994). Here the complex was allowed to form in solution with differing concentrations of ligand and a fixed concentration of ligate. The initial rate of binding was found to be proportional to the free concentration of ligate in the premix and thus the affinity constant could be determined. In a similar manner, Nieba et al (1996) also used the biosensor as a concentration monitor but used the on-rate to determine the free concentration of ligate. Hall and Winzor (1997) have proposed using IAsys to produce a binding isotherm without the need for regeneration between ligate additions. This equilibrium titration methodology is similar to that used in chromatography (Nichol *et al.* 1981, Hogg *et al.* 1991) and takes advantage of the open format of the IAsys cuvette allowing sequential addition of ligate. Furthermore, Edwards and Leatherbarrow (1997) have used the initial rate of ligate binding to determine the association rate constant eliminating the need for the assumptions required during the use of the integrated rate equation.

In is the intention of this chapter to investigate the use of these methods in the analysis of the chymotrypsin/ CI-2 interaction and to compare values obtained by the more usual non-linear regression analysis of interaction profiles by integrated rate equations.

8.2 Determination of the association rate constant via initial rate analysis.

In addition to the association rate constant being determined from the slope of a plot of k_{on} against ligate concentration, this constant can be determined from initial rate analysis of the association phase. The initial rates of binding are ligate concentration dependent and the construction of a plot of initial rate against ligate concentration ([L]) yields a straight line that passes through the origin. The slope of this graph is the product of the association rate constant times the maximal binding capacity of the

ligand (R_{max}). This relationship can be derived from the integrated rate equation used to describe the binding phase shown in equation 8.1

$$R_t = \frac{R_{max}[L]}{K_D + [L]}\left(1 - \exp\left(-k_{ass}[L] + k_{diss}\right)t\right) \tag{8.1}$$

Differentiating with respect to time gives (8.2)

$$\frac{dR}{dt} = \frac{R_{max}[L]}{K_D + [L]}\left(k_{ass}[L] + k_{diss}\right)\left(\exp\left(-k_{ass}[L] + k_{diss}\right)t\right) \tag{8.2}$$

At t = 0 equation 8.2 simplifies to

$$\frac{dR}{dt} = \frac{R_{max}[L]}{K_D + [L]}\left(k_{ass}[L] + k_{diss}\right) = R_{max}[L]k_{ass} \tag{8.3}$$

Therefore providing the R_{max} is known then the association rate constant can be determined from the plot of initial rate against ligate concentration.

The chymotrypsin/CI-2 system was used to investigate this initial rate methodology. The immobilisation of 50μg/ml chymotrypsin resulted in an immobilisation response of 862 arc seconds. In order to obtain the R_{max} value, CI-2 at a concentration of 6.7μM was added and the binding followed for 20 minutes (figure 8.1).

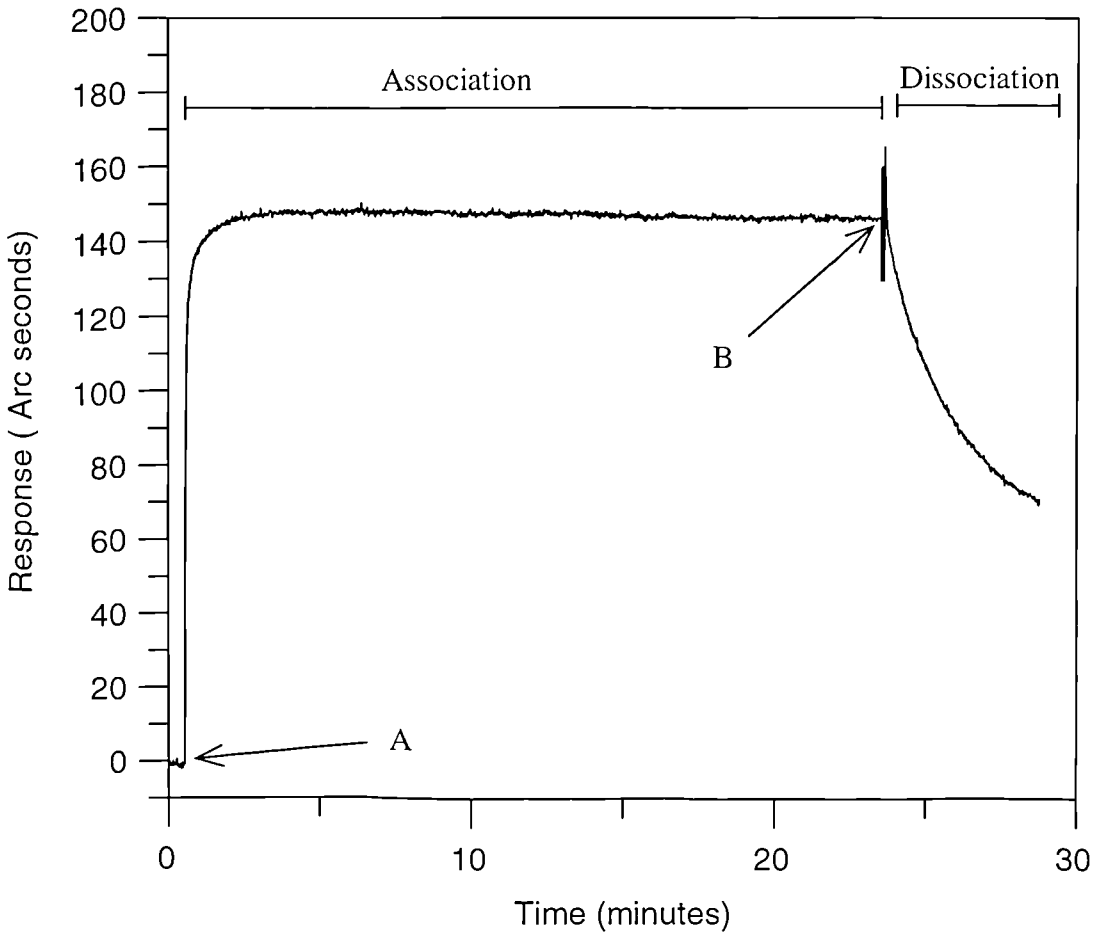

Figure 8.1: *CI-2 at 6.7 μM binding to chymotrypsin immobilised on CMD. An equilibrium response of 150 arc seconds is observed which, given the high concentration of CI-2, is also the capacity of the chymotrypsin (R_{max}). The dissociation phase is also shown upon replacement of the CI-2 solution with buffer at B.*

A R_{max} value of 150 arc seconds was obtained. This concentration of CI-2 was 2000 fold above the expected K_D of the system and should therefore represent saturation of the immobilised ligand. While the monitoring of the dissociation phase is not required for the determination of the association rate constant from initial rate analysis figure 8.1 also shows the dissociation induced by the addition of buffer (B). The initial rate of binding was determined using linear regression analysis of the binding of CI-2 at differing concentrations. The binding at each concentration was followed for 1 minute although most of this data was not used due to the curvature of the association profiles especially at the higher concentrations over this time range. Indeed, the data at

concentrations above 100 nM show a curvature over a time span of 20 seconds (figure 8.2). It was therefore necessary to fit individual concentrations over differing time periods, which at high concentrations reduces the number of data points fitted.

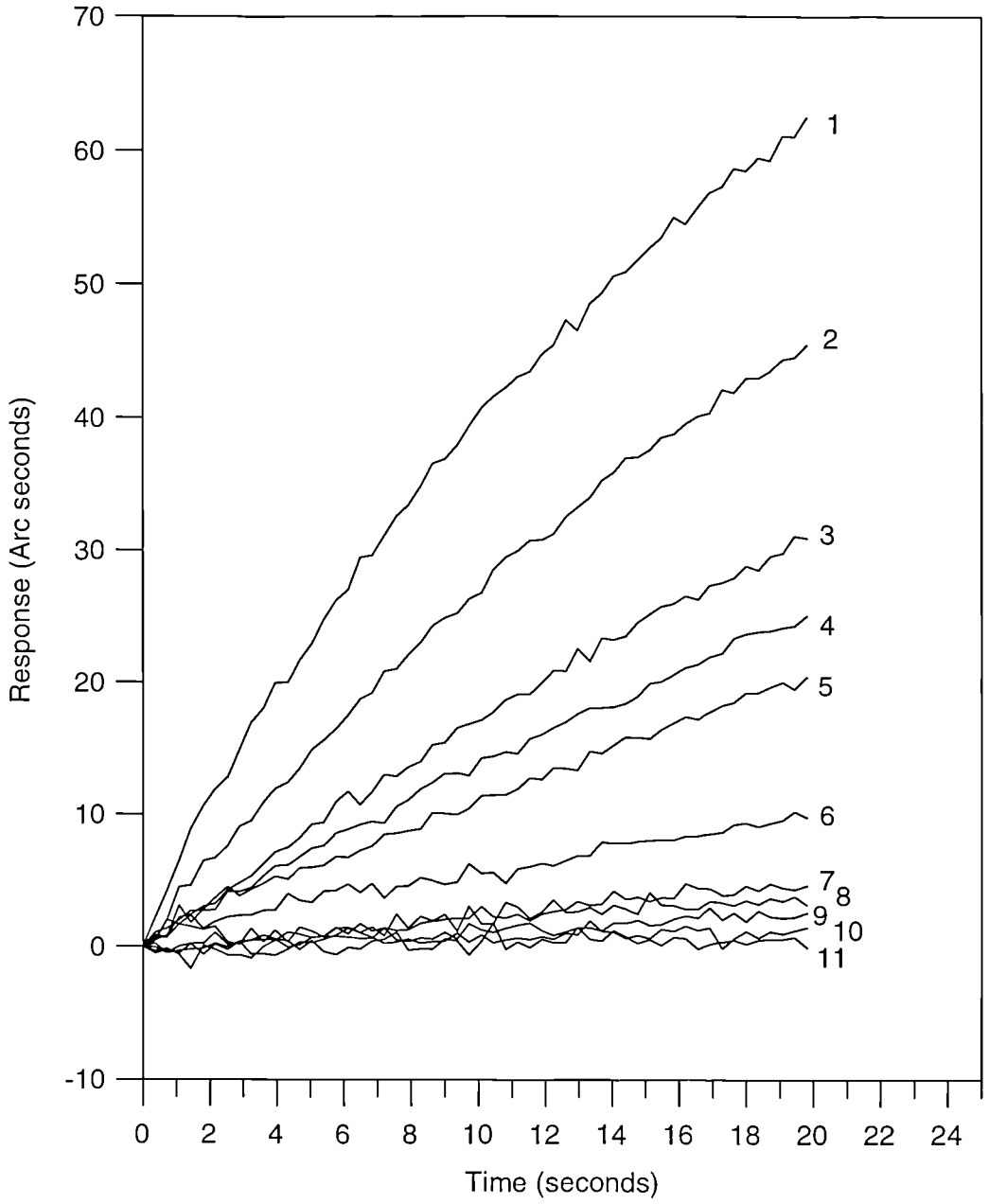

Figure 8.2: *Overlay of the initial portion of association data for CI-2 binding to immobilised chymotrypsin at a range of concentrations: 1, 200 nM; 2, 150 nM; 3, 100 nM; 4, 75 nM; 5, 50 nM; 6, 25 nM; 7, 10 nM; 8, 7.5 nM; 9, 5 nM; 10, 2.5 nM; 11, 1 nM.*

To ascertain the accuracy of using linear regression analysis to find the initial slope and hence the data range used for such analysis, data were modelled using the single exponential association equation using equally spaced time data. The initial rate of this data set was 1.0 and linear regression analysis of differing percentages of the maximal binding response performed. The linear regression slope (initial rate) is plotted against the percentage of R_{max} used as data in figure 8.3 showing that the higher the percentage R_{max} data used, the less accurate the returned initial rate

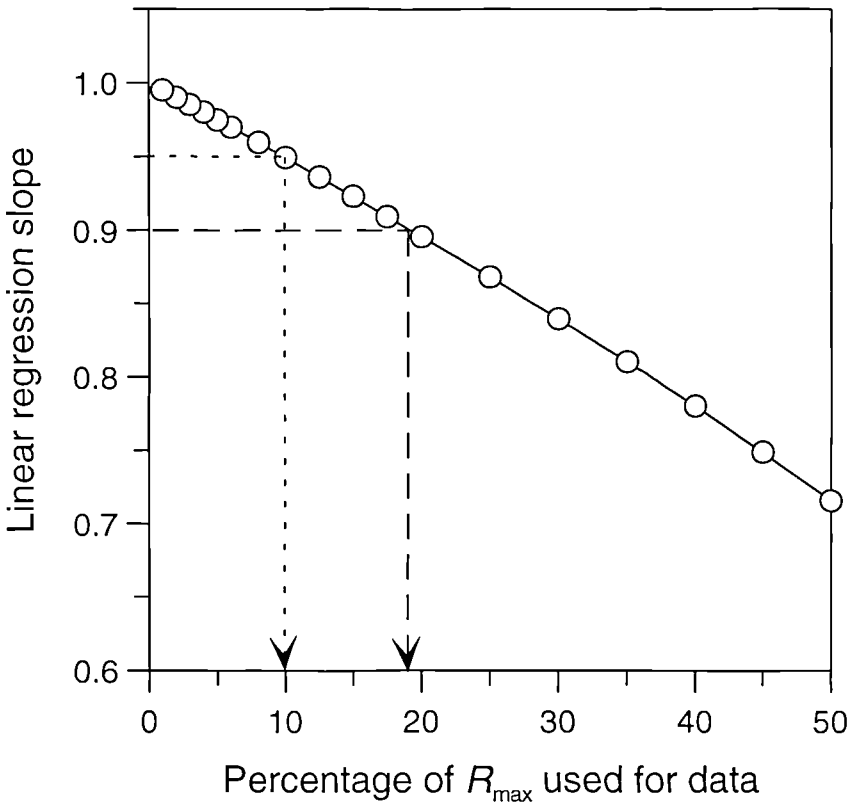

Figure 8.3: *Analysis of the effect of taking varying amounts of data describing a first-order process and fitting the initial data by linear regression. Simulated data having a theoretical initial rate of 1.0 were generated at equal time intervals. Groups of data that started a zero time and corresponding to varying percentages of the maximal response were taken, and the slopes of these data were calculated. The figure illustrates the fractions of the total response that correspond to 90 and 95% of the theoretical value.*

Using initial rate analysis to the CI-2 binding phase, ensuring that only the linear portion of each binding was used, the plot of initial rate against CI-2 concentration was constructed (figure 8.4). The slope of this plot was $1.84 \pm 0.03 \times 10^{7}$ arc s s^{-1} M^{-1}. Using the value of R_{max} determined previously the association rate constant was determined as $1.1 \pm 0.02 \times 10^{5}$ $M^{-1}s^{-1}$.

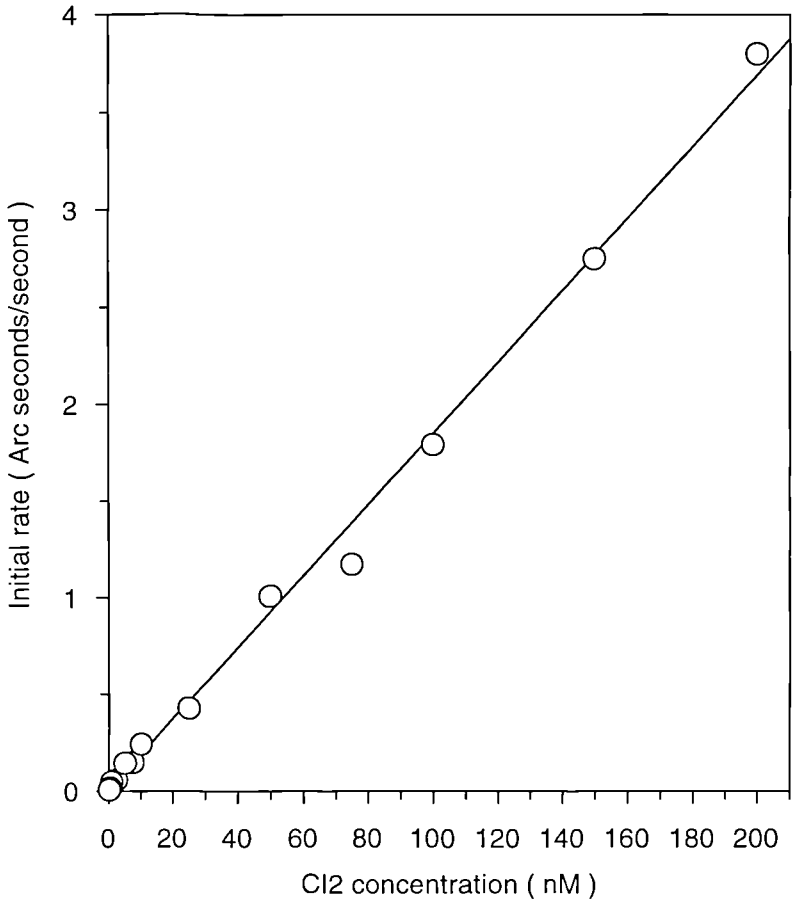

Figure 8.4: *Plot of initial binding rate of CI-2 against CI-2 concentration. The slope of the best fit line allows the association rate constant to be calculated provided the capacity (R_{max}) of the chymotrypsin is known.*

Fitting the dissociation phase in figure 8.1 to a single exponential dissociation equation containing an offset gave a value of $7.5 \pm 0.2 \times 10^{-3}$, making the calculated K_D equal to 68 ± 3 nM.

8.3 Equilibrium Titration

The open format of the cuvette allows the sequential addition of ligate and therefore an isotherm can be constructed without the requirement of regeneration between each ligate addition. Each addition of ligate forms a new response plateau (R_{eq}) and thus with the knowledge of the total ligate concentration in the cuvette the isotherm can be constructed. Figure 8.5 shows the IAsys profile for increasing additions of CI-2 to CMD immobilised chymotrypsin.

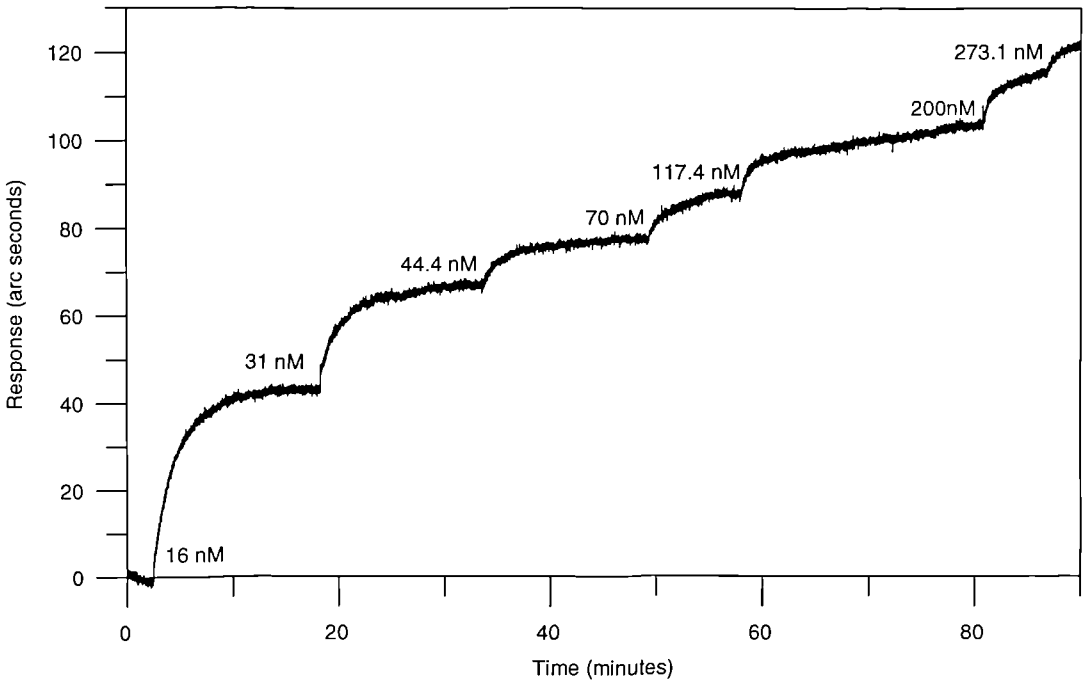

Figure 8.5: *An IAsys profile showing an equilibrium titration experiment. Increasing concentrations of CI-2 are bound to immobilised chymotrypsin and the equilibrium response for each concentration noted. The CI-2 concentrations within the cuvette are shown on the figure.*

The equilibrium response (R_{eq}) at each CI-2 concentration was plotted against the free concentration of CI-2. The free concentration of CI-2 was determined by converting the R_{eq} value to a concentration and subtracting this from the starting value. The conversion of response to concentration has been described in chapter 7, shown again in equation 8.4 below

$$\beta = \frac{R_{eq}\, S}{M\alpha\, V} \tag{8.4}$$

where S is the surface area of the sensor (m^2), V is the volume of ligate (litres), α is the calibration factor (arc s/g/m^2), and M the molecular weight of the ligate.

Figure 8.6 shows the isotherm constructed from the data in figure 8.5 together with the fitted Langmuirian isotherm equation (equation 8.5)

$$R_{eq} = \frac{R_{\max}[L]}{K_D + [L]} \tag{8.5}$$

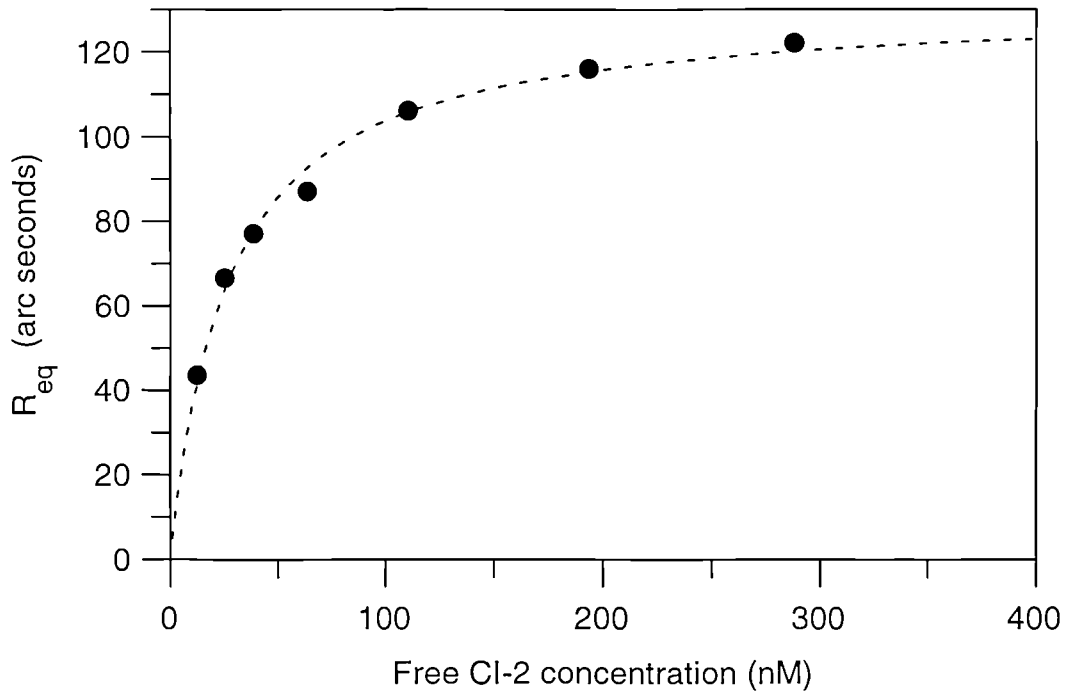

Figure 8.6: *A binding isotherm constructed from the data in figure 8.5. The equilibrium responses (R_{eq}) after each addition of CI-2 are plotted against the free concentration of CI-2. The free concentration of CI-2 is calculated by conversion of the R_{eq} value into a concentration term and subtracted from the total concentration within the cuvette. The dotted line shows the best fit to the corrected data using equation 8.5*

The K_D determined from this analysis was 22 ± 4 nM with a capacity (R_{max}) of 135 arc seconds.

8.4 Solution affinity using IAsys.

Premixes of ligate and competitor are preformed at differing ligand concentrations while maintaining a constant ligate concentration. After the attainment of equilibrium the IAsys can be used to determine the free concentration of ligate within each premix by either the initial rate (Karlsson. 1994) or on-rate (Nieba *et al.* 1995) of ligate binding to immobilised ligand. Both these approaches will be illustrated by the use of the chymotrypsin/CI-2 interaction.

8.4.1 Theory

The general derivation for the determination of the solution based affinity determination is shown below. The rate of binding is reduced in the presence of the competitor by the ratio of free ligate to total ligate as shown in equation 8.6. Here the concentration of the competitor, in this example also the free ligand, is given by G, and the ligate by L.

$$k_{on} = k_{on0} \frac{[L]_{free}}{[L]_{tot}} \tag{8.6}$$

i.e. When $[L]_{free} = [L]_{tot}$ then $k_{on} = k_{on0}$

The concentration of free L is given by Equation 8.7

$$[L]_{free} = [L]_{tot} - [GL] \tag{8.7}$$

where [GL] is the complex concentration in solution

Insert equation (8.7) into (8.6)

$$k_{on} = \frac{k_{on0}([L]_{tot} - [GL])}{[L]_{tot}} \tag{8.8}$$

The dissociation equilibrium constant, K_D, is defined by equation 8.9

$$K_D = \frac{[L]_{free}[G]_{free}}{[GL]} \tag{8.9}$$

The free concentration of G and L can not be determined directly. The concentration of bound complex is determined and this allows the free concentrations to be determined by simple subtraction such that equation 8.9 becomes

$$K_D = \frac{([L]_{tot} - [GL])([G]_{tot} - [GL])}{[GL]} \tag{8.10}$$

This can be arranged to give equation 8.11

$$[G]_{tot}[L]_{tot} - [GL]([G]_{tot} + [L]_{tot} + K_D) + [GL]^2 = 0 \tag{8.11}$$

This is now in the form ax^2+bx+c where a =1, b = $-([G]_{tot}+[L]_{tot}+K_D)$ and c = $[G]_{tot}[L]_{tot}$. Using the solution to the quadratic equation gives 8.12

$$[GL] = -\left(\frac{[L]_{tot} + [G]_{tot} + K_D}{2}\right) + \sqrt{\left(\frac{[L]_{tot} + [G]_{tot} + K_D}{2}\right)^2 - [G]_{tot}[L]_{tot}} \tag{8.12}$$

Inserting equation 8.12 defining the concentration of complex into equation 8.8 gives

$$k_{on} = k_{on0}\frac{1}{[L]_{tot}}\left\{[L]_{tot} - \left(\frac{[L]_{tot} + [G]_{tot} + K_D}{2}\right) + \sqrt{\left(\frac{[L]_{tot} + [G]_{tot} + K_D}{2}\right)^2 - [G]_{tot}[L]_{tot}}\right\} \tag{8.13}$$

Thus, by measuring the on-rate of L in the presence of differing concentrations of competitor, G., the K_D of the interaction in solution can be measured.

8.4.2 Experimental.

Premixes containing varying concentrations of chymotrypsin and 32 nM CI-2 were analysed by adding 200 µl of one premix at a time to a chymotrypsin immobilised surface and the binding of free CI-2 monitored for 5 minutes. Thus, in this example

the ligate, L, was the CI-2 and the competitor, G, was the chymotrypsin. Each of the binding profiles were fitted by non-linear regression analysis using the single exponential equation to obtain k_{on} values. A plot of on-rate against the $\log_{10}$ of the chymotrypsin concentration is shown in figure 8.7 where the data were fitted to equation 8.13. This approach to the determination of the free CI-2 concentration allowed a K_D of 18 ± 2 nM to be determined.

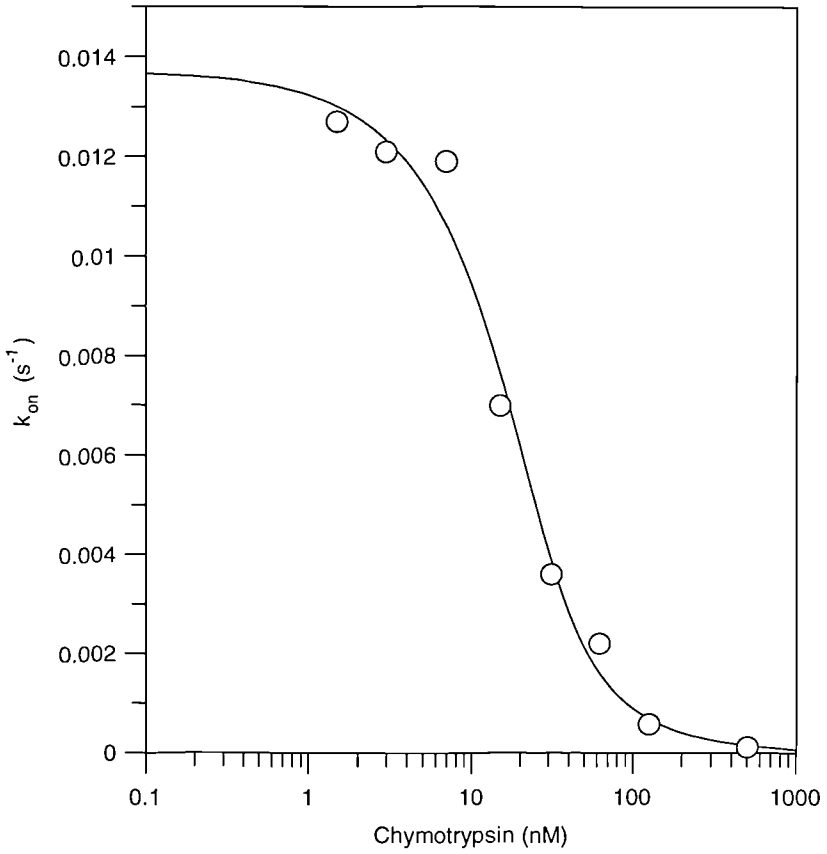

Figure 8.7: *A plot of on-rate from CI-2 binding, in the presence of differing concentrations of chymotrypsin in a premix, to CMD immobilised chymotrypsin. The solid line shows the fit from equation 8.13*

8.5 Discussion.

8.5.1 Initial rate measurements.

The use of initial rates has focused upon their use in concentration analysis. Holwill et al (1996) proposed the use of initial rate analysis for the monitoring of active protein within fermentation broth. Karlsson (1994) proposed that initial rates could be used

for concentration analysis providing mass transport conditions prevailed. Under these conditions the rate of reaction is only dependant upon the concentration of ligate and not its affinity for the immobilised ligand. It has however been noted that ensuring complete mass transport limitation is difficult. Chistensen (1997) has recently published a method for determining concentrations under conditions of partial mass transport limitation by measuring the initial rates of ligate binding at differing flow rates providing that the ligate molecular weight and diffusion coefficient are known. Richalet-Sécordel *et al* (1997) used this technique to determine the concentrations of monoclonal antibodies, Fab fragments from the monoclonal antibodies by papain digestion, and recombinant Fab fragments. The use of initial rate analysis in determining the association rate constant eliminates the potential complication arising from non-Langmuirian kinetics in that no assumption is made into the mode of binding. The linear regression analysis also has the advantage of allowing the association rate constant to be determined faster than exponential curve fitting of the entire binding profile as less experimental data points are required. This method does however require the accurate determination of the R_{max} value by saturation of the immobilised ligand with ligate. This may be considered a disadvantage only if insufficient material is available to ensure saturation over a reasonable time period. The K_D of the reaction may also be determined by following the dissociation from the saturating binding curve. This dissociation rate constant from this saturation response will be less susceptible to rebinding of the dissociated ligate due to a lower number of available ligand sites. The interaction of CI-2 with immobilised chymotrypsin analysed by exponential curve fitting and construction of a secondary plot has an association rate constant of 4×10^5 $M^{-1}s^{-1}$ at low R_{max} values. Comparison of this value with that determined from initial rate analysis reveals a four- fold difference in the two rates. While it is assumed that the initial rate analysis should reveal binding rates prior to the appearance of steric hindrance constraints, the difference in these values suggests that steric hindrance may occur in a more rapid time scale than expected. This steric hindrance will be worse at higher concentration of CI-2, concentrations which have a marked influence in the slope of the initial rate plot. Combination of the association rate constant with the dissociation rate constant determined from saturation gives a K_D value of 68 nM with a k_{diss} of 7.3×10^{-3} s^{-1}. Given the four-fold difference in the association rate constant, there is a corresponding

difference in the K_D value compared to the ratio the association rate constant from the slope of the secondary kinetic plot and the measured dissociation rate constant. This ratio gives a K_D of 15 nM.

8.5.2 Equilibrium titration

The equilibrium titration experiment allows the determination of the affinity constant by repeated additions of the CI-2 without regenerating between concentrations. The affinity determined by this method was found to be 22 nM and therefore in reasonable agreement with that determined from the ratio of rate constants. The titration experiment allows the affinity of an interaction to be determined even if the ligand is unstable to regeneration. Dissociation from the titration profile allows the dissociation rate constant to be determined from a saturating ligate concentration, a situation in which rebinding of the ligate will be low. Analysis of the dissociation phase of the titration experiment gives a value of $6.3 \pm 0.5 \times 10^{-3}$ s^{-1} and therefore an association rate constant of $2.86 \pm 0.56 \times 10^{5}$ $M^{-1}s^{-1}$ was determined.

8.5.3 Solution experiment

The K_D determined from the solution experiments in which the IAsys was used as a concentration gave 18 ± 2nM by the use of on-rate analysis. The assumption underlying this method is that the on-rate measured is proportional to the free concentration of CI-2 in the premix. This will not be the case if the binding to the immobilised ligand disturbs the established equilibrium such as under second order conditions where the free concentration of CI-2 alters with time. To ensure that the equilibrium is not disturbed upon addition, each premix is added by complete replacement of the solution rather than by dilution into the cuvette.

Chapter 9

Comparison of solution and IAsys kinetic parameters.

9.1 Introduction.

For any new technique it is important to make comparisons with a conventional, widely used method. This is especially important as the determination of kinetic parameters on IAsys requires that one of the reactants be immobilised to the sensor surface either directly or via a CMD matrix. In this chapter, stopped-flow fluorescence was used for the comparison. This has the advantage of being capable of monitoring fast reactions (k_{ass} of greater than 1 x 10^7 $M^{-1}s^{-1}$) in solution. Furthermore, this technique is widely used for the determination of kinetic parameters. The main disadvantage of this technique is that for general applicability it is usually necessary to fluorescently label one of the binding partners.

The interaction of anti-FITC mab with fluorescein was selected as a model for investigation. The fluorescein was attached to differing molecular weight proteins in order to investigate the sensitivity of the interaction to molecular weight. To simplify the kinetic analysis the proteins used were selected such that they only contained one free thiol group. This thiol group could then be used to link the fluorescein label using a maleimide derivative (Cardoza et al., 1984.). The proteins chosen were maltose binding protein (M_r 43,000), papain (M_r 25,000), and cytochrome c from yeast (M_r 12,000).

9.2 Stopped-flow fluorescence.

In order to determine the kinetics of the interaction between the conjugates and the anti-FITC mab in solution, use was made of the quenching of conjugate fluorescence resulting from the binding of the anti-FITC mab. In each case the concentration of the conjugate was fixed and the concentration of the antibody varied. Figures 9.1 shows the quenching data for the interaction of mbp-fluorescein conjugate with differing anti-FITC mab concentrations. The fluorescent data were fitted to a single exponential equation yielding a single on-rate (k_{on}) value These data were then used to construct a kinetic plot in a similar manner to that obtained for the IAsys data. The association rate constant was determined from the slope and the dissociation rate constant from the intercept of such a plot. Figures 9.2, 9.3, and 9.4 show kinetic plots for mbp, cytochrome c, and papain conjugates.

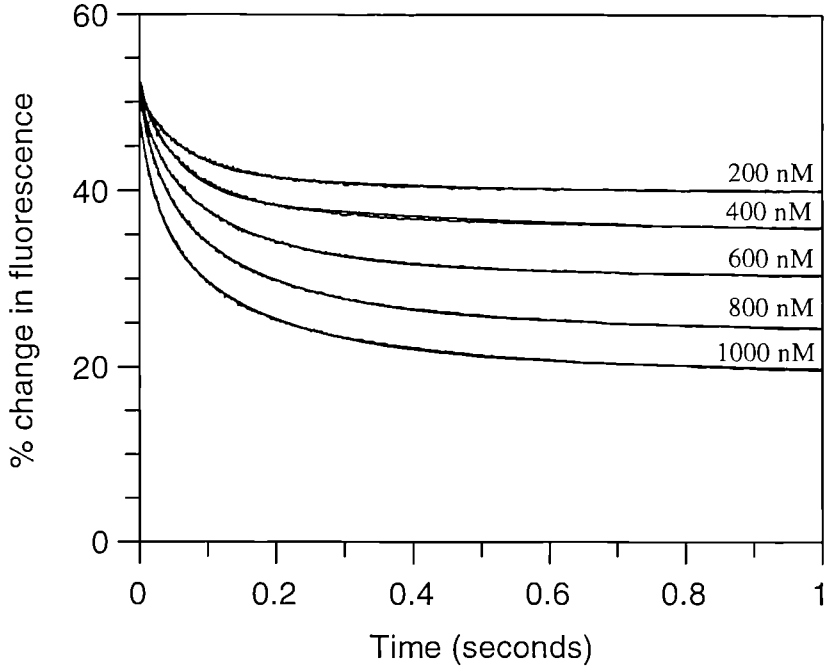

Figure 9.1: *The quenching of mbp-fluorescein conjugate fluorescence in the presence of differing concentrations of anti-FITC mab. The curves are fitted to single exponential equation containing an offset.*

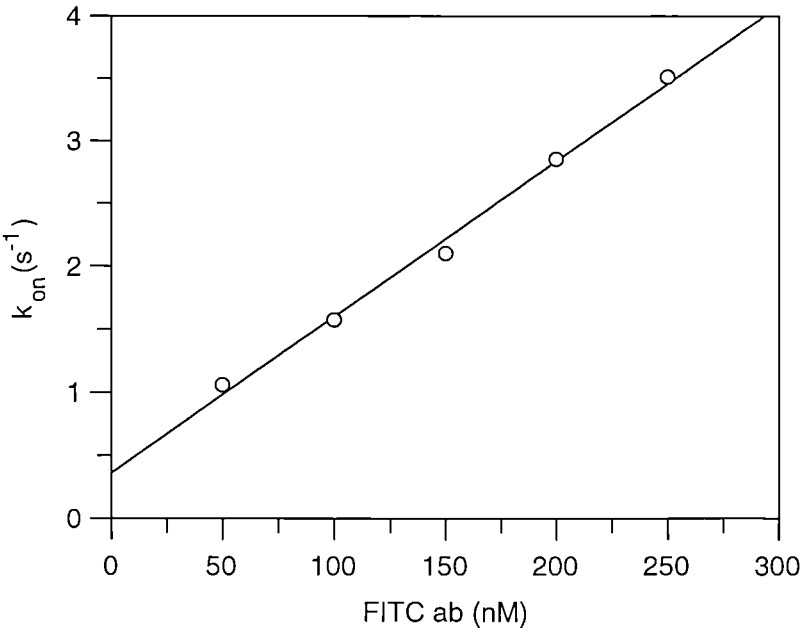

Figure 9.2: *Plot of on-rate against anti-FITC mab concentration for the quenching of mbp-fluorescein conjugate by anti-FITC mab*

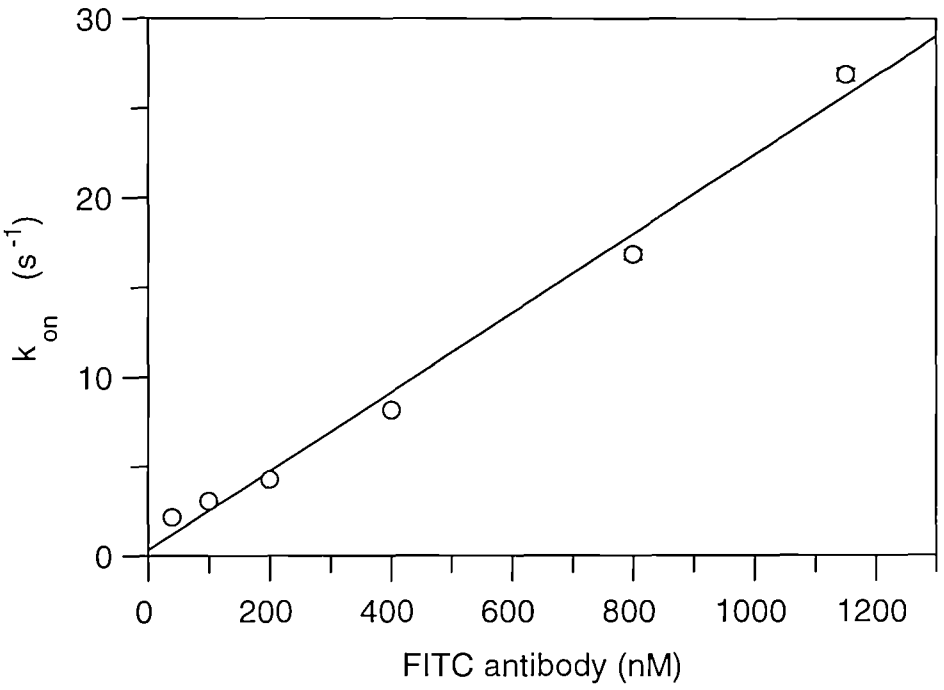

Figure 9.3: *Plot of on-rate against anti-FITC mab concentration for the quenching of cytochrome c-fluorescein conjugate by the anti-FITC mab*

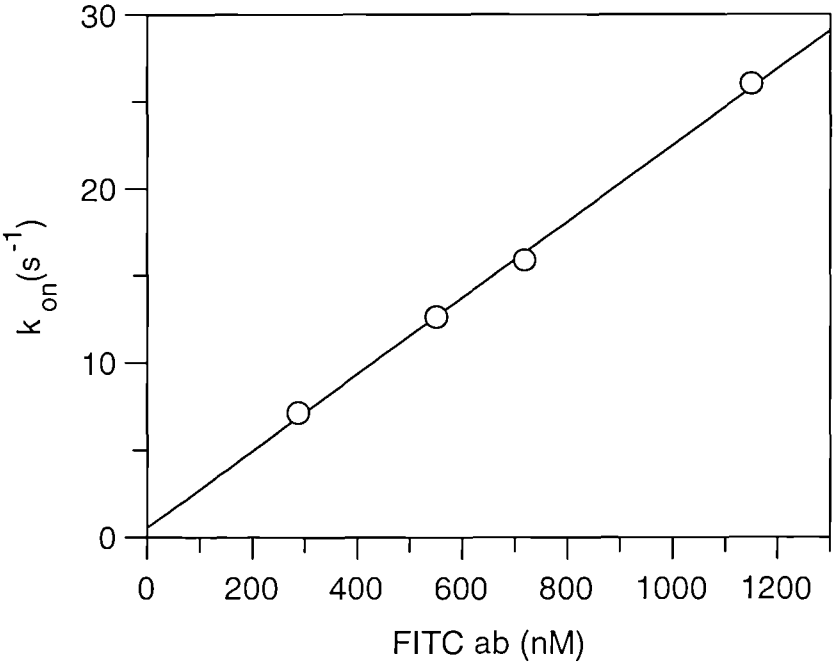

Figure 9.4: *Plot of on-rate against anti-FITC mab concentration for the quenching of the papain-fluorescein conjugate by the anti-FITC mab*

The derived rate constants are given in table 9.1

Conjugate	k_{ass} ($M^{-1}s^{-1}$)	k_{diss} (s^{-1})	K_D (nM)
mbp	$1.23 \pm 0.05 \times 10^{7}$	$3.59 \pm 0.92 \times 10^{-1}$	29.8 ± 7.7
Cytochrome c	$2.21 \pm 0.11 \times 10^{7}$	$3.36 \pm 6.89 \times 10^{-1}$	15.2 ± 31.2
Papain	$2.19 \pm 0.06 \times 10^{7}$	$5.68 \pm 4.7 \times 10^{-1}$	25.9 ± 21.4

Table 9.1: *The association and dissociation rate constants derived for the interaction of three fluorescein conjugates with anti-FITC mab from fluorescence quench measurements. The K_D shown was determined from the ratio of the two rate constants*

The association rate constants determined from the slope of the kinetic plot for each conjugate are similar with the cytochrome c and papain conjugates giving values of 2.2×10^{7} $M^{-1}s^{-1}$. The value from the mbp conjugate was slightly lower at 1.23×10^{7} $M^{-1}s^{-1}$. However, the dissociation rate constant from the intercept was poorly defined for both the cytochrome c and the papain conjugate with % errors of greater than 100%. The intercept from the mbp conjugate was better defined but still possessed a 20% error.

It is theoretically possible to determine directly the dissociation rate constant from fluorescence quenching experiments. This is achieved by preforming the complex then injecting this premix into buffer which causes the complex to dissociate and the fluorescence to recover. However, in the case of the interactions measured, the large amount of antibody required prevented a detailed investigation.

9.3 Interaction kinetics on IAsys.

In addition to a comparison of IAsys and stopped-flow techniques it was also decided to compare biosensor surfaces using this interaction.

9.3.1 CMD

9.3.1.1 Immobilisation of fluorescein labelled conjugates

9.3.1.1.1 Cytochrome c-fluorescein conjugate

Cytochrome c-fluorescein conjugate was immobilised to CMD sensor surfaces at a loading of 120 arc seconds. The binding of anti-FITC mab at differing concentrations allowed the rate constants to be determined. Figure 9.5 shows the kinetic plot obtained for this interaction on CMD.

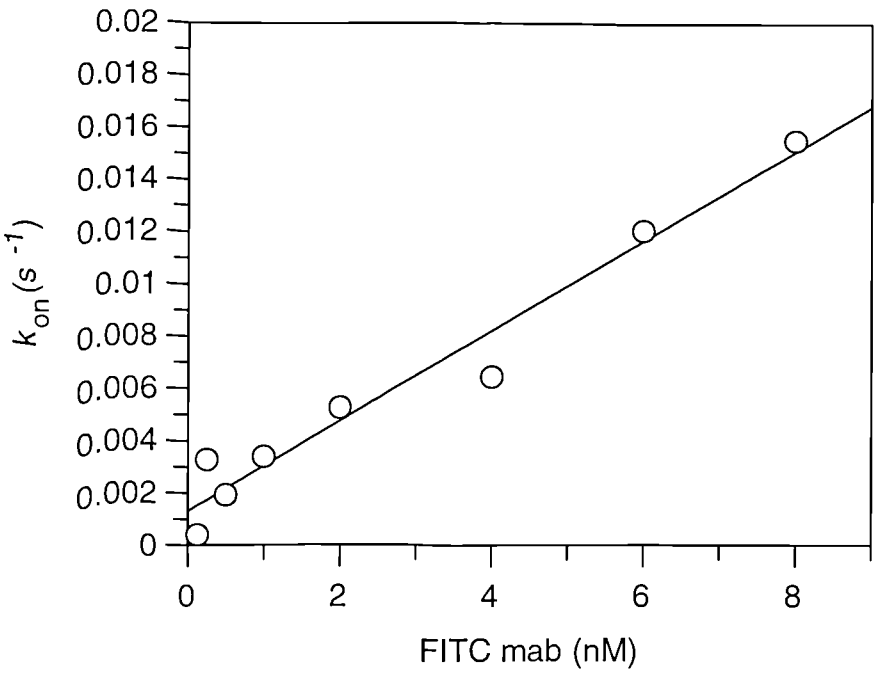

Figure 9.5: *Plot of on-rate against anti-FITC mab concentration for the interaction of the anti-FITC mab with cytochrome c-fluorescein conjugate immobilised to a CMD surface at 120 arc seconds.*

An association rate constant of 1.72 ± 0.15 x 10^6 $M^{-1}s^{-1}$ was obtained from the slope of figure 9.5 and a dissociation rate constant of 1.32 ± 0.55 x 10^{-3} s^{-1} from the

intercept. Combining these rate constants gives a K_D of 0.76 ± 0.32 nM. Direct fitting of the dissociation phase to a single exponential equation containing an offset value resulted in a k_{diss} of 2.62 ± 0.06 x 10^{-3} s^{-1}.

In order to further investigate the K_D value, a binding isotherm was constructed and is shown in figures 9.6. The K_D values from this isotherm was 0.92 ± 0.19 nM.

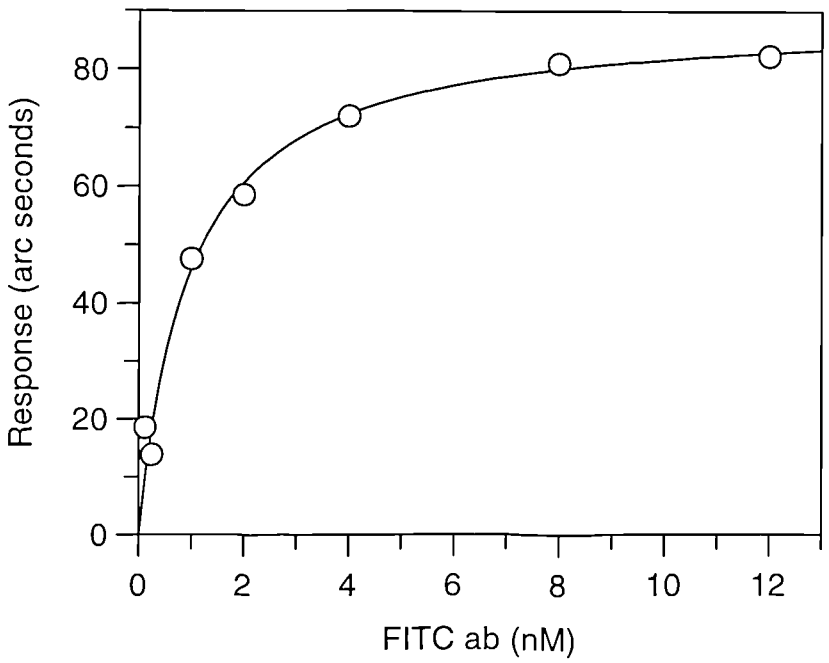

Figure 9.6: *Plot of equilibrium response against anti-FITC mab concentration for the interaction of the anti-FITC mab with cytochrome c-fluorescein conjugate immobilised to a CMD surface at 120 arc seconds.*

An equilibrium titration experiment was also performed on a CMD block with cytochrome c-fluorescein conjugate immobilised at 2500 arc seconds and the data are shown in figure 9.7 with the corresponding isotherm in figure 9.8. A value of 2.8 ± 0.09 nM with an R_{max} of 570 ± 7 arc seconds was determined.

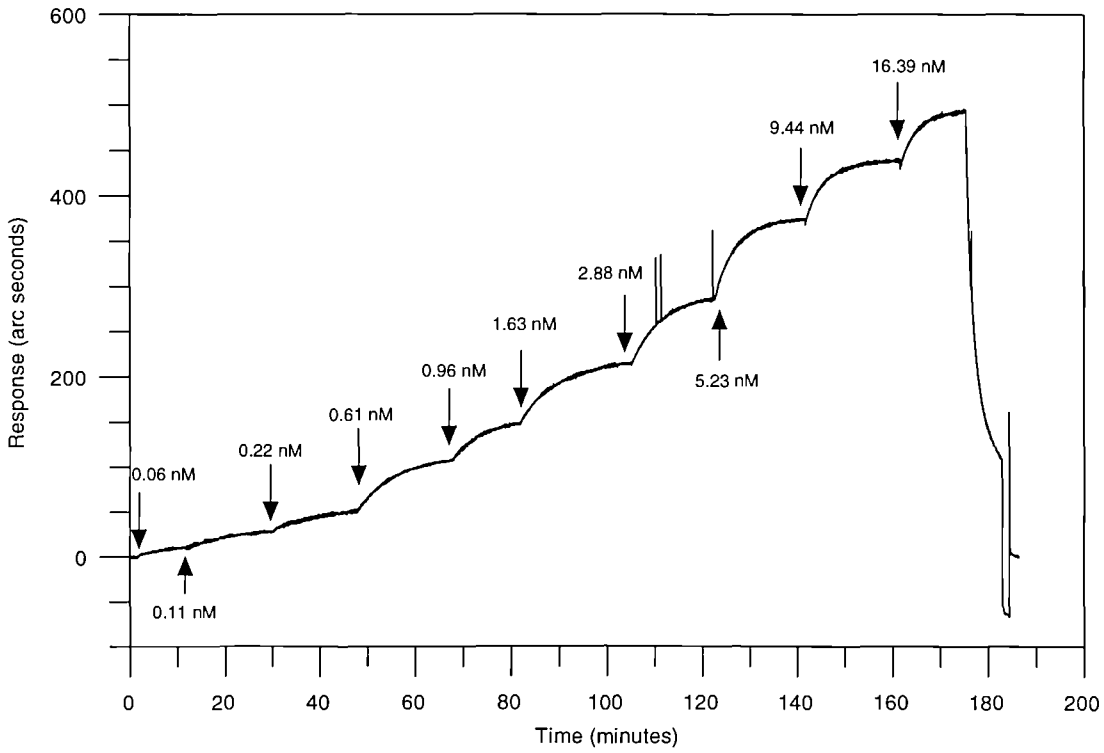

Figure 9.7: *Equilibrium titration for the interaction of anti-FITC mab with cytochrome c-fluorescein conjugate immobilised to CMD at 2500 arc seconds. The total concentration of anti-FITC mab in the cuvette is shown on the figure.*

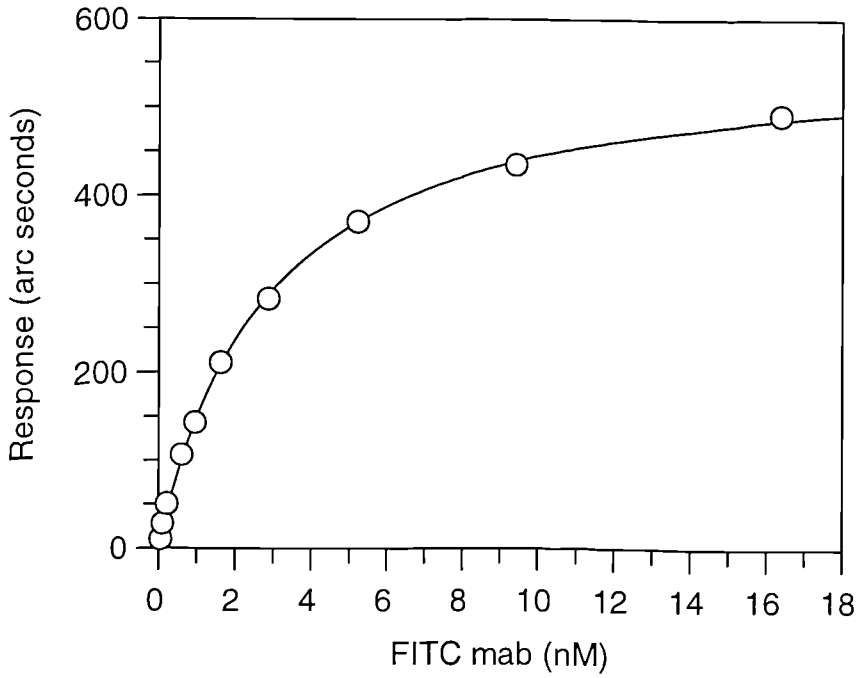

Figure 9.8: *Plot of equilibrium response against anti-FITC mab concentration from the equilibrium titration experiment in figure 9.7. The curve shows the best fit to the isotherm equation (equation 8.5)*

As a control, cytochrome c was immobilised to the CMD matrix and the interaction of anti-FITC mab monitored. No appreciable binding of the anti-FITC was observed (Data not shown).

9.3.1.1.2 Papain-fluorescein conjugate

Papain-fluorescein conjugate was immobilised to CMD at a level of 167 arc seconds. The kinetics of the interaction with anti-FITC mab are shown in figure 9.9. No appreciable binding of anti-FITC mab to papain immobilised on CMD was observed.

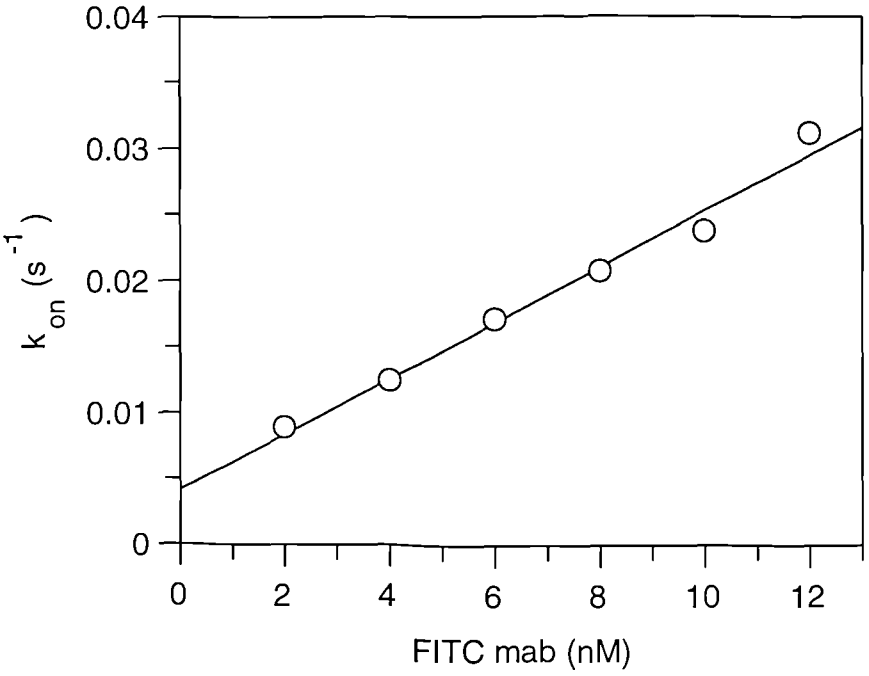

Figure 9.9: Plot of on-rate against anti-FITC mab concentration for the interaction of the anti-FITC mab with papain-fluorescein conjugate immobilised to a CMD surface at 167 arc seconds.

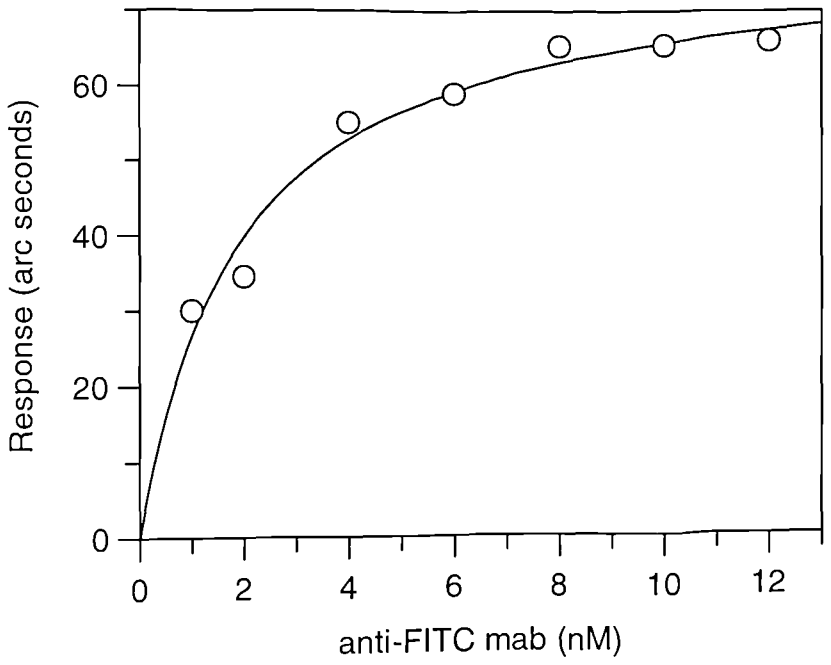

Figure 9.10: Plot of equilibrium response against anti-FITC mab concentration for the interaction of the anti-FITC mab with papain-fluorescein conjugate immobilised to CMD at 167 arc seconds.

An association rate constant of $2.12 \pm 0.14 \times 10^{6} M^{-1}s^{-1}$ was obtained from the slope of figure 9.9 and a dissociation rate constant of $4.18 \pm 1.10 \times 10^{-3} s^{-1}$ from the intercept. Combining these rate constants gives a K_D of 1.91 ± 0.52 nM. Direct fitting of the dissociation phase to a single exponential equation containing an offset value resulted in a k_{diss} of $2.56 \pm 0.05 \times 10^{-3} s^{-1}$. The binding isotherm in figure 9.10 gave a K_D of 1.94 ± 0.34 nM.

A K_D value of 4.4 ± 0.5 nM with an R_{max} of 1620 ± 71 arc seconds was determined from an equilibrium titration experiment on a CMD surface with 1988 arc seconds immobilised. The experimental data is shown in figure 9.11 with the isotherm shown in figure 9.12.

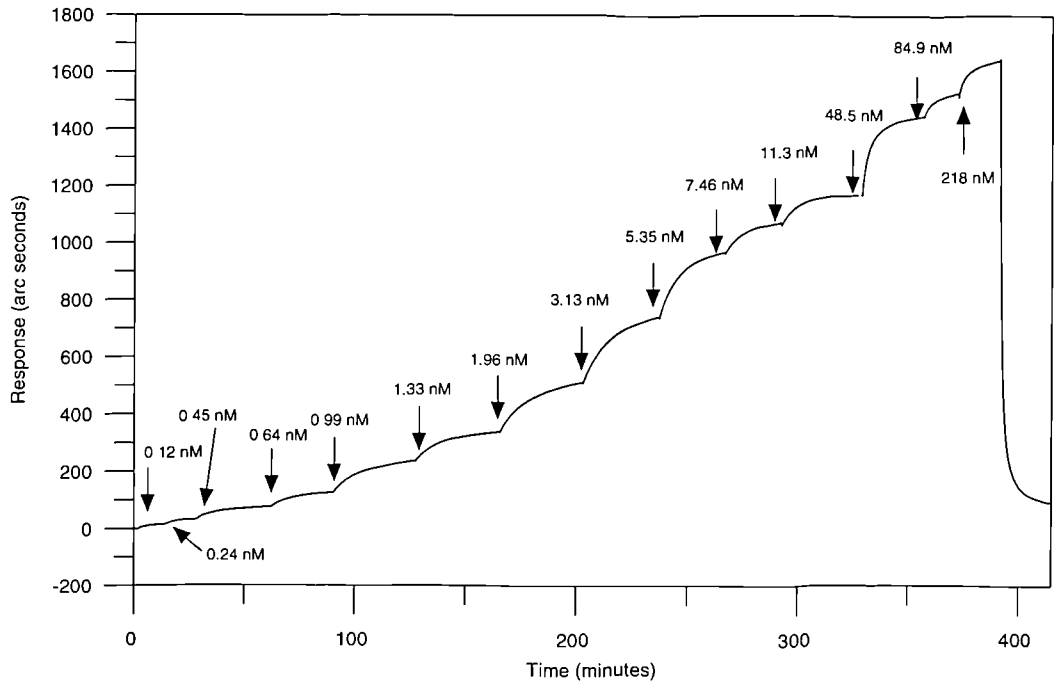

Figure 9.11: *Equilibrium titration for the interaction of anti-FITC mab with papain-fluorescein conjugate immobilised to a CMD surface at 1988 arc seconds. The total concentration of anti-FITC mab in the cuvette is shown on the figure.*

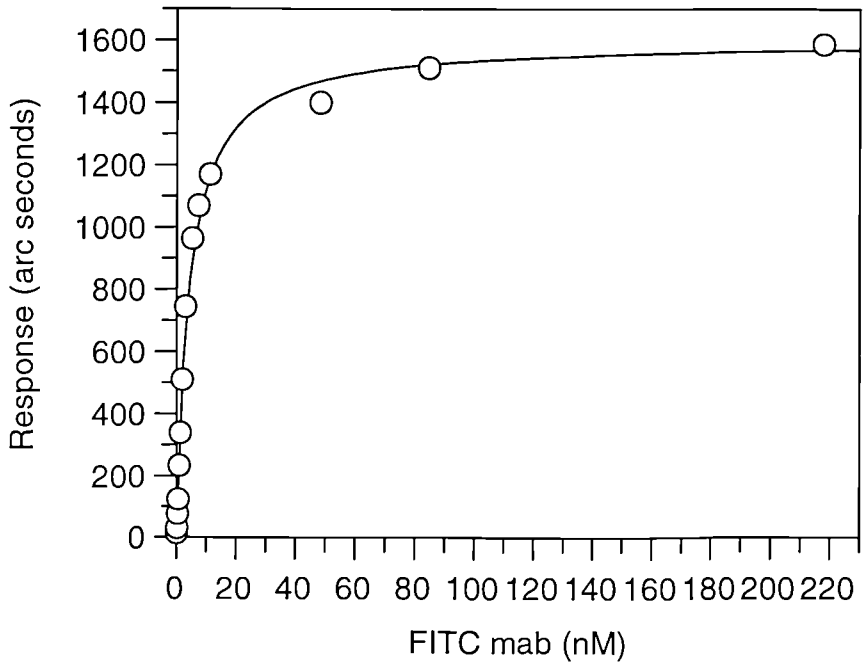

Figure 9.12: *Plot of equilibrium response against anti-FITC mab concentration from the equilibrium titration experiment in figure 9.11. The curve shows the best fit to the isotherm equation (equation 8.5)*

9.3.1.1.3 Maltose binding protein-fluorescein conjugate

Figure 9.13 shows the kinetic plot from this loading while figure 9.15 shows the isotherm from this data. The kinetic and equilibrium values are shown in table 9.2.

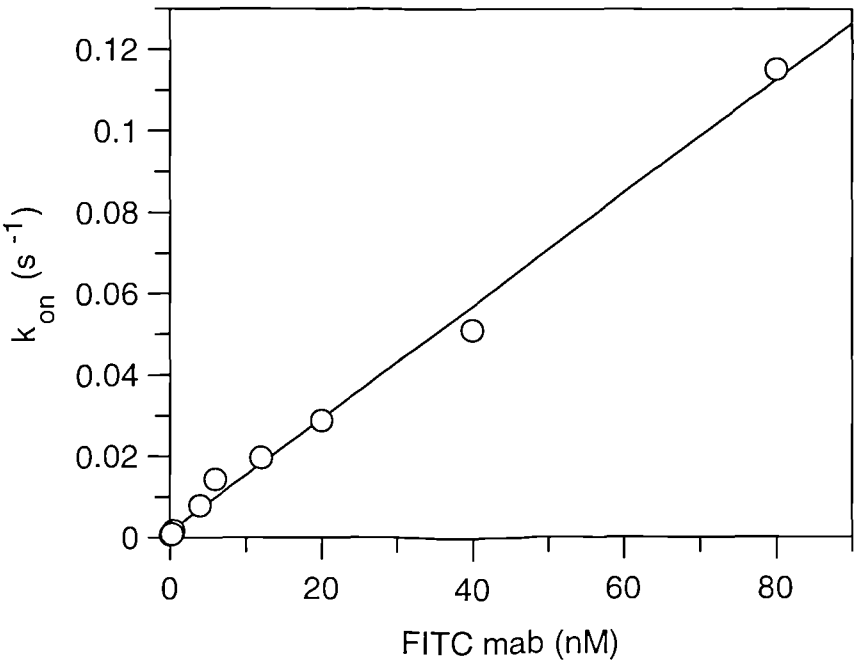

Figure 9.13: *Plot of on-rate against anti-FITC mab concentration for the interaction of the anti-FITC mab with mbp-fluorescein conjugate immobilised to a CMD surface at 240 arc seconds*

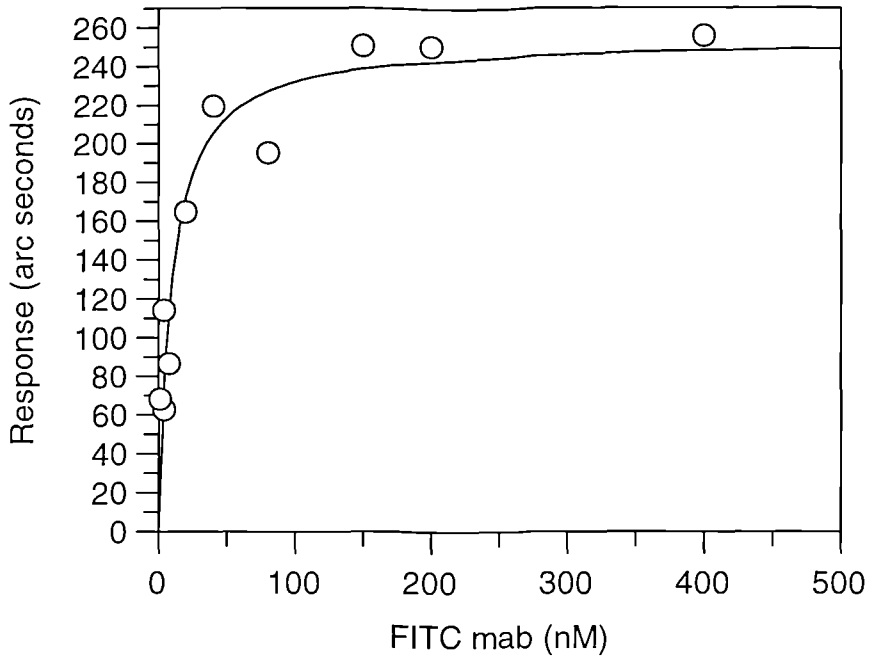

Figure 9.14: *Plot of equilibrium response against anti-FITC mab concentration for the interaction of the anti-FITC mab with mbp-fluorescein conjugate immobilised to a CMD surface at 240 arc seconds*

k_{ass} ($M^{-1}s^{-1}$)	k_{diss} (s^{-1})	K_D (nM)	K_D from isotherm (nM)
$1.38 \pm 0.04 \times 10^{6}$	$1.58 \pm 1.25 \times 10^{-3}$	1.14 ± 0.90	9.37 ± 2.62

Table 9.2: *The association and dissociation rate constants determined from the slope and intercept of plots such as figure 9.13 for the interaction of anti-FITC mab binding to CMD immobilised mbp-fluorescein conjugate.*

No binding of anti-FITC mab to unconjugated mbp immobilised on CMD was observed

9.3.1.2 Binding of conjugates to immobilised anti-FITC mab.

The anti-FITC mab used was acid labile and as such another regenerant was used. For all three conjugates a two minute wash with 4M $MgCl_2$ removed the bound conjugate and retained the activity of the immobilised antibody. The kinetic plots for each of the three conjugates are shown in figures 9.15 to 9.17 and the data are summarised in table 9.3.

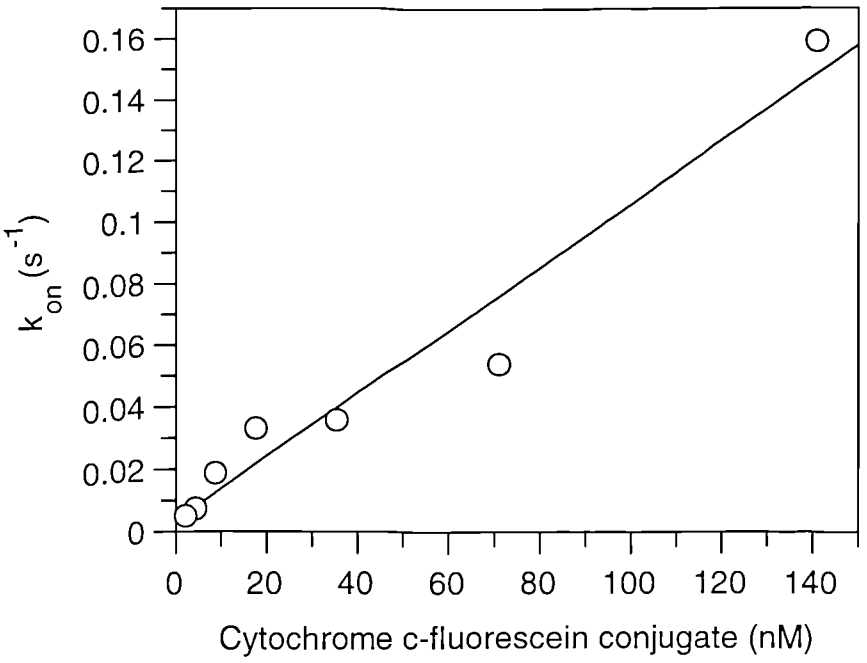

Figure 9.15: *Plot of on-rate against cytochrome c-fluorescein concentration for the interaction of the conjugate with anti-FITC mab immobilised to a CMD surface at 550 arc seconds*

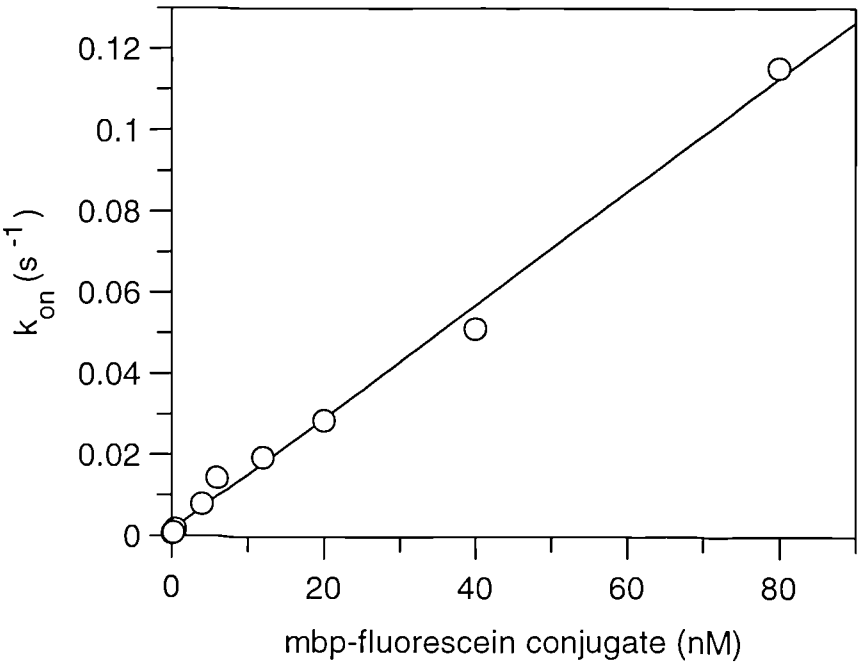

Figure 9.16: *Plot of on-rate against mbp-fluorescein concentration for the interaction of the conjugate with anti-FITC mab immobilised to a CMD surface at 550 arc seconds*

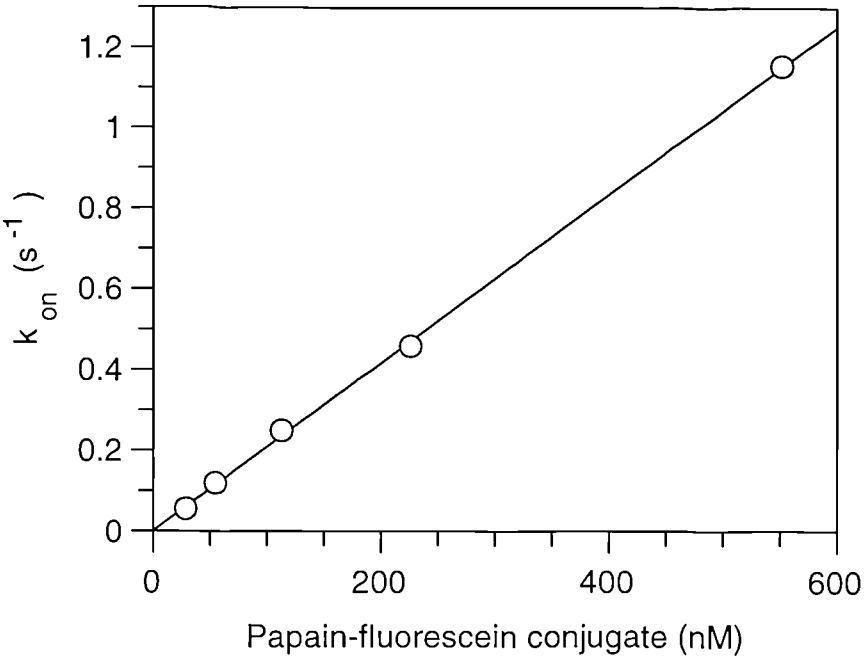

Figure 9.17: *Plot of on-rate against papain-fluorescein concentration for the interaction of the conjugate with anti-FITC mab immobilised to a CMD surface at 550 arc seconds*

Conjugate	k_{ass} ($M^{-1}s^{-1}$)	k_{diss} (s^{-1})	K_D (nM)
Cytochrome c	$1.03 \pm 0.10 \times 10^{6}$	$3.4 \pm 6.2 \times 10^{-3}$	3.30 ± 6.02
mbp	$1.38 \pm 0.04 \times 10^{6}$	$1.58 \pm 1.25 \times 10^{-3}$	1.14 ± 0.90
papain	$2.08 \pm 0.03 \times 10^{6}$	$1.17 \pm 7.8 \times 10^{-4}$	0.56 ± 3.71

Table 9.3: *The association and dissociation rate constants derived for the interaction of three fluorescein conjugates with CMD immobilised anti-FITC mab. The K_D shown was determined from the ratio of the two rate constants.*

The fitted k_{diss} values determined from the dissociation phase for each of the three conjugates were found to be similar with values of $5.4 \pm 0.5 \times 10^{-3}$ s^{-1}, $4.7 \pm 0.7 \times 10^{-3}$ s^{-1}, and $5.9 \pm 0.6 \times 10^{-3}$ s^{-1} for the cytochrome c, papain, and mbp conjugates respectively.

9.3.1.3 Immobilisation of RAMFc as a capture system

RAMFc was immobilised on the CMD sensor surface and a response of 2200 arc seconds was achieved. The anti-FITC mab was then bound followed by the conjugate.

As expected the binding responses were lower than those obtained from direct binding of the conjugates to immobilised anti-FITC mab. Figure 9.18 shows the kinetic plot for the cytochrome c conjugate while figures 9.19 and 9.20 show similar plots for the papain and mbp conjugates.

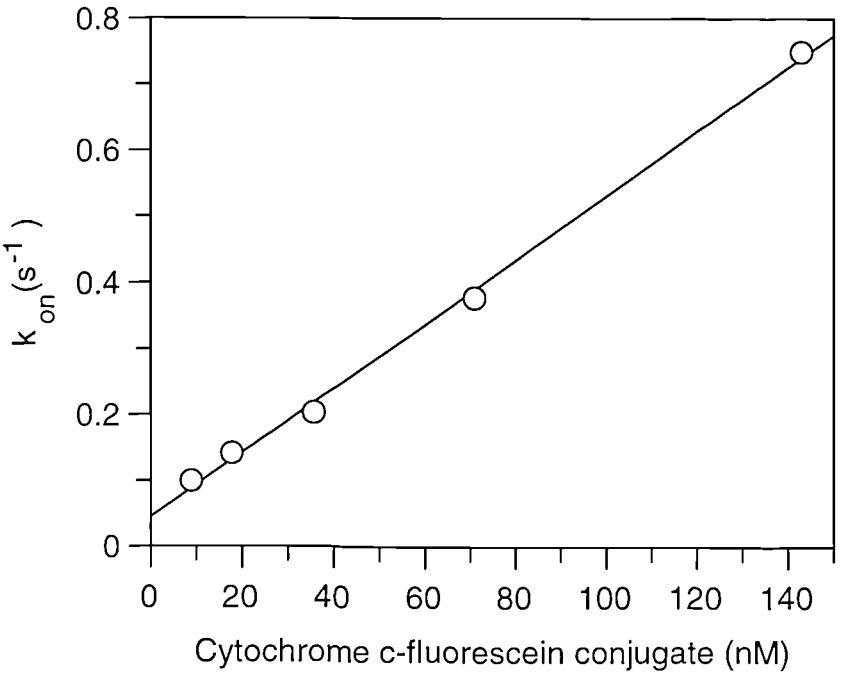

Figure 9.18: *Plot of on-rate against cytochrome c-fluorescein concentration for the interaction of the conjugate with anti-FITC mab bound to RAMFc immobilised to a CMD surface at 2200 arc seconds*

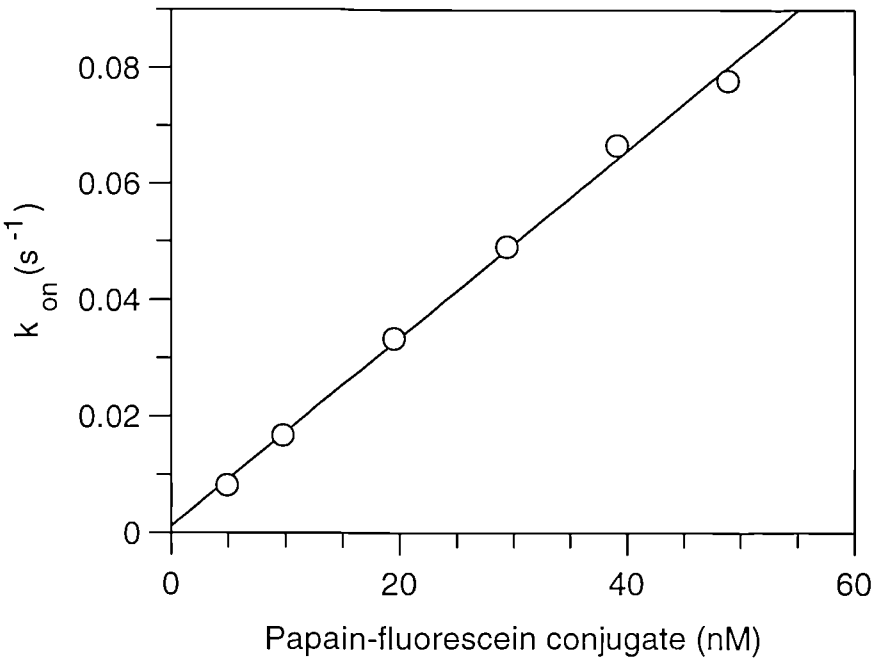

Figure 9.19: *Plot of on-rate against papain-fluorescein concentration for the interaction of the conjugate with anti-FITC mab bound to RAMFc immobilised to a CMD surface at 2200 arc seconds*

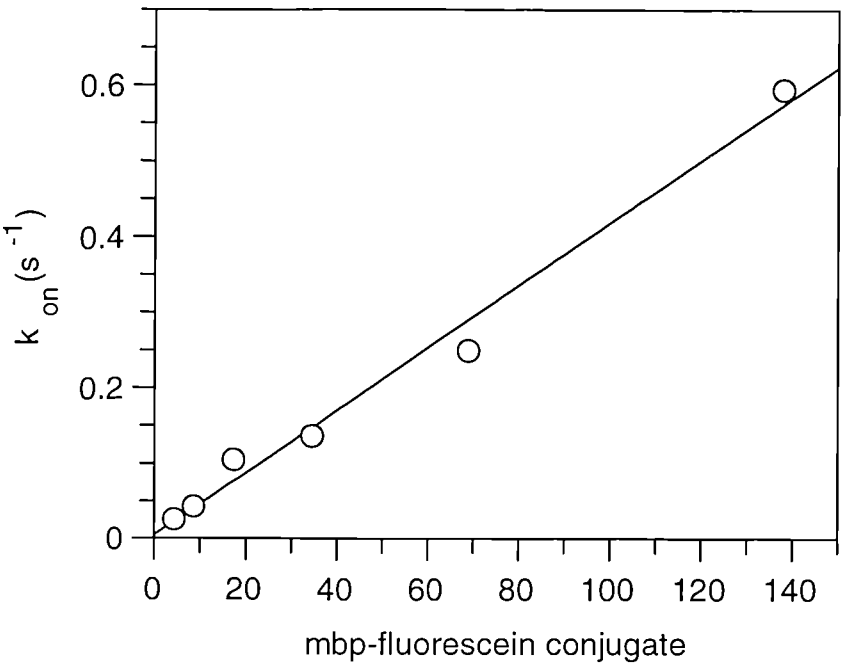

Figure 9.20: *Plot of on-rate against mbp-fluorescein concentration for the interaction of the conjugate with anti-FITC mab bound to RAMFc immobilised to a CMD surface at 2200 arc seconds*

The rate constants determined are shown in table 9.4 below.

Conjugate	k_{ass} ($M^{-1}s^{-1}$)	k_{diss} (s^{-1})	K_D (nM)
Cytochrome c	$4.62 \pm 0.14 \times 10^{6}$	$7.00 \pm 1.01 \times 10^{-2}$	15.1 ± 2.3
mbp	$4.16 \pm 0.23 \times 10^{6}$	$5.13 \pm 15.2 \times 10^{-3}$	1.22 ± 3.56
papain	$1.62 \pm 0.04 \times 10^{6}$	$1.21 \pm 1.36 \times 10^{-3}$	0.71 ± 0.79

Table 9.4: *The association and dissociation rate constants derived for the interaction of three fluorescein conjugates with anti-FITC mab bound to RAMFc immobilised on CMD. The K_D shown was determined from the ratio of the two rate constants.*

The fitted k_{diss} values were similar for each conjugate with values of $6.2 \pm 0.3 \times 10^{-3}$ s^{-1}, $5.6 \pm 0.6 \times 10^{-3}$ s^{-1}, and $5.4 \pm 0.6 \times 10^{-3}$ s^{-1} for cytochrome c, papain and mbp conjugates respectively.

9.3.2 Planar carboxylate surface

9.3.2.1. Immobilisation of anti-FITC mab

The immobilisation of the FITC antibody to the planar carboxylate surface gave a response of 360 arc seconds. Using this antibody immobilised surface the conjugates were bound at differing concentrations in order to determine the kinetic constants Figures 9.21,9.22 and 9.23 show the kinetic plots for the cytochrome c, mbp and papain conjugates respectively.

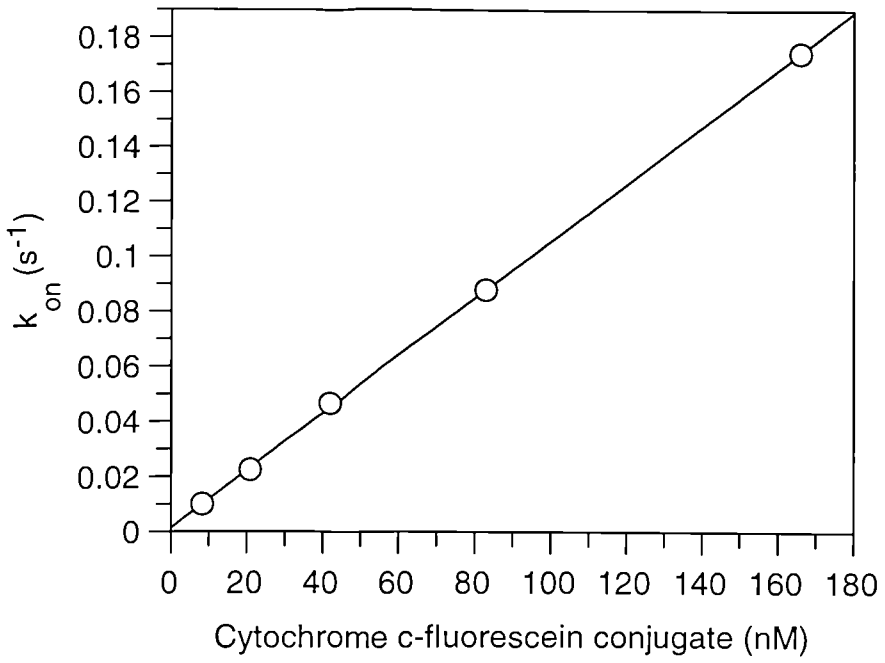

Figure 9.21: *Plot of on-rate against cytochrome c-fluorescein concentration for the interaction of the conjugate with anti-FITC mab immobilised to a carboxylate surface at 360 arc seconds*

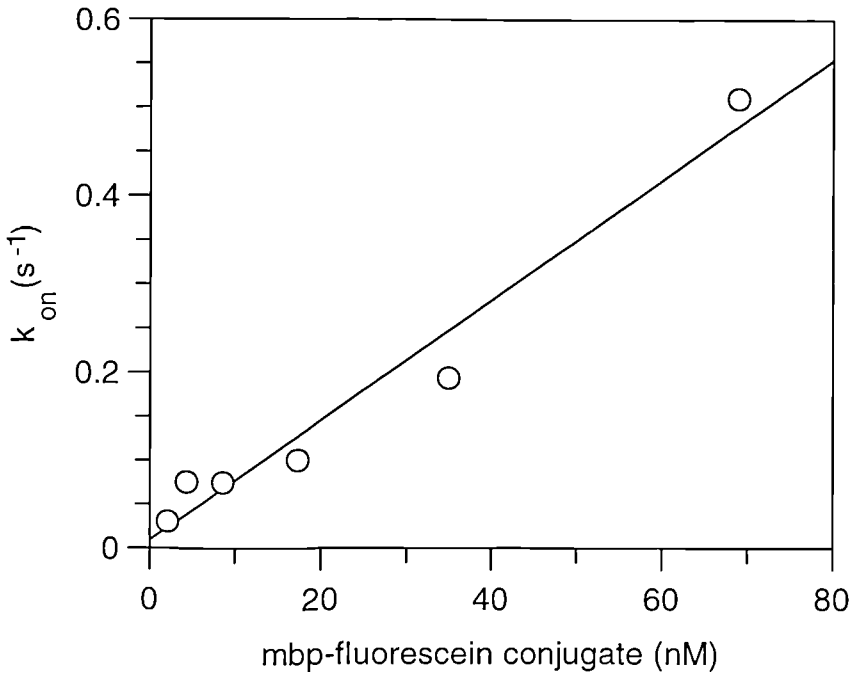

Figure 9.22: *Plot of on-rate against mbp-fluorescein concentration for the interaction of the conjugate with anti-FITC mab immobilised to a carboxylate surface at 360 arc seconds*

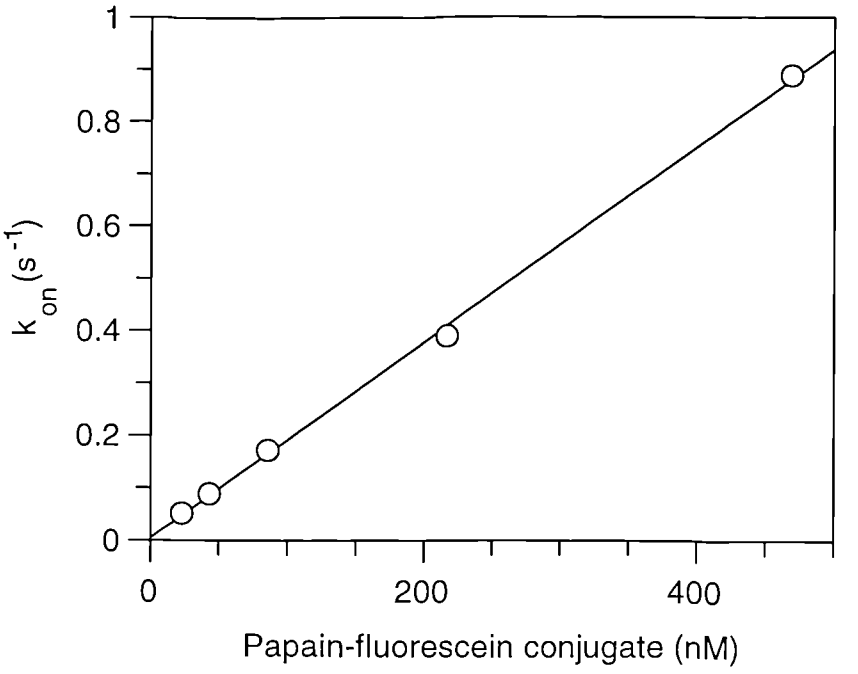

Figure 9.23: *Plot of on-rate against papain-fluorescein concentration for the interaction of the conjugate with anti-FITC mab immobilised to a carboxylate surface at 360 arc seconds*

The kinetic values for each conjugate are shown in table 9.5

Conjugate	k_{ass} ($M^{-1}s^{-1}$)	k_{diss} (s^{-1})	K_D (nM)
Cytochrome c	$1.04 \pm 0.08 \times 10^{6}$	$1.41 \pm 0.7 \times 10^{-3}$	1.35 ± 0.67
mbp	$6.81 \pm 0.69 \times 10^{6}$	$9.5 \pm 22.2 \times 10^{-3}$	1.39 ± 3.25
papain	$1.87 \pm 0.04 \times 10^{6}$	$5.01 \pm 8.5 \times 10^{-3}$	2.68 ± 4.55

Table 9.5: *The association and dissociation rate constants derived for the interaction of three fluorescein conjugates with anti-FITC mab immobilised on the carboxylate surface. The K_D shown was determined from the ratio of the two rate constants*

The fitted k_{diss} values for each conjugate were $6.2 \pm 0.4 \times 10^{-3}$ s^{-1}, $6.6 \pm 0.7 \times 10^{-3}$ s^{-1}, and $7.1 \pm 0.6 \times 10^{-3}$ s^{-1} for mbp , papain and cytochrome c conjugates respectively.

9.3.2.2 RAMFc capture system

An immobilisation response of 1100 arc seconds was obtained on the carboxylate surface. The anti-FITC mab binding response was 230 arc seconds.

The kinetic plots for the binding of cytochrome c, papain and mbp conjugates are shown in figures 9.24,9.25 , 9.26 respectively.

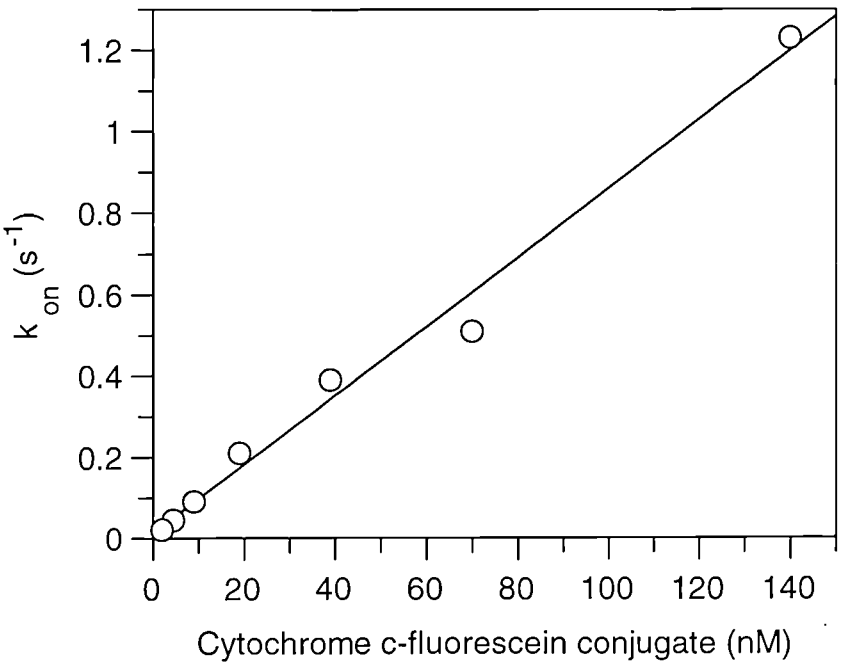

Figure 9.24: *Plot of on-rate against cytochrome c-fluorescein concentration for the interaction of the conjugate with anti-FITC mab bound to RAMFc immobilised to a carboxylate surface at 1100 arc seconds*

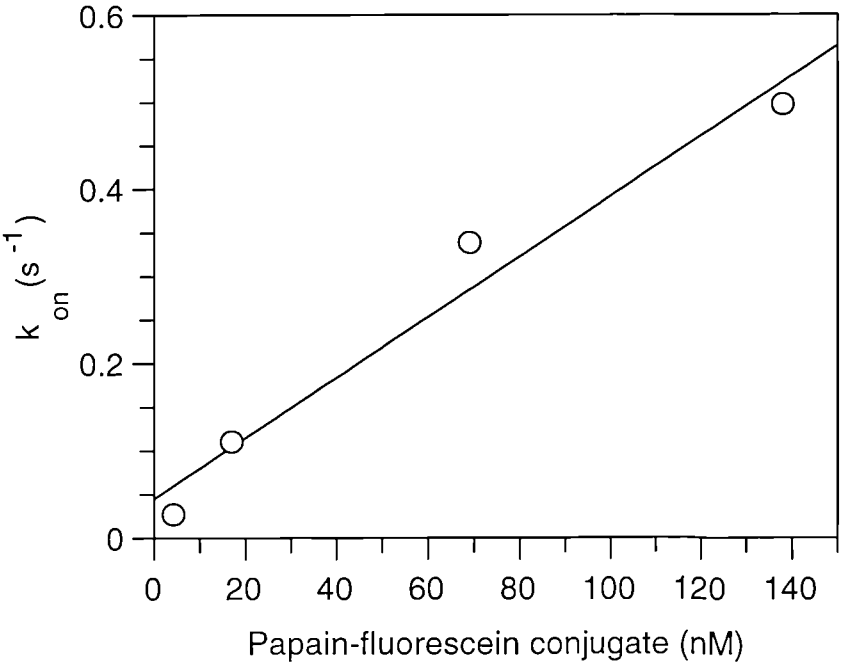

Figure 9.25: *Plot of on-rate against papain-fluorescein concentration for the interaction of the conjugate with anti-FITC mab bound to RAMFc immobilised to a carboxylate surface at 1100 arc seconds*

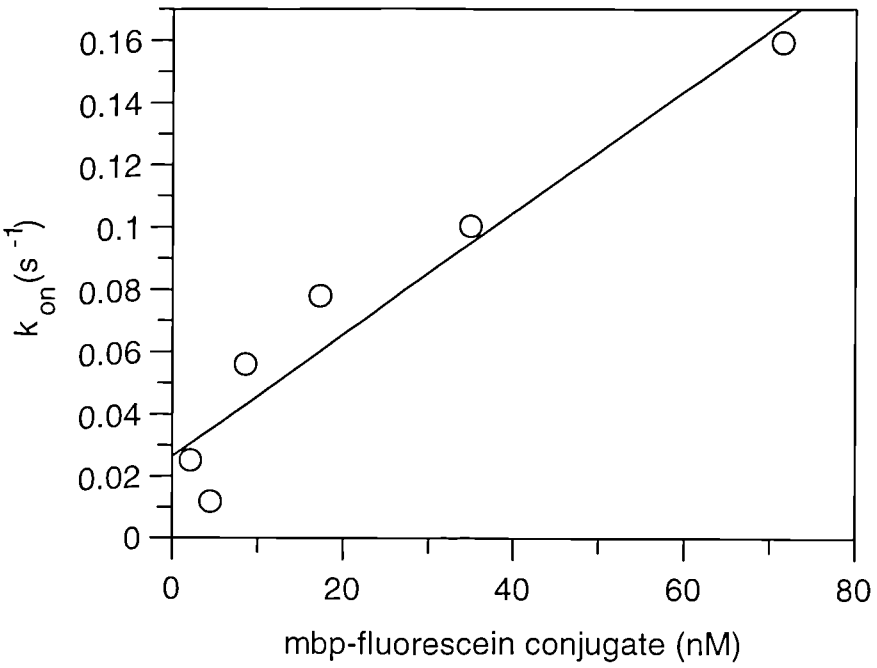

Figure 9.26: *Plot of on-rate against mbp-fluorescein concentration for the interaction of the conjugate with anti-FITC mab bound to RAMFc immobilised to a carboxylate surface at 1100 arc seconds*

The rate constants are tabulated below in table 9.6

Conjugate	k_{ass} ($M^{-1}s^{-1}$)	k_{diss} (s^{-1})	K_D (nM)
Cytochrome c	$8.90 \pm 0.46 \times 10^{6}$	$4.5 \pm 2.8 \times 10^{-3}$	0.56 ± 0.31
mbp	$1.95 \pm 0.28 \times 10^{6}$	$2.6 \pm 0.9 \times 10^{-2}$	13.33 ± 4.98
papain	$3.46 \pm 0.46 \times 10^{6}$	$4.5 \pm 3.6 \times 10^{-2}$	13.00 ± 10.5

Table 9.6: *The association and dissociation rate constants derived for the interaction of three fluorescein conjugates with anti-FITC mab bound to RAMFc immobilised on the carboxylate surface. The K_D shown was determined from the ratio of the two rate constants*

The association rate constant derived from the binding of conjugate to anti-FITC mab on the amino surface shows a conjugate dependency. From highest to lowest, the order of the k_{ass} was ; cytochrome c-, papain- and then mbp- fluorescein conjugates. The

dissociation rate constant determined from the rate suggests that the k_{diss} for the mbp conjugte may be lower than that of the other conjugates. However, the error in the intercept makes this uncertain. The fitted k_{diss} values for each conjugate with values of $4.5 \pm 0.4 \times 10^{-3}$ s^{-1}, $5.6 \pm 0.7 \times 10^{-3}$ s^{-1}, and $4.9 \pm 0.6 \times 10^{-3}$ s^{-1} for cytochrome c, papain and mbp conjugates respectively. Therefore there seems little discernable difference between the dissociation rate of the conjugates.

9.3.3 Planar amino surface

9.3.3.1 Immobilisation of anti-FITC mab

Anti-FITC antibody was immobilised to the amino surface via glutaraldehyde. Conjugates were then bound at differing concentrations in order to construct kinetic plots. Each conjugate concentration was removed by a two minute wash with 4M $MgCl_2$. Figures 9.27,9.28, and 9.29 show the kinetic plots for the cytochrome c, papain and mbp conjugates.

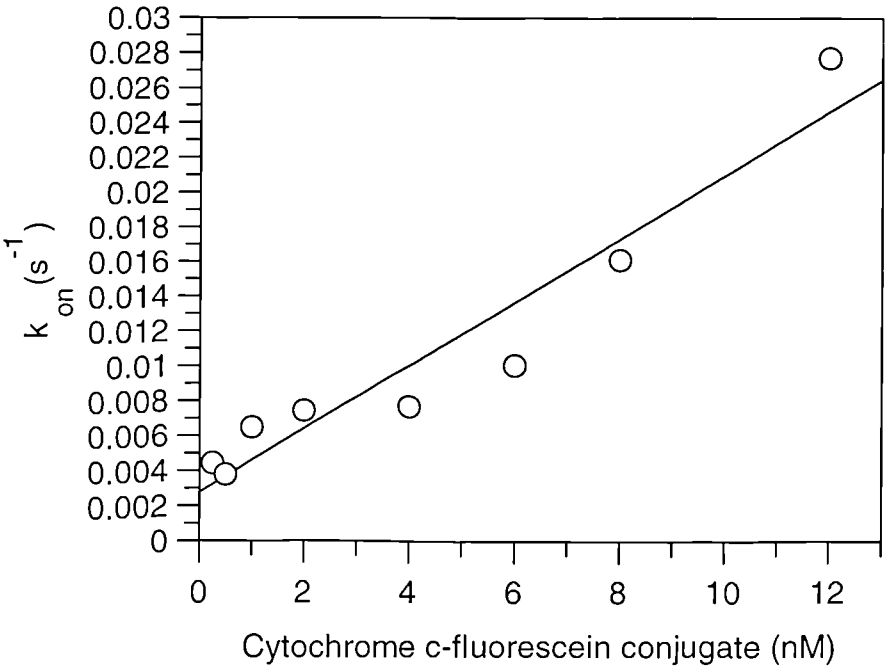

Figure 9.27: *Plot of on-rate against cytochrome c-fluorescein concentration for the interaction of the conjugate with anti-FITC mab immobilised to an amino surface at 600 arc seconds*

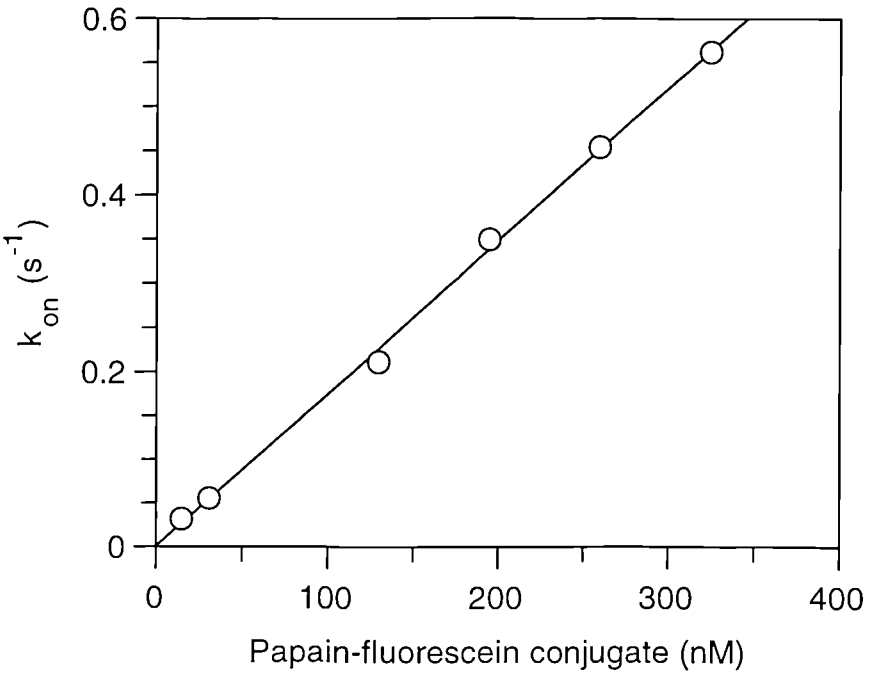

Figure 9.28: *Plot of on-rate against papain-fluorescein concentration for the interaction of the conjugate with anti-FITC mab immobilised to an amino surface at 600 arc seconds*

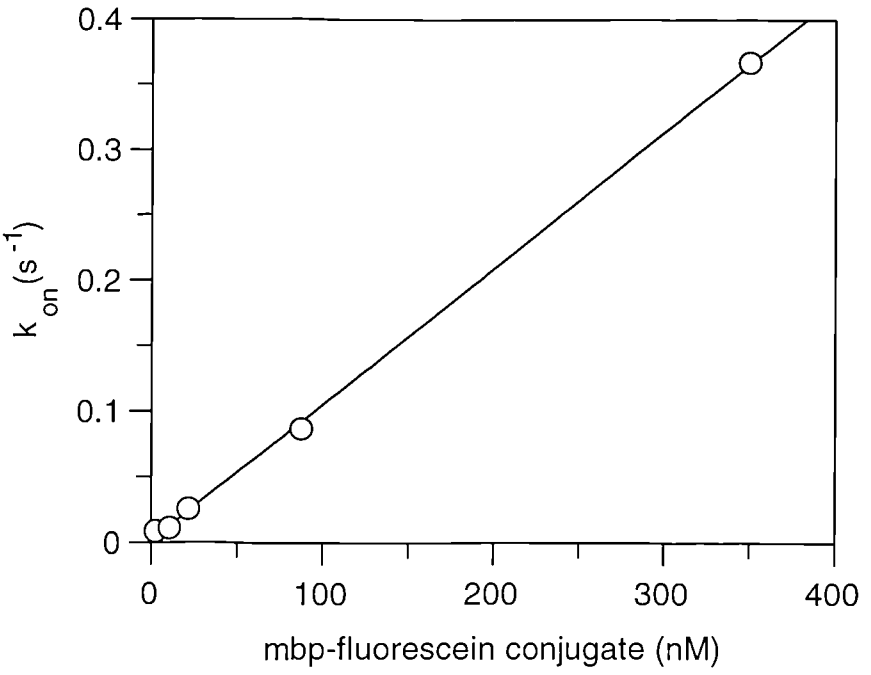

Figure 9.29: *Plot of on-rate against mbp-fluorescein concentration for the interaction of the conjugate with anti-FITC mab immobilised to an amino surface at 600 arc seconds*

The rate constants derived from the binding of fluorescein conjugates to anti-FITC mab immobilised to amino surfaces are shown in table 9.7 below

Conjugate	k_{ass} ($M^{-1}s^{-1}$)	k_{diss} (s^{-1})	K_D (nM)
Cytochrome c	$1.82 \pm 0.22 \times 10^{6}$	$2.72 \pm 1.21 \times 10^{-3}$	1.49 ± 0.68
mbp	$1.04 \pm 0.015 \times 10^{6}$	$1.23 \pm 2.41 \times 10^{-3}$	1.18 ± 2.31
papain	$1.73 \pm 0.03 \times 10^{6}$	$1.11 \pm 6.71 \times 10^{-3}$	0.64 ± 3.86

Table 9.7: *The association and dissociation rate constants derived for the interaction of three fluorescein conjugates with anti-FITC mab immobilised on the amino surface. The K_D shown was determined from the ratio of the two rate constants.*

The fitted k_{diss} values were once again similar for each conjugate with values of $5.3 \pm 0.3 \times 10^{-3}$ s^{-1}, $5.2 \pm 0.6 \times 10^{-3}$ s^{-1}, and $6.1 \pm 0.6 \times 10^{-3}$ s^{-1} for cytochrome c, papain and mbp conjugates respectively.

9.4 Discussion

It was found necessary to reduce the positive charge on the papain and cytochrome c conjugates in order to eliminate non-specific binding. This was accomplished by succinylation of the conjugates with succinic anhydride, converting the free amino groups to carboxylic acids.

9.4.1 Kinetic constants from stopped-flow fluorescence

The kinetic constants from the fluorescence data were determined by monitoring the fluorescence quench when an anti-FITC mab binds to a fluorescently labelled protein conjugate. In this experiment, the labelled protein is the ligand and therefore its concentration is fixed. The concentration of the mab was varied and allowed the rate constants to be determined. The association rate constant for cytochrome c and papain conjugates was 2.2×10^{7} $M^{-1}s^{-1}$. This rate constant for the mbp conjugate was approximately two-fold lower at 1.23×10^{7} $M^{-1}s^{-1}$. As the fluorescence technique monitors reactions in solution, it was expected that all three values would be similar given that the reaction is via the fluorescein label and the antibody. It may be that the larger mbp may influence the binding of the mab by steric means. The dissociation

rate constant from these experiments is poorly defined with the exception of that from the mbp conjugate. However, even the intercept from the mbp conjugate experiment has a 20% error associated with it. The dissociation rate constant was also expected to be independent of conjugate and the values suggest this to be so although the errors in the values from the papain and cytochrome c conjugate make any conclusion doubtful. Despite this, an intercept value of 4×10^{-1} s^{-1} seems a plausible estimate.

9.4.2 Kinetic constants from IAsys

For the IAsys comparison several different methodologies and surfaces were investigated. The immobilisation of the conjugates to the CMD matrix followed by antibody binding allowed the rate constants to be determined in a similar manner to that from the fluorescence experiment. Namely that the concentration of the conjugate was constant and the concentration of the mab was varied. An association rate constant for the anti-FITC mab interacting with CMD immobilised cytochrome c conjugate of $1.72 \pm 0.15 \times 10^{6}$ $M^{-1}s^{-1}$ was determined. The dissociation rate constant determined from the intercept was $1.32 \pm 0.55 \times 10^{-3}$ s^{-1}. Directly fitting the dissociation data gave a k_{diss} value of $2.62 \pm 0.06 \times 10^{-3}$ s^{-1}. The binding isotherm resulted in a K_D of 0.92 ± 0.19 nM which agree well to 0.76 ± 0.32 nM obtained from the ratio of the association to the dissociation rate constants from the kinetic plot. Using the dissociation rate constant determined directly gives a K_D of 1.52 ± 0.14 nM. Finally for this interaction, a K_D of 2.8 nM was determined by equilibrium titration.

For the papain-fluorescein conjugate immobilised on CMD the association rate constant was $2.12 \pm 0.14 \times 10^{6}$ $M^{-1}s^{-1}$ and the dissociation rate constant from the intercept was $4.18 \pm 1.10 \times 10^{-3}$ s^{-1}. Combining these rate constants gives a K_D of 1.91 $\pm$ 0.52 nM. Direct fitting of the dissociation phase to a single exponential equation containing an offset value resulted in a k_{diss} of $2.56 \pm 0.05 \times 10^{-3}$ s^{-1} but the dissociation rate could be increased by the inclusion of fluorescein in the dissociation buffer. A value of 3.7×10^{-2} s^{-1} was then determined. This has been found previously for the interaction of the mab with immobilised FITC on CMD sensor surfaces. (see chapter 6). It is assumed that the fluorescein competes with the fluorescein on the conjugates surface for the mab and therefore reduces the rebinding on the dissociated mab. This reduction in rebinding and therefore increase in the dissociation rate

constant has been reported by other authors (Glaser, 1993. Felder et al., 1993. Takano et al., 1994. Johanson et al., 1995. MacKenzie et al., 1996). The binding of antibody to mbp conjugate was performed at a ligand loading of 240 arc seconds. Values of $1.38 \pm 0.04 \times 10^{6}\ M^{-1}s^{-1}$ for the association rate constant and $1.58 \pm 1.25 \times 10^{-3}\ s^{-1}$ for the dissociation rate constant from the intercept agree well with the constants determined from the other immobilised conjugates. The dissociation rate constant could be increased by the inclusion of fluorescein in the dissociation buffer to $2.8 \times 10^{-2}\ s^{-1}$. The K_D determined from the ratio of the rate constants determined from the kinetic plot were 1.14 ± 0.90 nM while from the isotherm plot a K_D of 9.37 ± 2.62 nM was determined.

It was the intention of this study to determine whether there was a molecular weight dependence upon the rate constants determined. A situation which could only be investigated by the immobilisation of the antibody. The antibody used for this investigation was acid labile and therefore normal acidic regenerants resulted in an inactive ligand. It was found that a two-minute wash with 4M $MgCl_2$ removed bound conjugate while maintaining the activity of the immobilised antibody.

The immobilisation of the antibody to either the amino, CMD or carboxylate surfaces gave association rate constants which were indistinguishable from each other. All the values were between 1.04 to $2.08 \times 10^{6}\ M^{-1}s^{-1}$ with the exception of the mbp conjugate binding which resulted in a value of $6.81 \times 10^{6}\ M^{-1}s^{-1}$. The reason for this difference is unclear but may reflect the difference in charge between the three proteins. The cytochrome c and the papain had to be succinylated to reduce their positive charge and hence non-specific binding on CMD. The fact that the association rate constant from the mbp conjugate on CMD is not higher than the other conjugate may be due to the differences in surface morphology between planar carboxylate and CMD. The dissociation rates determined from the intercept are largely independent of both surface and conjugate with the exception of the mbp conjugate binding to mab on a carboxylate surface with a value of $9.5 \times 10^{-3}\ s^{-1}$. However, the errors associated with some of the intercepts make comparison difficult. The fitted values from the conjugate bindings also reveal no significant difference between conjugates and surfaces with values of between 4.7 and $7.1 \times 10^{-3}\ s^{-1}$.

A sandwich assay was also employed as a further comparison. RAMFc was immobilised on the CMD and carboxylate surfaces only and the FITC followed by the conjugates were bound. The regenerant used was 100mM HCl. The association rate constant ranged between 1.62 and 4.62 x 10^6 $M^{-1}s^{1}$ although a value of 8.9 x 10^6 $M^{-1}s^{-1}$ was determined for cytochrome c on the carboxylate surface. The dissociation rate constant from the intercept was again poorly defined with similar values to those obtained on the direct determination from immobilised antibody. Direct fitting of the dissocaition phase failed to highlight any differences in the conjugates or surfaces with k_{diss} values of between 4.5 and 6.2 x 10^{-3} s^{-1}. It should be mentioned that the association rate constants from the RAMFc system may be higher than those the direct analysis. It may be that the RAMFc is able to orientate the anti-FITC mab and therefore retain a greater activity.

Both the association and dissociation rate constants are therefore about 10-fold lower using IAsys on this system but because of the fact that both the constants are lowered by the same amount the K_D value determined from the ratio are similar to those from the fluorescence data.

9.4.3 Comparisons by other authors

There have been several publications comparing the affinities determined by optical biosensors with more conventional techniques such as calorimetry and fluorescence.
For example, Ito and Kurosawa (1993) investigated the interaction of hen egg lysozyme (HEL) with Fv fragments of anti-HEL antibody using BIAcore, fluorescence quench, and calorimetry. The fluorescence quench was used to determine the association rate constant while calorimetry used to determine K_A. From these values, the dissociation rate constant was calculated. It was found that the both the association and dissociation rate constants were slower by a factor of ten with values of 1.2 x 10^5 $M^{-1}s^{-1}$ and 2 x 10^{-3} s^{-1} respectively. However, given that both values have dropped by the same factor, the affinity constant agreed well with that from the calorimetry.

Bondeson et al. (1993) investigated the kinetics for the interaction of lactose repressor with operator DNA by SPR, electrophoretic mobility shift assay, and filter assay using

nitro-cellulose membranes. The association rate constant determined by SPR was 2 x 10^6 $M^{-1}s^{-1}$ while that obtained by the filter assay was 1 x 10^9 $M^{-1}s^{-1}$. The dissociation rate constants from the same methods were 3 x 10^{-4} s^{-1} and 2 x 10^{-2} s^{-1} respectively.

In addition, others workers have noted differences in the rate constants determined by biosensor technology (Guichard et al., 1994. Gruen et al., 1993., Takano et al., 1994). In contrast to differences in the measured affinities and kinetics, several workers have obtained constants which are in general agreement to those obtained by different methods. These include Johanson et al., 1995., MacKenzie et al., 1996, and Wu et al., 1995.

In conclusion the data collected suggest that the maximum association rate constant that can be measured by IAsys is in the order of 5 x 10^6 $M^{-1}s^{-1}$. Higher values may be possible by utilising the RAMFc system. There seems to be no molecular weight dependence upon the rate constants on the CMD surface; a situation that may have occurred given the nature of the CMD matrix. The determination of the dissociation rate constant is more complex. The intercept of the kinetic plot is often poorly defined and as such the degree of uncertainty of the dissociation rate constant from this method is high.. A more accurate method is to fit the dissociation data using one of the dissociation rate equations. Both these methods generally gave k_{diss} values of 5 x 10^{-3} s^{-1} although the errors from direct fitting were lower. However, the k_{diss} was still 100-fold lower than that determined from the fluorescence data. A ten-fold increase in the k_{diss} value was achieved by performing the dissociation in the presence of a competing species such as the ligand to prevent rebinding.

CONCLUSIONS.

Both the association and dissociation data obtained from optical biosensors have been shown to be inadequately described by the expected equations. The association data are frequently poorly fitted to an integrated first order rate equation containing a single exponential term. Only at low ligate concentrations does this equation seem to give an adequate description of the data. At higher ligate concentrations the data must be fitted to an equation containing two exponential terms in order to describe the data. This deviation from the expected behaviour is, at least in part, due to steric hindrance within the CMD matrix. The binding of ligate to a particular site may prevent binding of other ligate molecules to an adjacent site. In addition to the biphasic nature of the association curve, the determined association rate constant is also influenced by ligand loading. At low loadings the association rate constant is found to be significantly higher than at higher loadings. This steric problem may obviously be reduced by the use of low loadings of ligand. The dissociation phase also deviates from that expected with a poor fit to the data given by a single exponential decay equation. A better fit is achieved by the inclusion of an offset term which allows for the incomplete dissociation of the ligate often seen in biosensor data. This incomplete dissociation has been shown to be due to rebinding of the dissociated ligate.

Efficient delivery of the ligate to the immobilised ligand is achieved by the use of stirring in IAsys. It was found that the on-rate was independent of stir rate at the rate used for all the data contained within this thesis. The on-rate was also independent of viscosity changes up to a value of 10% glycerol (w/w). Above this value the on-rate was lowered. An unstirred layer thickness of between 5 and 9 μm was calculated using initial rates allowing rapid transfer of ligate from bulk to immobilised ligand. Given these points it was concluded that the data collected in this thesis were not significantly controlled by mass transport.

The closed nature of the IAsys cuvette means that the assumption of pseudo-first order conditions within the cuvette may not be valid. Second order equations were derived allowing the equilibrium and kinetic constants to be determined under conditions of ligate depletion. It was found that depletion is more severe over extended time periods

and therefore the equilibrium constant determined from the use of equilibrium responses may be greatly affected. Simulated equilibrium data at differing concentrations of ligate were used to construct a binding isotherm. Depletion causes the isotherm to be shifted to the right resulting in a higher K_D value. It is possible to correct for these depletion by three methods: (i) by correcting the K_D determined using Langmuirian conditions; (ii) by correcting the concentrations for depletion prior to construction of the isotherm; and (iii) by fitting the experimental data to an isotherm allowing for depletion. In the case of the association phase of data, depletion causes a higher than expected on-rate value. This can be observed in plots of on-rate against ligate concentration as a positive curvature at the lower ligate concentrations. This curvature causes an under-estimate in the association rate constant and an over-estimate in the dissociation rate constant. Low ligand loadings are therefore recommended in order to reduce depletion. If a positive curvature is observed, then selection of the higher ligate concentrations or the use of second order equations should be made.

For the dissociation phase, the closed nature of the cuvette favours the rebinding of dissociated ligate. This is seen in an IAsys profile as incomplete dissociation which is poorly fitted to the expected single exponential decay equation but well described by the addition of an offset into the decay equation. It has, however, been shown that the use of the offset equation may result in an over-estimate of the dissociation rate constant. In general, the extent of depletion is influenced by the capacity of the immobilised ligand for the ligate, the affinity of the interaction, and the concentration of ligate used. In addition, the degree of rebinding in the dissociation phase is also dependent upon the response from which the dissociation is initiated compared to the capacity of the ligand. To accurately measure the dissociation rate constant from direct analysis, it is recommended that low ligand loadings are used and the dissociation fitted from the higher ligate concentrations which approach saturation.

A comparison of the kinetics of differing biological systems on CMD, and planar carboxylate and amino surfaces revealed only small differences in rate constants. Immobilisation of anti-HSA mab revealed that the binding of HSA was faster when immobilised onto aminosilane compared to the other surfaces. However,

immobilisation of the HSA and binding of anti-HSA showed no surface dependency. A similar finding was observed by immobilising lysozyme and binding D1.3Fv fragments. In contrast, the immobilisation of chymotrypsin and binding of CI-2 illustrated a potential problem with planar surfaces. Binding of CI-2 was only observed when the chymotrypsin was immobilised to CMD, when immobilised to planar surfaces the CI-2 failed to bind. This is assumed to be due to the chymotrypsin being denatured by the planar surface.

The study using fluorescently labelled proteins possessing a single thiol group revealed differences in the rates obtained from stopped-flow and IAsys. IAsys determined association rate constants which were about ten-fold lower (2×10^6 $M^{-1}s^{-1}$) on dextran cuvettes with FITC mab immobilised. The data, although not conclusive, suggest that higher rates may be possible on planar surfaces such as the carboxylate surface or by the use of RAMFc capture system. In these cases association rate constants increased to values at best two-fold (8.9×10^6 $M^{-1}s^{-1}$) below the fluorescent data values of 2×10^7 $M^{-1}s^{-1}$. The dissociation rate constant determined from the intercept of the kinetic plot for fluorescence data revealed large errors in this value. However, it was assumed that the value was around 0.3 s^{-1}. The dissociation rate constant determined from the intercept or by direct fitting of the IAsys data were approximately 5×10^{-3} s^{-1}. It was possible to increase this rate by the addition of free ligand, such as fluorescein (sodium salt), into the dissociation buffer. Values of around 5×10^{-2} s^{-1} were then determined. It would seem the maximum association and dissociation rate constants that may be determined at present using the IAsys are about 1×10^7 $M^{-1}s^{-1}$ and 5×10^{-2} s^{-1} respectively. However, it may be necessary to investigate both the surface, the method of attachment (i.e. via orientation using RAMFc) and the addition of a competing ligand into the dissociation buffer to gain a complete insight into biomolecular interactions using biosensor technology.

In conclusion, the IAsys optical biosensor is capable of determining the equilibrium and kinetic constants arising from the interaction of ligate with surface immobilised ligand. While this surface attachment does influence the values determined, the differences between this and more conventional solution techniques such as fluorescence can be minimised by careful experimental design. Low levels of immobilised ligand should be used in order to minimise steric constraints within the CMD matrix. Non-linear regression analysis of the ligate binding data will, at moderate to high concentrations, be poorly fitted by the expected single exponential equation but better described by the addition of a further exponential term. At these concentrations the first, rapid k_{on} value should be used in the subsequent k_{on} vs. [ligate] plot. Alternatively, the amount of data used for fitting may be reduced until well described by the single exponential equation. The association rate constant determined from the slope of the k_{on} vs. [ligate] should reflect the true rate constant for the interaction provided that the data points lie on a straight line. Curvature is often seen at high ligate concentrations and is believed to be due to steric constraints. At the lower concentrations, a positive curvature is an indication of depletion, while a negative curvature suggests mass transport limitations. Under these circumstances, correct selection of the ligate concentrations to be used is vital. The dissociation rate constant rate constant determined from the intercept of the k_{on} vs. [ligate] is often close to zero and hence poorly defined. A better approach is to directly fit the dissociation profile. Ligate dissociation is often incomplete and the data are therefore better fitted by the inclusion of an offset term in the expected single exponential dissociation equation or via the use of a second order equation. In order to determine dissociation rate constants, the level of immobilised ligand should be low and the ligate concentration high to ensure that its binding saturates the free ligand sites. To further minimise rebinding, the rate should be data using data towards the initiation of dissociation and preferably the dissociation should proceed with competing ligand in the dissociation buffer.

The rate constants determined on CMD should be compared to planar surfaces on which it may be possible to determine higher association rate constants due to the absence of the CMD layer. In addition, it may also be preferable to attempt orientated

immobilisation, such as via RAMFc or Protein A, in order to increase the confidence in the rate and equilibrium constants.

Despite the work carried out within this thesis, further comparative work on kinetics is needed between optical biosensors and conventional techniques. This will provide further confidence in the kinetic constants published by various authors and provides a starting point to further expand the range of constants that can be reliably determined. Some of the data within this thesis suggest that planar surfaces may be able to determine higher association rate constants than CMD surfaces. Further investigation of this is therefore warranted together with an investigation into the possible advantages of orientated immobilisation on rate constant determination.

References.

Arwin, H., and Lundstrom, I. (1985) *Anal.Biochem* **145** 113-119

Beatty, J.D., Beatty, B.G., and Vlahos, W.J. (1987a) *J.Immunol.Methods.* **100** 173-179

Beatty, J.D., Beatty, B.G., Vlahos, W.J., and Hill, L.R. (1987b) *J. Immunol. Methods.* **100** 161

Berg, O.G., and von Hippel, P.H. (1985) *Ann. Rev. Biophys. Biophys. Chem* **14** 131-160

Bernard, A and Bosshard, H.R. (1995) *Eur. J. Biochem.* **230** 416-423

Bhat, T.N., Bentley, G.A., Fischmann, T.O, Boulot, G., and Poljak, R.J. (1990) *Nature* **347** 483-485

Bhat, T.N., Bentley, G.A., Boulot, G., Greene, M., Tello, D., Dall'Acqua, W., Souchon, H., Schwarz, F.P., Mariuzza, R.A., and Poljak, R.J. (1994) *Proc. Natl. Acad. Sci. USA.* **91** 1089-1093

Bhatia, S.K.,Shriver-Lake, L.C., Prior, K.J., Georger, J.H., Calver, J.M., Bredehorst, R., and Ligler, F.S. (1989) *Anal.Biochem.* **178** 408-413

Bondenson, K., Frostell-Karlsson, A., Fägerstam, L., and Magnusson, G. (1993) *Analytical Biochemistry*, **214** 245-251

Borchert, A., Larsson, P., and Mosbach, K. (1982) *J.Chromatog.* **244** 49-56

Bowles, M.R., Hall, D.R., Pond, S.M., and Winzor, D.J. (1997) **244** 133-143

Brandenburg, A., and Gombert, A. (1993) *Sensors and Actuators B* **17** 35-40

Brecht, A., Ingenhoff, J., and Gauglitz, G. (1992) *Sensors and Actuators B* **6** 96-100

Buckle, M., Williams, R.M., Negroni, M., and Buc, H. (1996) *Proc. Natl. Acad. Sci. USA.* **93** 889-894

Buckle, P.E., Davies, R.J., Kinning, T., Yeung, D., Edwards, P.R., Pollard-Knight, D. and Lowe, C.R. (1993) *Biosensors and Bioelectronics* **8** 355-363

Buijs, J., Van den Berg, P., Lichtenbelt, J.W.Th., Norde, W., and Lyklema, J. (1996) *J.Colloid Interface Sci.* **178** 594-605

Butler, J.E., Ni, L., Nessler, R., Joshi, K.S. Suter, M., Rosenberg, B., Chang, J., Brown, W.R., and Cantarero, L.A. (1992) *J.Immunol. Methods.* **150** 77-90

Cantor, C.R. and Schimmel, P.R. (1980) *Biophysical Chemistry Part II: Techniques for the study of biological structure and function.* W.H. Freeman and Co. New York 584

Cardoza, J.D., Kleinfeld, A.M., Stallcup, K.C., and Mescher, M.F (1984) *Biochemistry* **23** 4401-4409

Cha, W., and Beissinger, R.L. (1996) *J.Colloid Interface Sci.* **177** 666-674

Christensen, L.L.H (1997) *Anal. Biochem.* **249** 153-164

Chacko, S., Silverston, E.W., Kam-Morgan, L., Smith-Gill, S.J., Cohen, G., and Davies, D.R. (1995) *J.Mol.Biol.* **245** 261-274

Checovich, W.J., Bolger, R.E., and Burke, T. (1995) *Nature* **375** 254-256

Clerc, D., and Lukosz, W. (1993) *Sensors and Actuators B* **11** 461-465

Clerc, D., and Lukosz, W. (1994) *Sensors and Actuators B* **18-19** 581-586

Clerc, D., and Lukosz, W. (1997) *Biosensors and Bioelectronics* **12** 184-194

Colman, P.M., Laver, W.G., Varghese, J.N., Baker, A.T., Tulloch, P.A., Air, G.M., and Webster, R.G. (1987) *Nature* **326** 358-363

Corr, M., Slanetz, A.E., Boyd, L.F., Jelonek, M.T., Khilko, S., Al-Ramadi, B.K., Kim, Y.S., Maher, S.E., Bothwell, A.L.M., and Margulies, D.H. (1994) *Science* **265** 946-949

Cowen, R., and Underwood, P.A. (1988) *J. Theor. Biol.* **132** 319-335

Cram, D.J. (1983) *Science* **219** 709-713

Creighton, T.E. (1993) *Proteins: Structure and Molecular Properties. 2nd Edition* Freeman and Co. New York.

Cush, R., Cronin, J.M., Steward, W.J., Maule, C.H., Molloy, J., and Goddard, N.J. (1993) *Biosensors and Bioelectronics* **8** 347-353

Dandliker, W.B and Levison, S.A. (1967) *Immunochemistry* ,**5** , 171-183

Day, E. (1990) *Advanced Immunochemistry,* 2nd edition, Wiley-Liss, NY, 693

DelMar, E.G., Largman, C., Brodrick, J.W., and Geokas, M.C. (1979) *Anal. Biochem.* **99** 316-320

Domenici, C., Schirone, A., Celebre, M., Ahluwalia, A., and De Rossi, D. (1995) *Biosensors and Bioelectronics* **10** 371-378

Dunn, B.M., and Chaiken, I.M. (1974) *Proc. Natl. Acad. Sci. USA.* **71** 2382-2385

Duschl, C., and Hall, E.A.H (1991) *J.Colloid Interface Sci. B* **144** 368-380

Eddowes, M.J. (1987/88) *Biosensors* **3** 1-15

Edwards, P.R., Gill, A., Pollard-Knight, D.V., Hoare, M., Buckle, P.E., Lowe, P.A., and Leatherbarrow, R.J. (1995) *Anal. Biochem.*, **231**, 210-217.

Edwards, P.R. and Leatherbarrow, R.J. (1997) *Anal. Biochem.*, **246** 1-6

Edwards, P.R., Lowe, P.A., and Leatherbarrow, R.J. (1997) *Journal of Molecular Recognition.* **10** 128-134

Eilat, D., and Chaiken, I. M. (1979) *Biochemistry* **18** 790

Ernst-Cabrera, K., and Wilchek, M. (1987) *J.Chromatog.* **397** 187-196

Fattinger, Ch., Koller,H., Schlatter, D., and Wehrli, P. (1993) *Biosensors and Bioelectronics* **8** 99-107

Fattinger, Ch. (1993) *Appl. Phys. Lett.* **62** 1460-1462

Feldman, S.F., Uzgiris, E.E., Penney, C.M., Gui, J.Y., Shu, E.Y., and Stokes, E.B. (1995) *Biosensors and Bioelectronics* **10** 423-434

Felder, S., Zhou, M., Hu., P., Ureña, J., Ullrich, A., Chaudhuri, M., White, M., Shoelson, S., and Schlessinger,J. (1993) *Mol. Cell. Biol.* **13** 1449-1455

Fisher, R.J., and Fivash, M. (1994) *Current Opin.Biotech.* **5** 389-395

Fisher, R.J., Fivash, M., Casas-Finet, J., Erickson, J.W., Kondoh, A., Bladen, S.V., Watson, D.K., and Papas, T. (1994) *Protein Science* **3** 257-266

Friguet, B., Chaffotte, A.F., Djavadi-Ohaniance, L., and Goldberg, M.E. (1985) *J.Immunol.Methods.* **77** 305-319

Fuchs, H., Orberger, G., Tauber, R., and Gebner, R. (1995) *J.Immunol. Methods.* **188** 197-208

Gao, H., Sänger, M., Luginbühl, R., and Sigrist, H. (1995) *Biosensors and Bioelectronics* **10** 317-328

Gauglitz, G., Brecht, A., Kraus, G., and Nahm, W. (1993) *Sensors and Actuators B* **11** 21-27

Gershon, P.D., and Khilko, S. (1995) *J.Immunol.Methods* **183** 65-76

Glaser, R.W. (1993) *Anal. Biochem.* **213** 152-161

Gomez, J., Hilser, V.J., Xie, D., and Freire, E. (1995) *Proteins* **22** 404-412.

Gruen, L.C., Kortt, A.A., and Nice, E. (1993) *European Journal of Biochemistry* **217** 319-325

Guichard, G., Benkirane, N., Zeder-Lutz, G., Van Regenmortel, M.H.V., Briand, J., and Muller, S. (1994) *Proc. Natl. Acad. Sci. USA* **91** 9765-9769

Hale, Z.M., Payne, F.P., Marks, R.S., Lowe, C.R., and Levine, M.M. (1996) *Biosensors and Bioelectronics* **11** 137-148

Hall, D.R., Cann, J.R., and Winzor, D.J. (1996) *Anal.Biochem.* **235** 175-184

Hall, D.R., Gorgani, N.N., Altin, J.G., and Winzor, D.J. (1997) *Anal.Biochem* **253** 145-155

Hall, D.R., and Winzor, D.J. (1997) *Anal.Biochem.* **244** 152-160

Harrick, N (1967) *Internal Reflection Spectroscopy* New York Interscience 274

Hogg, P.J., and Winzor, D.J. (1985) *Biochem. Biophys. Acta* **843** 159

Hogg, P.J., Jackson, C.M., and Winzor, D.J. (1991) *Anal.Biochem.* **192** 303-311

Holland, G.P., and Stewart, M.W. (1991) *J. Immunol. Methods.* **138** 245-255

Holwill, I., Gill, A., Harrison, J., Hoare, M., and Lowe, P.A. (1996) *Process Control and Quality* **8** 133-145

Honig, B., and Nicholls, A. (1995) *Science* **268** 1144-1149

Huber, W., Barner, R., Fattinger, Ch., Hübscher, J., Koller, H., Müller, F., Schlatter, D., and Lukosz, W. (1992) *Sensors and Actuators B* **6** 122-126

Ito, W., and Kurosawa, Y. (1993) *J.Biol.Chem.* **268** 20668-20675

Janin, J. (1995) *Proteins* **21** 30-39

Johanson, K., Appelbaum, E., Doyle, M., Hensley, P., Zhao, B., Abdel-Meguid, S.S., Young, P., Cook, R., Carr, S., Matico, R., Cusimanos, D., Dul, E., Angelichio, M., Brooks, I., Winborne, E., McDonnell, P., Morton, T., Bennett, D., Sokoloski, T., McNulty, D., Rosenberg, M., and Chaiken, I. (1995) *J.Biol.Chem.* **270** 9459-9471

Johnson, E.M., Berk., D.A., Jain, R.k., and Deen, W.M. (1995) *Biophys. J.* **68** 1561-1568

Johnson, E.M., Berk., D.A., Jain, R.k., and Deen, W.M. (1996) *Biophys. J.* **70** 1017-1026

Johnsson, B., Löfås, S., and Lindquist, G. (1991) *Anal. Biochem.* **198** 268-277

Johnsson, B., Löfas, S., and Lindquist, G., Edström, Å., Müller Hillgren, R.-M and Hansson, A. (1995) *J.Mol. Recogn.* **8** 125-131

Jönsson, U., Malmqvist, M., and Rönnberg, I. (1985) *Biochem.J.* **227** 363-371

Jost, J-P., Munich, O., Andersson, T. (1991) *Nucleic acids Res.* **19** 2788-

Kalinin, N.L., Ward, L.D., and Winzor, D.J. (1995) *Anal.Biochem.* **228** 238-244

Karlsson, R., Michaelsson, A., and Mattson, L. (1991) *J. Immunol. Methods* **145** 229-240

Karlsson,R., Roos, H., Fägerstam, L., and Persson, B. (1994) *Methods: A companion to Methods in Enzymology* **6** 99-110

Karlsson, R. (1994) *Anal. Biochem.* **221** 142-151

Karlsson,R., and Ståhlberg,R. (1995) *Anal. Biochem.* **228** 274-280

Karlsson, R., and Fält, A. (1997) *J.Immunol. Methods.* **200** 121-133

Khilko, S.N., Corr, M., Boyd, L.F., Lees, A., Inman, J.K., and Marguiles, D.H. (1993) *J.Biol.Chem.* **268** 15425-15434.

Khilko, S.N., Jelonek, M.T., Corr, M., Boyd, L.F., Bothwell, A.L.M., and Margulies, D.H. (1995) *J. Immunol. Methods* **183** 77-94

Klapper,I., Hagstrom, R., Fine, R., Sharp, K., and Honig, B. (1986) *Proteins* **1** 47-79

Kortt, A.A., Oddie, G.W., Iliades, P., Gruen, L.Clem. and Hudson, P.J. (1997) *Anal.Biochem.* **253** 103-111

Koppenol, W.H., and Margoliash, E. (1982) *J. Biol.Chem.* **257** 4426-4437

Kozack, R.E., and Subramaniam,S. (1993) *Protein Science* **2** 915-926

Kurrat, R., Prenosil, J.E., and Ramsden, J.J. (1997) *J.Colloid.Interface. Sci.* **185** 1-8

Langmuir, I.M. (1918) *J. Am. Chem. Soc.* **40** 1361

Larvor, M-P., Djavadi-Ohaniance, L., Nall, B., and Goldberg, M.E. (1994) *J. Immunol. Methods.* **170** 167-175

Lassen, B., and Malmsten, M. (1996) *J.Colloid Interface Sci.* **186** 9-16

Lassen, B., and Malmsten, M. (1997) *J.Colloid Interface Sci.* **179** 470-477

Leatherbarrow, R.J (1990) *Trends Biol. Sci.* **15** 455-458

Liedberg, B., Nylander, C., and Lundstrom, I (1983) *Sensors and Actuators* **4** 299-304

Löfas, S., and Johnsson, B. (1990) *J. Chem. Soc. Chem. Commun* **21** 1526-1528

Löfås, S., Malmqvist, M., Ronnberg, I., Stenberg, E., Lieberg,B., and Lundstrom, I. (1991) *Sensors and Actuators B* **5** 79-84

Löfås, S., Johnsson, B., Tegendal, K., and Rönnberg, I. (1993) *Colloids and Surfaces B: Biointerfaces* **1** 83-89

Löfås, S., Johnsson, B., Edström, Å., Hansson, A., Lindquist, G., Hillgren, R.M., and Stigh, L. (1995) *Biosensors and Bioelectronics* **10** 813-822

Longstaff, C., Campbell, A.F., and Fersht, A.R. (1990) *Biochemistry* **29** 7339-7347

Lukosz, W., Clerc, D., Nellen, P, M., Stamm, Ch., and Weiss, P. (1991a) *Biosensors and Bioelectronics* **6** 227-232

Lukosz, W., Clerc, D., Nellen, P, M. (1991b) *Sensors and Actuators A* **25-27** 181-184

Lukosz, W. (1991) *Biosensors and Bioelectronics* **6** 215-225

MacCullum, R.M., Martin, A.C.R., and Thornton, J.M. (1996) *J.Mol.Biol.* **262** 732-745

MacKenzie, C.R., Hirama, T., Deng, S., Bundle, D.R., Narang, S., and Young, N.M. (1996) *J.Biol.Chem.* **271** 1527-1533

Malmborg, A-C., Michaëlsson, A., Ohlin, M., Jansson, B., and Borrebaeck, B. (1992) *Scand. J. Immunol.* **35** 643-650

Martensson, J., Arwin, H., Lunstrom, I., and Ericson,T. (1993) *J.Coll. Int. Sci.* **155** 130-136

McPhalen, C.A. and James, M.N.G. (1988) *Biochemistry* **27** 6582-6598

Model, M.A., and Omann, G.M. (1995) *Biophys. J.* **69** 1712-1720

Moore, R.M., and Walters, R.R. (1987) *J.Chromat.* **384** 91-103

Morgan, C.L., Newman, D.J. and Price, C.P. *Clin.Chem.* (1996) **42:2** 193-209.

Morton, T.A., Bennett, D.B., Appelbaum, E.R., Cusimano, D.M., Johanson, K.O., Matico, R.E., Young, P.R., Doyle, M., and Chaiken, I.M. (1994) *J. Mol. Recogn.* **7** 47-55

Morton, T.A., Myszka, D.G., and Chaiken, I.M. (1995) *Anal. Biochem.* **227** 176-185

Mosbach, K (1991) *Biosenors and Bioelectronics* **6** 179-18

Munro, P.D., Winzor, D.J., and Cann, J. (1994) *J Chromat. A* **659** 267-273

Myszka, G.G., Morton, T.A., Doyle, M.L., and Chaiken, I.M. (1997) *Biophys. Chem.* **64** 127-137

Náray-Szabó, G. (1993) *J. Mol. Recogn.* **6** 205-210

Nellen, P., and Lukosz, W. (1990) *Sensors and Actuators B* **1** 592-596

Nichol, L.W., Ogston, A.G., Winzor, D.J., and Sawyer, W.H. (1974) *Biochem. J.* **143** 435-443

Nichol, L.W., Ward, L.D., and Winzor, D.J. (1981) *Biochemistry* **20** 4856-

Nicholls, A., Sharp, K.A., and Honig, H. (1991) *Proteins* **11** 281-296

Nieba, L., Krebber, A., and Plückthun, A. (1996) *Anal.Biochem.* **234** 155-165

Nieto, A., Gaya, A., Jansa, M., Moreno, C., and Vives, J. (1984) *Mol. Immunol.* **21** 537

Niveleau, A., Sage, D., Reynaud, C., Bruno, C., Legastelois, S., Thomas, V., and Dante, R. (1993) *J. Immunol. Methods* **159** 177-187

Northrup, S.H., and Erickson, H.P. (1992) *Proc. Natl. Acad. Sci. USA.* **89** 3338-3344

Novotny, J., and Sharp, K. (1992) *Prog. Biophys. Molec. Biol.* **58** 203-224

Noy, N., Leonard, M., and Zakim, D. (1992) *Biophys. Chem* **42** 177-188

Nygren, H. (1993) *Biophys. J.* **65** 1508-1512

Nygren, N., and Stenberg, M. (1985) *J.Colloid Interface Sci.* **107** 560-566

Nygren, N., Werthen, M., and Stenberg, M. (1987) *J. Immunol. Methods.* **101** 63-71

Oddie, G.W., Gruen, L.Clem., Odgers, G.A., King, L.G., and Kortt, A.A. (1997) *Anal. Biochem.* **244** 301-311

O'Shannessy, D.J., Brigham-Burke, M., and Peck, K. (1992) *Anal.Biochem.* **205** 132-136

O.Shannessy,D.J., Brigham-Burke, M., Soneson, K.K., Hensley, P. and Brooks, I. (1993) *Anal. Biochem.* **212** 457-468

O'Shannessy, D.J. (1994) *Curr.Opin.Biotech.* **5** 65-71

O'Shannessy, D.J., and Winzor, D.J., (1996) *Anal. Biochem.* **236** 275-283

Ockman, N. (1978) *Bioploymers* **17** 1273-1284

Parsons, I.D., and Stockley, P.G. (1997) *Anal. Biochem.* **254** 82-87

Piehler, J., Brecht, A., Gauglitz, G., Maul, C., Grabley, S., and Zerlin, M. (1997) *Biosensors and Bioelectronics* **12** 531-538

Pellequer, J.L., and Van Regenmortel., M.H.V. (1993) *J. Immunol. Methods* **166** 133-143

Place, J.F., Sutherland, R.M., and Dahne, C. (1985) *Biosensors* **1** 321-353

Plowman, T.E., Reichert, W.M., Peters, C.R., Wang, H.K., Christensen, D.A., and Herron, J.N. (1996) *Biosensors and Bioelectronics* **11** 149-160

Polzius, R., Bier, F.F., Bilitewski, U., Jäger, V., and Schmid, R.D. (1993) *Biotechnology and Bioengineering* **42** 1287-1292

Richalet-Sécordel, P.M., Rauffer-Bruyère, N., Christensen, L.L.H., Ofenloch-Haehnle, B., Seidel, C., and Van Regenmortel, M.H.V. (1997) *Anal. Biochem* **249** 165-173

Rova, U., Goodtzova, K., Ingemarson, R., Behravan, G., Gräslund, A., and Thelander, L. (1995) *Biochemistry* **34** 4267-4275

Ruzgas, T.A., Razumas, V.J., and Kulys, J.J. (1992) *Biosensors and Bioelectronics* **7** 305-308

Sadana, A., and Sii, D. (1991) *J.Coll.Int.Sci.* **151** 166-177

Santore, M.M., and Kaufman, M.J. (1996) *J.Polymer Sci. B.* **34** 1555-1568

Scatchard, G. (1949) *Ann. N.Y. Acad. Sci.* **51** 660-672

Schipper, E.F., Kooyman, R.P.H., Borreman, A., and Greve, J. (1996) *Biosensors and Bioelectronics* **11** 295-304

Schipper, E.F., Kooyman, R.P.H., Heideman, R.G., and Greve, J. (1995) *Sensors and Actuators B* **24-25** 90-93

Schlatter, D., Barner, R., Fattinger, Ch., Huber, W., Hubscher, J., Hurst, J., Koller, H., Mangold, C., and Muller, F. (1993) *Biosensors and Bioelectronics* **8** 109-116

Schuck, P. (1996) *Biophys. J.* **70** 1230-1249

Schuck, P. and Minton, A.P (1996) *Anal. Biochem.* **240** 262-272

Schuck, P. (1997) *Curr. Opin. Biotech.* **8** 492-502

Sharp, K., and Honig, B. (1990) *J. Phys. Chem.* **94** 7694-7692

Shoup, D., and Szabo, A. (1982) *Biophys. J.* **40** 33-39

Stamm, Ch., and Lukosz, W. (1993) *Sensors and Actuators B* **11** 177-181

Stamm, Ch., and Lukosz, W. (1996) *Sensors and Actuators B* **31** 203-207

Stenberg, M., and Nygren, H. (1982) *Anal. Biochem.* **127** 183-192

Stenberg, M., and Nygren, H. (1985) *J. Theor. Biol.* **113** 589-597

Stenberg, M., Stiblert, L., and Nygren, H. (1986) *J. Theor.Biol.* **120** 129-140

Stevens, F.J. (1987) *Mol. Immunol.* **24** 1055-1060

Striebel, Ch., Brecht, A., and Gauglitz, G. (1994) *Biosensors and Bioelectronics 9 139-146*

Sutherland, R., and Dahne, C. (1987) in *Biosensors: Fundamentals and Applications* (eds. A.P.F. Turner, I. Karube and G.S.Wilson) Oxford Science Publicxations 655-678

Takano, E., Hatanaka, M., and Maki, M. (1994) *FEBS Letters* **352** 247-250

Thompson, M., Kipling, A.L., Duncan-Hewitt, W.C., Rajakovic, L.V., and Cavic-Vlasak, B.A. (1991) *Analyst* **116** 881-890

Tiefenthaler, K., and Lukosz, W. (1989) *J. Opt. Soc. Am.* **6** 209-220

Tiefenthaler, K (1993) *Biosensors and Bioelectronics* **8** 35-37

Tronin, A., Dubrovsky, T., Denitti, C., Gussoni, A., Erokhin, V., and Nicolini, C. (1994) *Thin Solid Films* **238** 127-132

Ulbrich, R., Golbik, R., and Schellenberger, A. (1991) *Biotech. and Bioeng.* **37** 280-287

Underwood, P.A. and Steele, J.G. (1991) *J.Immunol. Methods.* **142** 83-94

Vadgama, P., Spoors, J., Tang, L.X., and Battersby, C. (1989) *Biomed. Biochim. Acta* **48** 935-942

Van Leeuwen, J.W. (1983) *Biochem. Biophys. Acta* **743** 408-421

Voss, E.W. Jr. (1993) *J.Mol.Recogn.* **6** 51-58

Watts, H.J., Lowe, C.R., and Pollard-Knight, D.V. (1994) *Anal.Chem.* **66** 2465-2470

Wigren, R., Billsten, P., Erlandsson, R., Löfås, S., and Lundström, I. (1995) *J.Coll.Int.Sci.* **174** 521-523

Williams, R.A. and Blanch, H.W. (1994) *Biosensors and Bioelectronics* **9** 159-167

Williams, R.J.P. (1988) *Nature* **332** 393

Winzor, D.J., Munro, P.D., and Cann, J.R. (1991) *Anal.Biochem* **194** 54-63

Winzor, D. J., and Sawyer, W.H. (1995) *Quantitative Characterisation of Ligand Binding* Wiley-Liss, New York.

Wiseman, T., Williston, S., Brandts, J.F., and Lin, L-N. (1989) *Anal.Biochem.* **179** 131-137

Wu, Z., Johnson, K.W., Choi, Y., and Ciardelli, T.L. (1995) *J. Biol. Chem* **270** 16045-16051

Yarmush, M.L., Patankar, D.B., and Yarmush, D.M. (1997) *Mol. Immunol.* **33** 1203-1214

Ysern,X., Fields, B.A., Bhat., T.N., Goldbaum, F.A., Dall'Acqua, W., Schwarz, F.P., Poljak, R.J., and Mariuzza, R.A. (1994) *J.Mol.Biol. 238 496-500*

Zellers, E.T., White, R.M., and Wenzel, S.W. (1988) *Sensors and Actuators* **14** 35

APPENDIX

Experimental Controls.

A1 Introduction.

In order to have confidence upon any conclusions made from the experimental data, the data must represent specific binding with the absence of no, or insignificant, non-specific binding. Non-specific binding is often a major problem with the use of planar surfaces such as those used for ELISA techniques where the protein of interest adsorbs to the surface together with any specific binding to its partner on the surface. This adsorption can be dramatically reduced by blocking the surface with a non-specific protein. Common examples are proteins used as blocking reagents include BSA and β-casein. The non-specific adsorption can also be reduced by surfactants such as Tween and by masking any surface change by the inclusion of NaCl in buffers. Therefore planar surface biosensor experiments are performed by blocking the surface with a non-specific protein and performing binding reactions in the presence of surfactant and at physiological or higher salt concentrations.

The presence of the CMD matrix reduces the likelihood of adsorption to the surface. However, given the high negative charge of the carboxylated matrix, proteins possessing a positive charge under the conditions of the experiment may cause a non-specific response by the interaction with the matrix. This interaction can be reduced by increasing the salt concentration in the interaction buffer.

This chapter therefore includes control data for the experimental data detailed in previous chapters.

A2 Chymotrypsin/CI-2 interaction.

To determine any non-specific binding to the CMD matrix, RAMFc was immobilised using EDC/NHS chemistry to a response of 2500 arc seconds. CI-2 was then added to the cuvette at a concentration of 124nM in PBS/T and allowed to interact for four minutes. The overlay of CI-2 binding at 124nM to chymotrypsin and RAMFc is shown in figure A1.

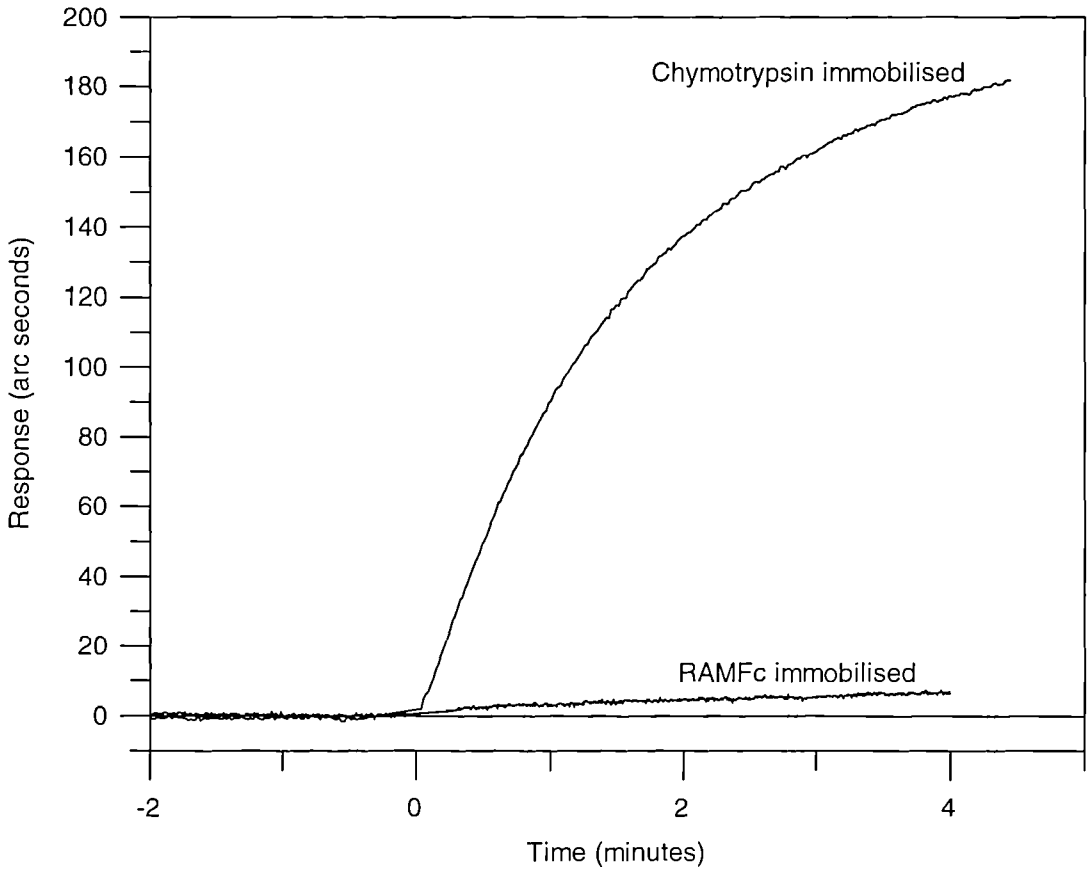

Figure A1: *The binding of 124 nM CI-2 to chymotrypsin or RAMFc immobilised on CMD with immobilisation signals of 1110 and 1960 arc seconds respectively.*

CI-2 at 124nM in PBS/T showed only a small increase in response on the RAMFc immobilised surface (less than 10 arc seconds), whereas on a chymotrypsin immobilised block a response of 190 arc seconds was observed.

A3 HSA/anti-HSA mab.

The HSA/anti-HSA mab system was investigated on differing surfaces with either partner immobilised.

A3.1 Binding of HSA to immobilised anti-HSA mab

A3.1.1 CMD

RAMFc was immobilised to the CMD surface and HSA at 15μM in PBS/T and allowed to bind. Figure A2 shows the responses obtained at the same concentration on RAMFc and anti-HSA mab immobilised CMD surfaces.

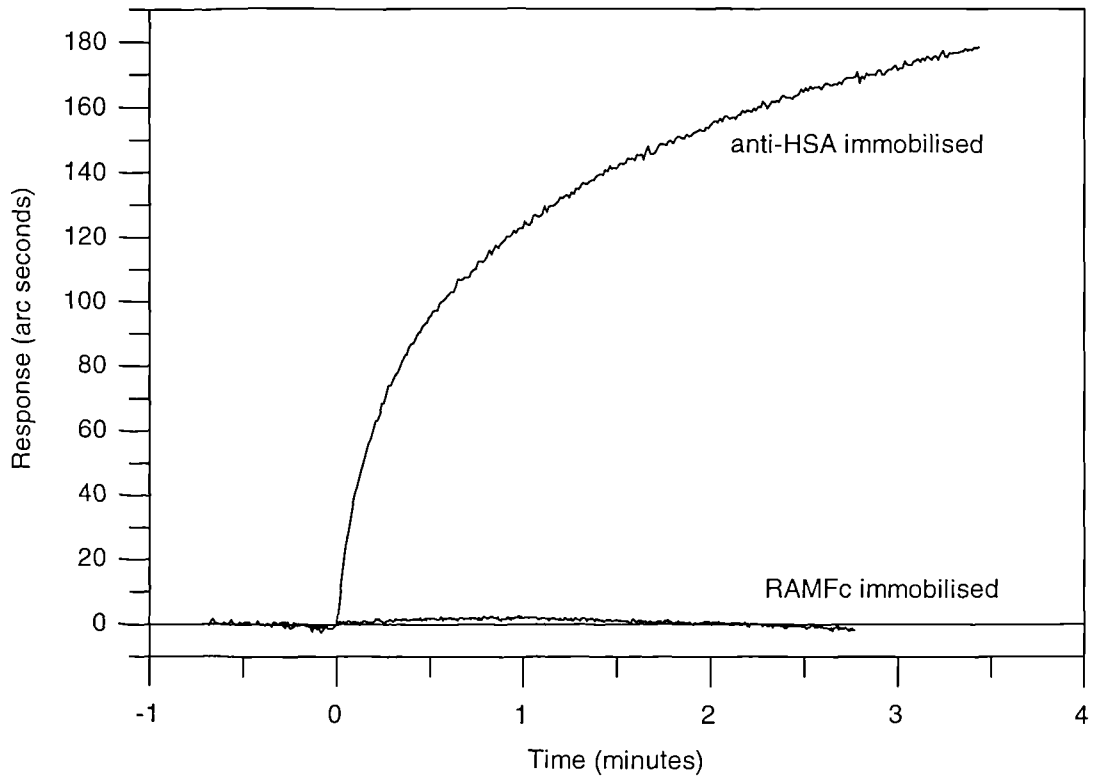

Figure A2: *The binding of 15 μM HSA to anti-HSA mab or RAMFc immobilised on CMD with immobilisation signals of 2100 and 1960 arc seconds respectively.*

There was no observable binding to RAMFc after 3 minutes compared to 170 arc seconds on the anti-HSA mab CMD surface.

A3.1.2 Carboxylate

The specific block was blocked with β-casein and therefore a carboxylate surface possessing immobilised β-casein to the same total immobilisation response. Figure A3 shows the binding response of 15 μM HSA on both the casein immobilised and the anti-HSA mab immobilised surfaces.

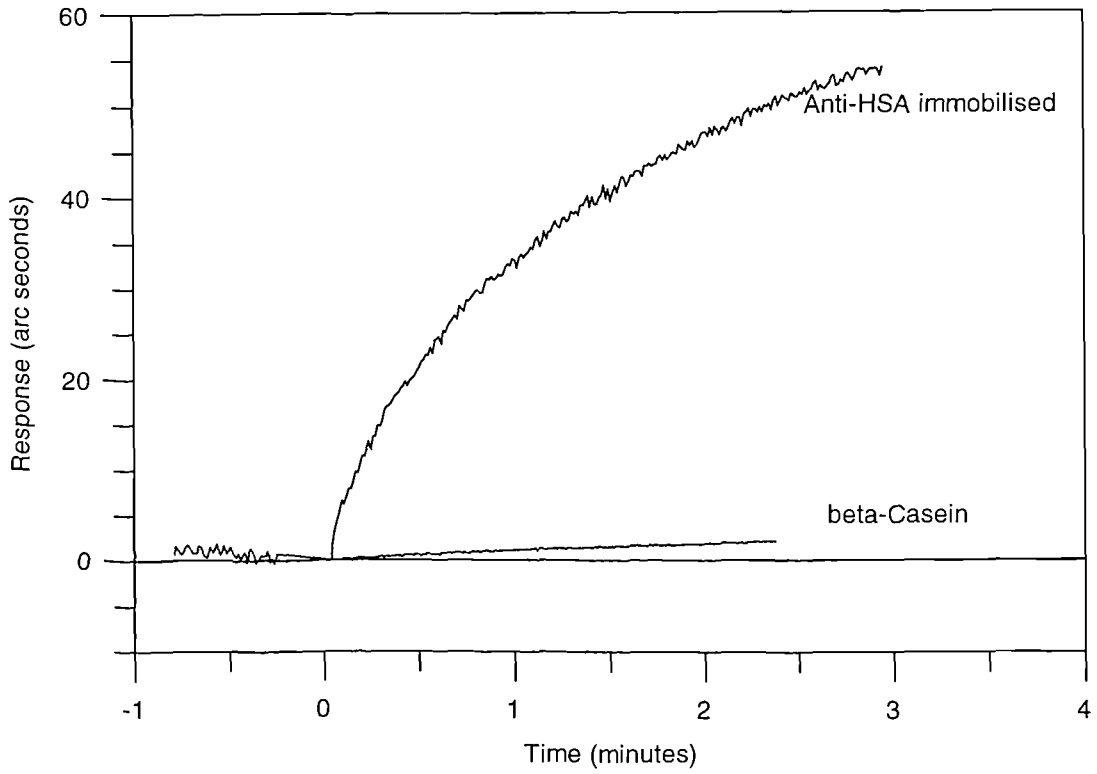

Figure A3: *The binding of 15 μM HSA to anti-HSA mab or β-casein immobilised on carboxylate surfaces with immobilisation signals of 660 and 850 arc seconds respectively.*

The specific signal is approaching 50 arc seconds after two minutes, whereas on the casein only surface a response of less than five arc seconds is observed.

A3.1.3 Amino surfaces

In common with the carboxylate surface, as the amino surface was routinely blocked with β-casein, the control for the amino surfaces was immobilised casein. Figure A4 shows the binding of 15 μM HSA to anti-HSA mab and casein only surfaces.

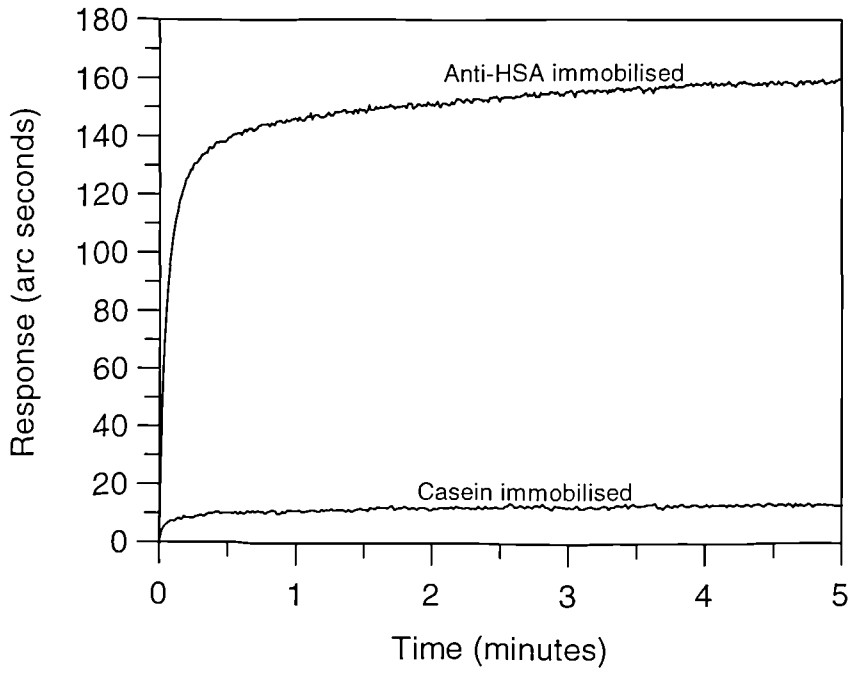

Figure A4: *The binding of 15 μM HSA to anti-HSA mab or casein immobilised on amino surfaces with immobilisation signals of 750 and 940 arc seconds respectively.*

After five minutes the binding response had reached 160 arc seconds on the anti-HSA mab surface while the casein only surface achieved a binding response of less than 20 arc seconds.

A3.2 Binding of anti-HSA mab to immobilised HSA

A3.2.1 CMD

The RAMFc could not be used for the control in this instance as binding of the anti-HSA mab would be observed and BSA was therefore used as a control. The binding of 2.2 μM anti-HSA mab in PBS/T to BSA and HSA immobilised CMD surfaces is shown in figure A5

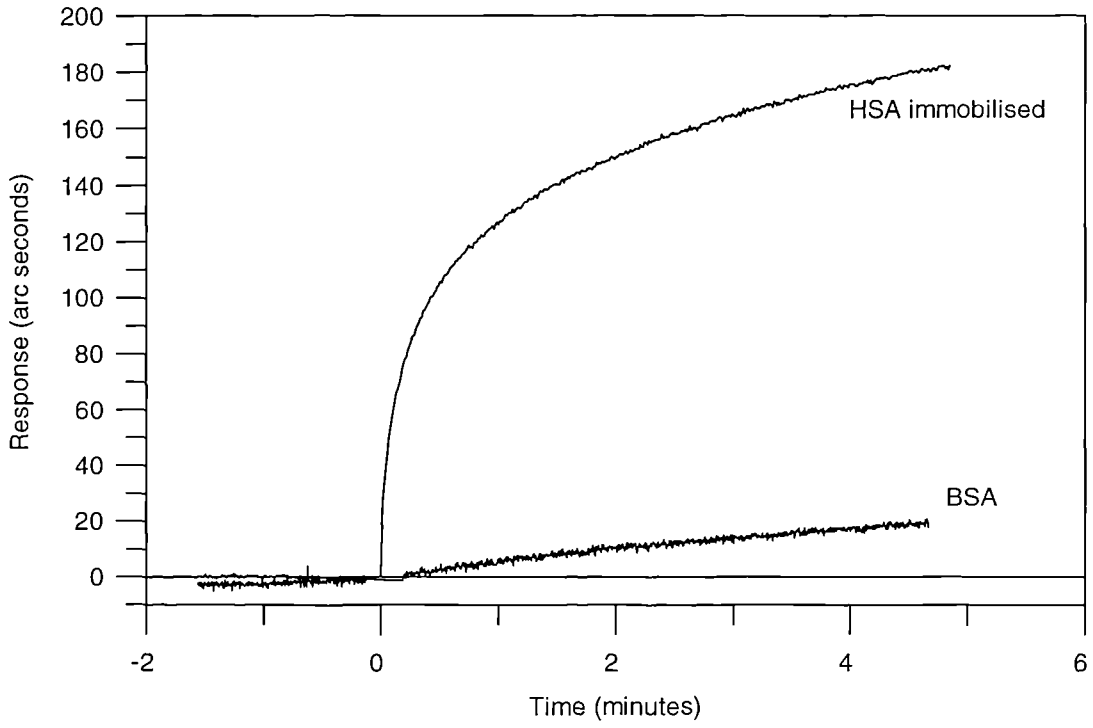

Figure A5: *The binding of 2.2 μM anti-HSA mab to HSA or BSA immobilised on CMD surfaces with immobilisation signals of 1020 and 1960 arc seconds respectively.*

A response of 180 arc seconds after 5 minutes was observed on the HSA immobilised surface compared to 20 arc seconds on the BSA immobilised surface.

A3.2.2 Carboxylate surface.

Once again the control was the immobilisation of β-casein used to block the specific surface. Figure A6 shows the binding of anti-HSA mab at 2.2 μM in PBS/T on casein and HSA immobilised carboxylate surfaces.

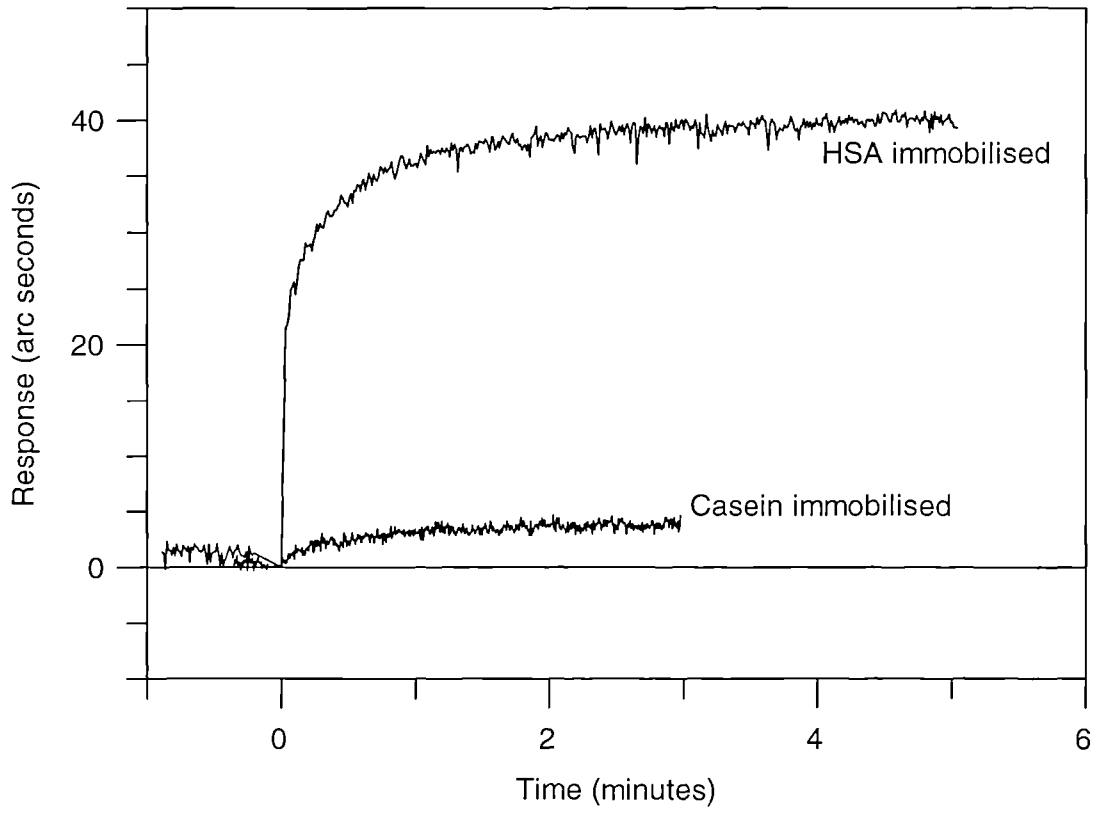

Figure A6: *The binding of 2.2 μM anti-HSA mab to HSA or casein immobilised on carboxylate surfaces with immobilisation signals of 450 and 850 arc seconds respectively.*

A3.2.3 Amino surface

Figure A7 shows the binding of anti-HSA mab at 2.2 μM in PBS/T to casein and HSA immobilised amino surfaces.

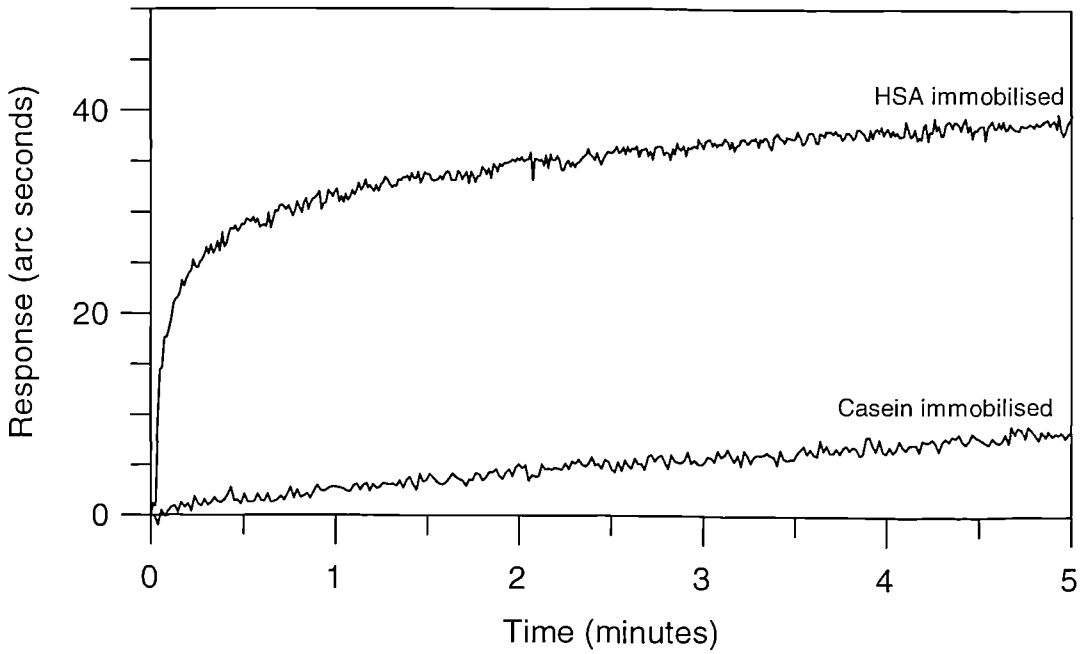

Figure A7: *The binding of 2.2 μM anti-HSA mab to HSA or casein immobilised on amino surfaces with immobilisation signals of 680 and 940 arc second respectively.*

The specific response from anti-HSA mab binding was 40 arc seconds after 5 minutes while that of the non-specific was less than 10 arc seconds.

A4 Lysozyme/D1.3Fv

A4.1 CMD

D1.3Fv at 15 nM was bound to lysozyme or RAMFc immobilised to CMD surfaces. The binding is shown in figure A8

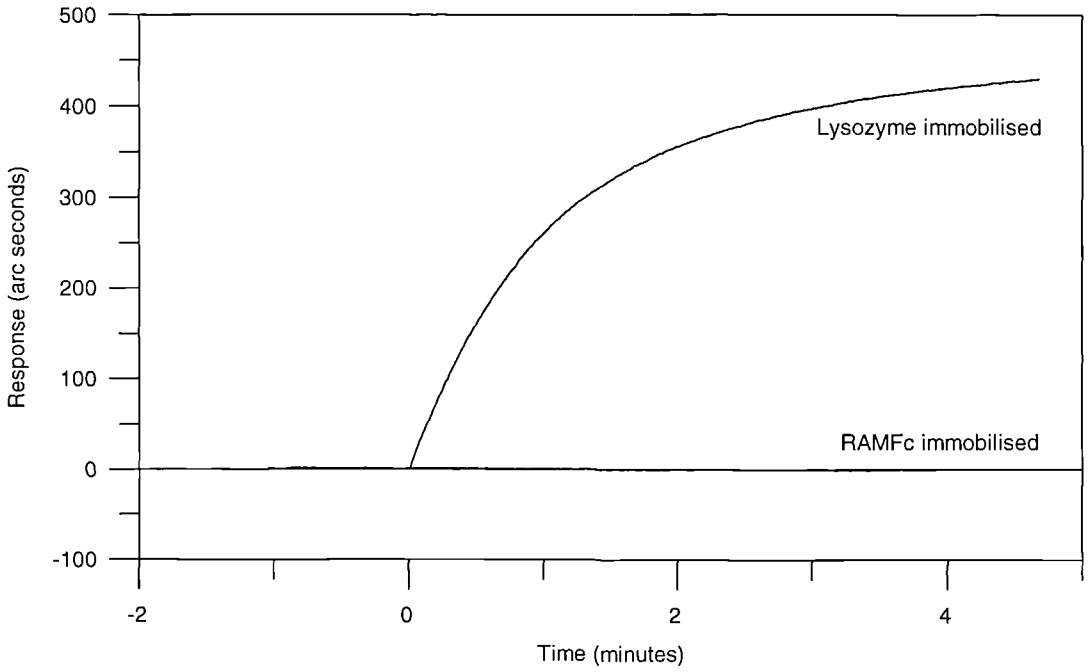

Figure A8: *The binding of 15 nM D1.3Fv to lysozyme or RAMFc immobilised on CMD surfaces with immobilisation signals of 1500 and 1980 arc second respectively*

No binding of D1.3Fv was observed to the RAMFc after four minutes whereas on the lysozyme immobilised surface 400 arc seconds was obtained.

A4.2 Carboxylate surface

D1.3Fv at 15 nM was bound to lysozyme or casein immobilised to carboxylate surfaces

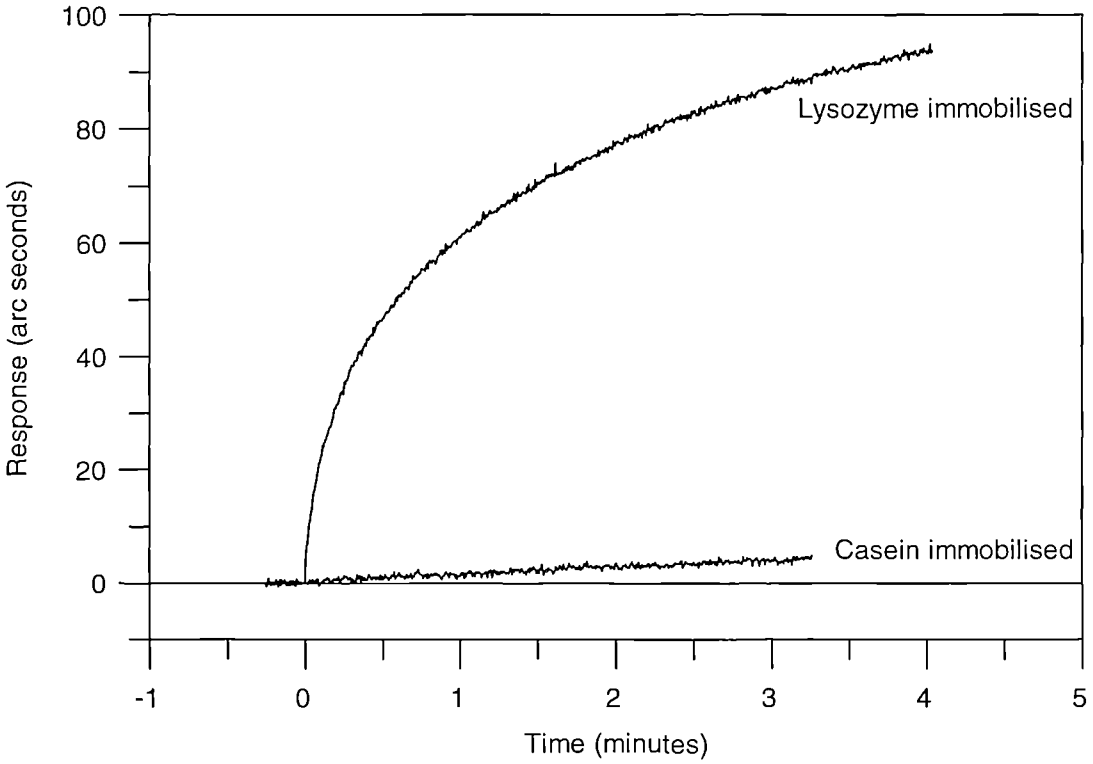

Figure A9: *The binding of 15 nM D1.3Fv to lysozyme or casein immobilised on carboxylate surfaces with immobilisation signals of 790 and 850 arc second respectively*

A4.3 Amino surface

β-Casein also acted as a control for the binding of D1.3Fv to lysozyme immobilised on an amino surface

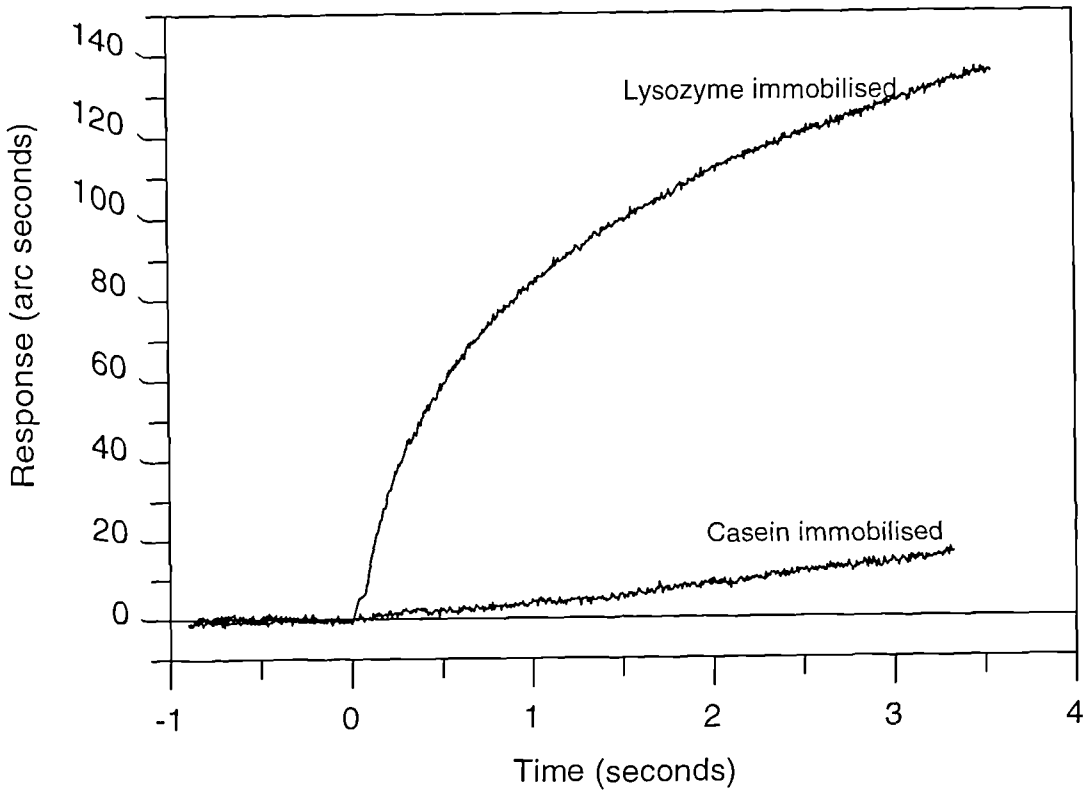

Figure A10: *The binding of 15 nM D1.3Fv to lysozyme or casein immobilised on amino surfaces with immobilisation signals of 880 and 940 arc seconds respectively*

A5 Discussion.

In all cases the instrument responses arising from specific binding were higher than those from the non-specific interaction. The low non-specific responses on the CMD surfaces may be expected due to its hydrophilic nature although the residual negative charge may increase the non-specific binding of positively charged material. It should be stressed that these charges may be screened by an increase in the ionic strength of the interaction buffer such a physiological (0.15M NaCl) or above. The interaction on planar surfaces may be expected to result in higher non-specific interactions with lower specific response compared to the equivalent conditions on CMD. The lower specific response is due the lower amount of active ligand on the surface. The high non-specific binding (adsorption) is a inherent problem with planar surfaces although this fact is used to often used to coat ELISA plates with antibody. The non-specific binding resulting from surface adsorption can be minimised by the introduction of a surfactant such as Tween 20 and increasing the ionic strength of buffers upon ligate

binding. Furthermore blocking of the surface with a non-specific protein such as casein or BSA has been shown to reduce later ligate adsorption.